DETERMINING THE ROLE OF GABAERGIC SIGNALING IN THE CRANIOFACIAL DEVELOPMENT OF LARVAL ZEBRAFISH

by

LINDSEY L. BEEBE

(Under the Direction of James D. Lauderdale)

ABSTRACT

Although best known as an inhibitory neurotransmitter, intriguing evidence has implicated GABA as a key signaling molecule in craniofacial development in mammals. Glutamate is converted to GABA by an enzyme called glutamic acid decarboxylase (GAD), which exists in two isoforms, GAD67 and GAD65. The GAD1 and GAD2 genes encode these isoforms, respectively. A decrease in GAD activity in the human brain is often associated with epilepsy, schizophrenia and related neurological disorders. In mice and humans, mutations in *gad1,* but not *gad2*, result in defects in palate development, and mutations in the Gabrb3 gene, which encodes the β3 subunit of the $GABA_A$ receptor, exhibit a comparable phenotype to *gad1* mutations. These results suggest that GABA signaling, through the $GABA_A$ receptor, can play an important and conserved role in craniofacial development. However, the mechanism of this process is not known and cannot be easily investigated in a mammalian system. In this work, translation-blocking morpholinos against the GAD genes were used to alter expression within the larval zebrafish. While *gad2* morphants looked phenotypically normal, *gad1* morphant animals exhibited altered cranial structures at 1 and 7 dpf. Yet, both *gad1* and *gad2* morphants

exhibited spontaneous seizure-like neural activity. Through the use of photoactivatable caged-morpholinos, the craniofacial deformities could be bypassed when photolysis was carried out at 24 hpf. Electrophysiological recordings showed that while dark-raised CyHQ-*gad1* morphant animals looked phenotypically comparable to wild-type animals, they exhibited abnormal, seizure-like neural activity. These findings support the idea that *gad1* exhibits a novel function in craniofacial development, independent of its activity in GABA synthesis.

INDEX WORDS: GABA, *gad1*, *gad2*, GAD67, GAD65, zebrafish, knockdown, translation blocking morpholinos, neural activity, seizures, cleft palate

# DETERMINING THE ROLE OF GABAERGIC SIGNALING IN THE CRANIOFACIAL DEVELOPMENT OF LARVAL ZEBRAFISH

by

LINDSEY L. BEEBE

BS, Michigan State University, 2010

A Dissertation Submitted to the Graduate Faculty of The University of Georgia in Partial Fulfillment of the Requirements for the Degree

DOCTOR OF PHILOSOPHY

ATHENS, GEORGIA

2015

# DETERMINING THE ROLE OF GABAERGIC SIGNALING IN THE CRANIOFACIAL DEVELOPMENT OF LARVAL ZEBRAFISH

by

LINDSEY L. BEEBE

| | |
|---|---|
| Major Professor: | James D. Lauderdale |
| Committee: | Brian Condie |
| | Scott Dougan |
| | Douglas Menke |
| | John Wagner |

Electronic Version Approved:

Julie Coffield
Interim Dean of the Graduate School
The University of Georgia
May 2015

## DEDICATION

I dedicate this work to my parents and to my husband, Steve. They have been my biggest support throughout my graduate career. My parents and Steve have continued to encourage and motivate my work and progress, and I know that I would not have made it through the rough spots without their support.

ACKNOWLEDGEMENTS

I would like to thank my mentor and major professor Dr. James D. Lauderdale for all of the guidance and insights that he has given me throughout my undertakings as a graduate student. He has not only helped me develop and carry out my research projects, but he has also given continued support in helping me reach my goals as an educator. He has not only stood in the stead of an academic advisor, but he has been a mentor to whom I could truly confide in. Without his continued support, I would not have made it thus far in my graduate career.

I would also like to thank all of the members of my lab, especially Vani Hariharan, Kenji Johnson, Tyler page, Ariel VanLeuven, Ana Bobilov, Vijay Kalaskar and Rebecca Ball. You all have not only been there to discuss my experiments, but you have also made my time in the Lauderdale lab fun and filled with laughter. Rebecca has been instrumental in teaching and helping me carry out many of my experiments. She has not only been there to give me advice, but she has also helped me turn into the scientist that I am today.

I'd like to thank Dr. Andrew Sornborger for serving as a mentor and continued help with analyses. I also would like to thank my committee members, Dr. Brian Condie, Dr. Scott Dougan, Dr. Douglas Menke and Dr. John Wagner for their critical and helpful advice and guidance along the way.

TABLE OF CONTENTS

Page

LIST OF FIGURES

Page

# CHAPTER 1

# INTRODUCTION AND LITERATURE REVIEW

## GABA and its functions as a neurotransmitter

GABA (γ-aminobutyric acid) is the principle inhibitory neurotransmitter in the central nervous system (CNS) of all vertebrates. In adults, GABA is synthesized in 20-30% of all neurons present within the CNS (Varju et al., 2001). The functional CNS depends on a fine balance of excitatory and inhibitory neurotransmission, so GABA serves a very important role in neural activity. Therefore, a key step in the regulation of GABA signaling must involve the modulation of GABA synthesis.

The major pathway through which GABA is synthesized is by the α-decarboxylation of glutamic acid to GABA by the action of glutamic acid decarboxylase (GAD) (Tillakaratne et al., 1995, Martin et al., 1998, Maddox and Condie, 2001, Kim et al., 2004). In vertebrates, GAD exists in two protein isoforms, each of which is encoded by a separate gene (Bu et al., 1992, Tillakaratne et al., 1995, Martin et al., 1998). In mammals, the GAD1 gene encodes for the protein isoform called GAD67, which has a molecular weight of ~67 kilodaltons (kDa), and the GAD2 gene encodes the protein isoform GAD65, which has a molecular weight of ~65 kDa (Erlander et al., 1991, Bu et al., 1992, Asada et al., 1997, Bosma et al., 1999, Maddox and Condie, 2001, Delgado and Schmachtenberg, 2008). These enzymes are highly conserved and have been described in *Drosophila*, avian and mammalian species (Martin et al., 1998). There is evidence of a third GAD gene (*gad3*) in the armored grenadier (*Coryphaenoides armatus*), a

scavenging deep sea fish (Bosma et al., 1999), but *gad1* and *gad2* have only been described in the zebrafish genome (Martin et al., 1998).

As an inhibitory neurotransmitter, the response to synaptic GABA is mediated through the activation of ionotropic $GABA_A$ and $GABA_C$, as well as metabotropic $GABA_B$ receptors in active post-synaptic neurons. Activation of the ionotropic receptors causes an influx of $Cl^-$ into the active neuron, which results in hyperpolarization, and ultimately inhibition of neuronal firing and action potential conduction (Cherubini et al., 1991, Johnston, 1996, McKernan and Whiting, 1996, Bormann, 2000). $GABA_A$ receptor activation mediates the primary bulk of rapid inhibitory synaptic transmission throughout the CNS, whereas the $GABA_C$ receptor primarily modulates activity within the retina (Feigenspan et al., 1993, Lukasiewicz, 1996). When GABA is bound to the metabotropic $GABA_B$ receptor of a post-synaptic neuron, GABA instead activates $K^+$ ion channels, resulting in hyperpolarization of the neuron and subsequent inhibition of action potential generation (Macdonald and Olsen, 1994, Mott and Lewis, 1994). The inhibitory activity established when these GABA receptors are activated is what characterizes the mature GABAergic network.

In mature neurons, GABA is present in two distinct compartments of the neuron: the synaptic terminal and the cell body. The pool of GABA present in each compartment is thought to perform a distinct function. GABA present within the synaptic terminal is released from vesicles and functions as a neurotransmitter. On the other hand, GABA within the cell body seems to exhibit a metabolic function, where it participates in the Tricarboxylic Acid (TCA) cycle (Martin and Rimvall, 1993, Tillakaratne et al., 1995). This pathway is shown in Figure 1.1. Three enzymes including glutamic acid

decarboxylase (GAD), GABA-transaminase (GABA-T) and succinic semialdehyde dehydrogenase (SSADH), are involved in the GABA shunt pathway of the TCA cycle. While the GAD enzymes synthesize GABA, the other two components are responsible for catabolism (Martin and Rimvall, 1993). This GABA shunt pathway is important for the disposal of GABA and it also provides energy upon breakdown (Hassel et al., 1998). Yet, this pathway remains secondary to GABA's role in neurotransmission.

GABA's functions during embryonic development

In addition to its role as an inhibitory neurotransmitter in the adult nervous system, GABA has been shown to exert excitatory and neurotrophic roles in the developing nervous system. Early in development, GABA exerts a depolarizing and excitatory action on immature neurons (Ben-Ari et al., 2007). These developmental actions are the result of elevated intracellular $Cl^-$ present within immature neurons. This increase in intracellular $Cl^-$ is primarily the result of high expression of the $Cl^-$ loader NKCC1 and low expression of the $Cl^-$ extruder KCC2 (Rivera et al., 1999, Yamada et al., 2004, Dzhala et al., 2005). In this scenario, the negatively charged chloride ions flow out of the post-synaptic neuron, generating an inward directed electrical current, and ultimately producing a depolarization. Yet, not all cells are excited by the depolarizing actions of GABA during embryonic development, even at the most immature state.

It has also been determined that the proportion of cells exhibiting an excitatory response rapidly decreases with age (Tyzio et al., 2006, Tyzio et al., 2007). During the first postnatal week in mice, GABA is found to depolarize neuronal membranes (Mueller et al., 1984, Ben-Ari et al., 1989, Cherubini et al., 1990, Zhang et al., 1990), most likely due to the modified chloride gradients resulting from the reversed operations of the $Cl^-$

membrane pumps (Misgeld et al., 1986). Though, as development progresses, the expression of the NKCC1 transporter is down regulated, allowing for GABA to exert a hyperpolarizing effect within the network. By the second postnatal week, in concomitance with the shift of GABA responses from depolarizing to hyperpolarizing, spontaneous GABA-mediated inhibitory potentials appear (Cherubini et al., 1991).

The postsynaptic responses in the early embryo seem to be mediated through the $GABA_A$ receptor (Khazipov et al., 2014). Activation of the $GABA_A$ receptor has not only been found to generate depolarizing effects, but it has also been associated with increased cell volumes and accumulation of stem cells in the S phase of the cell cycle. Inhibition of endogenous signaling in high-density stem cell cultures, through the addition of bicuculline (a competitive $GABA_A$ antagonist), significantly increased the number of cells and led to increased Bromodeoxyuridine (Brdu) incorporation (Andäng et al., 2008). This finding suggests that GABA, acting through the $GABA_A$ receptor, regulates cell migration and proliferation in an autocrine/paracrine-signaling manner (Condie et al., 1997, Hagiwara et al., 2003, Andäng et al., 2008).

Similar to the above findings, it seems that GABA can serve as a neurotrophic factor during synaptogenesis and neural differentiation (Lauder, 1993, Martin and Rimvall, 1993, Kim et al., 2004). Previous work has shown that GABA was able to induce ultrastructural changes in developing ganglion cells. These changes included the appearance of spine-like protrusions on dendrites and membrane thickening (Wolff et al., 1978). In murine neuroblastoma cells, incubation with GABA was found to increase the formation of synaptic contacts, induce proliferation of vesicles, promote the differentiation of terminal swellings and induce the formation of intermediate junctions

(Wolff, 1982, Madtes Jr and Redburn, 1983). Together, these findings suggest that GABA may play a role in embryonic development, distinct from and prior to its role as a neurotransmitter.

GABA dysregulation in epilepsy and other neurological disorders

It has been found that defects in amino acid neurotransmission are commonly associated with several pathologies, including neurodegeneration and epilepsy (Bosma et al., 1999). While GABA and glutamate (the primary excitatory neurotransmitter) are the most abundant in the brain, dysregulation of either has the potential to cause neurological problems. Epilepsy is one of the most prevalent neurological disorders in the United States, occurring at a rate of 5-10 out of every 1000 people (Theodore et al., 2006). It is characterized by periodic and unpredictable seizures that are mediated by the rhythmic firing of large groups of neurons and can be caused by trauma, stroke, tumors, congenital cortical dysgenesis and vascular malformations (Purves, 2012). More specifically, these recurrent seizures manifest due to the abnormal, excessive and hypersynchronous discharge of a population of neurons. This hyperexcitable state is often the result of either increased excitatory synaptic transmission or decreased inhibitory neurotransmission (Bromfield et al., 2006).

Seizures generated due to an increase in excitatory activity are commonly caused by an increase in glutamatergic signaling, through its ionotropic receptors. Prolonged activity of this pathway allows for accumulation of $Ca^{+2}$, $K^{+}$ and $Na^{+}$ ions, and a subsequent increase in action potential generation (Bromfield et al., 2006). Similarly, a switch in the GABAergic system from its hyperpolarizing activities to depolarizing effects, can also contribute to the enhanced excitability commonly observed in immature

or damaged networks. The actions of this pathway can lead to an accumulation of $Cl^-$ within postsynaptic neurons, establishing an increased susceptibility to the development of seizure activity (Holmes et al., 2002, Khazipov et al., 2014).

The decreased expression of genes related to GABAergic signaling has also been associated with epilepsy (Akbarian and Huang, 2006, Brooks-Kayal et al., 2009, Hortopan et al., 2010). Abnormal expression of the GAD genes and the GABA receptors have been linked to the depolarizing effects of GABA, as well as seizure and epilepsy generation in both humans and rodents. For example, block of $GABA_A$ receptors in rat hippocampal slices has been found to suppress drug-induced seizures or transform them into less severe interictal-like activity (Dzhala and Staley, 2003, Khalilov et al., 2003, Khazipov et al., 2004). Unlike GAD67 mutant mice, which die shortly after birth due to cleft palate, GAD65-/- mice are viable, but they exhibit temporal lobe epilepsy in the limbic regions of the brain (Condie et al., 1997, Kash et al., 1997). Similarly, when the $GABA_AR$ β3 subunit was knocked out in mice, mutants exhibited hyperactive responses to human contact and other stimuli (Homanics et al., 1997), and neuron-specific enolase expression of this subunit was able to rescue these neurological phenotypes (Hagiwara et al., 2003).

Due to the associations of GABAergic signaling with seizures and epilepsy, many pharmacologic therapies combating seizure development target this pathway. Anti-epileptic drugs (AEDs) utilize two approaches to reduce the likelihood that a seizure will develop. These methods include: 1) enhancing the functions of inhibitory synapses that use GABA or 2) limiting action potential generation, by acting on voltage-gated $Na^+$ channels (Leslie Iversen, 2008). Common AEDs that work to enhance GABAergic

synaptic effects include the benzodiazepines and barbiturates, which bind to the $GABA_A$ receptors and act to prolong GABA responses through increased $Cl^-$ conductance. Other AEDs target the GAT-1 transporter, preventing the reuptake and metabolism of GABA, and ultimately prolonging the effect of GABA at the synapse (Leslie Iversen, 2008).

Not only has GABAergic signaling been associated with epilepsy, but changes in this inhibitory signaling have also been implicated in autism, bipolar and schizophrenia literature (Harrison and Weinberger, 2004, Guidotti et al., 2005, Lewis et al., 2005, Akbarian and Huang, 2006, Brooks-Kayal et al., 2009, Hortopan et al., 2010). Studies have linked the dysfunction of GAD1 to the abnormal development and early (childhood) onset of schizophrenia (Addington et al., 2004, Rapoport et al., 2005) and bipolar disorder (Lundorf et al., 2005). Not surprisingly, GAD67 and GABA levels have been found to be greatly reduced within the prefrontal cortex and other cortical areas of schizophrenics (Akbarian and Huang, 2006), autistic individuals (Fatemi et al., 2002) and in the postmortem brain of those exhibiting bipolar disorder (Guidotti et al., 2000, Woo et al., 2004, Hossein Fatemi et al., 2005).

## Nonneural functions of GABA

Surprisingly, GABA isn't confined to the CNS, as it has also been detected within the peripheral nervous system, endocrine and several other tissues (Erdö and Kiss, 1986, Erdö et al., 1989, Tillakaratne et al., 1995). Nonneural GABAergic signaling has been implicated by the presence of GABA, its biosynthesizing enzymes and receptors within the pancreas (Baekkeskov et al., 1990, Yang et al., 1994), the oviduct and ovary (Erdö et al., 1989), the kidney (Párducz et al., 1992), the testis (Tillakaratne et al., 1992) and multiple embryonic sites in mice, including the mystacial vibrissae and limb buds

(Katarova et al., 2000, Maddox and Condie, 2001). Figure 1.2 shows examples of the nonneural GABA/Gad1 expression patterns within the embryonic mouse. The exact role of GABA within these nonneural tissues remains largely unknown, but there is data that gives insight into its varying functions. For example, GABA may be important to the local regulation of seminal function including the motility of spermatozoa, the stimulation of testosterone production and the regulation of uterotuberal and gut motility (Ritta et al., 1987, Boldizsár et al., 1992, László et al., 1992, Tillakaratne et al., 1995). GABA has also been implicated in the control of hormone release in the endocrine cells of the pancreas, adrenal medulla and gastrointestinal tract (Kataoka et al., 1984, Gilon et al., 1988, Castro et al., 1989, Young and Bordey, 2009). GABA's functions in craniofacial development have more recently been demonstrated in murine models.

GABA's functions in craniofacial development

Craniofacial anomalies are among the most common birth defects in the human population, with an estimated prevalence of 1 in 600 live births worldwide. These include oral clefts (lip and/or palate), jaw deformities, and defects in the ossification of facial or cranial bones. Factors that contribute to these conditions include poor nutrition, drug exposure, environmental factors and heredity (Organization, 2002). Studies in humans and rodents have implicated a rather unexpected causal agent in the form of disruptions in GABA signaling, however the cellular and molecular mechanisms involved have not been easily investigated using the existing mouse models or in human patients.

The involvement of GABAergic signaling in normal palate development has been thoroughly demonstrated through the use of mouse models, including mutants for Gad1 (encoding GAD67) and Gabarb3 (encoding the $GABA_AR$ β3 subunit) (Culiat et al., 1993,

Hagiwara et al., 2003, Ding et al., 2004). Mice lacking either of these genes die soon after birth, most likely due to feeding problems associated with a severe secondary cleft palate (Asada et al., 1997, Condie et al., 1997, Homanics et al., 1997, Maddox and Condie, 2001). Similarly, when GABA agonists, such as diazepam, or antagonists, such as picrotoxin, were administered to pregnant mice, cleft palate was induced in exposed embryos (Miller and Becker, 1975, Wee and Zimmerman, 1983, Jurand and Martin, 1994). When GABA itself was applied to organ culture, palate formation was also impaired (Wee and Zimmerman, 1983). Such observations suggest that deviation from a normal range of GABA signaling can severely affect development of the palate.

Determining functions of GABA: neurotransmission and craniofacial development

In the embryonic palate, the GABAergic system may be acting through neurons (innervating the palate, mouth or tongue) or through nonneural cells in or around the developing palate. GABA synthesized and released by the palatal epithelium has already been implicated in mediating cellular proliferation during palatal shelf elevation, cell migration and differentiation during the fusion process (Hagiwara et al., 2003). Therefore, it seems likely that GABA signaling can serve multiple roles in a developing animal: including one as a neurotransmitter and a second in early craniofacial development.

In order to separate the functions of GABA signaling during early embryonic development, a specific toolset was developed to isolate its activity in neurotransmission from that in craniofacial development. The first approach utilized both *ex vivo* and *in vivo* electrophysiological approaches. Although brain slice culture is a standard technique used for the study of cellular components of the mammalian brain (Haas et al., 1979,

Walther et al., 1986, MacVicar and Hochman, 1991, Owens et al., 1996), the preparation of these slices necessarily disrupts the overall neural network, thereby limiting their use to the study of local circuitry. The small size of the adult zebrafish brain suggests that it could be well suited for the development of a whole-brain preparation that could be used in conjunction with slice recordings. Therefore, I developed a system where an isolated adult zebrafish brain could remain functional and exhibit spontaneous neurological activity. This preparation was easily maintained in a solution of artificial cerebrospinal fluid (ACSF) for periods up to 4 hours, and it could be used to record electrophysiological alterations in the native neural activity when different pharmacological agents were applied.

While the whole brain preparation was able to maintain the original neural connections, I show that an *ex vivo* brain is unable to fully recapitulate the neural activity of a living fish. Acute slice preparations were also able to maintain functionality with our setup, but local neural circuits were necessarily disrupted when the brain was removed and/or sectioned. Changes in the neurological activity of *ex vivo* whole brain and slice setups, following chemical exposure, were similar to those seen in the living fish, though induced changes were not as complex as those observed with the *in vivo* setup. While electrophysiological data from intact adults gives a better idea of changes in native neurological activity of zebrafish, this setup was far more complex and time consuming than the *ex vivo* approaches. Analysis of *in vivo* data was also much more difficult than that of the whole brain and slice approaches because sensory inputs and other higher-order circuits had to be considered when observing this data. Thus, a combination of both

approaches was useful when observing the neurological functions of GABA within the nervous system.

To study GABA's role in craniofacial development, caged-morpholinos were utilized to separate GABA's functions in early development from its later role as a neurotransmitter. The design of the photoactivatible morpholinos to *gad1* was similar to those created by James Chen's laboratory (Ouyang et al., 2009, Yamazoe et al., 2012), but they were more sensitive in a biological system due to the quinoline-based photoremovable protecting groups (PPGs) BHQ and CyHQ, which were developed in the Dore laboratory (Zhu et al., 2006). Early injection of these compounds, under red light conditions, allowed us to control the timing of photolysis, and ultimately the timing of morpholino activation. Specifically, when embryos were exposed to light immediately following injection, zebrafish exhibited altered craniofacial phenotypes at 1 dpf, but these alterations were not observed when animals were not exposed to light until 1 dpf or later. Caged-morphant animals exposed to light at 24 hpf were phenotypically comparable to their wild-type counterparts, but they exhibited increased electrophysiological activity *in vivo*. These findings support the idea that GABA signaling participates in two distinct developmental pathways. This work also supports that our established toolset can allow for the separation of GABA's early activity in craniofacial development from its later role in neurotransmission.

Figures

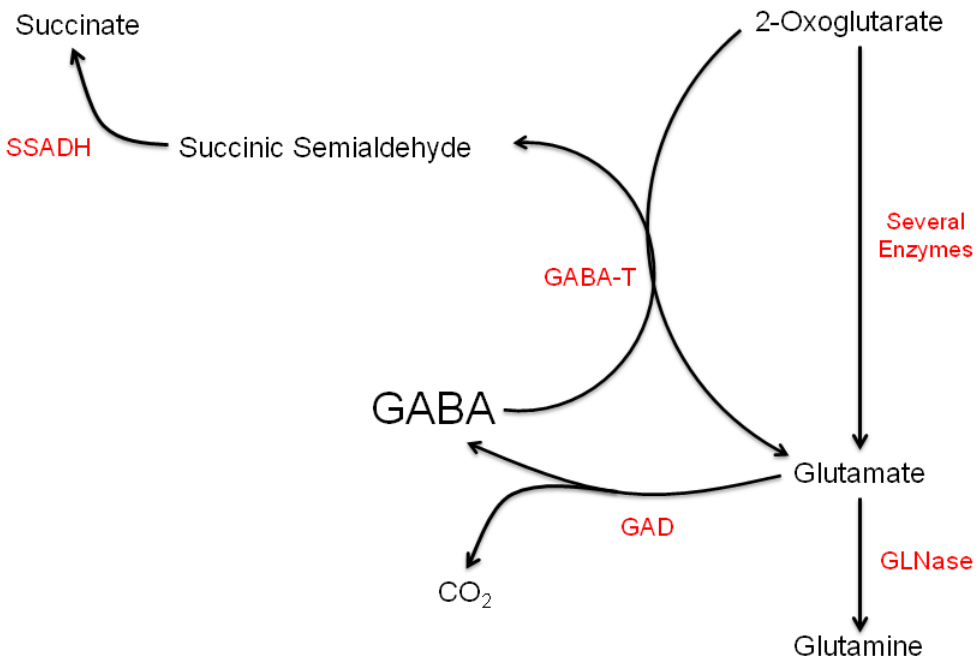


**Figure 1.1. GABA metabolism.** Adapted from (Martin and Rimvall, 1993). Production of GABA by the GABA shunt pathway of the TCA cycle involves conversion of oxoketoglutarate (2-oxoglutarate) to glutamate, which is then converted to GABA by the GAD enzymes. For GABA disposal, GABA-T and SSADH catabolize GABA into succinate. GAD, glutamic acid decarboxylase; GABA-T, GABA transaminase; GLNase, glutaminase; SSADH, succinic semialdehyde dehydrogenase

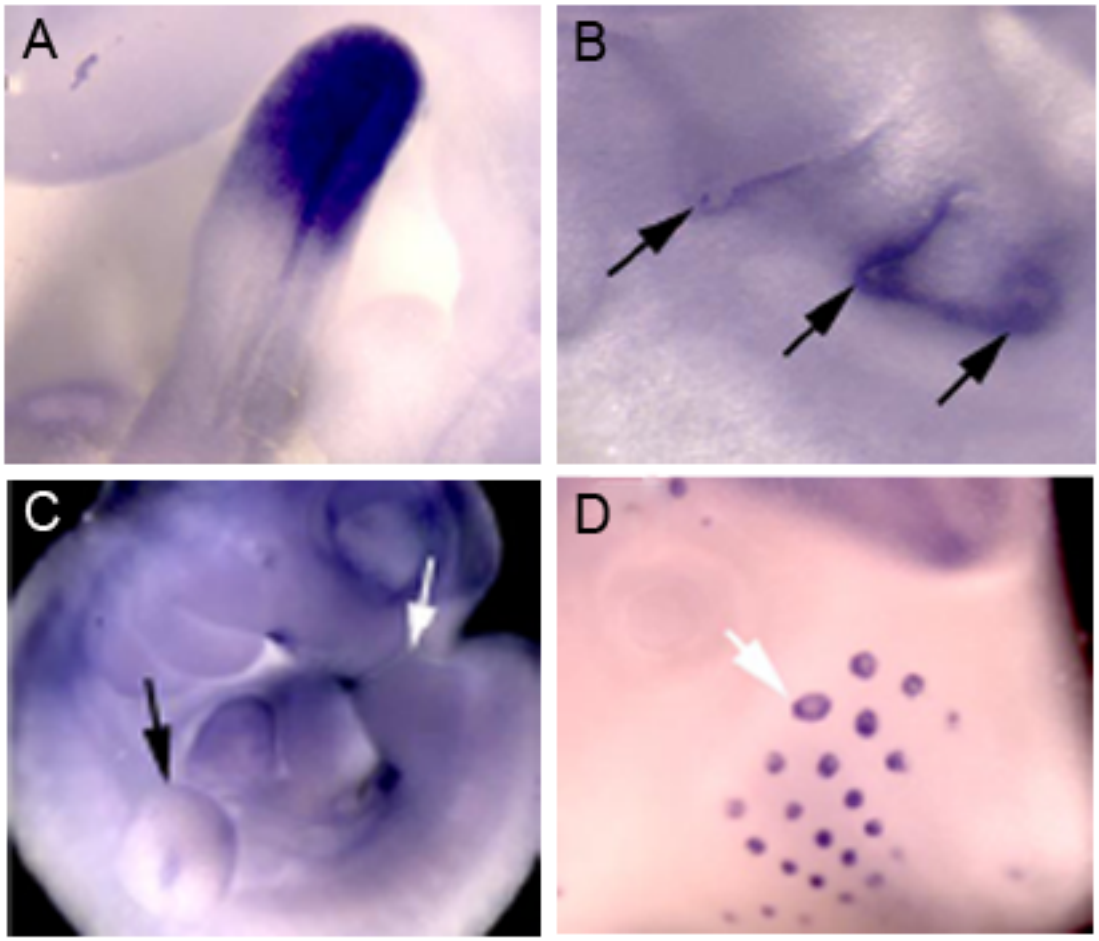


**Figure 1.2. Nonneural expression of GABA, as shown by Gad1 mRNA, in the embryonic mouse.** Adapted from (Maddox and Condie, 2001). (A-D) *in situ* hybridizations showing nonneural Gad1 expression in embryonic mice. (A) Gad1 expression in the tail at E10.5. (B) Gad1 expression in the developing pharyngeal pouches at E9.5 (black arrows). (C) Lateral view of E10.5 embryo indicating the forelimb (black arrow) and hindlimb (white arrow). Expression is observed in the proximal forelimb. (D) Gad1 mRNA in the lateral nasal/maxillary (white arrow) rows of vibrissae.

References

Addington A, Gornick M, Duckworth J, Sporn A, Gogtay N, Bobb A, Greenstein D, Lenane M, Gochman P, Baker N (2004) GAD1 (2q31. 1), which encodes glutamic acid decarboxylase (GAD67), is associated with childhood-onset schizophrenia and cortical gray matter volume loss. Molecular psychiatry 10:581-588.

Akbarian S, Huang H-S (2006) Molecular and cellular mechanisms of altered *GAD1*/*GAD67* expression in schizophrenia and related disorders. Brain research reviews 52:293-304.

Andäng M, Hjerling-Leffler J, Moliner A, Lundgren TK, Castelo-Branco G, Nanou E, Pozas E, Bryja V, Halliez S, Nishimaru H (2008) Histone H2AX-dependent GABAA receptor regulation of stem cell proliferation. Nature 451:460-464.

Asada H, Kawamura Y, Maruyama K, Kume H, Ding R-G, Kanbara N, Kuzume H, Sanbo M, Yagi T, Obata K (1997) Cleft palate and decreased brain γ-aminobutyric acid in mice lacking the 67-kDa isoform of glutamic acid decarboxylase. Proceedings of the National Academy of Sciences 94:6496-6499.

Baekkeskov S, Aanstoot H-J, Christgai S, Reetz A, Solimena M, Cascalho M, Folli F, Richter-Olesen H, Camilli P-D (1990) Identification of the 64K autoantigen in insulin-dependent diabetes as the GABA-synthesizing enzyme glutamic acid decarboxylase.

Ben-Ari Y, Cherubini E, Corradetti R, Gaiarsa J (1989) Giant synaptic potentials in immature rat CA3 hippocampal neurones. The Journal of physiology 416:303-325.

Ben-Ari Y, Gaiarsa J-L, Tyzio R, Khazipov R (2007) GABA: a pioneer transmitter that excites immature neurons and generates primitive oscillations. Physiological reviews 87:1215-1284.

Boldizsár HK, Wekerle L, Vén E, Sarlós P, Barna J (1992) Neurotransmitter Amino Acids as Modulators of Biological Processes of Spermatozoa. In: GABA Outside the CNS (Erdö, S., ed), pp 199-211: Springer Berlin Heidelberg.

Bormann J (2000) The 'ABC'of GABA receptors. Trends in Pharmacological Sciences 21:16-19.

Bosma PT, Blázquez M, Collins MA, Bishop J, Drouin G, Priede IG, Docherty K, Trudeau VL (1999) Multiplicity of glutamic acid decarboxylases (GAD) in vertebrates: molecular phylogeny and evidence for a new GAD paralog. Molecular biology and evolution 16:397-404.

Bromfield EB, Cavazos JE, Sirven JI (2006) Basic mechanisms underlying seizures and epilepsy.

Brooks-Kayal AR, Raol YH, Russek SJ (2009) Alteration of epileptogenesis genes. Neurotherapeutics 6:312-318.

Bu D-F, Erlander MG, Hitz BC, Tillakaratne N, Kaufman DL, Wagner-McPherson CB, Evans GA, Tobin AJ (1992) Two human glutamate decarboxylases, 65-kDa GAD and 67-kDa GAD, are each encoded by a single gene. Proceedings of the National Academy of Sciences 89:2115-2119.

Castro E, Oset-Gasque MJ, González MP (1989) GABAA and GABAB receptors are functionally active in the regulation of catecholamine secretion by bovine chromaffin cells. Journal of neuroscience research 23:290-296.

Cherubini E, Gaiarsa JL, Ben-Ari Y (1991) GABA: an excitatory transmitter in early postnatal life. Trends in neurosciences 14:515-519.

Cherubini E, Rovira C, Gaiarsa J, Corradetti R, Ari YB (1990) GABA mediated excitation in immature rat CA3 hippocampal neurons. International Journal of Developmental Neuroscience 8:481-490.

Condie BG, Bain G, Gottlieb DI, Capecchi MR (1997) Cleft palate in mice with a targeted mutation in the γ-aminobutyric acid-producing enzyme glutamic acid decarboxylase 67. Proceedings of the National Academy of Sciences 94:11451-11455.

Culiat CT, Stubbs L, Nicholls RD, Montgomery CS, Russell LB, Johnson DK, Rinchik EM (1993) Concordance between isolated cleft palate in mice and alterations within a region including the gene encoding the beta 3 subunit of the type A gamma-aminobutyric acid receptor. Proceedings of the National Academy of Sciences 90:5105-5109.

Delgado L, Schmachtenberg O (2008) Immunohistochemical localization of GABA, GAD65, and the receptor subunits GABAAα1 and GABAB1 in the zebrafish cerebellum. The Cerebellum 7:444-450.

Ding R, Tsunekawa N, Obata K (2004) Cleft palate by picrotoxin or 3-MP and palatal shelf elevation in GABA-deficient mice. Neurotoxicology and teratology 26:587-592.

Dzhala VI, Staley KJ (2003) Excitatory actions of endogenously released GABA contribute to initiation of ictal epileptiform activity in the developing hippocampus. The Journal of neuroscience 23:1840-1846.

Dzhala VI, Talos DM, Sdrulla DA, Brumback AC, Mathews GC, Benke TA, Delpire E, Jensen FE, Staley KJ (2005) NKCC1 transporter facilitates seizures in the developing brain. Nature medicine 11:1205-1213.

Erdö S, Kiss B (1986) Presence of GABA, glutamate decarboxylase, and GABA transaminase in peripheral tissues: a collection of quantitative data: Raven Press, New York.

Erdö SL, Joo F, Wolff JR (1989) Immunohistochemical localization of glutamate decarboxylase in the rat oviduct and ovary: further evidence for non-neural GABA systems. Cell Tissue Res 255:431-434.

Erlander MG, Tillakaratne NJ, Feldblum S, Patel N, Tobin AJ (1991) Two genes encode distinct glutamate decarboxylases. Neuron 7:91-100.

Fatemi SH, Halt AR, Stary JM, Kanodia R, Schulz SC, Realmuto GR (2002) Glutamic acid decarboxylase 65 and 67 kDa proteins are reduced in autistic parietal and cerebellar cortices. Biological psychiatry 52:805-810.

Feigenspan A, Wassle H, Bormann J (1993) Pharmacology of GABA receptor CI-channels in rat retinal bipolar cells. Nature 361:159-162.

Gilon P, Campistron G, Geffard M, Remacle C (1988) Immunocytochemical localisation of GABA in endocrine cells of the rat entero-pancreatic system. Biology of the Cell 62:265-273.

Guidotti A, Auta J, Davis JM, Dong E, Grayson DR, Veldic M, Zhang X, Costa E (2005) GABAergic dysfunction in schizophrenia: new treatment strategies on the horizon. Psychopharmacology 180:191-205.

Guidotti A, Auta J, Davis JM, Gerevini VD, Dwivedi Y, Grayson DR, Impagnatiello F, Pandey G, Pesold C, Sharma R (2000) Decrease in reelin and glutamic acid decarboxylase67 (GAD67) expression in schizophrenia and bipolar disorder: a postmortem brain study. Archives of general psychiatry 57:1061-1069.

Haas HL, Schaerer B, Vosmansky M (1979) A simple perfusion chamber for the study of nervous tissue slices in vitro. Journal of neuroscience methods 1:323-325.

Hagiwara N, Katarova Z, Siracusa LD, Brilliant MH (2003) Nonneuronal expression of the $GABA_A$ β3 subunit gene is required for normal palate development in mice. Developmental biology 254:93-101.

Harrison P, Weinberger D (2004) Schizophrenia genes, gene expression, and neuropathology: on the matter of their convergence. Molecular psychiatry 10:40-68.

Hassel B, Johannessen CU, Sonnewald U, Fonnum F (1998) Quantification of the GABA shunt and the importance of the GABA shunt versus the 2‐oxoglutarate dehydrogenase pathway in GABAergic neurons. Journal of neurochemistry 71:1511-1518.

Holmes GL, Khazipov R, Ben-Ari Y (2002) New concepts in neonatal seizures. Neuroreport 13:A3-A8.

Homanics GE, DeLorey TM, Firestone LL, Quinlan JJ, Handforth A, Harrison NL, Krasowski MD, Rick CE, Korpi ER, Mäkelä R (1997) Mice devoid of γ-aminobutyrate type A receptor β3 subunit have epilepsy, cleft palate, and hypersensitive behavior. Proceedings of the National Academy of Sciences 94:4143-4148.

Hortopan GA, Dinday MT, Baraban SC (2010) Spontaneous seizures and altered gene expression in GABA signaling pathways in a mind bomb mutant zebrafish. The Journal of Neuroscience 30:13718-13728.

Hossein Fatemi S, Stary JM, Earle JA, Araghi-Niknam M, Eagan E (2005) GABAergic dysfunction in schizophrenia and mood disorders as reflected by decreased levels of glutamic acid decarboxylase 65 and 67 kDa and Reelin proteins in cerebellum. Schizophrenia research 72:109-122.

Johnston GAR (1996) $GABA_C$ receptors: relatively simple transmitter-gated ion channels? Trends in pharmacological sciences 17:319-323.

Jurand A, Martin LVH (1994) Cleft palate and open eyelids inducing activity of lorazepam and the effect of flumazenil, the benzodiazepine antagonist. Pharmacology & toxicology 74:228-235.

Kash SF, Johnson RS, Tecott LH, Noebels JL, Mayfield RD, Hanahan D, Baekkeskov S (1997) Epilepsy in mice deficient in the 65-kDa isoform of glutamic acid decarboxylase. Proceedings of the National Academy of Sciences 94:14060-14065.

Kataoka Y, Gutman Y, Guidotti A, Panula P, Wroblewski J, Cosenza-Murphy D, Wu JY, Costa E (1984) Intrinsic GABAergic system of adrenal chromaffin cells. Proceedings of the National Academy of Sciences 81:3218-3222.

Katarova Z, Sekerková G, Prodan S, Mugnaini E, Szabó G (2000) Domain‐restricted expression of two glutamic acid decarboxylase genes in midgestation mouse embryos. Journal of Comparative Neurology 424:607-627.

Khalilov I, Holmes GL, Ben-Ari Y (2003) In vitro formation of a secondary epileptogenic mirror focus by interhippocampal propagation of seizures. Nature neuroscience 6:1079-1085.

Khazipov R, Khalilov I, Tyzio R, Morozova E, Ben‐Ari Y, Holmes GL (2004) Developmental changes in GABAergic actions and seizure susceptibility in the rat hippocampus. European Journal of Neuroscience 19:590-600.

Khazipov R, Valeeva G, Khalilov I (2014) Depolarizing GABA and Developmental Epilepsies. CNS neuroscience & therapeutics.

Kim Y-J, Nam R-H, Yoo YM, Lee C-J (2004) Identification and functional evidence of GABAergic neurons in parts of the brain of adult zebrafish (*Danio rerio*). Neuroscience letters 355:29-32.

László Á, Nádasy GL, Monos E, Zsolnai B, Erdö SL (1992) The GABAergic System in Human Female Genital Organs. In: GABA Outside the CNS (Erdö, S., ed), pp 183-197: Springer Berlin Heidelberg.

Lauder JM (1993) Neurotransmitters as growth regulatory signals: role of receptors and second messengers. Trends in neurosciences 16:233-240.

Leslie Iversen SI, Floyd E. Bloom, and Robert H. Roth (2008) Introduction to Neuropsychopharmacology: Oxford University Press.

Lewis DA, Hashimoto T, Volk DW (2005) Cortical inhibitory neurons and schizophrenia. Nature Reviews Neuroscience 6:312-324.

Lukasiewicz P (1996) GABAC receptors in the vertebrate retina. Mol Neurobiol 12:181-194.

Lundorf M, Buttenschøn HN, Foldager L, Blackwood D, Muir W, Murray V, Pelosi A, Kruse T, Ewald H, Mors O (2005) Mutational screening and association study of glutamate decarboxylase 1 as a candidate susceptibility gene for bipolar affective disorder and schizophrenia. American Journal of Medical Genetics Part B: Neuropsychiatric Genetics 135:94-101.

Macdonald RL, Olsen RW (1994) GABAA receptor channels. Annual review of neuroscience 17:569-602.

MacVicar B, Hochman D (1991) Imaging of synaptically evoked intrinsic optical signals in hippocampal slices. The Journal of neuroscience 11:1458-1469.

Maddox DM, Condie BG (2001) Dynamic expression of a glutamate decarboxylase gene in multiple non-neural tissues during mouse development. BMC developmental biology 1:1.

Madtes Jr P, Redburn DA (1983) GABA as a trophic factor during development. Life sciences 33:979-984.

Martin DL, Rimvall K (1993) Regulation of γ - aminobutyric acid synthesis in the brain. Journal of neurochemistry 60:395-407.

Martin SC, Heinrich G, Sandell JH (1998) Sequence and expression of glutamic acid decarboxylase isoforms in the developing zebrafish. The Journal of comparative neurology 396:253-266.

McKernan RM, Whiting PJ (1996) Which $GABA_A$-receptor subtypes really occur in the brain? Trends in neurosciences 19:139-143.

Miller RP, Becker BA (1975) Teratogenicity of oral diazepam and diphenylhydantoin in mice. Toxicology and applied pharmacology 32:53-61.

Misgeld U, Deisz R, Dodt H, Lux H (1986) The role of chloride transport in postsynaptic inhibition of hippocampal neurons. Science 232:1413-1415.

Mott D, Lewis DV (1994) The Pharmacology and Function of Central GABA~ B Receptors. International review of neurobiology 97-97.

Mueller AL, Taube JS, Schwartzkroin PA (1984) Development of hyperpolarizing inhibitory postsynaptic potentials and hyperpolarizing response to gamma-aminobutyric acid in rabbit hippocampus studied in vitro. The Journal of neuroscience 4:860-867.

Organization WH (2002) The World health report: 2002: Reducing the risks, promoting healthy life.

Ouyang X, Shestopalov IA, Sinha S, Zheng G, Pitt CLW, Li W-H, Olson AJ, Chen JK (2009) Versatile Synthesis and Rational Design of Caged Morpholinos. Journal of the American Chemical Society 131:13255-13269.

Owens DF, Boyce LH, Davis MB, Kriegstein AR (1996) Excitatory GABA responses in embryonic and neonatal cortical slices demonstrated by gramicidin perforated-patch recordings and calcium imaging. The Journal of neuroscience 16:6414-6423.

Párducz A, Dobo E, Wolff J, Petrusz P, Erdö S (1992) GABA-immunoreactive structures in rat kidney. Journal of Histochemistry & Cytochemistry 40:675-680.

Purves D (2012) Neuroscience: Sinauer Associates.

Rapoport JL, Addington AM, Frangou S, Psych M (2005) The neurodevelopmental model of schizophrenia: update 2005. Molecular psychiatry 10:434-449.

Ritta MN, Campos MB, Calandra RS (1987) Effect of GABA and benzodiazepines on testicular androgen production. Life sciences 40:791-798.

Rivera C, Voipio J, Payne JA, Ruusuvuori E, Lahtinen H, Lamsa K, Pirvola U, Saarma M, Kaila K (1999) The K+/Cl− co-transporter KCC2 renders GABA hyperpolarizing during neuronal maturation. Nature 397:251-255.

Theodore WH, Spencer SS, Wiebe S, Langfitt JT, Ali A, Shafer PO, Berg AT, Vickrey BG (2006) Epilepsy in North America: a report prepared under the auspices of the global campaign against epilepsy, the International Bureau for Epilepsy, the International League Against Epilepsy, and the World Health Organization. Epilepsia 47:1700-1722.

Tillakaratne NJ, Erlander MG, Collard MW, Greif KF, Tobin AJ (1992) Glutamate decarboxylases in nonneural cells of rat testis and oviduct: differential expression of GAD65 and GAD67. Journal of neurochemistry 58:618-627.

Tillakaratne NJ, Medina-Kauwe L, Gibson KM (1995) Gamma-aminobutyric acid (GABA) metabolism in mammalian neural and nonneural tissues. Comparative Biochemistry and Physiology Part A: Physiology 112:247-263.

Tyzio R, Cossart R, Khalilov I, Minlebaev M, Hübner CA, Represa A, Ben-Ari Y, Khazipov R (2006) Maternal oxytocin triggers a transient inhibitory switch in GABA signaling in the fetal brain during delivery. Science 314:1788-1792.

Tyzio R, Holmes GL, Ben‐Ari Y, Khazipov R (2007) Timing of the developmental switch in GABAA mediated signaling from excitation to inhibition in CA3 rat hippocampus using gramicidin perforated patch and extracellular recordings. Epilepsia 48:96-105.

Varju P, Katarova Z, Madarász E, Szabó G (2001) GABA signalling during development: new data and old questions. Cell Tissue Res 305:239-246.

Walther H, Lambert J, Jones R, Heinemann U, Hamon B (1986) Epileptiform activity in combined slices of the hippocampus, subiculum and entorhinal cortex during perfusion with low magnesium medium. Neuroscience letters 69:156-161.

Wee EL, Zimmerman EF (1983) Involvement of GABA in palate morphogenesis and its relation to diazepam teratogenesis in two mouse strains. Teratology 28:15-22.

Wolff J (1982) Morphological changes induced by sodium bromide in murine neuroblastoma cells in vitro. Cell Tissue Res 222:379-388.

Wolff JR, Joó F, Dames W (1978) Plasticity in dendrites shown by continuous GABA administration in superior cervical ganglion of adult rat.

Woo T-UW, Walsh JP, Benes FM (2004) Density of Glutamic Acid Decarboxylase 67 Messenger RNA–ContainingNeurons That Express the N-Methyl-D-AspartateReceptor Subunit NR2A in the Anterior Cingulate Cortex in Schizophreniaand Bipolar Disorder. Archives of general psychiatry 61:649-657.

Yamada J, Okabe A, Toyoda H, Kilb W, Luhmann HJ, Fukuda A (2004) Cl− uptake promoting depolarizing GABA actions in immature rat neocortical neurones is mediated by NKCC1. The Journal of physiology 557:829-841.

Yamazoe S, Shestopalov IA, Provost E, Leach SD, Chen JK (2012) Cyclic caged morpholinos: conformationally gated probes of embryonic gene function. Angewandte Chemie, International Edition 51:6908-6911.

Yang W, Reyes AA, Lan NC (1994) Identification of the $GABA_A$ receptor subtype mRNA in human pancreatic tissue. FEBS letters 346:257-262.

Young SZ, Bordey A (2009) GABA's control of stem and cancer cell proliferation in adult neural and peripheral niches. Physiology 24:171-185.

Zhang L, Spigelman I, Carlen P (1990) Whole-cell patch study of GABAergic inhibition in CA1 neurons of immature rat hippocampal slices. Developmental Brain Research 56:127-130.

Zhu Y, Pavlos CM, Toscano JP, Dore TM (2006) 8-Bromo-7-hydroxyquinoline as a photoremovable protecting group for physiological use: mechanism and scope. Journal of the American Chemical Society 128:4267-4276.

# CHAPTER 2

# RECORDING FIELD POTENTIALS IN ISOLATED WHOLE BRAIN FROM ADULT ZEBRAFISH [1]

[1] Beebe, L.L., Page, A.T., Clark, J.K., Ball, R.E. and J.D. Lauderdale. To be submitted to *Journal of Neuroscience Methods*.

Abstract

Understanding the detailed organization of a neuronal network is required for elucidating the complex responses of brain function. Yet, to fully understand the functional circuitry, it is necessary to manipulate the activity of neural networks. In mammals and large vertebrates, selective perturbations of neural activity are often difficult to carry out due to their size and complexity of the nervous system. The zebrafish central nervous system exhibits all of the fundamental aspects characterizing the nervous system of larger, more complex vertebrates, but in a much simpler structure. Due to their small size and relatively simple neurological architecture, zebrafish have developed as a model system for behavior, addiction, and seizure research. *Ex* vivo procedures are already established for rodents, but similar approaches are necessary to study how drugs and/or mutations influence synaptic excitability and neuroplasticity within the fish. In this paper, we describe an *ex vivo* method to remove an adult zebrafish brain and carry out extracellular recordings on both whole brain and acute slice preparations. The procedure allows for the intact neural network to maintain function, as shown by the presence of spontaneous neurological activity. This method also permits optical imaging to determine the cellular and functional mechanisms contributing to neural plasticity. Based upon these findings, it was determined that electrophysiological changes in the native spontaneous activity of the optic tectum could be elicited following the introduction of different pharmacological compounds. Ultimately, this method could help determine the functionality of the different circuits involved in the neuroadaptations caused by diseases, such as epilepsy or drug dependence.

## Introduction

Understanding the detailed organization of the neurological network is key for elucidating the computational responses of brain function (Callaway and Katz, 1993), yet the ability to manipulate the activity of neural networks is required to understand such functional circuitry (Friedrich et al., 2010, Warther et al., 2010). Selective perturbations of neural activity are often difficult in mammals due to their size and complexity of the nervous system; therefore utilizing a small model organism with fewer neurons is advantageous (Friedrich et al., 2006, Friedrich et al., 2010). Studies in mammals have shown that learning and memory are controlled by several distinct brain circuits (Baxendale et al., 2012), yet the rodent models used for elucidating the mechanisms of such behaviors involve high costs and labor-intensive work. Zebrafish lend themselves as good systems for these types of manipulations due to their small size and relatively simple neurological structure (McLean and Fetcho, 2004). The adult zebrafish has also been found to display a full repertoire of these mature behaviors and it is the ease of being able to apply drugs and having robust behavioral assays that have solidified the zebrafish as a good model to study to the circuits involved in learning, memory, anxiety and other related behaviors (Norton and Bally-Cuif, 2010). As a result of this work, studies of the adult zebrafish are now helping to uncover the genetic pathways and neural circuits that control these complex behaviors (Bally-Cuif and Vernier, 2010, Norton and Bally-Cuif, 2010).

While studies in rodents have revealed only a few hints at the neurobiology of drug-induced neuroadaptations, zebrafish have proven themselves as a useful animal model for the study of genetic and complex neurobiological phenotypes involved in drug

abuse (Yuferov et al., 2005, Krasnova et al., 2008, Cadet, 2009, Norton and Bally-Cuif, 2010, Klee et al., 2012). Several studies have reported alterations in cellular structure following the administration of amphetamine, suggesting that structural adaptations of the brain circuitry are a characteristic of addictive processes (Robinson and Kolb, 2004, Cadet, 2009). Through the use of mutagenesis screens and selective pharmacological manipulations, it has been possible to identify some of the molecular substrates involved in drug addiction. This work suggested that dopamine, serotonin, GABA, and the noradrenergic systems could all be involved in the addiction response cascade (Norton and Bally-Cuif, 2010, Klee et al., 2012).

Alterations in these neurotransmitter systems have also been associated with the pathogenesis and mechanisms involved in seizure development. To study the etiology of seizure development, *in vivo* and *in vitro* methods have been utilized. In rodents, seizure activity is commonly induced by exposure to chemiconvulsants via kindling (Sloviter, 2008), trauma due to cranial insult (Buckmaster and Jongen-Relo, 1999, Sutula et al., 2003), among other induction techniques (Galanopoulou, 2013). Similar models and induction paradigms have also been used in other vertebrates, including turtles (Volanschi and Servit, 1969), frogs (Servit and Strejckova, 1970b, Hewapathirane et al., 2008), and fish (Strejckova, 1969, Servit and Strejckova, 1970a, Baraban et al., 2005). Zebrafish are now emerging as a model for epilepsy because of its stereotypic behaviors and response to seizure-inducing drugs. Seizure-like behaviors in the zebrafish have been characterized by tracking swimming patterns and examining alterations in brain electrophysiology (Baraban et al., 2005, Baraban et al., 2007, Mei et al., 2013), and this activity has been observed in both larval and adult fish (Baraban et al., 2005, Baraban et

al., 2007, Pineda et al., 2011, Ball et al., In preparation). Unlike other animal models, one key advantage of the zebrafish stems from the transparency of its embryo, which facilitates three-dimensional analysis of gene expression patterns. Due to these aspects, the zebrafish is emerging as an excellent model vertebrate for *in vivo* analysis of complex behaviors, as well as for decoding the mechanisms involved in the neuroadaptations caused by diseases, such as epilepsy or drug dependence. Yet, this also creates a need for an *ex vivo* approach in order to fully study how drugs or neurological alterations influence excitability and changes in neuroplasticity.

***What is the problem?***

Adult zebrafish have a bony skull that develops following the larval stage; therefore detailed studies of the adult brain require the development of similar tools and techniques necessary for studying the mammalian brain. We have previously described a procedure to study neurological changes with an *in vivo* approach for adult zebrafish (Johnston et al., 2013), but the small craniotomy and remaining skull hinder the ability to study the region where electrophysiological recordings were obtained. This problem can be overcome by the application of a bare-brain (Tomizawa et al., 2001) or *ex vivo* preparation (Vargas et al., 2011b). An *ex vivo* approach would not only remove the requirement of keeping an animal alive, but it would allow for optical imaging of the region of interest, allowing one to elucidate the cellular and functional mechanisms contributing to functional and structural plasticity.

***Why perfused whole brain instead of slice?***

Although brain slice culture is a standard technique used for the study of cellular components of the mammalian brain (Haas et al., 1979, Walther et al., 1986, MacVicar

and Hochman, 1991, Owens et al., 1996), the preparation of these slices necessarily disrupts the overall neural network, thereby limiting the use of these preparations to the study of local circuitry. Whole brain preparations have already been utilized (Mühlethaler et al., 1993, De Curtis et al., 1994, Pakhotin and Pakhotina, 1994, Federico and MacVicar, 1996, de Curtis et al., 1998, Vargas et al., 2011a, Vargas et al., 2011b), but these methodologies tend to require complex and expensive equipment. While this is a necessary limitation because of the demands of keeping tissue alive during an experiment, the small size of the adult zebrafish brain suggests that is ideally suited to the development of a whole-brain preparation, which could be used in conjunction with slice recordings. Previously, Tomizawa et al., reported that isolated adult zebrafish brains could be cultured *ex vivo* over the period of a week (2001). It was also determined that *ex vivo* slice and whole brain preparations of the telencephalon could elicit post-synaptic responses when they were electrically stimulated (Nam et al., 2004, Ng et al., 2012).

Here, we show that an isolated adult zebrafish brain can exhibit spontaneous neurological activity while maintained in artificial cerebrospinal fluid (ACSF) and that it can be used to record electrophysiological alterations in this activity when exposed to different pharmacological agents. We also show that field excitatory post-synaptic potentials can be generated within the optic tectum when the optic nerve is stimulated over a wide range of stimulus inputs. Not surprisingly, fEPSP responses were found to be comparable between mouse and zebrafish preparations, suggesting that the zebrafish brain could serve as a useful model to study long distance circuitry within the brain.

## Materials and Methods

### *Animals and maintenance*

Adult zebrafish (*Danio rerio*) of WIK strain, obtained from the Zebrafish International Research Center (ZIRC), were maintained in an Aquatic Habitats (Apopka, FL) multi-rack system according to standard procedures (Westerfield, 2000). Habitat water consisted of reverse osmosis filtered/sterilized water to which sodium bicarbonate and other salts (Instant Ocean, Aquarium Systems, Inc., Mentor, OH, USA) were added to maintain pH from 7.0 -7.4 and conductivity between 400 and 430 μS. All experimental procedures were conducted in accordance with National Institutes of Health guidelines for use of zebrafish in research under protocols approved by the University of Georgia Institutional Animal Care and Use Committee.

### *Preparation of whole brains and slices for extracellular field recordings*

Zebrafish brains were removed from healthy animals of both sexes and of ages 7 to 24 months old. Fish were anesthetized in ice-cold water before decapitation. The brain was removed in ice-cold, oxygenated (95% O2/5% CO2) dissection artificial cerebrospinal fluid (ACSF) in a 60x15 mm Corning Not-TC treated petri dish (Corning Inc., Tewksbury, MA). Detailed dissection methods are described in the Supplemental Methods section. Briefly, for whole brain preparations, the intact zebrafish brain was transferred from the dissection dish to new petri dish and mounted, dorsal side up, in a droplet of 1.2% agarose (Thermo Fisher Scientific, Waltham, MA). Enough zebrafish ACSF was added so that the final volume, after chemical addition, would be 3 mL. For

slice preparations exposed to drugs, the brain was hemisected along the coronal plane and a brain half was placed distal (uncut) side down in bath of oxygenated ACSF.

For fEPSP slice preparations, the brain was hemisected along the sagittal plane and each brain half was placed medial (cut) side down in a submersion recording chamber and perfused at approximately 1 mL/min with oxygenated (95% O2/5% CO2) standard ACSF. Brains were allowed to recover for 90 minutes at room temperature (25°C) before experiments began.

***Preparation of fish for in vivo field recordings***

Adult fish were immobilized and prepped for craniotomy following the protocol established in Johnston et al. (2013). Briefly, adult zebrafish were immobilized by bath application of 630 µM tricaine methanesulfonate. Once movement had ceased, 1µg/g fish weight of pancuronium bromide was injected intraperitoneally. The fish was intubated and a craniotomy was carried out in the region of skull covering the optic tectum (TeO). This setup was moved to the electrophysiology microscope and the primary electrode was placed within the craniotomy opening while the reference electrode was placed in the contralateral nostril of the fish. Fish were perfused with system water at a rate of 1 mL/min for at least 45 minutes to wash out the tricaine. After this period, perfusion with 15 mM PTZ began and recording continued until consistent seizure-like activity had developed.

***Drugs***

All drugs used for this study were purchased from Sigma-Aldrich (St. Louis, MO). A solution of zebrafish ACSF was obtained following the procedure as previously

described (Edwards and Michel, 2003). ACSF was composed of 131mM NaCl, 20 mM $NaHCO_3$, 2 mM KCl, 1.25 mM $KH_2PO_4$, 2 mM $MgSO_4$, 10 mM glucose and 2.5 mM $CaCl_2$. The solution was chilled and equilibrated with 95% $O_2$/5% $CO_2$ for at least 1 hour, and a pH of 7.4 was established through the addition of NaOH. The ACSF was sterile filtered and stored at 4$^{o}$C until it was used. Before each use, a 10-15 mL sample was removed and bubbled with 95% $O_2$/5% $CO_2$ for at least 1 hour in an ice bath. For stimulated slice preparations, standard ACSF was composed of 120 mM NaCl, 3 mM KCl, 1.5 mM $MgCl_2$, 1 mM $NaH_2PO_4$, 2.5 mM $CaCl_2$, 26 mM $NaHCO_3$, and 10 mM glucose. Samples were bubbled with 95% $O_2$/5% $CO_2$ throughout the experiment.

Stock pentylenetetrazol (PTZ) of 300 mM was made in distilled water and stored in aliquots at -20°C. A working concentration of 15 mM PTZ in ACSF was used for all experiments. The concentration of adenosine triphosphate (ATP) used was 100 μM for each experiment. The concentration of CNQX used for stimulated slice experiments was 5μM (Tocris Bioscience, Minneapolis, MN). All neuromodulators were dissolved in phosphate buffered saline.

***Labeling and Immunohistochemistry***

For immunolabelling, adult brains were dissected and removed from the skull as described for *ex vivo* whole brain preparations. Brains were immersion fixed in 4% PFA/PBS at room temperature (24$^{o}$C) for 1 hour in Fisher 1.5 mL microcentrifuge tubes (Thermo Fisher Scientific, Inc., Waltham, MA ). Fixed samples were cryosectioned using a Leica CM1850 (Leica Microsystems, Buffalo Grove, IL) at 16–20 μm. Sections were collected on gelatin-coated slides and air dried for 1 hour. Slides were then washed with 37$^{o}$C phosphate buffered saline (PBS), pH 7.4, until all gelatin had dissolved.

Hematoxylin/eosin staining was performed according to standard procedures (Fischer et al., 2008). For tyrosine hydroxylase and serotonin staining, the protocol established by Kaslin et al. was followed, with modifications (Kaslin and Panula, 2001). Slides were blocked with a solution containing 0.3% Tween (PBS-Tw, pH 7.4), 2% dimethyl sulfoxide and 2% normal goat serum (NGS) in PBS for 45 minutes. The slides were then incubated with a primary antisera and blocking solution for 1 hour at room temperature. After incubation with primary antibody, slides were washed with PBS and incubated with Alexa-conjugated (488, 594) donkey anti-rabbit, goat anti-rabbit, or goat anti-mouse immunoglobulin G secondary antibody (Molecular Probes, Eugene, OR). Secondary antibodies were diluted 1/1000 in PBS-Tw and 2% normal goat serum and incubated for 30 minutes at room temperature.

For GABA and GAD staining, slides were first blocked in a solution containing 3% bovine serum albumin (BSA) in PBS for at least 1 hour. For GABA staining, slides were then incubated with the 1:1500 dilution of primary antisera (Sigma-Aldrich, St. Louis, MO) in blocking solution for 1 hour at room temperature. For GAD65/67 stains, slides were incubated with a 1:50 dilution of primary antisera (AnaSpec, Fremont, CA) in blocking solution overnight at $4^{o}$C. After incubation with primary antibody, slides were washed with PBS and incubated with Alexa-conjugated (488, 594) donkey anti-rabbit immunoglobulin G secondary antibody (Molecular Probes, Eugene, OR) diluted 1/1000 in the 3% BSA in PBS blocking solution and incubated for 30 minutes at room temperature.

All sample preparations were imaged using either a Zeiss Imager .D2 or a Zeiss LSM 510 Metal Confocal microscope, connected to a computer running Leica FireCam image capture software (Leica Microsystems, Buffalo Grove, IL).

## Experimental

### *Extracellular field recording set up*

For whole brain and slice preparations, a sharp glass pipet microelectrode (15 - 20 MΩ impedance), loaded with 2-3 µL of 2 M potassium chloride, was inserted into the optic tectum (TeO). The optic tectum was chosen to facilitate comparison with previously published data obtained from larval zebrafish (Baraban et al., 2005). Additionally, the simple, layered cytoarchitecture of the teleostean optic tectum appeared to be well suited for field recordings. Electrical activity was monitored with a field electrode placed under visual guidance in the posterior, left optic tectum. Stereotypical placement of the electrode is shown in Fig. 2.1A. Insertion ventrally beyond this area of the tectum greatly reduced the amplitude of electrical activity. A chloride-coated silver wire (0.010" A-M Systems, Inc. Sequim, WA) reference electrode was placed touching the medulla or remaining spinal cord.

In experiments assessing the effects of neuromodulators, baseline activity was recorded for 5 minutes followed by introduction of 15 mM PTZ or 100 µm ATP to the ACSF bath. Activity was recorded for a period of 1-2 hours after exposure began. In the experiments accessing the effect of neurotransmitters, two application methods were used. The first utilized administration of the compounds directly into the ACSF bath. The volume of compound was added such that the final working concentrations were

established within the bathing environment. In the second method, a second sharp glass pipet loaded with the desired neuromodulator was inserted into the optic tectum with the tip being positioned in close proximity (10-50 μm) to the tip of the primary electrode. This compound was then microinjected into the optic tectum and changes in neural activity were recorded. Collected recordings were found to be similar between each method. Field recordings were collected using Molecular Devices' Axoclamp software and data were digitized at 10 kHz, low-pass filtered at 1 kHz, and analyzed with pCLAMP 10.2 software (Axon Instruments, Sunnyvale, CA).

For experiments assessing fEPSPs, a bipolar stimulating electrode (Kopf Instruments, Tujunga, CA) was placed on the superficial surface of the optic nerve just before it enters the TeO, and an extracellular recording microelectrode (1.0 MΩ tungsten, World Precision Instruments, Sarasota, FL) was positioned in the most superficial layer of the medial lateral TeO. Field excitatory post-synaptic potentials (fEPSPs) were evoked using a single square wave stimulus pulse of 270 μs duration. Data were digitized at 10 kHz, low-pass filtered at 1 kHz, and analyzed with pCLAMP 10.2 software (Axon Instruments, Sunnyvale, CA). The initial slope of the population fEPSP was measured by fitting a straight line to a 1 ms window immediately following the fiber volley. Stimulus response curves were obtained at the beginning of each experiment with stimulus pulses at 40, 50, 60, 70, 90, 110, 130, 150, 170, and 190 μA delivered once every 60 s (0.0167 Hz). To begin baseline recording, the stimulation intensity was adjusted to obtain a fEPSP of approximately 35-40% of the linear range between the minimum and maximum response. For evaluation of glutamatergic synaptic activity, the AMPA glutamate receptor antagonist CNQX (5 μM, Tocris Bioscience, Minneapolis,

MN) was bath applied for 20 minutes and subsequently washed out for the remainder of the experiment. Baseline synaptic responses were normalized by dividing all fEPSP slope values by the average of the five responses recorded during the 5 minutes immediately prior to CNQX application.

## Results

### *Characterization of recording field*

Field potentials reflect the sum of extracellular currents generated by current sources relatively close to the recording electrode. If the electrode is placed very close to a neuron, these extracellular currents provide information about this cell and its immediate neighbors. However, large extracellular current flows can also be generated in neuropil formed by neurons with parallel dendrites. Under such conditions juxtadendritic action potentials can be recorded several hundred microns from the soma (Buzsaki et al., 1996). Figure 2.1A shows the setup used to collect extracellular field potentials using the *ex vivo* preparation described here.

To better understand the source of the extracellular currents that could contribute to the discharge patterns observed when recording from the optic tectum, DiI was focally applied using the same experimental set up as for the field recording. Instead of recording a field potential, DiI was loaded into the pipet and applied using gravity (Fig. 2.1B). Cryosections through the labeled regions revealed that the electrode tip was typically located 112 ± 24 μm (n = 4) from the dorsal surface of the tectum (Fig. 2.1C). In all cases, DiI fluorescence was observed spanning the stratum opticum (SO) and stratum griseum centrale (SGC) along the dorsal-ventral axis of the tectum and typically extended ~100 μm radially from the tip of the electrode (Fig. 2.1C). These results suggest that:

(1) the bulk of the field potentials recorded were generated by neurons with processes in the SGC, and (2) the electrode may be detecting action potentials up to a 100 μm or more from the soma of the active neuron.

Immunolabeling of these sections revealed a high-density of very diverse sets of neurons. Figure 2.2A shows the region of the optic tectum (TeO) that was visualized in each of the immunofluorescent labeled sections. Immunoreactive fibers for glutamic acid decarboxylase isoforms 65 and 67 (GAD65/67), GABA, serotonin (5-HT), and tyrosine hydroxylase were observed spanning the optic tectum (Fig. 2.2). These results suggest that inhibition via GABAergic signaling or administration of neurotransmitters such as 5-HT, glutamate, dopamine or ATP should lead to changes in the patterns of electrical discharge within each of these neuron types.

GABAergic neurons were observed in both the superficial and deep layers of the TeO. Labeled cell bodies were predominantly found in the deeper layers, similar to previous findings (Kim et al., 2004b). More specifically, GABA immunoreactivity was seen in cell bodies located within the stratum album centrale (SAC) and the stratum griseum periventriculare (SGP). A small number of GABA-positive cell bodies were also observed in the SO (Fig. 2.2B). Similar to this GABA distribution, GAD65/67 expression was observed most commonly in the SGC and SGP (Fig. 2.2C). This finding is not surprising considering that the GAD enzymes are known to synthesize GABA from glutamic acid (Bu et al., 1992, Delgado and Schmachtenberg, 2008). Both GABA and GAD65/67 positive axons could also be seen extending from the SGP through the more central layers of the TeO.

Previous work determined that serotonergic fibers were also present in both the superficial and deep layers of the adult zebrafish optic tectum, with the most prominent bands being present within the stratum fibrosum et griseum superficiale (SFGS) (Kaslin and Panula, 2001). Consistent with these findings, we observed similar serotonergic presence within the optic tectum (Fig. 2.2D). Serotonergic immunoractive fibers were distributed in several layers, but the highest density of fibers were in a medially located band at the approximate margin between the SFGS and the SGC.

High-densities of TH-immunoreactive fibers were observed primarily in the SFGS and as a band in the deeper part of the SGC. Immunoreactivity was also strongly observed in the more superficial SO and less-dense patterns were observed within the SAC (Fig. 2.2D). Our findings support those previously described by Kaslin and Panula (2001). Yet, we observed these tyrosine hydroxylase innervations to be more dispersed than what was previously described.

***ATP and PTZ induces electrical discharges in isolated brains***

To determine if recorded extracellular activity could detect action potentials up to a 100 μm or more from the soma of the active neuron, an excitatory compound was introduced into the TeO through microinjection. The representative field recording observed from an *ex* vivo preparation microinjected with100 μM ATP is shown in Figure 2.3. The *ex vivo* whole brain preparation presented a delayed response to ATP following microinjection into the optic tectum, but spontaneous activity generally developed and persisted starting about 5 minutes following the injection. At this time, spontaneous discharges developed and evolved into a stable pattern characterized by low amplitude (<0.25 mV) bursting events (Fig. 2.3B). Such discharges continued to occur until the

experiment was ended. Similarly, when ATP was microinjected into the optic tectum of an acute brain slice, low amplitude (0.25-0.5 mV) discharges developed and persisted until the experiment was ended (Fig. 2.3C). This spontaneous activity was never observed in baseline recordings for both preparations (Fig. 2.3A).

Exposure of isolated brains to 15 mM PTZ induced spontaneous epileptiform-like discharges within 3 to 5 minutes following bath application (Fig. 2.4B). These discharges were initially small (frequency, amplitude) but evolved into a stable discharge pattern characterized by high frequency, low amplitude discharges and low frequency, high amplitude (>0.5 mV) events. This spontaneous activity resembled the PTZ-induced activity seen with *in vivo* preparations. When adult zebrafish were exposed to 15 mM PTZ large amplitude discharges developed, but occurred more often than in the *ex vivo* preparations (Fig. 2.4C). This finding is consistent with that described in Ball et al. (In preparation). These events were not observed during baseline recording periods prior to PTZ exposure (Fig. 2.4A) and never occurred in control brains bathed in only ACSF for periods up to 1.5 hours (n=7; data not shown). Examination of isolated small-amplitude and large amplitude discharges revealed that they exhibited similar morphology to the discharges observed in living animals (Fig. 2.4D,E). In both *ex vivo* and *in vivo* setups, the induced changes in neural activity closely resembled the 'interictal' and 'ictal' bursts described by Baraban et al. following exposure of zebrafish larvae to 15 mM PTZ (Baraban et al., 2005, Baraban et al., 2007). Thus, our preparations seem to recapitulate those findings previously described (Baraban et al., 2005, Ball et al., In preparation). No differences were observed between recordings obtained from male or female animals.

### *Field Excitatory Post-Synaptic Potentials stimulated in the optic tectum*

To determine if zebrafish brain slices could respond to an electrical stimulus, similar to murine models, a bipolar stimulating electrode was placed on the surface of the optic nerve and subsequent synaptic activity was recorded from the ipsilateral TeO. Field excitatory post-synaptic potentials (fEPSPs) were evoked using a single square wave stimulus pulse of 270 μs duration. To evaluate the general synaptic response of ON-TeO synapses, a series of increasing input intensities stimulating the optic nerve resulted in subsequent increases in fEPSPs observed within the TeO (Fig. 2.5A).

To evaluate the glutamatergic synaptic activity within this pathway, the AMPA receptor antagonist CNQX was used to block glutamatergic synaptic transmission. After the establishment of stable fEPSP baseline activity, CNQX was bath applied to the slices for 20 minutes and then washed out for the remainder of the experiment. As shown in Figure 2.5B, application of CNQX (5 μM) resulted in a complete block of glutamatergic transmission. fEPSP slope values decreased to 0 within the first 10 minutes following antagonist application, and this decrease persisted until CNQX application was terminated (Fig. 2.5B, point 2). Following removal of the glutamate antagonist, fEPSP slope values slowly increased during the 50 min washout period, but never fully returned to baseline levels (Fig. 2.5B, point 3).

## Discussion

### *Characterization of recording field*

In the present study, we describe an *ex vivo* method to isolate the adult zebrafish whole brain and acute slices to record changes in neural activity, following exposure to different pharmacological agents. Zebrafish share extensive homology with mammals at

the genetic, neural and endocrine levels (Maximino et al., 2012), and the basic structure of the zebrafish's central nervous system contains all of the major domains found within the mammalian brain organization (Matsuda and Mishina, 2004, Bally-Cuif and Vernier, 2010, Friedrich et al., 2010). Many of the biological features and compounds present in higher vertebrates, such as major neurotransmitters, are also present within the zebrafish nervous system (Matsuda and Mishina, 2004, Bally-Cuif and Vernier, 2010).

Selective perturbations of neural activity are often difficult in mammals due to their size and complexity. The zebrafish lends itself as a good system for these types of manipulations due to its small size, with the adult brain averaging only 3 mm in length. The zebrafish brain is relatively simple in neurological structure (McLean and Fetcho, 2004), and it has been well characterized morphologically and structurally (Nevin et al., 2008, Bally-Cuif and Vernier, 2010, Neuhauss, 2010). For this work we focused on the optic tectum, simply due to its relative size, compared to the overall brain size and the fact that it is well characterized.

The optic tectum is one of the best systems for investigating multisensory processes because it plays a major role in visual and auditory inputs, such as controlling eye movement, fine motor programming and sensory-motor coupling (Meek, 1990, Kaslin and Panula, 2001, Bally-Cuif and Vernier, 2010). These functions closely mirror those of the superior colliculus in mammals, which plays a key role in eye movements (Mueller and Neuhauss, 2010). This region of the midbrain is also highly specialized for localization of objects and initiating body movements (Gahtan and Baier, 2004). Visual input from the retina is received within many of the superficial layers of the optic tectum, whereas the deeper central layers can receive input from various other sources. These

inputs seem to be processed as they move through the TeO, where motor outputs from the deeper layers of the tectum target premotor reticulospinal circuits within the hindbrain (Sato et al., 2007). Therefore, the neurotransmitter systems present are important for not only the integration, but also the modulation of multisensory input within the zebrafish.

Our immunohistochemical findings support those previously described (Kaslin and Panula, 2001, Kim et al., 2004b, McLean and Fetcho, 2004). Although function, distribution and localization of GABA and GAD have been examined in the larval zebrafish, such information has been minimally described within the adult. Kim et al. found that GABA-ir was localized to specific regions within the TeO, including the SAC and the SGP (2004a). Our findings support this work, but we also observed GABA-positive cells labeling within the more superficial SO and labeled axon tracts were seen spanning the depth of the TeO. Not surprisingly, the GAD65/67 staining patterns were similar to those described for the GABA staining. Because glutamic acid decarboxylase synthesizes GABA from glutamic acid, it is believed that the GAD enzymes should be present wherever GABA is found. In larval zebrafish, it has also been shown that the GAD enzymes and GABA tend to colocalize (Martin et al., 1998).

When the monoaminergic neurotransmitters were observed, we saw more dispersed TH-ir innervations throughout the TeO. The majority of TH staining was predominantly found in two major bands, within the SO and the SFGS. These two layers receive many of the retinal efferent neurons targeting the TeO (Kaslin and Panula, 2001, Bally-Cuif and Vernier, 2010). A weaker band was also observed in the deeper, central band within the SGC. Serotonin, on the other hand, was mainly found within the more central layers (SFGS, SGC) of the TeO. This non-uniform gradient of the aminergic

neurotransmitters suggest that information may not only be processed differently within these different regions, but also that many forms of information may be processed.

***PTZ and ATP induces electrical discharges in isolated brains***

We also showed that exposure of isolated brains or acute slices to 15 mM PTZ or 100 μM ATP could induce spontaneous epileptiform-like discharges within the first 5-10 minutes following addition. These discharges were initially small (frequency, amplitude), but gradually evolved into stable discharge patterns characterized by larger amplitude events. Similar activity has been reported within both *in vivo* preparations (Baraban et al., 2005, Baraban et al., 2007, Johnston et al., 2013, Ball et al., In preparation) and *ex vivo* whole brain and slice preparations (Vargas et al., 2011a). ). In both the *ex vivo* and *in vivo* setups, the induced changes in neural activity closely resembled the 'interictal' and 'ictal' bursts described by Barban et al., following the exposure of zebrafish larvae to 15 mM PTZ (Baraban et al., 2005, Baraban et al., 2007). Baraban's work was carried out in larval zebrafish, yet we have shown that both adult animals and *ex vivo* brain samples have the ability to show similar activity following exposure to PTZ. Even though these neurological changes were similar between setups, intact adult fish exhibited much more complex changes following PTZ exposure, when compared to the *ex vivo* preparations. This is likely due to the fact that adult fish maintain the capability to process sensory inputs within the mature TeO as recording is taking place (Sato et al., 2007, Mueller and Neuhauss, 2010). Together, these findings support the idea that an intact zebrafish brain can be removed from the body, while maintaining functionality similar to live fish.

Even though *ex vivo* whole brain and slice preparations are simple to carry out and maintain functionality when placed in ACSF, there are some negative aspects to

each. While the whole brain preparation maintains the original neural connections, we have shown that an *ex vivo* brain is unable to fully recapitulate the neural activity of a living fish (Fig. 2.4). Acute slice preparations were able to maintain functionality with this setup, but local neural circuits were necessarily disrupted when the brain was sectioned. Though, similar changes in the neurological activity of both *ex vivo* setups were established following chemical exposure, the induced changes were not as complex as those seen with the *in vivo* setups. While electrophysiological data from intact adults gives a better idea of changes in native neurological activity of zebrafish, this setup was far more complex and time consuming than the *ex vivo* approaches. Analysis of *in vivo* data was also much more complex than that of the whole brain and slice approaches because sensory inputs and other higher-order circuits must be taken into consideration when observing this data.

***fEPSPs generated through optic nerve stimulation in ex vivo slice preparations***

We were also able to show that field excitatory post-synaptic potentials could be generated within the optic tectum when the optic nerve was stimulated over a wide range of stimulus inputs, similar to what was previously shown within the zebrafish telencephalon (Nam et al., 2004, Ng et al., 2012). For these field potential experiments, a standard ACSF formulation, similar to what is commonly used in mouse studies, was used. Not surprisingly, fEPSP responses were comparable between mouse and zebrafish preparations. The average fEPSP activity generated a large primary wave response, similar to that often seen with mouse samples (Froc et al., 2003, Suwabe et al., 2008), yet this large response was followed by a smaller secondary wave (Fig. 2.5A, top inset). When CNQX was bath applied to these slice preparations, fEPSP slope values decreased

from baseline levels to 0, similar to what has been observed in mice (Liauw et al., 2003, Suwabe et al., 2008). These findings suggest that not only can zebrafish slice preparations respond to electrical stimulation, but that they can do so in a manner comparable to rodents, which are most commonly used in these types of preparations.

This setup also suggests that the zebrafish brain could serve as a useful model to study long distance circuitry within the brain. With our setup, the stimulating electrode was placed touching the optic nerve, before it enters the brain and synapses within the TeO, suggesting that responses can be recorded over long (mm) distances. With this technique, application of CNQX was also able to show that there was strong glutamatergic presence within this region of the TeO. Although no other areas were recorded from in this work, our findings support that this *ex vivo* approach may be applicable to the study of higher-order circuits involved in many of the sensory processes common to vertebrates.

The majority of neurons contributing to sensory and other higher-order circuits within the nervous system use either excitatory neurotransmitters, such as glutamate or aspartate, or inhibitory neurotransmitters, such as GABA or glycine. These systems are known to control and modify sensory, motor and integrated information to match the inner state of the animal to the interaction with the environment. Such mechanisms are the main substrate for behavioral processes such as reward, motivation and emotions, awareness, aggression, sleep, feeding and reproductive behaviors (Bally-Cuif and Vernier, 2010). Similarly, altered levels of neurotransmitters can lead to neural dysfunctions. For example, reduced levels of GABA and GAD expression in the brain have been shown to cause neurological dysfunctions such as mood disorders, seizures

and neuronal cell death (Erdo et al., 1991, Volk and Lewis, 2002, Brambilla et al., 2003, Powell et al., 2003, Kim et al., 2004b). Therefore, it is necessary to develop systems in which these neural functions can easily be studied and better understood.

## Conclusions

Following characterization of the neuronal populations present throughout the optic tectum, it could be assumed that this region could not only respond to a variety of compounds, both excitatory and inhibitory, but also to mutational changes which could alter the neuronal circuitry. Because of the non-uniform, layered architecture of the optic tectum, this midbrain structure lends itself to be a good system to the study specific neural networks involved in sensory processing. Ultimately, we have shown that an intact zebrafish brain can be removed and that the neural activity can be maintained and successfully altered through the introduction of synthetic compounds. We have also demonstrated that the observed changes in neural activity were similar between *ex vivo* and *in vivo* preparations. Not only have zebrafish become a useful model for mutational genetics, embryology and cellular biology, but they have also become important in the realm of neurobiology. Through studying the distribution and function of neural circuits within the zebrafish brain, we should be able to gain further insight into the behaviors and mechanisms involved in the neuroadaptations caused by diseases or drug addiction.

## Acknowledgements

This work was supported by NIH/NINDS Grant R01NS070159 (to T.M.D, J.D.L and A.T.S). We want to give special thanks to Drea Marlow for his hard work maintaining the zebrafish facility.

Figures

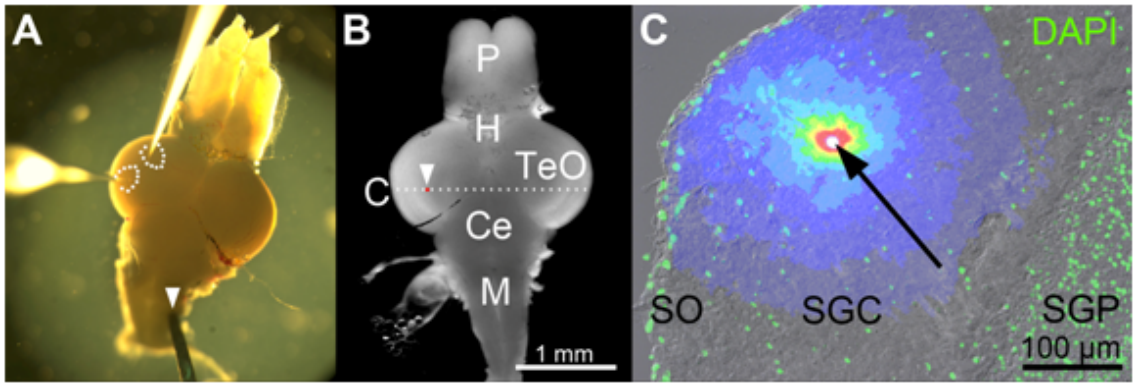


**Figure. 2.1. PTZ-induced electrographic activity in an *ex vivo* adult zebrafish preparation.** (A) Photograph of the configuration used to obtain tectal field recordings from adult zebrafish brain *ex vivo*. A glass microelectrode is placed into the optic tectum (dotted line). The reference electrode is placed touching the spinal cord (arrowhead). A glass micropipette is also placed in the optic tectum with the tip in close proximity to the microelectrode for microinjection. (B-C) Focal DiI labeling showing the typical placement of the primary microelectrode for field recordings. (B) Dorsal view of DiI labeled brain. DiI was applied using the same configuration as for field recording, allowing for the DiI to leak out of the primary electrode needle and slowly label microelectrode position. The brain was then photographed to show location of DiI label (arrowhead). The position of the section shown in C is denoted with a dotted line. (C) Section through the optic tectum at approximate site of needle tip (shown by arrow). A DiI heat map overlay was generated by integrating DiI fluorescence from labeled sections; hot colors denote regions of high intensity and cold colors of low intensity labeling. Nuclei were DAPI labeled and false colored to green. P, pallium; H, habenula; TeO, optic tectum; Ce, cerebellum; M, medulla; SO, stratum opticum; SGC, stratum griseum central; SGP, stratum griseum periventricular

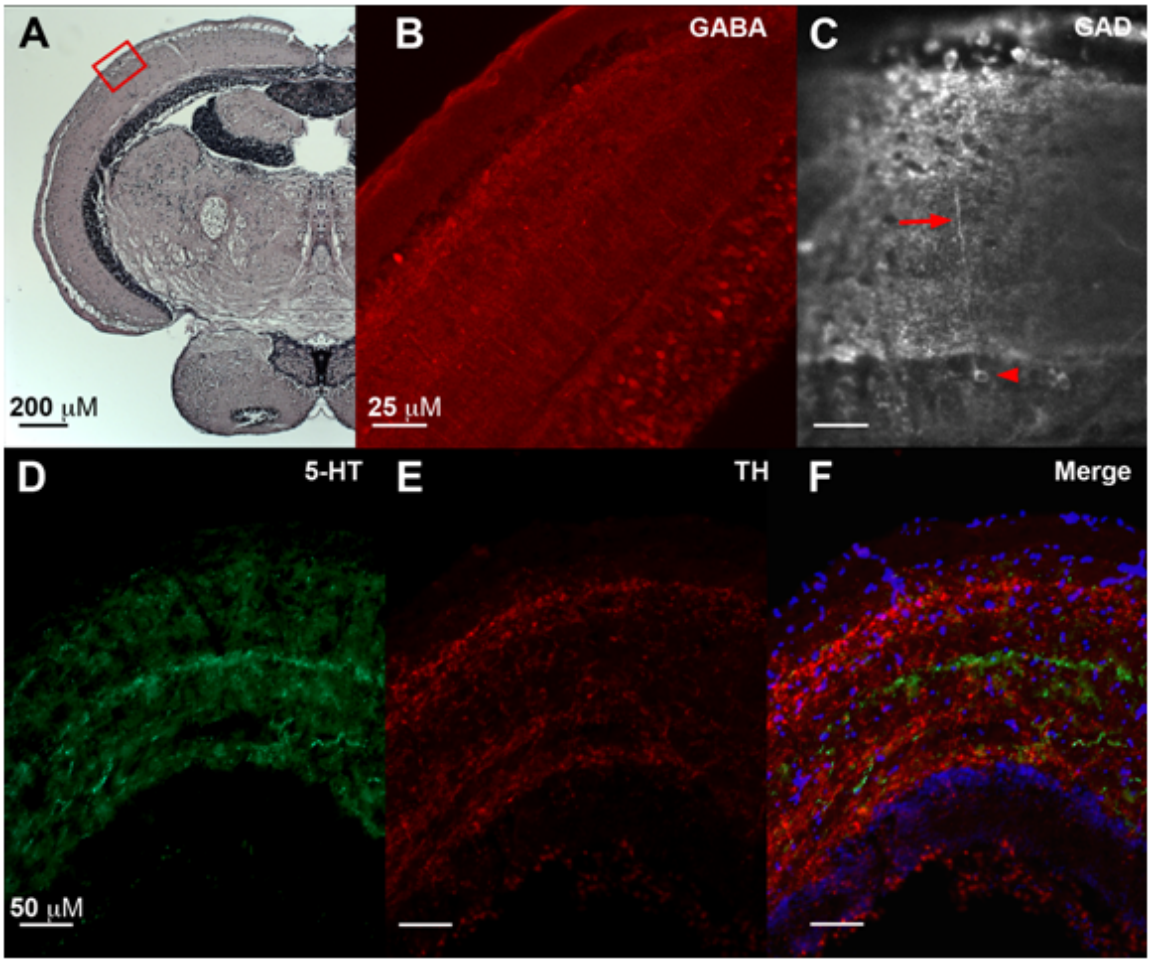


**Figure. 2.2. Amine immunoreactivity in the optic tectum; cross section view.** (A) Haematozylin Eosin (H&E) stained section of adult zebrafish brain. Red square represents the region observed in B-F. (B) Confocal image of a cross-section showing GABA expression. GABAergic neurons innervate both superficial and deep layers of the TeO. Labeled cell bodies are predominantly found in the deeper layers. Scale bar is consistent for panels B and C. (C) Confocal image of a cross-section showing GAD expression within the TeO. A single cell body (arrowhead) resides in the deep layer of the TeO with an axon extending into the more superficial layers (arrow). (D-F) Cross-section showing a network of TH- and serotonin (5-HT) –ir fibers in the TeO. (D) 5-HT-ir neurons are predominantly found in the deeper layers of the TeO. (E) TH-ir neurons innervate both superficial and deep layers of the TeO. (F) Merge of panel E and panel F showing the relative distribution of TH- and 5-HT –ir fibers. Nuclei were labeled with DAPI and included in the merged panel. Scale bar in D is consistent for panels E and F.

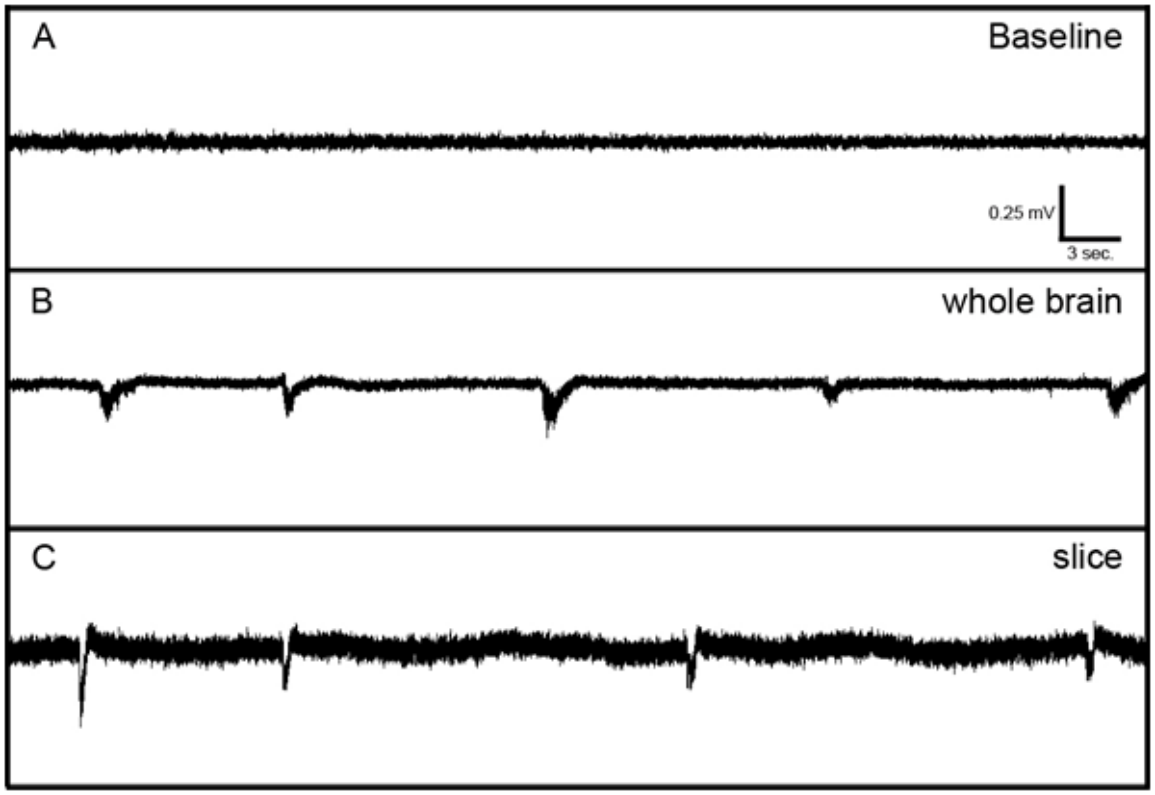


**Figure. 2.3. ATP-induced activity in an *ex vivo* preparation.** (A) A 1 min. period of baseline field recording showing very little activity, being stereotypical for the *ex vivo* preparations. (B) Representative field recording following the addition of 100 µM ATP to the preparation dish holding the intact *ex vivo* brain. Within 5 minutes of exposure, peaks (~0.25 mV) developed and persisted until the end of the trial. (C) Representative field recording from a slice preparation exposed to 100 µM ATP. In general, spontaneous activity only developed and persisted starting about 5-10 min. following exposure. Each panel represents 1 min. of a typical field recording for each preparation. All panels show a y-axis scale of 1 mV.

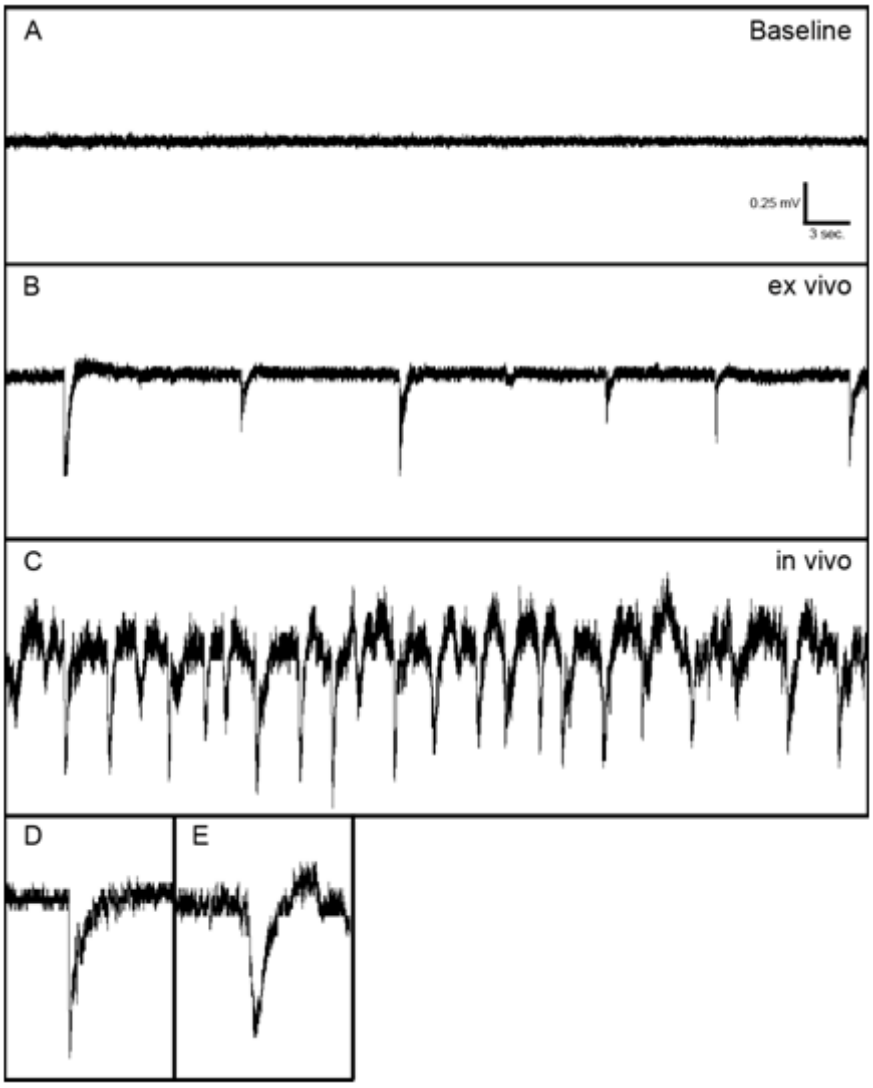


**Figure. 2.4. PTZ-induced activity in an *ex vivo* preparation.** (A) A 1 min. period of baseline field recording showing very little activity, being stereotypical for the *ex vivo* preparations. (B) Representative field recording following the addition of 300 mM PTZ to the preparation dish holding the *ex vivo* brain; this created a final concentration of 15 mM PTZ in the ACSF bath. Within 2 minutes of exposure, large amplitude peaks (0.25-2 mV) developed and persisted until the end of the trial. (C) Representative field recording from an *in vivo* preparation exposed to 15 mM PTZ. Large amplitude spontaneous activity developed and persisted starting 3-5 min after perfusion began. Intact fish exhibited similar large amplitude events as the *ex vivo* brain, but many more peaks were observed. (D) Single large amplitude peak from *ex vivo* brain exposed to PTZ. (E) Single large amplitude peak from intact adult fish. The peak morphology that developed following PTZ exposure was comparable between *ex vivo* and intact fish preparations. Each panel represents 1 min. of a typical field recording for each preparation. All panels show a y-axis scale of 1 mV.

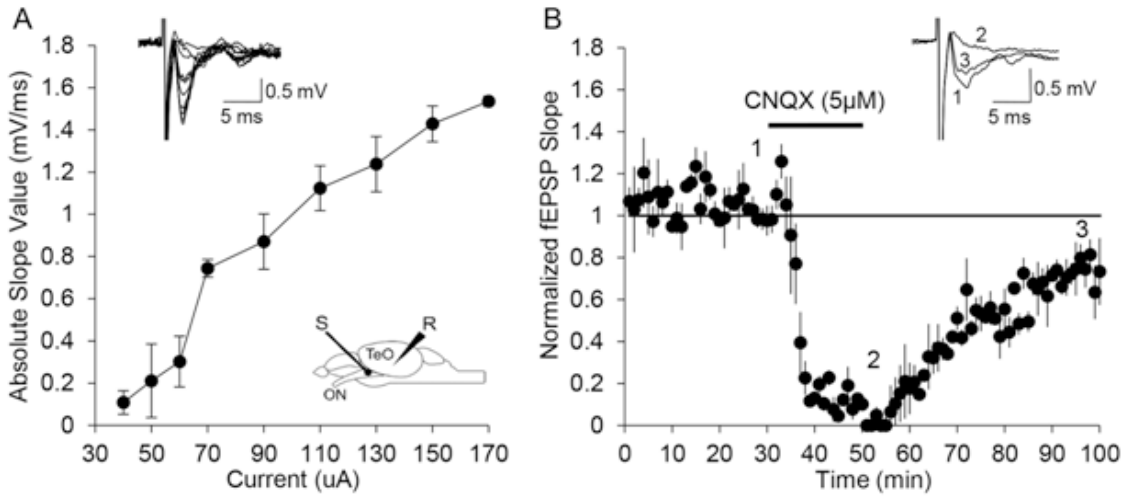


**Figure. 2.5. Field Excitatory Post-Synaptic Potentials (fEPSP) recorded from the optic tectum of adult zebrafish.** (A) Stimulus response curve at the indicated stimulus intensities (40, 50, 60, 70, 90, 110, 130, 150, 170, and 190 μA). Inset (top left) illustrates averaged fEPSP responses for the stimulus response curve. Inset (lower right) depicts a schematic of the hemisected adult zebrafish brain showing the approximate location of the stimulating electrode (S) and the recording electrode (R). ON: Optic Nerve; TeO: Tectum Opticum. (B) Summary plot of normalized fEPSP slope values for assessment of glutamatergic synaptic activity. CNQX (5μM) was bath applied for 20 minutes then subsequently removed for the remainder of the experiment. The inset above represents averaged fEPSP sweeps from 5 minutes before (1), during the last 5 minutes of application (2), and after a 50-minute washout (3) of CNQX. The vertical scale bars represent 0.5 mV and the horizontal scale bars represent 5 ms. Slope values represent the mean ± SEM from 3 different zebrafish brains.

References

Ball R, Page AT, Acuff S, Singer R, Gaudet J, Beebe LL, Keith CH, Sornborger AT, Lauderdale JD (In preparation) A Comparison of Evoked Seizure Activity in the Mature and Immature Zebrafish Brains.

Bally-Cuif L, Vernier P (2010) Organization and Physiology of the Zebrafish Nervous System. In: Fish Physiology: Zebrafish, vol. 29 (Perry, S. F. et al., eds).

Baraban SC, Dinday MT, Castro PA, Chege S, Guyenet S, Taylor MR (2007) A large-scale mutagenesis screen to identify seizure-resistant zebrafish. Epilepsia 48:1151-1157.

Baraban SC, Taylor MR, Castro PA, Baier H (2005) Pentylenetetrazole induced changes in zebrafish behavior, neural activity and c-fos expression. Neuroscience 131:759-768.

Baxendale S, Holdsworth CJ, Meza Santoscoy PL, Harrison MR, Fox J, Parkin CA, Ingham PW, Cunliffe VT (2012) Identification of compounds with anti-convulsant properties in a zebrafish model of epileptic seizures. Disease models & mechanisms 5:773-784.

Brambilla P, Perez J, Barale F, Schettini G, Soares JC (2003) GABAergic dysfunction in mood disorders. Molecular psychiatry 8:721-737, 715.

Bu D-F, Erlander MG, Hitz BC, Tillakaratne N, Kaufman DL, Wagner-McPherson CB, Evans GA, Tobin AJ (1992) Two human glutamate decarboxylases, 65-kDa GAD and 67-kDa GAD, are each encoded by a single gene. Proceedings of the National Academy of Sciences 89:2115-2119.

Buckmaster PS, Jongen-Relo AL (1999) Highly specific neuron loss preserves lateral inhibitory circuits in the dentate gyrus of kainate-induced epileptic rats. The Journal of neuroscience : the official journal of the Society for Neuroscience 19:9519-9529.

Buzsaki G, Penttonen M, Nadasdy Z, Bragin A (1996) Pattern and inhibition-dependent invasion of pyramidal cell dendrites by fast spikes in the hippocampus in vivo. Proc Natl Acad Sci USA 93:9921-9925.

Cadet JL (2009) Amphetamine recapitulates developmental programs in the zebrafish. Genome biology 10:231.

Callaway EM, Katz LC (1993) Photostimulation using caged glutamate reveals functional circuitry in living brain slices. Proceedings of the National Academy of Sciences of the United States of America 90:7661-7665.

De Curtis M, Biella G, Forti M, Panzica F (1994) Multifocal spontaneous epileptic activity induced by restricted bicuculline ejection in the piriform cortex of the isolated guinea pig brain. Journal of neurophysiology 71:2463-2476.

de Curtis M, Manfridi A, Biella G (1998) Activity-dependent pH shifts and periodic recurrence of spontaneous interictal spikes in a model of focal epileptogenesis. The Journal of neuroscience 18:7543-7551.

Delgado L, Schmachtenberg O (2008) Immunohistochemical localization of GABA, GAD65, and the receptor subunits GABAAα1 and GABAB1 in the zebrafish cerebellum. The Cerebellum 7:444-450.

Edwards J, Michel W (2003) Pharmacological characterization of ionotropic glutamate receptors in the zebrafish olfactory bulb. Neuroscience 122:1037-1047.

Erdo S, Michler A, Wolff JR (1991) GABA accelerates excitotoxic cell death in cortical cultures: protection by blockers of GABA-gated chloride channels. Brain research 542:254-258.

Federico P, MacVicar B (1996) Imaging the induction and spread of seizure activity in the isolated brain of the guinea pig: the roles of GABA and glutamate receptors. Journal of neurophysiology 76:3471-3492.

Fischer AH, Jacobson KA, Rose J, Zeller R (2008) Hematoxylin and eosin staining of tissue and cell sections. Cold Spring Harbor Protocols 2008:pdb. prot4986.

Friedrich RW, Jacobson GA, Zhu P (2010) Circuit neuroscience in zebrafish. Current biology : CB 20:R371-381.

Friedrich RW, Mack-Bucher JA, Li J (2006) Opto-and electrophysiological approaches in the central nervous system of zebrafish. Using Zebrafish to Study Neuroscience 33.

Froc DJ, Eadie B, Li AM, Wodtke K, Tse M, Christie BR (2003) Reduced synaptic plasticity in the lateral perforant path input to the dentate gyrus of aged C57BL/6 mice. Journal of neurophysiology 90:32-38.

Gahtan E, Baier H (2004) Of lasers, mutants, and see-through brains: functional neuroanatomy in zebrafish. Journal of neurobiology 59:147-161.

Galanopoulou AS (2013) Basic mechanisms of catastrophic epilepsy - Overview from animal models. Brain & development.

Haas HL, Schaerer B, Vosmansky M (1979) A simple perfusion chamber for the study of nervous tissue slices in vitro. Journal of neuroscience methods 1:323-325.

Hewapathirane DS, Dunfield D, Yen W, Chen S, Haas K (2008) In vivo imaging of seizure activity in a novel developmental seizure model. Experimental neurology 211:480-488.

Johnston L, Ball RE, Acuff S, Gaudet J, Sornborger A, Lauderdale JD (2013) Electrophysiological Recording in the Brain of Intact Adult Zebrafish. e51065.

Kaslin J, Panula P (2001) Comparative anatomy of the histaminergic and other aminergic systems in zebrafish (Danio rerio). The Journal of comparative neurology 440:342-377.

Kim Y-J, Nam R-H, Yoo YM, Lee C-J (2004a) Identification and functional evidence of GABAergic neurons in parts of the brain of adult zebrafish (*Danio rerio*). Neuroscience letters 355:29-32.

Kim YJ, Nam RH, Yoo YM, Lee CJ (2004b) Identification and functional evidence of GABAergic neurons in parts of the brain of adult zebrafish (Danio rerio). Neuroscience letters 355:29-32.

Klee EW, Schneider H, Clark KJ, Cousin MA, Ebbert JO, Hooten WM, Karpyak VM, Warner DO, Ekker SC (2012) Zebrafish: a model for the study of addiction genetics. Human genetics 131:977-1008.

Krasnova IN, Li SM, Wood WH, McCoy MT, Prabhu VV, Becker KG, Katz JL, Cadet JL (2008) Transcriptional responses to reinforcing effects of cocaine in the rat hippocampus and cortex. Genes, brain, and behavior 7:193-202.

Liauw J, Wang G, Zhuo M (2003) NMDA receptors contribute to synaptic transmission in anterior cingulate cortex of adult mice. Sheng li xue bao:[Acta physiologica Sinica] 55:373-380.

MacVicar B, Hochman D (1991) Imaging of synaptically evoked intrinsic optical signals in hippocampal slices. The Journal of neuroscience 11:1458-1469.

Martin SC, Heinrich G, Sandell JH (1998) Sequence and expression of glutamic acid decarboxylase isoforms in the developing zebrafish. The Journal of comparative neurology 396:253-266.

Matsuda N, Mishina M (2004) Identification of chaperonin CCT gamma subunit as a determinant of retinotectal development by whole-genome subtraction cloning from zebrafish no tectal neuron mutant. Development 131:1913-1925.

Maximino C, Lima MG, Araujo J, Lieveira K, Herculano AM, Stewart AM, Kyzar EJ, Cachat J, Kalueff AV (2012) The Serotonergic System of Zebrafish: Genomics, Neuroanatomy and Neuropharmacology.

McLean DL, Fetcho JR (2004) Ontogeny and innervation patterns of dopaminergic, noradrenergic, and serotonergic neurons in larval zebrafish. The Journal of comparative neurology 480:38-56.

Meek HJ (1990) Tectal morphology: connections, neurones and synapses. In: The Visual System of Fish, pp 239-277: Springer.

Mei X, Wu S, Bassuk AG, Slusarski DC (2013) Mechanisms of prickle1a function in zebrafish epilepsy and retinal neurogenesis. Disease models & mechanisms 6:679-688.

Mueller KP, Neuhauss SC (2010) Behavioral neurobiology: how larval fish orient towards the light. Current biology : CB 20:R159-161.

Mühlethaler M, Curtis M, Walton K, Llinas R (1993) The Isolated and Perfused Brain of the Guinea‐pig In Vitro. European Journal of Neuroscience 5:915-926.

Nam RH, Kim W, Lee CJ (2004) NMDA receptor-dependent long-term potentiation in the telencephalon of the zebrafish. Neuroscience letters 370:248-251.

Neuhauss SC (2010) Zebrafish Vision: Structure and Function of the Zebrafish Visual System. In: Fish Physiology: Zebrafish, vol. 29 (Perry, S. F. et al., eds).

Nevin LM, Taylor MR, Baier H (2008) Hardwiring of fine synaptic layers in the zebrafish visual pathway. Neural development 3:36.

Ng MC, Tang TH, Ko MC, Wu YJ, Hsu CP, Yang YL, Lu KT (2012) Stimulation of the lateral division of the dorsal telencephalon induces synaptic plasticity in the medial division of adult zebrafish. Neuroscience letters 512:109-113.

Norton W, Bally-Cuif L (2010) Adult zebrafish as a model organism for behavioural genetics. BMC neuroscience 11:90.

Owens DF, Boyce LH, Davis MB, Kriegstein AR (1996) Excitatory GABA responses in embryonic and neonatal cortical slices demonstrated by gramicidin perforated-patch recordings and calcium imaging. The Journal of neuroscience 16:6414-6423.

Pakhotin PI, Pakhotina ID (1994) Preparation of isolated perfused ground squirrel brain. Brain research bulletin 33:719-721.

Pineda R, Beattie CE, Hall CW (2011) Recording the adult zebrafish cerebral field potential during pentylenetetrazole seizures. Journal of neuroscience methods 200:20-28.

Powell EM, Campbell DB, Stanwood GD, Davis C, Noebels JL, Levitt P (2003) Genetic disruption of cortical interneuron development causes region- and GABA cell type-specific deficits, epilepsy, and behavioral dysfunction. The Journal of neuroscience : the official journal of the Society for Neuroscience 23:622-631.

Robinson TE, Kolb B (2004) Structural plasticity associated with exposure to drugs of abuse. Neuropharmacology 47 Suppl 1:33-46.

Sato T, Hamaoka T, Aizawa H, Hosoya T, Okamoto H (2007) Genetic single-cell mosaic analysis implicates ephrinB2 reverse signaling in projections from the posterior tectum to the hindbrain in zebrafish. The Journal of neuroscience : the official journal of the Society for Neuroscience 27:5271-5279.

Servit Z, Strejckova A (1970a) An electrographic epileptic focus in the fish forebrain. Conditions and pathways of propagation of focal and paroxysmal activity. Brain research 17:103-113.

Servit Z, Strejckova A (1970b) Epileptic focus in the frog forebrain. Triggering of the focal discharge with sensory stimuli. Experimental neurology 28:371-383.

Sloviter RS (2008) Hippocampal epileptogenesis in animal models of mesial temporal lobe epilepsy with hippocampal sclerosis: the importance of the "latent period" and other concepts. Epilepsia 49 Suppl 9:85-92.

Strejckova A (1969) Epileptogenic focus in the fish telencephalon (in the common tench--Tinca tinca). Physiologia Bohemoslovaca 18:209-216.

Sutula TP, Hagen J, Pitkanen A (2003) Do epileptic seizures damage the brain? Current opinion in neurology 16:189-195.

Suwabe T, Fukami H, Bradley RM (2008) Synaptic responses of neurons controlling the parotid and von Ebner salivary glands in rats to stimulation of the solitary nucleus and tract. Journal of neurophysiology 99:1267-1273.

Tomizawa K, Kunieda J, Nakayasu H (2001) Ex vivo culture of isolated zebrafish whole brain. Journal of neuroscience methods 107:31-38.

Vargas R, Johannesdottir IT, Sigurgeirsson B, Thornorsteinsson H, Karlsson KA (2011a) The zebrafish brain in research and teaching: a simple in vivo and in vitro model for the study of spontaneous neural activity. Advances in physiology education 35:188-196.

Vargas R, Johannesdottir IT, Sigurgeirsson B, Thorsteinsson H, Karlsson KA (2011b) The zebrafish brain in research and teaching: a simple in vivo and in vitro model for the study of spontaneous neural activity. Advances in physiology education 35:188-196.

Volanschi D, Servit Z (1969) Epileptic focus in the forebrain of the turtle. Experimental neurology 24:137-146.

Volk DW, Lewis DA (2002) Impaired prefrontal inhibition in schizophrenia: relevance for cognitive dysfunction. Physiology & behavior 77:501-505.

Walther H, Lambert J, Jones R, Heinemann U, Hamon B (1986) Epileptiform activity in combined slices of the hippocampus, subiculum and entorhinal cortex during perfusion with low magnesium medium. Neuroscience letters 69:156-161.

Warther D, Gug S, Specht A, Bolze F, Nicoud JF, Mourot A, Goeldner M (2010) Two-photon uncaging: New prospects in neuroscience and cellular biology. Bioorganic & medicinal chemistry 18:7753-7758.

Westerfield M (ed.) (2000) The zebrafish book: A guide for the laboratory use of zebrafish (Danio rerio): University of Oregon Press.

Yuferov V, Nielsen D, Butelman E, Kreek MJ (2005) Microarray studies of psychostimulant-induced changes in gene expression. Addiction biology 10:101-118.

## Supplementary Methods

### *Preparation of whole brains and slices for extracellular field recordings*

Adult zebrafish were caught in a net and anesthetized in iced aquarium water before decapitation. Once movement had subsided, the fish was quickly removed from the water and transferred to a clean surface. A sterile scalpel was used to remove the head by creating an incision just dorsal to the gills. The intact head was transferred to a 60x15 mm Corning Not-TC treated petri dish (Corning Inc., Tewksbury, MA ) filled with approximately 10-15mL ice cold ACSF (recently bubbled with 95% $O_2$/5% $CO_2$, pH 7.4). The remaining body was transferred to a plastic zip-lock bag for storage.

To remove the brain, a pair of Super Fine #5 Dumonts forceps (Fine Science Tools, Foster City, CA) was used to orient the head such that the dorsal side was facing up. A second set of forceps was used to remove the eyes from the cranium by positioning the forceps tips into the eye socket and gently pulling away. The head was then rotated so the ventral side was facing up. Using one set of forceps to steady the head, the lower jaw and excess tissue were removed by gently pulling away from the skull with the second set of forceps. Once all excess tissue was removed from the ventral portion of the cranium, one tip of the forceps was used to gently apply pressure along the midline of the skull from the anterior region to the spinal cord, creating a small crack. Once the skull was fractured, the two sets of forceps were used to grab each side of the cranium and carefully pull the skull apart. If the brain was not immediately released, the forceps were used to gently tease away any remaining bony material around the brain.

A small droplet of liquefied 1.2 % agarose (Thermo Fisher Scientific, Waltham, MA) was placed in the center of a 35x10 mm BD Falcon Petri Dish (BD Biosciences, Bedford, MA). After allowing the droplet to cool slightly, the brain was transferred from the previous dish using forceps and placed, dorsal side up, in the agarose. The agarose was allowed to set before fresh ACSF was added to the dish, creating a bath in which the brain would remain for the remainder of the experiment. Enough ACSF was added so that the final volume, after drug addition, would be 3 mL. Any agarose around the spinal cord was gently teased away using a probe to allow for better exposure to drugs.

# CHAPTER 3

# ELECTROPHYSIOLOGICAL RECORDING IN THE BRAIN OF INTACT ADULT ZEBRAFISH [1,2]

[1]Johnston, L., Ball, R. E., Acuff, S., Gaudet, J., Sornborger, A., Lauderdale, J. D. 2013. *Journal of Visusalized Experiments*. 81.



[2] Previously published as Lindsey L. Johnston (maiden name)

Short Abstract

This paper describes how an adult zebrafish can be immobilized, intubated, and used for *in vivo* electrophysiological experiments to allow recordings and manipulation of neural activity in an intact animal.

Long Abstract

Previously, electrophysiological studies in adult zebrafish have been limited to slice preparations or to eye cup preparations and electrorentinogram recordings. This paper describes how an adult zebrafish can be immobilized, intubated, and used for *in vivo* electrophysiological experiments, allowing recording of neural activity. Immobilization of the adult requires a mechanism to deliver dissolved oxygen to the gills in lieu of buccal and opercular movement. With our technique, animals are immobilized and perfused with habitat water to fulfill this requirement. A craniotomy is performed under Tricaine methanesulfonate (MS-222; tricaine) anesthesia to provide access to the brain. The primary electrode is then positioned within the craniotomy window to record extracellular brain activity. Through the use of a multi-tube perfusion system, a variety of pharmacological compounds can be administered to the adult fish and any alterations in the neural activity can be observed. The methodology not only allows for observations to be made regarding changes in neurological activity, but it also allows for comparisons to be made between larval and adult zebrafish. This gives researchers the ability to identify the alterations in neurological activity due to the introduction of various compounds at different life stages.

## Introduction

In this article, a protocol is described for obtaining *in vivo* recordings of neural activity in adult zebrafish. Extracellular recording methods are used, providing voltage measurements of electrical activity within a small region of neural tissue. This method of investigation involves monitoring a large number of cells in a behaving animal (Henze et al., 2000). Previously, slice recordings have been performed in both adults and larvae, as have eye cup preparations and electroretinogram recordings. These experiments have largely been performed to detail physiological responses of various sensory systems (Brockerhoff et al., 1995, Makhankov et al., 2004, Gabriel et al., 2008, Vargas et al., 2011). Until recently, intact brain preparations have only been available for performing electrophysiology with zebrafish larva (Baraban et al., 2005, Baraban et al., 2007, Vargas et al., 2011), where respiration and oxygen diffusion can occur through the skin. Our preparation allows the native neurological activity of an adult zebrafish to be measured while the animal remains fully conscious and aware of its surroundings.

Zebrafish (*Danio rerio*) currently play a fundamental role as a model for genetic, toxicological, pharmacological and physiopathological studies (Vargas et al., 2011). Zebrafish have gained visibility within the field of neuroscience because they share extensive homology with mammals at the genetic, neural and endocrine levels (Maximino et al., 2012). Over the past decade, standard neuroanatomic and immunohistochemical techniques have been used to determine the detailed characteristic organization of the zebrafish nervous system (Kaslin et al., 2004, McLean and Fetcho, 2004, Mueller et al., 2004, Bally-Cuif and Vernier, 2010) and of the distribution of different neurotransmitters (Higashijima et al., 2004, Vargas et al., 2011, Maximino et al.,

2012). More recently, researchers have shifted their focus to functional studies (Fan et al., 2007, Tao et al., 2011), many of which center on behavioral processes (Burgess and Granato, 2007, Burgess et al., 2010, Haug et al., 2010, Mueller and Neuhauss, 2010) and electrophysiological characteristics of sensory systems (Higashijima et al., 2004, Fetcho et al., 2008, Gabriel et al., 2008). A small number of these studies have concentrated on the electrical activity of specific areas of the adult zebrafish brain (Kim et al., 2004, Sato et al., 2007, Connaughton et al., 2008), but were not carried out using an *in vivo* approach.

This protocol can be adapted for electrophysiological studies of both spontaneous and evoked activity within the zebrafish nervous system to describe the patterns of activity in specific brain regions. The use of this technique allows comparisons to be made between the neurological activity of young larval stages and adults. Further, our protocol permits comparisons between genetic or pharmacological alterations. Together with other approaches, such as genetic engineering or pharmacological tests, this method offers a new possibility for the functional analysis of neuronal communication and plasticity in the intact adult animal, as well as for potential applications, such as studying late onset epilepsy or neurodegenerative processes.

## Protocol

All experimental procedures were conducted in strict accordance with the National Institutes of Health Guide for the Care and Use of Laboratory Animals and followed protocol #A2011 09-003, which was reviewed, approved, and overseen by the University of Georgia Institutional Animal Care and Use Committee.

***1. Equipment Setup***

*1.1) Perfusion system for craniotomy*

Immobilization of the adult necessitates an intubation system to deliver dissolved oxygen to the fish. A variety of systems can be utilized, but a simple gravity system consisting of a 60cc syringe is used. Elevate the pressure head to a height that consistently yields a flow rate of ~1 ml/min. This syringe can be placed in series with the syringes that are then used for the electrophysiological perfusion system.

1.1.1) Obtain a single 60cc luer-lock syringe tube and remove the plunger.

1.1.2) Suspend the syringe approximately 8 inches above the base of a ring-stand using a clamp.

1.1.3) Connect a one-way stopcock to the end of the syringe. To the opposite end of the stopcock, connect a piece of tubing, 2 mm in diameter, which is long enough to extend to the intubation base.

*1.2) Perfusion system for electrophysiology*

For electrophysiological experiments, it is often necessary to introduce a variety of compounds during the course of an experiment. A variety of systems are available, but a gravity system consisting of 60cc syringes in series can be used. This setup allows for simple, serial introduction of solutions to be carried out by opening the corresponding stopcock.

1.2.1) Obtain two or more 60cc luer-lock syringes and remove the plungers from each. One syringe is required to administer habitat water to the fish while each subsequent tube can be used to administer a variety of pharmacological compounds to the fish.

1.2.2) Connect each syringe to a 3-way stopcock with a luer connection.

1.2.3) Use $^{1}/_{8}$ in. outer diameter (O.D.) tubing to connect the syringes in series with a male luer-lock on one end.

1.2.4) Secure the device such that the pressure head is elevated to a height of 27 inches above the base, or a height that consistently yields a flow rate of ~1 ml/min.

*1.3) Intubation cannula*

The intubation cannula facilitates the introduction of fluid to the fish. This setup provides both flexibility and firmness to best position the cannula within the animal's mouth.

1.3.1) Using any general pair of scissors (e.g. Fiskars) or a razorblade, remove a 1.5 cm section from the wide end of a P-200 pipette tip.

1.3.2) Insert a 6 cm x 1 mm piece of tubing into a reducing valve with a female luer lock cap and silicone ferrule, i.e. a Tuohy Borst adapter, and insert this cannula into the modified pipette tip. Hold the pipette tip in position with the luer-lock using a short portion of $^{1}/_{8}$ in. diameter tubing. (Figure 3.1)

*1.4) Intubation base*

This dish is used to hold the immobilized animal in a stable, upright position and to facilitate the removal of the fluid entering the animal through intubation. If this is not established correctly, pooling can occur, leading to intrusive vibrational signals in the electrophysiological recording.

1.4.1) Obtain the base dish of a 100 x 15 mm plastic petri dish.

1.4.2) Using a soldering tool, melt a hole, 6 mm in diameter and 7.5 mm below the lip of the rim, into the side of the dish. Using the same tool, melt a hole, 10 mm in diameter and

11 mm below the lip of the dish ~ 74$^{o}$ counter-clockwise from the smaller hole. This hole will serve as the drainage hole.

1.4.3) Insert a tube, 1 cm in diameter, into the hole with the end lifted such that the end cannot be blocked. Then insert a P-200 pipetteman tip into the small hole; this will serve as a dummy cannula.

1.4.4) With the petri dish slightly elevated on the side of the larger hole, pour melted canning wax into the dish such that the cannula hole is just covered. The region will serve as a stop, allowing the cannula to be inserted ~3 mm into the mouth of the fish. This set up should be allowed to solidify.

1.4.5) Using a flame-heated metal edge, carve a channel to hold the fish so that the channel begins from the tip of the cannula and extends approximately 1-2 inches.

1.4.5.1) Caution must be taken to ensure that a continuous downward angle from the cannula area to the drainage port is formed. (Figure 3.2)

*1.5) Perfusion setup*

1.5.1) Before beginning, flush the perfusion set-ups with habitat water, ensuring that all air bubbles are removed.

1.5.2) Add ~30 ml of 0.016% (630 μM) tricaine solution to the craniotomy perfusion setup and allow ~2 ml to run through tubing to ensure that tricaine will be delivered to the animal upon perfusion initiation. See step 2.2 for dilution.

1.5.3) To the main perfusion setup, add ~50 ml of habitat water to the first tube. Add any desired experimental compounds to each of the remaining tubes.

1.5.4) Place the cannula setup into the small hole of the intubation base.

1.5.5) Twist a 1 inch-wide strip of 42 cm KimWipe into a tight spiral and insert it into the drainage tube such that the KimWipe extends on both ends. This tissue will serve as a wick to remove the perfused liquid and to prevent fluid buildup within the intubation base, which could interfere with electrophysiological recording.

1.5.6) Insert one end of the tubing into the large hole of the petri dish, allowing the lower end to extend into an inert dish that is large enough to collect all perfusion waste. This dish will serve as the outflow reservoir for the setup. Position the tissue so that one end will lie near the animal's abdomen region and the lower extension can drip into the dish.

1.5.7) Place this completed intubation base near the dissecting microscope. Connect the luer lock of the cannula to the tricaine perfusion tubing.

*1.6) Capillary needle and electrodes*

1.6.1) Obtain a primary electrode consisting of 2.5 in. of 0.010 in. silver wire and a secondary electrode which should be made up of 15 in. of the same wire to ground the setup. For the secondary electrode, use a 15 in. section of 0.010 in. silver wire with a soldered tip, which allows it to fit in back of a head-stage.

1.6.1.1) Electroplate the tips of both the primary and secondary silver wires with chloride ions.

1.6.2) Using a micropipette puller, pull a thin-walled, borosilicate capillary needle with a resistance of <15 mOhms.

1.6.2.1) Fill the capillary needle with 2-3 µl of 2 M potassium chloride, or enough to partially cover the chloride-coated tip of the silver wire.

1.6.2.2) Insert the primary electrode into the capillary head and mount it in the electrode holder.

1.6.2.3) Mount the head-stage into a micromanipulator and then mount the secondary electrode into a second micromanipulator. With the setup, first position each electrode and then fit the soldered tip of the secondary electrode into the back of the head-stage.

***2. Preparation of solutions, perfusion system, and electrophysiological recording equipment***

2.1) Obtain 1 L of habitat water from aquarium of fish.

2.2) 0.016% Tricaine methanesulfonate (tricaine) (50 ml of 630 μM) (Westerfield, 1993)

2.2.1) Thaw an aliquot of 0.4% Tris-buffered tricaine, pH 7.2.

2.2.2) Add 2.1 ml of 0.4% Tris-buffered tricaine to 47.9 ml of habitat water and mix.

2.3) Thaw stock concentration of desired water-soluble experimental compound (e.g. 300 mM Pentylenetetrazol, a common chemoconvulsant).

2.4) Thaw out an aliquot of 1μg/μl pancuronium bromide in Ringer's solution.

2.5) Fill both anesthetizing and experimental intubation systems with habitat water and drain at least enough to remove all bubbles from tubes. This must be done because bubbles obstruct fluid flow, leading to asphyxiation of the animal.

2.5.1) Completely drain the perfusion tubes that will hold drugs without allowing air into the connecting tubing.

2.5.2) Fill the anesthetizing tube with 0.016% (630 μM) tricaine solution and place any experimental compound(s) in additional tube(s) on experimental perfusion system.

2.5.2.1) The first tube of experimental perfusion should contain only habitat water.

2.6) Moisten the small pore sponge with habitat water and place in an empty 60 x 15 mm petri dish. This dish will be used to hold the fish while the anesthetic is injected.

Procedure

***3. Craniotomy***

3.1) Add enough of the 630 μM tricaine solution to a 15 x 60 mm petri dish to fill it about three-quarters of the way. Weigh the filled dish. This will be used to immobilize the animal so that further anesthesia can be injected intraperitoneally.

3.2) Immerse the animal into the dish containing tricaine and weigh the dish again.

3.2.1) Subtract the difference between the weights from steps 1 and 2 to obtain the weight of the fish.

3.2.2) Allow the animal to remain in the tricaine solution until calm and most movement has ceased.

3.3) Using a pair of broad forceps, transfer the fish to the pre-moistened sponge and position it laterally. Transferring the fish by the tail works well for this process.

3.3.1) Place the sponge and fish under the dissecting microscope.

3.4) With a Nanofil syringe containing a 34 gauge needle, measure out enough pancuronium bromide such that there is 1 μg/g of fish weight.

3.5) Using a popsicle stick along the dorsal side of the fish to hold it steady, administer the pancuronium bromide intraperitoneally using the Nanofil syringe.

3.6) Using the fine forceps, grab the fish by the lower jaw and quickly transfer the animal to the intubation base.

3.7) Position the animal so that it is dorsal-up on the wax form and such that the 1 mm cannula can be inserted into the mouth. Use blunt forceps to maneuver the fish and open the mouth around the cannula. Due to the makeup of the intubation tray, a stop was

engineered into the base, allowing the cannula to be inserted 3 mm into the mouth of the fish.

3.7.1) Once in position, turn on the gravity-fed perfusion tube containing tricaine.

3.8) Cut a 3 $cm^2$ section of KimWipe tissue and wet it with habitat water.

3.8.1) Place the tissue over the animal to prevent desiccation. The KimWipe section can also be positioned to aid in holding the animal dorsal-up.

3.9) Under the dissection microscope, use vanna spring scissors to remove ~2 $mm^2$ section of the cranium covering the optic tectum. This area looks like a dark, bony plate that sits behind the eye. (Figure 3.3)

3.9.1) Insert one blade of the vanna scissors at the edge of the plate and push with enough force to penetrate the bone, without piercing the brain. Close the scissors to snip the bone.

3.9.2) Remove the piece of bone using a pair of fine forceps (e.g. watchmaker's forceps).

3.9.3) If any blood is present, remove using the edge of a KimWipe. Bleeding generally stops shortly after carrying out the craniotomy.

***4. Electrophysiology***

4.1) Shut off the intubation stop-cock and quickly disconnect the luer-lock connecting the intubation base to the tricaine drip.

4.1.1) Move the intact intubation setup to the electrophysiology microscope and connect to the perfusion system.

4.1.2) Turn on the habitat water and perfuse at a rate of 1 ml/min for about one hour, in order to wash out the tricaine.

4.2) Using a micromanipulator under visual control, position the secondary electrode so that the electrode tip can be inserted into the animal's nostril or into the dip behind the upper jaw.

4.3) Insert the primary electrode needle into the craniotomy opening. Insert the needle into the tissue, such that the tip is positioned fairly superficial within the optic tectum. (Figure 3.4)

4.3.1) If the electrode is too deep, the electrical signal may be small.

4.4) Collect and analyze the electrical difference recorded between the primary and secondary reference electrodes. This process will allow for extracellular recordings to be obtained.

4.4.1) Collect the data in Gap-free mode at a 5000 Hz sample rate, with a low pass filter of 0.1 kHz and a high pass filter of 1 Hz.

4.4.2) Do not begin recording electrophysiological activity until habitat water has perfused for a minimum of 45 minutes.

4.4.3) Record a baseline of native activity for at least 15 minutes prior to the addition of experimental drugs. Begin perfusion with experimental drugs of choice and record for the desired amount of time. In healthy preparations, it is possible to record the neurological activity for 2-3 hours.

***5. Clean Up***

5.1) At the end of the experiment, remove the electrodes from the cranium and nostril and remove the intubation setup.

5.1.1) Euthanize the animal by drug overdose using tricaine in accordance with the accepted practices, as outlined by the American Veterinary Medical Association (AVMA) Guidelines for the Euthanasia of Animals (2013).

5.1.2) Zebrafish to be euthanized should be placed in a tricaine solution at 200-500 mg/liter. Fish are to be left in the solution for a minimum of 10 minutes after cessation of rhythmic opercular activity, after which they are subjected to a physical means of euthanasia (cervical transection) to ensure death.

5.2) Disconnect the luer-lock connecting the intubation base to the perfusion setup. Collect any remaining liquid in the perfusion system for appropriate disposal.

5.2.1) Run DI water through all tubes and collect for appropriate disposal, if hazardous.

5.3) To sanitize the perfusion system, run 70% ethanol through all tubes and collect for appropriate disposal.

5.3.1) Leave the stopcocks for each tube in the open position to facilitate air-drying.

5.3.2) Soak the electrodes in 70% ethanol and allow to air dry.

5.4) Dispose of the capillary needle used for the primary electrode in a sharps container.

5.5) Dismantle the intubation setup and rinse all pieces with water.

5.5.1) Clean each piece with 70% ethanol and allow to air dry.

## Representative Results

This protocol has been used to measure the neural activity of adult zebrafish *in vivo*. These electrophysiological recordings are consistently and reproducibly obtained. Figure 3.5 shows a representative example of native and induced alterations of the neural activity of an adult zebrafish when pentylenetetrazol (PTZ), a common chemoconvulsant

(Lazarova and Samanin, 1983, Loscher et al., 1991, Baraban et al., 2005, Baraban et al., 2007), is introduced in the intubation setup.

The native neurological activity of the adult zebrafish was monitored for each experiment (Fig. 3.5A). It was consistently observed that this activity was spontaneous and small in amplitude during the duration of the recording. Following the introduction of 15 mM PTZ to the system, spontaneous epileptiform-like discharges began to develop about 5 minutes following introduction. This activity was initially brief, small amplitude and occurred frequently, similar to what was observed within larval zebrafish (Baraban et al., 2005, Baraban et al., 2007). With continued exposure to the PTZ, a consistent pattern of large amplitude discharges developed that were followed by smaller, more frequent bursts of activity and a subsequent quiet period (Fig. 3.5B).

This technique has been used successfully to introduce other chemoconvulsants through the intubation system. With these compounds, changes in native neurological activity were also effectively evoked. Pentylenetetrazol was used here as an example due its ability to robustly alter the native neural activity of the zebrafish in a stereotypical manner.

## Discussion

This protocol has been used to measure the neural activity of adult zebrafish *in vivo*. With practice, neural activity can be observed consistently, though the characteristics (amplitude and shape of events) of the recorded activity can vary between individual fish. Utilization of the extracellular recording technique can explain this observation. The method provides simultaneous monitoring of a large number of cells within a region (Henze et al., 2000), so variations in the positioning of the primary

electrode can play a role in the observed activity. Depth of the primary electrode also changes the region being measured. If the tip of the electrode is positioned too deep within a region, the observed signal will be smaller than expected and alterations in activity will be harder to observe; if this occurs, simply pull back the primary electrode so that the tip is sitting more superficially. Take note that this is characteristic of the optic tectum and has not been looked at in depth in other regions of the brain. However, this procedure could be carried out within a different region of the brain. If the observed neural activity decreases to baseline levels during the experiment and it is uncertain if the fish is still alive, remove the electrodes from the cranium and check to see if there is still blood flow throughout the animal. This can be checked by observing the large vessels in the lip or nasal area of the fish. Blood flow can be easily seen in these regions. If the electrodes are removed to check for blood flow in the middle of a recording, when re-positioning the electrodes, they will be in a slightly different location than they were initially, negating the ability to directly compare this portion of the recording to the original baseline.

Before beginning this procedure, it must be ensured that the intubation tubes, as well as the perfusion tubes for both the craniotomy and the electrophysiology setups, are free of any bubbles. If bubbles do collect, they can be run out of the system by opening the stopcock and allowing some of the habitat water to run through. If this does not eliminate the problem, a small syringe can be attached to the end of the tube, where the cannula would be placed, and light suction can be applied to remove any remaining air within the system. For stubborn bubbles, habitat water can be forced through the tubing. Also, make sure that the perfusion tubes are primed and dripping before intubating the

fish. If a flow rate of ~1 ml/min. is not obtained, the height of the pressure head can be altered in order to achieve this. This will ensure that the fish has access to sufficient water flow. When the electrophysiology perfusion setup was configured with numerous tubes in series, it was determined that it took about ~1 min. for the new solution to be introduced to the animal, though resulting changes in the recorded neurological activity were dependent upon the compound being introduced. It is advised that this flow rate be measured prior to carrying out any experiments. Previous work has shown that tricaine can attenuate neural activity, requiring it to be removed from the system in order to obtain accurate recordings (Arnolds et al., 2002, DeMicco et al., 2010). Through previous work, it was determined that a period of 45-60 minutes of intubation with habitat water is required to wash out the tricaine and for neural activity to reach native levels. Similarly, washout of pentylenetetrazol was also carried out, and it was determined that a period of 20 minutes was required to return neural activity to baseline levels. Therefore, experimenters should complete trials to determine washout times for each compound of interest being introduced into the system.

This technique requires some practice. When carrying out the craniotomy, extra care must be taken to ensure that a small region of the bony plate that covers the head can be punctured and removed without damaging the brain. This can be done by introducing the vanna scissors at an acute angle with respect to the head. The bony area covering the optic tectum has fusions near the midline that are weak and serve as good entry points for the scissors. Once a small break has been made within the plate, use scissors to trim a small area of the bone, and remove using a pair of fine forceps. Younger fish often have softer, more pliable craniums, so fish that are 1 year of age or less are suggested for use

while learning this technique. Occasionally, blood will begin to collect around the region of the craniotomy, but this can be removed by dabbing a KimWipe gently around the area. With this procedure, the craniotomy is very small, being about 2 $mm^2$ in area. Due to this small size, desiccation of the cranial region has not occurred. However, if the craniotomy is larger in size, it is possible to apply agar or some other material to prevent moisture loss from the brain if this does become a problem.

A point of interest is the use of the pancuronium bromide. This chemical is stored in aliquots of 10 µl in order to prevent repetitive freezing and thawing. The suggested volume to be used in an experiment, being 1 µl per gram of weight, is usually sufficient to immobilize an adult fish. On occasion, however, this volume is not adequate. When this occurs and paralysis is not obtained, more pancuronium bromide can be administered intraperitoneally to the fish, as long as recording has not begun. When carrying out the injection, do not try to inject through the tough side scales; inject the fish in the softer abdomen region, near the vent. If the fish begins to move once the primary electrode has been positioned, there is a good chance that the needle has been broken off within the craniotomy, and the procedure must be repeated using a new animal. Through this work, it has been determined that pancuronium bromide can reduce the recorded neural activity in larval zebrafish (≤50% of baseline amplitude) and it is assumed that the same holds true for adults. However, in recent experience, the neural activity in an adult is robust enough that any dampening effects attributed to pancuronium bromide do not appear to adversely affect the ability to collect and analyze data. In contrast, confounds associated with motion can be significant. For this procedure, the benefits of complete immobility of the animal are of value beyond this limitation and the neural changes that are introduced

are robust enough to persist beyond any dampening effects. Also, any motion from the animal can displace the electrode, be registered by the electrophysiology recording equipment and possibly endanger the animal.

The limitations of this technique primarily lie in the fact that extracellular recording is the only possible way of recording neurological activity within the intact adult zebrafish. When positioning the primary electrode, the needle must be inserted into the craniotomy, preventing one from seeing exactly where the electrode is being placed. Though, with practice, it is possible to position the electrode within the same region and at the same depth consistently.

*In vivo* electrophysiology has largely been limited to zebrafish larvae. This is due to the ability to easily immobilize the small fish and the fact that they do not require intubation. Therefore, electrophysiological studies have focused on the larval stages and little has been done regarding the electrophysiological activity within the adult brain. This has prevented any comparisons between juvenile and adult neurological activity to be made. The use of the multi-tube intubation system permits for easy introduction of a variety of compounds to the fish. This also allows for the effects of different chemicals or drugs to be studied within both the larval and adult systems.


## Acknowledgements

This work was supported by NIH/NINDS Grant R01NS070159 (to T.M.D, J.D.L and A.T.S).


## Disclosures

The authors declare that they have no competing financial interests.

Figures

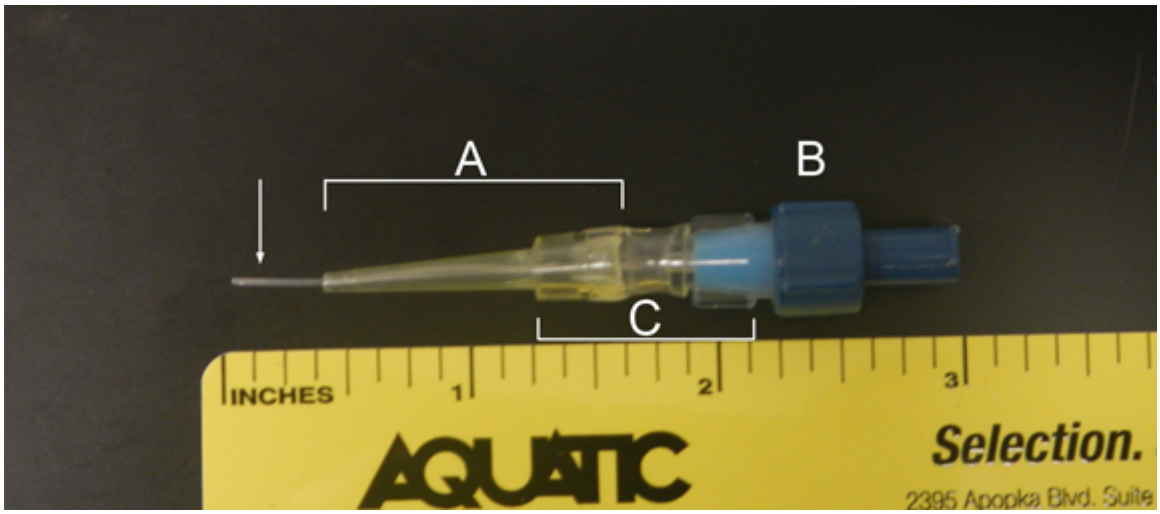


**Figure 3.1. Intubation Cannula.** Remove a 1.5 cm section from the wide end of a yellow P-200 pipetteman tip (A). Insert a 6 cm x 1 mm piece of tubing (arrow) into a luer-lock reducing connector (B) and insert this cannula into the modified pipette tip. Hold the pipette tip in position with the luer-lock using a short portion of $^{1}/_{8}$ in. tubing (C).

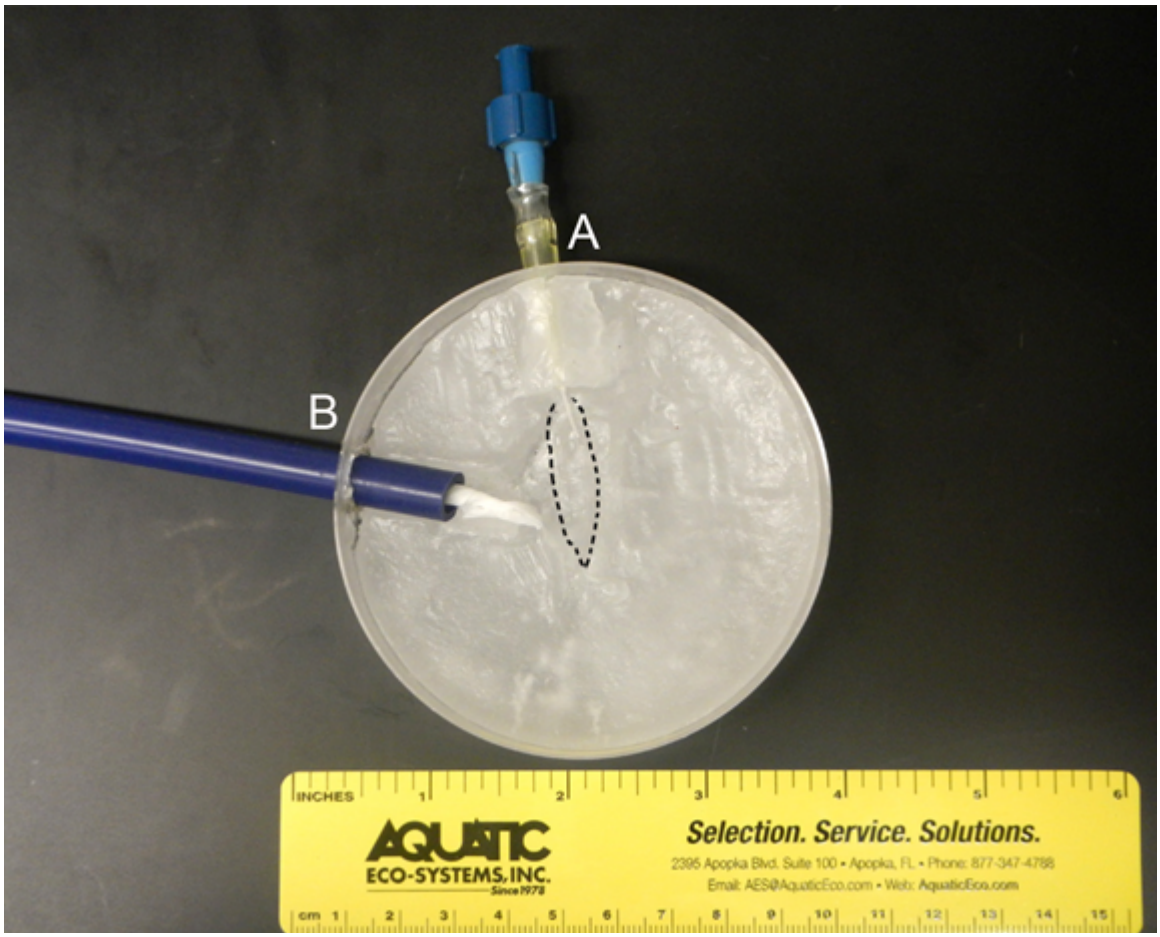


**Figure 3.2. Finished intubation base setup.** Once the Gulf Wax has cooled, place the cannula setup into the smaller hole of the intubation base (A). Twist a 1 inch-wide strip of 42 cm KimWipe into a tight spiral and insert it into the drainage tube such that the KimWipe extends on both ends. Insert one end of the drainage tubing into the large hole of the petri dish (B), allowing the lower end to extend into a 30 x 100 mm crystallizing dish (not in view). Position the tissue so that one end will lie near the animal's stomach area (outlined with black-dashed line) and the lower extension can drip into the dish.

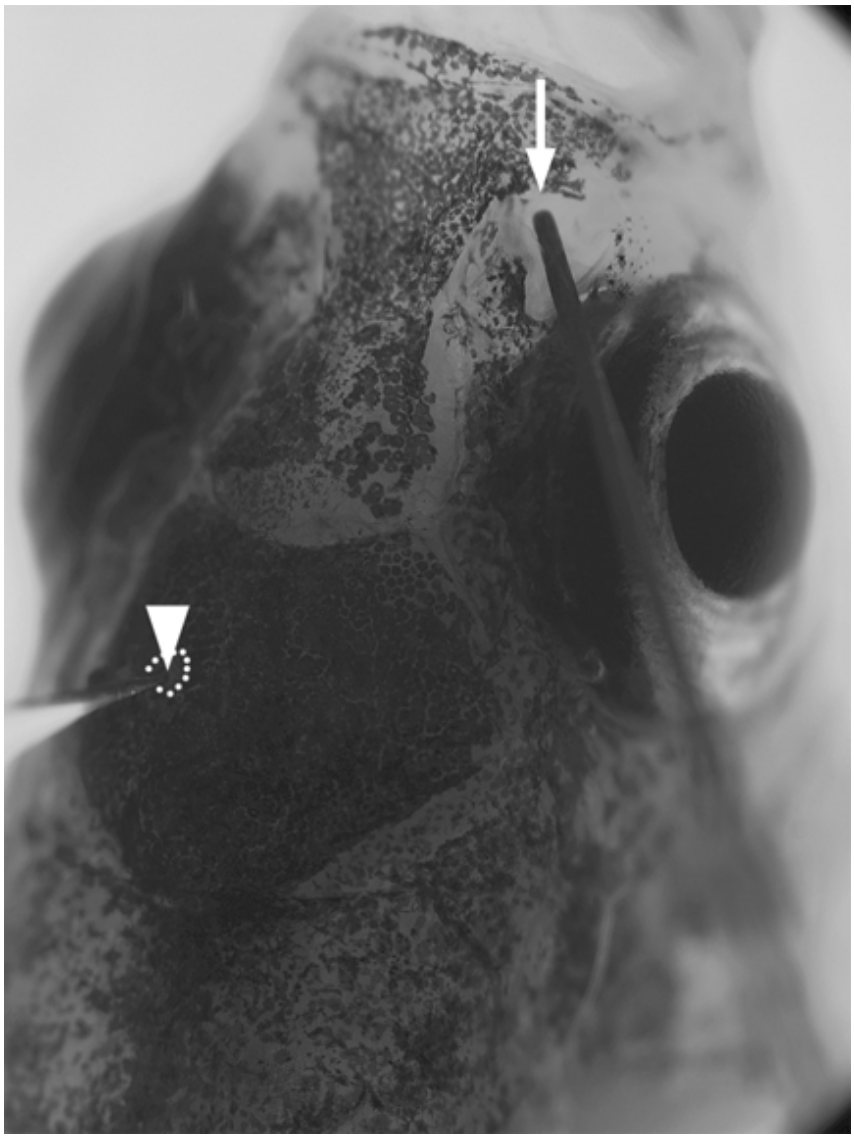

**Figure 3.3. Craniotomy.** Under the dissection microscope, use vanna spring scissors to remove ~2 $mm^2$ section of the cranium covering the optic tectum. This area looks like a dark, trapezoidal bony plate that sits behind the eye. The dotted circle demarcates where the craniotomy is positioned. The arrowhead shows there the needle of the primary electrode is positioned within the hole of the craniotomy. The primary electrode consists of a 2.5 in. section of 0.010 in. silver wire that has been electroplated with chloride ions and inserted into a borosilicate capillary needle. The capillary needle is filled with 2-3 µl of 2 M potassium chloride, or enough to partially cover the chloride-coated tip of the silver wire. The secondary electrode consists of a 15 in. section of the same wire used for the primary electrode except that a tip is soldered at one end, allowing it to be inserted into the back of the head-stage. The end of the secondary wire that is to be positioned touching the fish must also be electroplated with chloride ions. The arrow shows where the secondary electrode has been positioned within the right nostril of the adult fish.

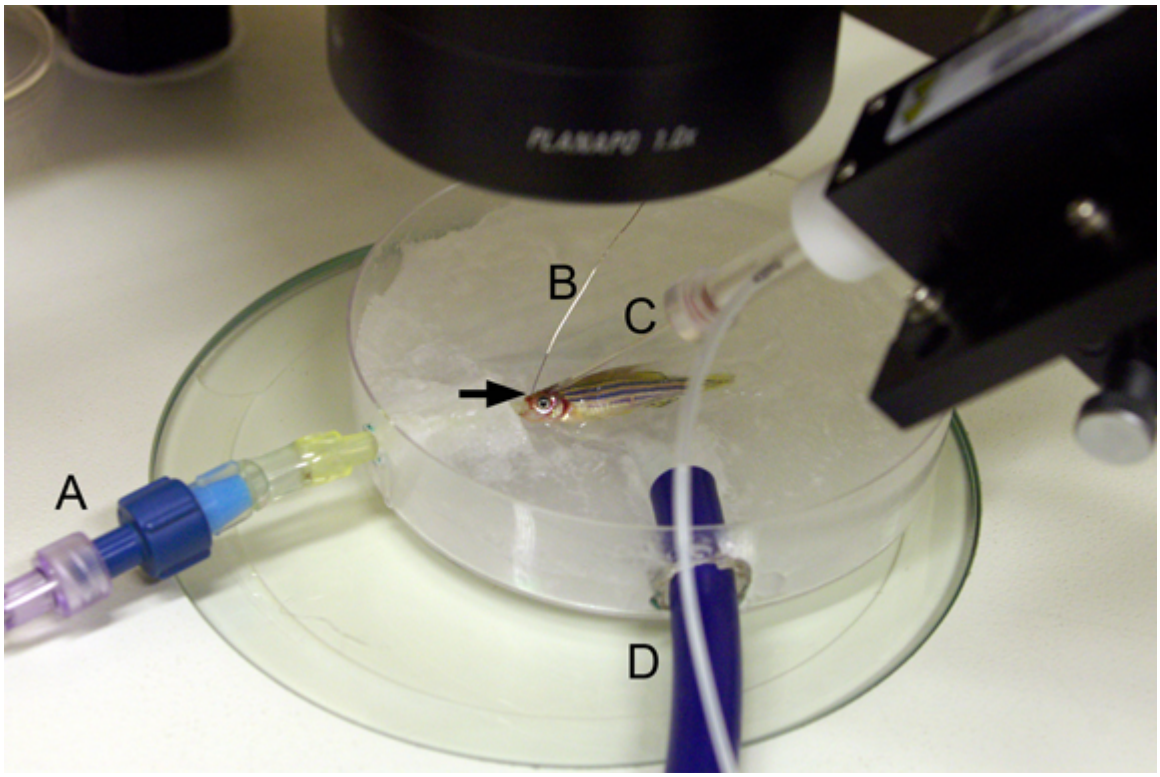


**Figure 3.4. Setup for collection of electrophysiological activity.** The intact intubation setup is moved to the electrophysiology microscope and the cannula is connected to the perfusion system (A). The system water must be turned on, allowing perfusion to start immediately. Using the micromanipulator, position the secondary electrode (B) so that the electrode tip is inserted into the animal's nostril or into the dip behind the upper jaw (Arrow). Insert the primary electrode needle (C) into the craniotomy opening. Insert the needle such that it is positioned fairly superficial within the optic tectum. The large drainage tube (D) extends from the intubation dish, out of the field of view, and the other end empties into the collection dish.

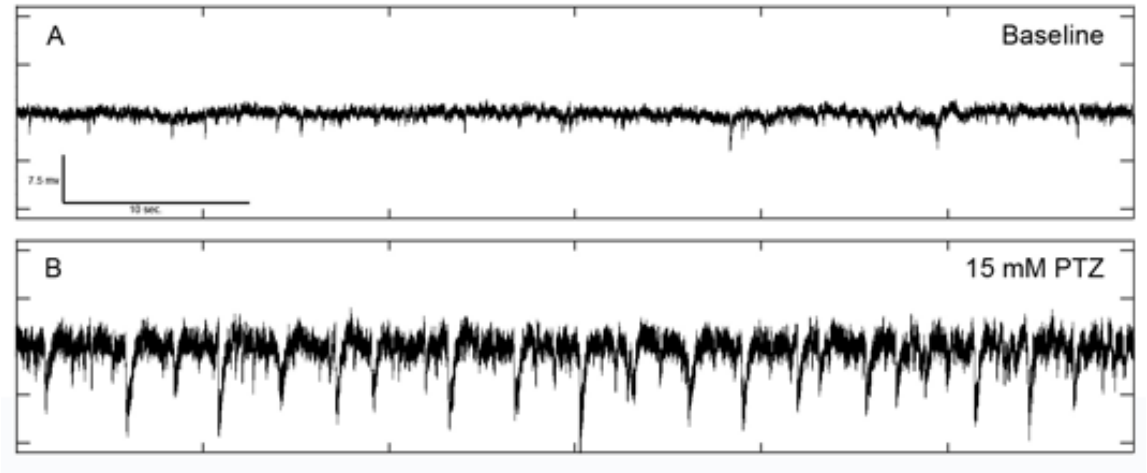


**Figure 3.5. Electrophysiological recordings within the optic tectum.** A) It was consistently observed that the native activity within the optic tectum of the adult zebrafish is stereotypically spontaneous, showing small amplitude (2-10 mV) activity throughout the duration of the recording. B) Following the introduction of 15 mM PTZ to the system, spontaneous epileptiform-like discharges began to develop about 5 min. following introduction. This activity was initially brief, small amplitude. With continued exposure to the PTZ, a consistent pattern of large amplitude (15-30 mV) discharges developed that were followed by smaller, more frequent bursts of activity.

References

Arnolds DE, Zottoli SJ, Adams CE, Dineen SM, Fevrier S, Guo Y, Pascal AJ (2002) Physiological effects of tricaine on the supramedullary/dorsal neurons of the cunner, Tautogolabrus adspersus. The Biological bulletin 203:188-189.

Bally-Cuif L, Vernier P (2010) Organization and Physiology of the Zebrafish Nervous System. In: Fish Physiology: Zebrafish, vol. 29 (Perry, S. F. et al., eds).

Baraban SC, Dinday MT, Castro PA, Chege S, Guyenet S, Taylor MR (2007) A large-scale mutagenesis screen to identify seizure-resistant zebrafish. Epilepsia 48:1151-1157.

Baraban SC, Taylor MR, Castro PA, Baier H (2005) Pentylenetetrazole induced changes in zebrafish behavior, neural activity and c-fos expression. Neuroscience 131:759-768.

Brockerhoff SE, Hurley JB, Janssen-Bienhold U, Neuhauss SC, Driever W, Dowling JE (1995) A behavioral screen for isolating zebrafish mutants with visual system defects. Proceedings of the National Academy of Sciences of the United States of America 92:10545-10549.

Burgess HA, Granato M (2007) Sensorimotor gating in larval zebrafish. The Journal of neuroscience : the official journal of the Society for Neuroscience 27:4984-4994.

Burgess HA, Schoch H, Granato M (2010) Distinct retinal pathways drive spatial orientation behaviors in zebrafish navigation. Current biology : CB 20:381-386.

Connaughton VP, Nelson R, Bender AM (2008) Electrophysiological evidence of GABAA and GABAC receptors on zebrafish retinal bipolar cells. Visual neuroscience 25:139-153.

DeMicco A, Cooper KR, Richardson JR, White LA (2010) Developmental neurotoxicity of pyrethroid insecticides in zebrafish embryos. Toxicological sciences : an official journal of the Society of Toxicology 113:177-186.

Fan X, Majumder A, Reagin SS, Porter EL, Sornborger AT, Keith CH, Lauderdale JD (2007) New statistical methods enhance imaging of cameleon fluorescence resonance energy transfer in cultured zebrafish spinal neurons. Journal of biomedical optics 12:034017.

Fetcho JR, Higashijima S, McLean DL (2008) Zebrafish and motor control over the last decade. Brain research reviews 57:86-93.

Gabriel JP, Mahmood R, Walter AM, Kyriakatos A, Hauptmann G, Calabrese RL, El Manira A (2008) Locomotor pattern in the adult zebrafish spinal cord in vitro. Journal of neurophysiology 99:37-48.

Haug MF, Biehlmaier O, Mueller KP, Neuhauss SC (2010) Visual acuity in larval zebrafish: behavior and histology. Frontiers in zoology 7:8.

Henze DA, Borhegyi Z, Csicsvari J, Mamiya A, Harris KD, Buzsaki G (2000) Intracellular features predicted by extracellular recordings in the hippocampus in vivo. Journal of neurophysiology 84:390-400.

Higashijima S, Schaefer M, Fetcho JR (2004) Neurotransmitter properties of spinal interneurons in embryonic and larval zebrafish. The Journal of comparative neurology 480:19-37.

Kaslin J, Nystedt JM, Ostergard M, Peitsaro N, Panula P (2004) The orexin/hypocretin system in zebrafish is connected to the aminergic and cholinergic systems. The Journal of neuroscience : the official journal of the Society for Neuroscience 24:2678-2689.

Kim YJ, Nam RH, Yoo YM, Lee CJ (2004) Identification and functional evidence of GABAergic neurons in parts of the brain of adult zebrafish (*Danio rerio*). Neuroscience letters 355:29-32.

Lazarova M, Samanin R (1983) Potentiation by yohimbine of pentylenetetrazol-induced seizures in rats: role of alpha 2 adrenergic receptors. Pharmacological research communications 15:419-425.

Loscher W, Honack D, Fassbender CP, Nolting B (1991) The role of technical, biological and pharmacological factors in the laboratory evaluation of anticonvulsant drugs. III. Pentylenetetrazole seizure models. Epilepsy research 8:171-189.

Makhankov YV, Rinner O, Neuhauss SC (2004) An inexpensive device for non-invasive electroretinography in small aquatic vertebrates. Journal of neuroscience methods 135:205-210.

Maximino C, Lima MG, Araujo J, Lieveira K, Herculano AM, Stewart AM, Kyzar EJ, Cachat J, Kalueff AV (2012) The Serotonergic System of Zebrafish: Genomics, Neuroanatomy and Neuropharmacology.

McLean DL, Fetcho JR (2004) Ontogeny and innervation patterns of dopaminergic, noradrenergic, and serotonergic neurons in larval zebrafish. The Journal of comparative neurology 480:38-56.

Mueller KP, Neuhauss SC (2010) Behavioral neurobiology: how larval fish orient towards the light. Current biology : CB 20:R159-161.

Mueller T, Vernier P, Wullimann MF (2004) The adult central nervous cholinergic system of a neurogenetic model animal, the zebrafish Danio rerio. Brain research 1011:156-169.

Sato Y, Miyasaka N, Yoshihara Y (2007) Hierarchical regulation of odorant receptor gene choice and subsequent axonal projection of olfactory sensory neurons in zebrafish. The Journal of neuroscience : the official journal of the Society for Neuroscience 27:1606-1615.

Tao L, Lauderdale JD, Sornborger AT (2011) Mapping Functional Connectivity between Neuronal Ensembles with Larval Zebrafish Transgenic for a Ratiometric Calcium Indicator. Frontiers in neural circuits 5:2.

Vargas R, Johannesdottir IT, Sigurgeirsson B, Thornorsteinsson H, Karlsson KA (2011) The zebrafish brain in research and teaching: a simple in vivo and in vitro model for the study of spontaneous neural activity. Advances in physiology education 35:188-196.

Westerfield M (1993) The zebrafish book : a guide for the laboratory use of zebrafish (Brachydanio rerio). Eugene, OR: M. Westerfield.

Materials List

| Name of Reagent/ Equipment | Company | Catalog Number | Comments/ Description |
|---|---|---|---|
| 70 % Ethanol | | | |
| 2 M Potassium Chloride | J.T. Baker | | |
| 2 M Sodium Chloride | J.T. Baker | | |
| 0.4 % Tris-Buffered Tricaine | Sigma-Aldrich | E10521 | pH 7.2-7.4; stored at -20 $^{o}$C |
| Pancuronium Bromide | Sigma-Aldrich | P1918 | Diluted to 1 μg/μl in 1x phosphate buffered saline |
| Aquarium water | Sigma-Aldrich | | pH 7.0-7.4, conductivity of 400-450 μS; maintained by Instant Ocean and Sodium Bicarbonate |
| Pentylenetetrazol | Sigma-Aldrich | P6500 | Diluted to 300 mM in 1x phosphate buffered saline |
| Nanofil syringe | World Precision Instruments, Inc. | 06A | |
| 34 guage beveled needle | World Precision Instruments, Inc. | NF34BV | |
| Sponge | | | |
| Foam-backed find sand paper | | | 5x5 $cm^2$ is large enough |
| 9V battery | | | |
| With with alligator clips | | | Need 2 |
| 37x42 cm KimWipe | Kimberly-Clark Professional | TW31KEM | |
| 11x21 cm KimWipe | Kimberly-Clark Professional | TW31KWP | |
| Tube | | | |
| Tube | | | |
| Microscope (Leica MZ APO) | | | Another microscope can be used |
| Vanna scissors | Roboz Surgical Instruments Co., Inc. | 15018-10 | |
| 60 cc luer-lock syringe tubes | Becton, Dickinson and Company | 309653 | |
| 3-way stopcocks with | | | |

| | | | |
|---|---|---|---|
| luer connections | | | |
| 1-way stopcock with luer connection | | | |
| Fisherbrand 100x15 mm petri dish | Fisher Scientific | NC9299146 | |
| Fisherbrand 60x15 mm petri dish | Fisher Scientific | S67961 | |
| 4” capillary tube | World Precision Instruments | TW100F-4 | |
| P-97 Flaming/Brown Micropipette Puller | Sutter Instrument Co. | | |
| Digidata 1440 | Molecular Devices | | |
| Axon Aloclamp 900A | Molecular Devices | | |
| Axoclamp software | Molecular Devices | | |
| HS-9Ax 1U headstage | Molecular Devices | | |
| 0.010” Silver wire | A-M Systems, Inc. | | |
| Q-series electrode holder | Warner Instruments | QSW-A10P | |
| 10cc luer lock syringe | | | |
| 1 mm x 15” tubing | | | Connect luer lock syringe to Q-series electrode holder |
| Micromanipulator | Warner Instruments | | Need 2 |
| Microsoft-based PC | Dell | | |
| Faraday Cage | | | |
| Air Table | | | |
| Dissecting Microscope | | | |

# CHAPTER 4

# A COMPARISON OF EVOKED SEIZURE ACTIVITY IN THE MATURE AND IMMATURE ZEBRAFISH BRAINS [1]

[1] Beebe, L.L., Ball, R.E., Page, A.T., Acuff, S., Singer, R., Gaudet, J., Keith, C.H., Sornborger, A.T., and James D. Lauderdale. To be submitted to *Journal of Neuroscience*.

Abstract

Zebrafish are now being used as a model to study seizure expression as a function of developmental stage. However, the developmental endpoint (adult) has not yet been studied. In this paper, we studied seizures at two fiducial points in the development of the zebrafish, 7 dpf and the adult (> 6 months). We compared the behavioral and electrographic correlates of pentylenetetrazol (PTZ)-induced seizures in adult zebrafish to those observed in larval zebrafish. Using electrophysiological techniques, we compared how adults and larvae responded to an array of anti-epileptic drugs (AEDs). In order to understand large-scale dynamics in the CNS, we imaged seizure-related $Ca^{2+}$ events using the ratiometric $Ca^{2+}$ indicator, *cameleon*. The results of our study were that larval zebrafish exhibited fundamentally different seizure characteristics as compared to the adult. Additionally, AEDs differentially modulated these two developmentally distinct nervous systems.

## Introduction

Approximately 0.6% of the human population has epilepsy (Granieri et al., 1983, Hauser et al., 1991, Forsgren et al., 2005). Of these individuals, approximately one quarter are children (Granieri et al., 1983, Hauser et al., 1991, Forsgren et al., 2005). Causes of this disorder can be primary genetic (no underlying gross neuropathology) (Pandolfo, 2013), inherited metabolic disease (Rahman, 2012), chromosomal abnormality (Singh et al., 2002) and abnormal cortical development (Sisodiya, 2004) and trauma (Frey, 2003), among others. The seizures symptomatic of epilepsy are dynamic neurological events that evolve in time from second to second (Schindler et al., 2007). Their onset is modulated by circadian rhythms (Sanchez Fernandez et al., 2013) and their severity typically changes over the duration that an individual has the disorder (Watanabe et al., 1999). Pediatric seizures are known to disrupt the underlying functional neuroanatomy, impacting cognitive development (Vannest et al., 2013).

Animal models have played a key role in elucidating the different pathogenic mechanisms underlying seizure activity. Of the animal models, the rat, and in particular the rat hippocampus, is the most widely used (e.g. a PUBMED search on 'rat seizure' shows 16026 results and 'rat hippocampus seizure' shows 5557 at the time of writing). In the rat, both *in vivo* and *in vitro* seizures have been induced by exposure to chemoconvulsants for both short- and long-terms (via kindling) (Sloviter, 2008) and by trauma due to cranial insult (causing large-scale cell loss and subsequent proliferation of granule cell axons) (Buckmaster and Jongen-Relo, 1999, Ratzliff et al., 2002, Sutula et al., 2003), among other induction techniques. However, similar models and induction paradigms have been used in other mammals and vertebrates, including mice (reviewed

in Galanopoulou, 2013), turtles (Volanschi and Servit, 1969, Velluti et al., 1997), frogs (Servit et al., 1968, Servit and Strejckova, 1970b, Hewapathirane et al., 2008, Steinlein, 2010), and fish (Strejckova, 1969, Servit and Strejckova, 1970a, Baraban, 2005, Baraban et al., 2005), and also in non-vertebrates such as *Drosophila* and *C. elegans* (Baraban, 2007, Song and Tanouye, 2008, Parker et al., 2011), which suggests that many elements of seizure initiation and propagation are highly conserved.

Recently, the zebrafish larva has begun to be used to study pediatric seizures (Baraban et al., 2005, Berghmans et al., 2007, Winter et al., 2008, Hortopan et al., 2010, Vermoesen et al., 2011, Baxendale et al., 2012, Orellana-Paucar et al., 2012, Afrikanova et al., 2013). There are a number of reasons that the zebrafish is a useful addition to the above seizure models. Firstly, it has a short generation time in comparison to the mouse and rat, giving it an advantage for screening for primary genetic causes of seizure (Hortopan et al., 2010). Secondly, it is small, transparent (< 12 dpf) and can be used for whole-brain functional imaging of neuronal activity (Ahrens et al., 2013), including the propagation of seizure-related neural activity throughout the brain (Tao et al., 2011). Thirdly, a growing genetic toolset exists for studying its nervous system, including many genetically engineered proteins for the study of specific neuronal promoters such as the gal4 system (Scott et al., 2007, Halpern et al., 2008) and optogenetic tools (Douglass et al., 2008, Baier and Scott, 2009, Wyart et al., 2009, Friedrich et al., 2010, Akerboom et al., 2013, Portugues et al., 2013), which can be used to specifically perturb identified neuronal networks. Fourthly, standard seizure induction protocols have been shown to be effective for seizure induction (Baraban, 2005, Baraban et al., 2005, Winter et al., 2008, Hortopan et al., 2010, Tao et al., 2011, Vermoesen et al., 2011, Baxendale et al., 2012,

Afrikanova et al., 2013), and seizure-like electrical activity can be triggered by a range of chemoconvulsants in the larval (typically 5-7 dpf) zebrafish (Baraban, 2005, Baraban et al., 2005, Orellana-Paucar et al., 2012, Afrikanova et al., 2013). Lastly, zebrafish offer the potential as a high-throughput primary screen to identify novel anticonvulsants (Baraban et al., 2005, Berghmans et al., 2007, Winter et al., 2008, Baxendale et al., 2012, Orellana-Paucar et al., 2012, Afrikanova et al., 2013).

One of the main outstanding issues in using the zebrafish as a pediatric seizure model is whether seizure activity in the immature zebrafish is truly distinct from that in the mature zebrafish. We hypothesized that the adult brain would be more susceptible to PTZ-induced seizure-like activity than 7 days post fertilization (dpf) larval zebrafish because of ontogenetic differences in network complexity and neurotransmitter systems. To test this hypothesis, we compared the electrographic correlates of pentylenetetrazol (PTZ)-induced seizure in adult zebrafish to those observed in larval zebrafish at 7 days post fertilization (dpf). Using electrophysiological techniques, we compared how adults and larvae responded to an array of AEDs. Finally, to understand large-scale dynamics across the entire CNS, we imaged seizure-related $Ca^{2+}$ dynamics using the ratiometric $Ca^{2+}$ indicator, *cameleon*. Our results demonstrate that seizure activity in the immature zebrafish is distinct from that found in adults.

## Materials and Methods

### *Zebrafish lines and maintenance*

Adult and larval zebrafish (*Danio rerio*) were obtained from lines maintained in the University of Georgia Zebrafish Facility following standard procedures (Westerfield, 2007). Embryos and larvae were staged using standard staging criteria (Kimmel et al.,

1995, Westerfield, 2007). Wild-type fish of the WIK strain were originally obtained from the Zebrafish International Research Center (ZIRC). Zebrafish transgenic for Tg( *fli1a:EGFP)*y1, which were used to evaluate the vasculature in the optic tectum, were originally obtained from Dr. Brant Weinstein (Laboratory of Molecular Genetics in the National Institute of Child Health and Human Development). Zebrafish transgenic for Tg(*elavl3:cameleon*) (Higashijima et al., 2003) were originally provided by Dr. Joe Fetcho (Cornell University, NY). All adult fish were maintained in an Aquatic Habitats (Apopka, FL) multi-rack system. Habitat water consisted of reverse osmosis filtered/sterilized water to which sodium bicarbonate and other salts (Instant Ocean, Aquarium Systems, Inc., Mentor, OH, USA) were added to maintain pH from 7.0–7.4 and conductivity between 400 and 430 μS. All experimental procedures were conducted in strict accordance with the National Institutes of Health Guide for the Care and Use of Laboratory Animals and followed protocol #A2011 09-003, which was reviewed, approved, and overseen by the University of Georgia Institutional Animal Care and Use Committee.

***Drugs***

All drugs used for this study were purchased from Sigma-Aldrich (St. Louis, MO). Stock PTZ of 300 mM was made in distilled water and stored in aliquots at -20°C. Concentrations of baclofen (50 μM), ethosuximide (10 mM), and phenytoin (100 μM) were selected following Baraban et al. (2005). The concentration of valproic acid sodium salt (VPA, 5 mM) was selected per Baraban et al. (2005) and Lee et al. (2010). All drugs were prepared in aqueous solutions following protocols used for administration to mammals (e.g. Jutkiewicz et al., 2006). Presumably, compounds dissolved in the

intubation solutions were readily absorbed through the gills of the adult fish and entered the blood stream; although it is also possible that compounds were absorbed through the gastrointestinal tract. In the case of larvae, compounds dissolved in embryo medium are readily absorbed through the gastrointestinal tract or across the skin (Peterson and Fishman, 2004).

***Seizure induction and behavioral observations***

Adult zebrafish were placed in aquarium water in a 1000-mL beaker to which pentylenetetrazol (PTZ) was bath applied at 2.5, 5.0, 10, 15, 20, and 30 mM concentrations. After tonic seizure was reached (animal became immobile and inverted), the animal was removed to a recovery tank of system water. Behavior was monitored with a digital camera (Sony Digital Handycam Steady Shot DCR-TRV240 NTC) mounted on a tripod. Recordings were visually analyzed for seizure stage, locomotion, and swimming behavior.

***Craniotomy***

Craniotomy was performed following our standard protocol (Johnston et al., 2013). Briefly adult animals were anesthetized by bath application of 630 μM tris-buffered tricaine methanesulfonate (MS-222, tricaine; pH 7.2) in habitat water (see *Zebrafish lines and maintenance* section for composition), given an intraperitoneal (IP) injection of ~1 μg/g body weight of pancuronium bromide, and placed on an intubation tray. Tricaine anesthesia was maintained by perfusion at a flow rate of ~1 mL/min during the entire procedure, and the animal was kept moist by application of a habitat-water moistened tissue. Approximately 0.4 $mm^2$ of the cranium overlying the sinister optic

tectum was surgically and very carefully removed using Vannas scissors (Roboz Surgical Instruments Co., Inc., Gaithersburg, MD).

***Electrophysiology***

While still being perfused with tricaine, a sharp glass pipet microelectrode (10–20 MΩ impedance) was inserted under visual control through the opening in the skull and into the optic tectum to a target depth of about 100 μm. Penetration ventrally into the presumptive stratum griseum periventricular greatly reduced the amplitude of electrical activity. A chloride-coated silver wire (0.010" A-M Systems, Inc. Sequim, WA) reference electrode was placed in the nostril or in the depression behind the upper mandible.

Larval zebrafish, 7 days post-fertilization (7 dpf) of age, were immobilized by exposure to 0.5 mM pancuronium bromide in normal Ringer's solution (116 mM NaCl, 2.9 mM KCl, 1.8 mM $CaCl_2$, 5.0 mM HEPES, pH 7.2.) and mounted in 1.2% agarose made with normal Ringer's in a 35 mm petri dish, to which 2850 μL Ringer's solution was added. A sharp glass pipet microelectrode (10–20 MΩ impedance), loaded with normal Ringer's solution, was inserted into the optic tectum and the chloride-coated silver reference wire was placed to touch the mid-dorsal side of the animal. After a 5-minute baseline was recorded, 150 μL of 300 mM PTZ solution was added to induce seizure. Once a consistent pattern of PTZ-induced spikes was established (40 to 60 min), an AED was added and recorded for at least 15 minutes.

Electrical activity was recorded using an Axoclamp 900a amplifier (Axon Instruments, Union City, Ca, USA). The amplified voltage was passed through a Hum Bug Noise Eliminator (AutoMate Scientific, Berkley, CA, USA), band-pass filtered from

1 Hz–0.1 kHz, and digitized at 10 kHz using a Digidata 1440 interface and stored on a PC using pClamp software (version 10.3, Molecular Devices). For some experiments, neuronal activity was recorded with an MDA-4I AC Differential Amplifier (Bak Electronics, Mount Airy, MD) and Tektronix DPO 3012 Digital Phosphor Oscilloscope (Beaverton, OR) then analyzed with custom scripts using MATLAB (MathWorks Inc.).

### *Focal Iontophoretic DiI Injections*

Focal iontophoretic DiI injections were performed as previously described (Birgbauer et al., 1995) except using a 10 MΩ resistor (Hodor and Ettensohn, 1998). DiI (1,1'-dioctadecyl-3,3,3',3'-tetramethylindocarbocyanine, perchlorate; Molecular Probes/Invitrogen) was diluted in absolute ethanol to make a 0.5% (w/v) solution. The DiI solution was back-loaded into sharp injection micropipettes (5–10 MΩ resistance if filled with KCl) pulled from thin-walled aluminosilicate glass capillaries (with filament) using a Sutter P-90/PC Micropipette Puller. The micropipettes were held in a pipette holder (Warner Instruments) with a silver wire that was immersed into the DiI solution. After positioning the micropipette into the optic tectum, DiI was injected iontophoretically (Myers and Bastiani, 1993) with a maximum of 900 nA for 2–10 seconds using a 9-volt battery through a 10 MΩ resistor.

### *Calcium Imaging*

Calcium imaging on larvae was performed as previously described (Fan et al., 2007, Tao et al., 2011), except that larvae were immobilized using pancuronium bromide in normal Ringer's solution as described above. Briefly, larvae were mounted in an imaging chamber using 1.2% agar. Confocal microscopy was performed on a Leica TCS SP5 confocal microscope (Leica DMI 6000 B, Leica Microsystems Inc.). Cameleon

YC2.1 fluorescence was excited with the 458 nm line of a 100-mW argon laser. Emission was imaged at 485±20 nm (cyan) and 535±15 nm (yellow). Larvae were continuously exposed to 15 mM PTZ. Images (8-bit, 128 x 128) were collected at a rate of 1 Hz. Data was analyzed using the Statistical Optimization for the Analysis of Ratiometric Signals (SOARS) algorithm (Broder et al., 2007).

***Histology, Immunolabeling, and Microscopy***

Sections were cut using one of two techniques. All sections cut through adult brains, and sections cut through larval brains transgenic for *fli1a:EGFP*, were performed following a vibratome sectioning protocol developed for visualizing vasculature in embryonic mice (Bryson et al., 2011); sections were either cut 100 µm thick and used for antibody staining or visualization of neuroanatomy or 200 µm thick and used to visualize *fli1a:EGFP* expression in the tectum. Frozen sections made from larva for immunolabeling were prepared as previously described (Barthel and Raymond, 1990).

To detect GAD protein, sections were incubated with a rabbit polyclonal to GAD65 + GAD67 (1:1000; Abcam, ab11070) followed by Alexa Fluor 594 donkey anti-rabbit IgG (1:1000; Life Technologies, A-21207), both in blocking solution (see below). For immunolabeling experiments using frozen sections, sections were blocked with 3% BSA/1% donkey serum/PBS (phosphate buffered saline; Sambrook and Russell, 2001) for 1 h, incubated with the primary antibody for 1 h, washed several times in PBS, incubated for 30 min with the secondary antibody, rinsed several times in PBS, and coverslipped using VECTASHIELD (Vector) mounting media; all steps were performed at room temperature. Immunolabeling experiments using vibratome sections were performed as previously described (Bryson et al., 2011) with some modification. Briefly,

sections were blocked overnight at 4°C in 10% donkey serum/PBSTx (phosphate buffered saline, pH 7.2; 0.15% Triton X-100) and then incubated overnight at 4°C with the primary antibody. After removal of the primary antibody, sections were washed three to four times with PBSTx over an 8 hour period and incubated overnight at 4°C with the secondary antibody. Samples were washed with PBSTx, dehydrated with a graded MeOH series, and cleared with Benzyl Alcohol:Benzyl Benzoate (BABB) in a 1:2 ratio. Sections were mounted in depression slides with BABB. Specific signals were visualized using either standard fluorescence microscopy using a Zeiss Axio Imager.D2 or laser scanning confocal microscopy using a Zeiss LSM 510 Meta Confocal Microscope. Images of whole brains were captured using a dissecting microscope (Zeiss SV11) outfitted for epifluorescence (Photofluor II, Chroma; GFP Illuminator, Kramer Scientific Corp.).

## Results

### *Behavior of adult zebrafish during PTZ-induced seizure*

To characterize the behavior of adult zebrafish to PTZ-exposure, healthy wild-type animals of both sexes and 7 to 24 months of age, with body weights ranging from 0.24 g to 1.32 g (with an average of 0.62 mg), were exposed to PTZ concentrations ranging from 2.5 to 30 mM (Fig. 4.1). Behavior was recorded following the staging convention originally established for larvae by Baraban et al. (2005) where Stage I was characterized by increased swimming activity, Stage II was characterized by a loss of normal swimming movement and posture, and Stage III was characterized by tetanic muscle contractions leading to a loss of posture, e.g. fish falls to one side and remains immobile. The types of behavior and the time spent in each behavior changed in a

concentration-dependent manner. Stage III behavior was the easiest to score and illustrated the trend in the data for all behaviors (Fig. 4.1).

Adult zebrafish normally swim in an upright posture with a smooth, sinusoidal motion and directional changes are preceded by characteristic changes in body shape called 'C' and 'J' bends. These changes were similar to those described for larvae (Budick and O'Malley, 2000, Danos and Lauder, 2007, Liu et al., 2012). When exposed to PTZ concentrations between 2.5 mM and 30 mM, all adult fish (n = 178) exhibited a significant increase in swimming activity (Stage I), which included increased velocity, distance moved, and abrupt turning behavior. At PTZ concentrations ≥ 10 mM, all animals (n = 110) exhibited progressively exaggerated C and J bends followed by an arching behavior that was much more violent than that observed in control animals. This was followed by Stage II behavior, in which the animal no longer swam primarily in the horizontal plane, but began breaching out of the water in a corkscrew fashion. Some fish performed these maneuvers upside-down. Typically, this behavior was rapidly followed by tetanus (Stage III) wherein the fish became rigid, with gills and fins splayed and a slight backwards arch to the posture.

Fish exhibiting changes in behavior were observed for all concentrations of PTZ tested; however, the numbers of animals affected and time to seizure-associated behaviors were dose-dependent (Fig. 4.1). At PTZ concentrations ≥ 10 mM, all animals (n = 110) progressed to tetanus within 23 minutes of exposure to the drug. At PTZ concentrations of 2.5 and 5 mM, latency to Stage III seizure behavior was variable, and some fish (~30% at 2.5 mM and ~11% at 5 mM) never exhibited tetanus during a 90 minute period of exposure. However, these fish did exhibit Stage I and, to a lesser degree,

Stage II behaviors. At PTZ concentrations ≤ 10 mM, fish exhibiting tetany often quickly recovered on their own and resumed swimming without assistance. However, fish exposed to PTZ concentrations ≥ 15 mM had to be removed immediately upon a tetany to a recovery tank or they would not survive. This was most likely due to hypoxia from the lack of operculum motion: fish intubated prior to exposure to high concentrations of PTZ (15–30 mM) recovered. Under these test conditions, we did not observe any statistical differences in the response of animals to PTZ based on sex, weight, or age (data not shown).

***Electrophysiological correlates of PTZ-seizure activity in adult zebrafish***

Field recordings were taken from the optic tectum of healthy adult wild-type fish (Fig. 4.2). A PTZ concentration of 15 mM was chosen for these experiments because in the behavioral assays all animals exhibited tetany within a 1 to 3 minute time period. Additionally, this concentration permitted direct comparison with the electrographic results reported for 7 dpf zebrafish larvae by others (Baraban, 2005, Baraban et al., 2005, Baraban et al., 2007, Afrikanova et al., 2013) and our results below. Adult fish of both sexes were anesthetized with tricaine, given an intraperitoneal (IP) injection of the muscle relaxant pancuronium bromide, and placed on an intubation tray that allowed sterile habitat water to gently flow into the animal's mouth, over its gills, and out through the opercula. Electrical activity was monitored with a field electrode placed under visual guidance through a small (~0.4 $mm^2$) opening over the left optic tectum made by craniotomy (Fig. 4.2A). Because tricaine is a known sodium channel blocker (Arnolds et al., 2002), and was observed to dampen native brain activity (data not shown), animals were allowed to recover from anesthesia prior to starting the experiment. Full recovery

from tricaine anesthesia as measured by electrographic activity typically took between 20 and 40 minutes (data not shown, n = 7). Animals remained immobile during the entire time of the experiment due to the administration of pancuronium bromide.

A stable discharge pattern characterized by high frequency, low-amplitude discharges and relatively low-frequency, high-amplitude (>4 mV) events was established within 10 minutes of exposure to PTZ (Fig. 4.2B-C). Examination of isolated small-amplitude discharges and isolated high-amplitude discharges revealed that they were similar in character to the 'interictal' and 'ictal' bursts reported for zebrafish larvae exposed to 15 mM PTZ (Baraban et al., 2005). These events were not observed during baseline recording periods prior to PTZ exposure (Fig. 4.2B) and never occurred in control fish treated with pancuronium bromide and intubated with habitat water for periods up to 1.5 hours (n = 7; data not shown). Time-frequency analyses (Mitra and Pesaran, 1999, Mitra and Bokil, 2008) of the evolution of PTZ-evoked changes in electrographic activity revealed that in all cases after a delay the electrographic log-spectrum approached a regular pattern with peak at low frequencies, but increased power across all frequencies, with occasional temporal modulation (Fig. 4.2C). The power in recordings of PTZ-induced discharges increased by 10-15 dB over baseline and peaked at approximately 0.5 Hz (Fig. 4.2D).

***Characterization of recording field***

To characterize electrode placement, DiI was focally applied using the same experimental setup as for the field recording except that, instead of recording a field potential, DiI was applied using iontophoresis. The typical region of electrode placement is shown in Fig. 4.2E-F. Cryosections through the labeled regions revealed that the

electrode tip was typically located 118±24 μm (n = 5) from the dorsal surface of the tectum (Fig. 4.2F). In all cases, DiI fluorescence was observed spanning the stratum opticum and stratum griseum along the dorsal-ventral axis of the tectum and typically extended ~100 μm radially from the tip of the electrode (Fig. 4.2F). Labeled cell bodies and tracts in the stratum griseum periventricular were also observed. These results suggest that the bulk of the field potentials recorded were generated by neurons with processes in the stratum griseum centrale.

***Pharmacology of PTZ-induced seizures in adult zebrafish***

We tested how the compounds valproic acid (VPA), ethosuximide, phenytoin, and baclofen modulated synaptic transmission during PTZ-evoked seizure activity. These are all compounds that have been tested on both rodents and larval zebrafish (Oliver et al., 1977, Krall et al., 1978, Piredda et al., 1986, Swinyard et al., 1986, Ferrendelli et al., 1989, Baraban, 2005, Baraban et al., 2005, Berghmans et al., 2007, Baxendale et al., 2012, Afrikanova et al., 2013). For these experiments, baseline activity was recorded for 5 min followed by introduction of 15 mM PTZ into the intubation solution, which was then perfused until a stable pattern of epileptiform activity developed (typically 30–45 min exposure). Pharmacological compounds were then introduced in combination with 15 mM PTZ for up to an hour. Electrographic activity was recorded the entire time.

VPA has been shown to be very effective at blocking PTZ-induced burst discharges in both rodents and larval zebrafish (Krall et al., 1978, Ferrendelli et al., 1989, Baraban et al., 2005, Watanabe et al., 2010, Afrikanova et al., 2013), and similar results were obtained in adult zebrafish (Fig. 4.3A-C and data not shown). Time-frequency analyses revealed that addition of VPA changed the power spectrum of PTZ-induced

electrographic activity over time (Fig. 4.3A-C). In the high alpha/low beta band (12 - 30 Hz) activity characteristic of oscillatory potentials at isolated frequencies was evident (see annotated frequencies at 15 Hz (Fig. 4.3B) and 12 Hz (Fig. 4.3C). This activity drifted somewhat over time, but not by more than a few Hz.

Ethosuximide, another classic AED that is used to treat absence seizures in humans, has been reported to be effective at blocking PTZ-induced seizures in rodents (Krall et al., 1978, Mirski and Ferrendelli, 1986, Ferrendelli et al., 1989, Jutkiewicz et al., 2006, Watanabe et al., 2010), but has mixed results reported for larval zebrafish, with one group reporting a block of PTZ-induced discharge (Afrikanova et al., 2013) and another reporting little effect (Baraban et al., 2005). In adults, ethosuximide added to PTZ significantly changed the frequency dynamics of electrographic activity over time (Fig. 4.3E); notably, it induced an overall depression in which the high amplitude power at low frequencies became narrower (Fig. 4.3E). However, intermittent bursts with power at higher frequencies were evident.

Phenytoin, an anticonvulsant that prolongs $Na^+$ channel inactivation (Mantegazza et al., 2010), has been reported to reduce PTZ-burst discharge in larval zebrafish in one study (Baraban et al., 2005) but have no effect in another (Afrikanova et al., 2013). In adults, phenytoin did not significantly modulate PTZ induced activity (data not shown). Conversely, baclofen, a $GABA_B$ receptor agonist, is known to potentiate PTZ-evoked seizure activity in zebrafish larvae (Baraban et al., 2005), and also potentiated activity in adult fish (Fig. 4.3F).

***Comparison of electrographic seizure activity in adults and larvae***

In the adult zebrafish, putative ictal and interictal events were generated in rapid succession, typically with one or two sharp deflections of the potential per five-second interval in the field recording. This gave rise to a smooth spectrum as a function of time once PTZ-evoked activity stabilized (Fig. 4.4A-C). By contrast, electrographic activity in the larva was fundamentally different (Fig. 4.4D-F). The overall amplitude of putative ictal and interictal spikes was from 3 to 8 dB lower than in the adult (compare, for instance, colorbars in Fig. 4.4C,F) and bursts of spikes were separated by longer times (Fig. 4.4D-F) relative to the adult. This led to a characteristic spectral response with sharp changes at all frequencies in the spectrogram corresponding to the bursts (Fig. 4.4F).

To compare the larval and adult responses to synaptic modulation, we tested whether PTZ-evoked electrographic activity changed in response to the compounds VPA, ethosuximide, and phenytoin (Fig. 4.5). Burst separation time after PTZ-evoked activity stabilized in the larvae typically varied from approximately 20 to 60 s with some separations of 100 s or more. Relative to these inter-event intervals, exposure to VPA gave rise to longer event intervals (~80-100, Fig. 4.5C). Ethosuximide also had a tendency toward longer intervals, but this was not as consistent (Fig. 4.5E), and phenytoin had no obvious effect (Fig. 4.5G).

***Synaptic $Ca^{2+}$ release due to bursting activity in zebrafish larvae and adults***

To characterize the spatial distribution of neuronal activity, we imaged $Ca^{2+}$, a proxy for synaptic transmission, with the genetically encoded calcium indicator *cameleon*. Typical imaging data showed widespread $Ca^{2+}$ release in the CNS, including regions in the forebrain, tectum, tegmentum, hindbrain and spinal cord (Fig. 4.6C,E). The

dominant contributor to the variability of the imaging data typically showed $Ca^{2+}$ release at a rate comparable to the burst rate measured with electrophysiological methods (Fig. 4.6D, compare 31 anti-correlated $Ca^{2+}$ events/1000 s in Fig. 4.6D with 15 events/500 s in Fig. 4.4F).

Because of its much larger size, we could only image part of the adult CNS. We chose to image the tectum to compare with our larval imaging results, since the larval tectum regularly exhibited PTZ-evoked $Ca^{2+}$ waves. In contrast to the larval imaging experiments, no statistically significant waves were seen in the adult (data not shown).

## Discussion

One of the main outstanding issues in using the zebrafish as a seizure model is an understanding of how seizure activity in the larval zebrafish compares to that of the adult. In mammals, seizure susceptibility and dynamics correlate with maturity of the brain. In humans, there is a higher incidence of seizures in younger children than adults (Hauser, 1992, 1995, Cowan, 2002), and rat pups have been shown to be more susceptible than adult rats to pentylenetetrazol (PTZ), kainic acid, and pilocarpine induced seizures (Haas et al., 1990). In the developing rat neocortex, the incidence and characteristics of epileptiform activity induced by pharmacological manipulation of glutamatergic and GABAergic systems were age-dependent (Wong and Yamada, 2001); and kindling antagonism, a phenomenon where alternating stimulation between two limbic sites results in suppression of seizure formation at one or both sites, is not found in rat pups (Haas et al., 1990). These, and other studies, indicate that—in mammals at least—developmentally related network properties contribute to seizure proneness and dynamics.

A large set of underlying mechanisms that cause, sustain or have an effect upon seizure activity have been identified. These include: neurotransmitter failure—both synapses that are too weak (Feng and Durand, 2004, van Drongelen et al., 2005) and too strong (Wong et al., 1986, Dichter and Ayala, 1987), neuronal mutations favoring multiple consecutive action potentials (there are a large set of these) (Spampanato and Goldin, 2008), slow channel activation that enhances overall network activity (resembling the action of pharmacoagonists) (Fransen et al., 2006) and network topology (including differences between small- and large-world networks) (Dyhrfjeld-Johnsen et al., 2007), and the strength of network connections and the number of recurrent connections (Traub and Wong, 1982, Traub and Miles, 1991, Dyhrfjeld-Johnsen et al., 2007). In the normal developing brain, it is likely that the most important network properties are those associated with ontogenic differences in neurotransmitter systems, network topology, and/or synaptic connectivity.

We hypothesized that the adult zebrafish brain would respond to PTZ differently than the 7 dpf larval brain because of differences in the brain at these two life stages. Consistent with this idea, PTZ-evoked electrographic activity in the adult was characterized by a pattern of high frequency, low-amplitude discharges and relatively low-frequency, high-amplitude discharges that gave rise to a smooth spectrum as a function of time. This pattern was markedly different from the PTZ-evoked electrographic events in larvae, which had longer latency and a burst-like character. From our imaging results, we infer that these bursts in the larval CNS corresponded to waves of $Ca^{2+}$ release. These results suggest that, contrary to the results found in developing

mammals, the 7 dpf larval zebrafish brain is more resistant than the adult brain to seizure initiation and propagation.

A significant contributing factor to the differences in PTZ-induced electrographic activity is likely to be the neuroanatomical differences between larval and adult brains. The brain of an adult zebrafish (n=25, average brain weight = 13.4 mg, range = 8.1 to 19.7 mg) is about 6 times larger than the larval brain at 7 dpf, and this difference in size is generally reflected in the number of neurons and amount of neuropil contributing to different regions of the brain. An example of this can be seen by comparing GAD expression in adult and larval tecta (Supplementary Fig 4.1). Whereas GAD 65 + GAD 67 expression in the larva is broadly expressed in its small tectum, GAD 65 + GAD 67 dominates the outer layers of the adult tectum. These layers receive input primarily from the visual system and in wild-type zebrafish exhibit responses primarily to visual stimuli. The inner layers express GAD 65 + GAD 67 at lower levels and consist of excitatory neuropil. The intermediate and deep layers receive inputs from a very diverse set of sensory and motor structures. Therefore, when inhibition is down-regulated, the adult tectal neuropil has a large number of excitatory inputs that can more readily excite the tectum leading to ictal events. Furthermore, the layered structure that has developed by the adult stage is likely to provide more recurrent connections between the tectal layers. Such feedback is known to induce susceptibility to seizure in neural tissues (Traub and Miles, 1991, Soltesz and Staley, 2008).

A second possible contributing mechanism for shorter latencies in adults relative to larva and the bursting behavior observed in larva comes from computational models of possible electrical and network mechanisms underlying seizure onset and propagation

(Traub and Miles, 1991, Soltesz and Staley, 2008). These simulations now include detailed reconstructions of the rat hippocampus (Ropireddy et al., 2008), studies of neuronal mutations causing generalized epilepsy (Spampanato and Goldin, 2008), neocortical (van Drongelen et al., 2004) and corticothalamic feedback networks (Destexhe, 2000) and many others. Of particular interest here, a simple computational model showing bursting behavior may be modeled from a pyramidal neuron coupled with a feed-forward inhibitory neuron (Zeldenrust and Wadman, 2013). In such a model, spike rate is modulated independently of burst rate. Increasing the strength of activation of the inhibitory interneuron causes both a decrease in the spiking rate of the circuit and induces bursting. If an extension of such a model applies to larval zebrafish, then differential sensitivity of the inhibitory component to PTZ could explain both the lower strength and bursting behavior of the larval versus adult electrographic response to PTZ.

A likely third contributing factor for the differences in PTZ-induced electrographic activity between adults and 7 dpf larva is developmental differences in the expression of ionotropic glutamate receptors, most likely those of the N-methyl-D-aspartate (NMDA) receptor family. PTZ seizures are mediated by glutamatergic synaptic transmission (Velisek et al., 1990, Velisek et al., 1991), and the same is true for larval zebrafish (Baraban et al., 2005). Importantly, Baraban et al. (2005) showed by application of antagonists that PTZ-evoked epileptiform discharge activity in larva required activation of N-methyl-D-aspartate (NMDA) and/or non-N-methyl-D-aspartate (non-NMDA) receptors. Although we did not specifically test this in our study, it seems reasonable to assume that ionotropic glutamate receptors are required for propagating PTZ-induced bursting activity in the adult zebrafish. Glutamatergic synapse development

involves interactive signaling of the $GABA_A$, NMDA, and AMPA ionotropic receptors (reviewed in Ewald and Cline, 2009). Although all three receptors are important, NMDA receptors (NMDARs) appear to be the key players in the developing brain and at nascent synapses (Durand et al., 1996, Wu et al., 1996, Isaac et al., 1997, Zhu et al., 2000, Aizenman and Cline, 2007). Of particular interest, the subunit composition of NMDARs changes as a function of development (Cull-Candy et al., 2001, Wenthold et al., 2003, Cull-Candy and Leszkiewicz, 2004). For NR2-containing NMDARs, developmentally regulated subunit expression results in NMDARs that differ in glutamate sensitivity and deactivation kinetics (Monyer et al., 1994, Cull-Candy et al., 2001). During vertebrate brain development, NMDAR decay kinetics shorten as the brain matures due to a developmental change of the NR2 subunits (Carmignoto and Vicini, 1992, Hestrin, 1992, Cline et al., 1996, Shi et al., 1997, Roberts and Ramoa, 1999). This developmental decrease in NMDAR decay kinetics would be expected to result in developmental differences in synaptic $Ca^{2+}$ influx (Sobczyk et al., 2005), as was observed in our data.

Adult zebrafish exhibit an AED profile directly comparable to adult rodents for the compounds tested. Valproate and ethosuximide, but not phenytoin, counteract PTZ-evoked electrographic bursting in both rodents (Krall et al., 1978, Swinyard et al., 1986, Ferrendelli et al., 1989, White, 2003, Watanabe et al., 2010) and zebrafish (our data). Although comparable data is not available for rodents, in adult fish VPA and ethosuximide changed the frequency dynamics of PTZ-induced electrographic activity in different ways. VPA induced an overall potentiation in the electrographic signal in a narrow frequency band in the high-alpha/low-beta frequency range, and ethosuximide induced an overall depression in which the high amplitude power at low frequencies

became narrower. Because the AEDs changed seizure dynamics in different ways, our results reinforce the evidence that these two AEDs act through different cellular mechanisms, likely different channels (Macdonald and McLean, 1986, Crunelli and Leresche, 2002, Stahl, 2004, Rosenberg, 2007), to modulate the action of PTZ. By focusing on the dynamics of electrographic activity, this type of study may help further our understanding of how manipulating these mechanisms at the cellular level contributes to modulating seizure activity at the network level.

Comparison of the responses between adult zebrafish and 7 dpf larva to modulators of neural activity revealed both similarities and differences. The anesthetic tricaine, the depressant ETOH, and phenytoin all had identical effects in both adults and larva. However, VPA and ethosuximide exhibited different effects on PTZ-induced bursting in larva compared to adults under our experimental conditions. Previous reports have shown that VPA is effective at reducing the number of PTZ-induced bursting in larval zebrafish (Baraban, 2005, Baraban et al., 2005, Afrikanova et al., 2013), and this is true for our study as well. However, to facilitate comparison with data from adults, we have chosen to compare spectrograms, where comparing the number of events between two conditions is roughly equivalent to comparing the integrated power during a recording. Thus, VPA was effective at reducing PTZ-induced burst events in larva (the event count decreased), but was different from the adult (in which there was a significant change in the high-alpha/low-beta frequency range). Our results for ethosuximide are more consistent with Afrikanova et al. (2013), who reported that this compound significantly shortened the average duration of interictal events and decreased the number of ictal-like discharges, rather than Baraban et al. (2005) who reported that ethosuximide

had little effect. In our study, ethosuximide was less effective than VPA in larva, and the frequency dynamics observed in larva were different than those in the adult. Together, the results from our studies as well as those of others (Baraban, 2005, Afrikanova et al., 2013) indicate that the larval brain differs from the adult brain in its response to specific pharmacological agents, which suggests that there are differences in the neurophysiology between these two stages.

The finding that larval zebrafish appear to be more resistant to seizure initiation whereas developing mammals appear to be less resistant is potentially very interesting. One possible explanation for the apparent difference between fish and rodents may be due to our use of a single acute bath application rather than a kindling (multiple exposure) paradigm, which has been used by many of the studies investigating the incidence and characteristics of seizures during mammalian development. Thus, our investigation precluded contributions to seizure activity from long-term potentiation of the CNS. Alternatively, the 7 dpf reference point may be too early in development to serve as a comparable time point for early post-natal mammalian studies. A more interesting explanation, however, is that the differences in resistance to seizure initiation may reflect ontogenic differences in brain development between teleosts and mammals. Although comparative studies between developing mouse embryos at mid-gestation (~E12.5/13.5 days) and hatching zebrafish larva (~ 3 dpf) have revealed that a remarkable degree of similarity exists between the two species at the level of expression patterns of genes involved in neurogenesis and patterns of GABA-expressing cells (Wullimann and Puelles, 1999, Mueller et al., 2006), there are also significant differences in both the numbers of neurons contributing to the developing brain and the establishment of the

tracts and commissures (Mastick and Easter, 1996). Thus it is possible that the developing postnatal mammalian brain is more susceptible to seizure initiation than the immature fish brain because it possesses a greater degree of connectivity.

One potential caveat is associated with our use pancuronium bromide as a muscle relaxant. Pancuronium bromide is known to act as a competitive acetylcholine antagonist for nicotinic acetylcholine receptors (Buckett, 1968, Buckett et al., 1968, Durant et al., 1979, Savage et al., 1980, Garland et al., 1998). In addition to the neuromuscular junction, these receptors are also present on autonomic neurons and adrenal chromaffin cells in the peripheral nervous system and on many neurons found in the brain and spinal cord (reviewed in Albuquerque et al., 2009). We have determined that pancuronium bromide can reduce the recorded neural activity in larval zebrafish (≤50% of baseline amplitude; data not shown), and we assume the same to be true for adults. Therefore, we know that pancuronium bromide was having a moderating effect on PTZ-evoked neural responses. Comparison of the electrophysiological data obtained from larva treated with pancuronium bromide versus untreated larva (but still embedded in agar) indicated that the effect of pancuronium bromide was to reduce the overall amplitude of the baseline signal, but did not affect the bursting pattern induced by PTZ exposure. Conversely, motion associated with muscle twitches created confounds that were problematic in analyzing frequency data. In the case of adults, confounds associated with motion were significant and necessitated the use of a muscle relaxant.

The results presented here, in conjunction with the published results using embryonic and larval stages, help solidify zebrafish as a seizure model and raise several

interesting questions, including at what developmental time point do "adult-like" seizure behaviors manifest, and what role do NMDARs play in this process?

## Acknowledgements

Dr. Timothy M. Dore provided useful comments on the manuscript. Ms. E. Hope Foskey participated in this research through the University of Georgia Center for Undergraduate Research Opportunities, and Ms. Cynthia M. Bledsoe and M. Caroline Tarallo participated in this research as part of the University of Georgia Young Dawgs high school internship program. The authors thank Mr. Michael L. Ball for help with experiments and Mr. Drea Marlow for expert fish care. Confocal microscopy was performed at the Center for Ultrastructural Research (Leica SP5 Confocal microscope) and Biomedical Microscopy Core (Zeiss LSM 510 Meta Confocal microscope) at the University of Georgia.

Figures

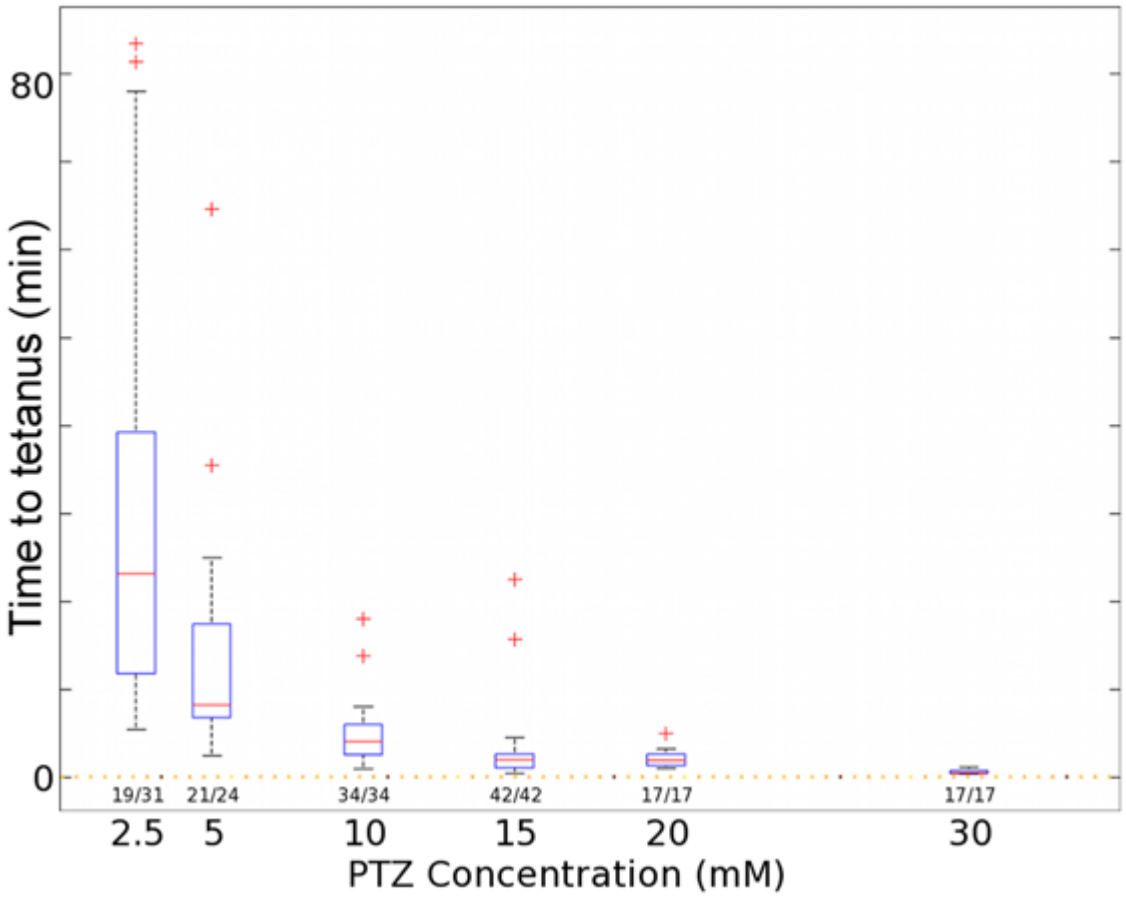


**Figure 4.1. Time to tetanic muscle contractions as a function of PTZ concentration.** Box plots at various concentrations of PTZ are shown with the number of tetanal fish/total assayed indicated. For each box, the central mark denotes the median, the edges of the box are the 25th and 75th percentiles, the whiskers extend to the most extreme data points not considered outliers, and outliers are plotted individually. Adult animals were 7 to 24 months of age, with an average body weight of 0.62 g (range 0.24 g to 1.32 g, mode = 0.71 g).

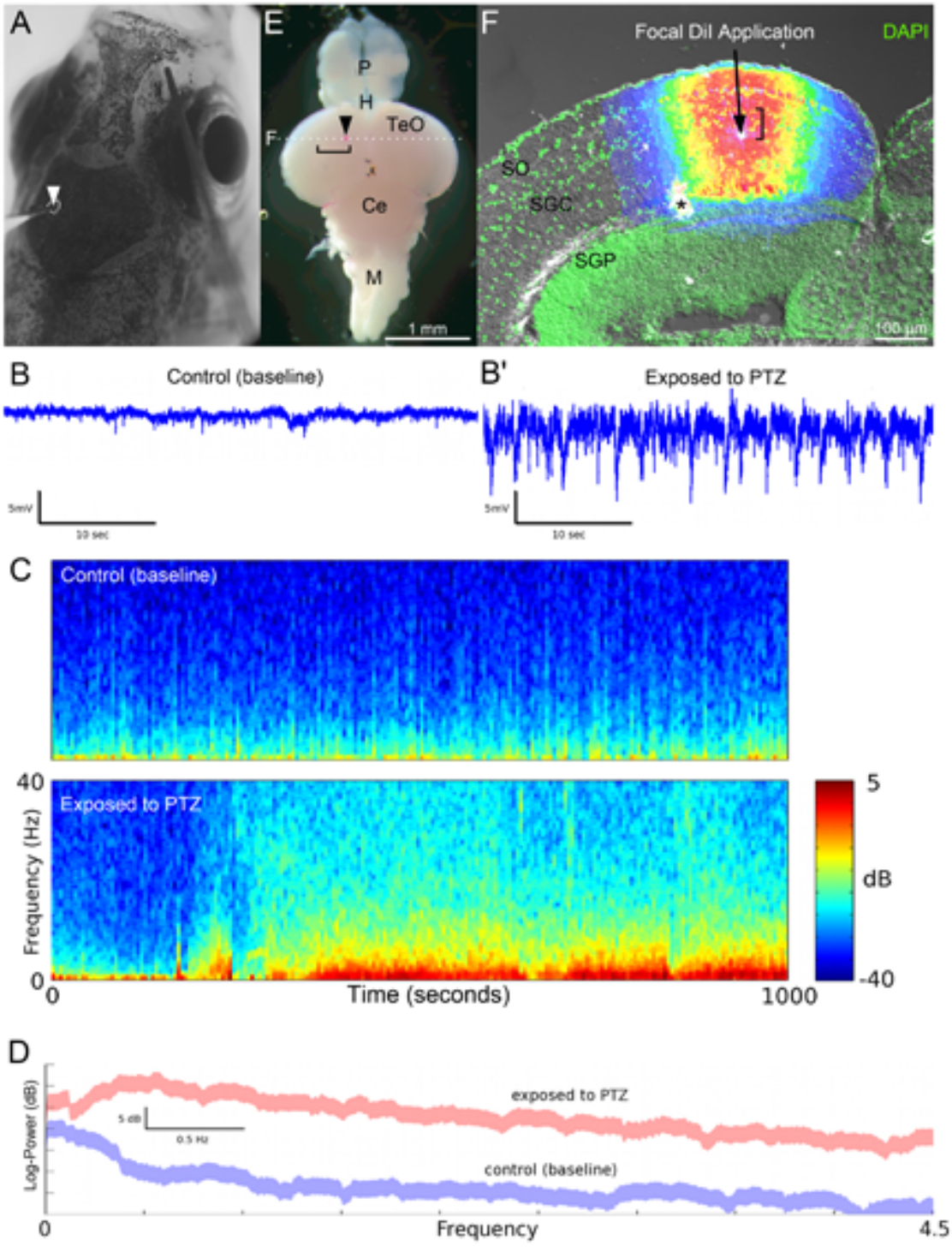
A
E
P
H
TeO
Ce
M
1 mm
F
Focal DiI Application
DAPI
SO
SGC
SGP
100 µm
B
Control (baseline)
B'
Exposed to PTZ
5mV
10 sec
C
Control (baseline)
Exposed to PTZ
40
0
Frequency (Hz)
0
Time (seconds)
1000
5
dB
-40
D
exposed to PTZ
control (baseline)
Log-Power (dB)
5 dB
0.5 Hz
0
Frequency
4.5

**Figure 4.2. Experimental preparation, PTZ-induced electrographic activity in an adult zebrafish, and recording region.** (A) Photograph of the configuration used to obtain tectal field recordings from adult zebrafish (dotted circle with arrowhead indicates tip of glass microelectrode within craniotomy). The reference electrode is placed in the right nostril. Note: The fish is also intubated. (B) Representative baseline field recording (n = 7/7). (B') Representative field recording after exposure to 15 mM PTZ for 15 min (n = 42/42). PTZ exposure was through intubation tube. (C, upper panel) Spectrogram of 1000 seconds of baseline activity in an adult zebrafish. Spectra here and for all subsequent figures were calculated in 5 second windows (25,000 measurements). (C, lower panel) Spectrogram of electrographic activity subsequent to exposure to 15 mM PTZ at time, t = 0. After a delay, the electrographic log-spectrum approaches a regular pattern with peak at low frequencies, but increased power across all frequencies (relative to baseline) with occasional temporal modulation. Log-power at a given time-frequency point is indicated with color (colorbar in lower panel). (D) Average frequency spectra of field recordings from 0 to 4.5 Hz. Red trace denotes power in electrographic signal subsequent to PTZ exposure. Blue trace denotes baseline activity. Width of lines indicates 95% jackknife confidence intervals. (E-F) Focal DiI labeling showing typical placement of microelectrode used for field recordings. (E) Dorsal view of DiI labeled brain. DiI was applied using the same configuration as for field recording except that, instead of recording a field potential, DiI was applied using iontophoresis. The brain was then removed and photographed to show location of DiI label (arrowhead). The bracket denotes the typical region of electrode placement (n=60/61). The position of the section shown in F is denoted with a dotted line. (F) Section through the optic tectum at approximate site of needle tip (shown by arrow). The bracket denotes the typical recording depth. A DiI heat map overlay was generated by integrating DiI fluorescence from all labeled sections; hot colors denote regions of high intensity and cold colors of low intensity. Nuclei were labeled with DAPI and (false) colored green. Asterisk denotes location of debris on section. P, pallium; H, habenula; TeO, optic tectum; Ce, cerebellum; M, medulla. SO, stratum opticum; SGC, stratum griseum centrale; and SGP, stratum griseum periventricular.

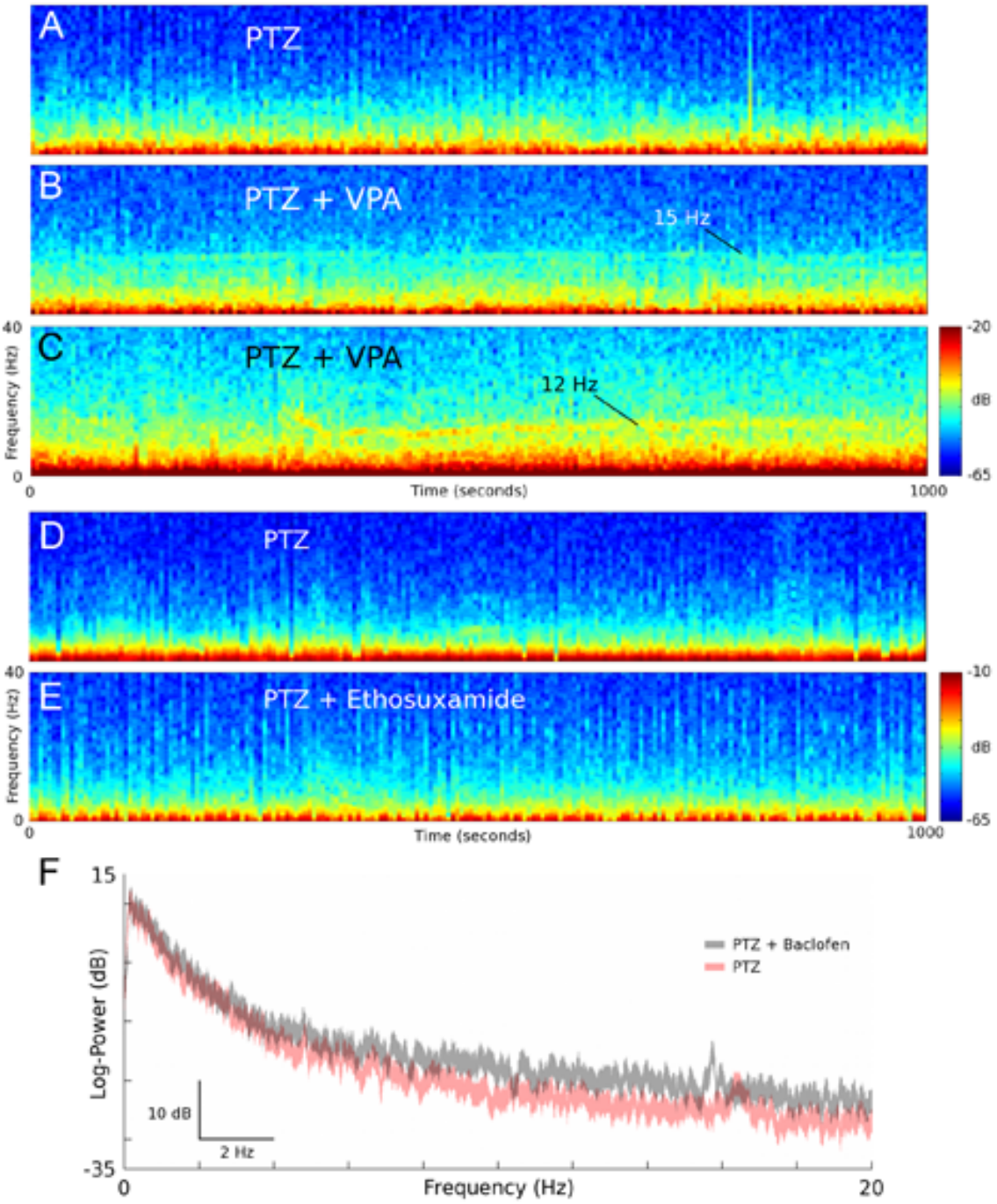
A
PTZ
B
PTZ + VPA
15 Hz
C
PTZ + VPA
12 Hz
40
Frequency (Hz)
0
Time (seconds)
1000
-20
dB
-65
D
PTZ
E
PTZ + Ethosuxamide
-10
F
15
Log-Power (dB)
-35
PTZ + Baclofen
PTZ
10 dB
2 Hz
0
Frequency (Hz)
20

**Figure 4.3: AEDs induce changes in electrographic spectrum and spectral dynamics.** (A-C) *Valproic acid induced variability in the low beta band.* Here, we plot spectrograms that allow us to visualize changes in the spectrum over time. (A) Spectrogram of 15 mM PTZ-induced electrographic activity. (B-C) Two typical examples from 6 total experiments of electrographic activity after exposure first to 15 mM PTZ for 1/2 hour, then to 5 mM valproic acid plus 15 mM PTZ. Log-power is denoted by color (colorbar). An overall potentiation was seen across all frequencies and slowly varying power, including harmonic lines (denoted in (B, 15 Hz) and (C, 12 Hz)) in the low beta band, was also evident. (D-E) *Ethosuximide induced intermittency in electrographic signal***.** (D) Spectrogram of electrographic signal after exposure to 15 mM PTZ. (E) Typical spectrogram (n = 3) of electrographic signal after exposure to 10 mM ethosuximide plus 15 mM PTZ. Ethosuximide/PTZ was administered subsequent to exposure to 15 mM PTZ for 30 mins. After exposure to ethosuximide/PTZ, average power decreased at frequencies below approximately 1 to 2 Hz, however, power increased intermittently across all frequencies (note the intermittent light blue lines). The intermittent changes in power due to ethosuximide were among the most consistent spectral signatures of all AEDs tested in adult zebrafish. (F) *Baclofen potentiated electrographic signal***.** Baclofen did not induce significant changes in the dynamics of the spectrum, therefore in this panel, we plot average spectra, not spectrograms. Spectra of electrographic signal upon exposure to 15 mM PTZ (red trace) and subsequent exposure to 50 μM baclofen plus 15 mM PTZ (black trace). Line widths indicate 95% jackknife confidence intervals. Approximately 4 dB potentiation was evident across frequencies greater than approximately 4 Hz.

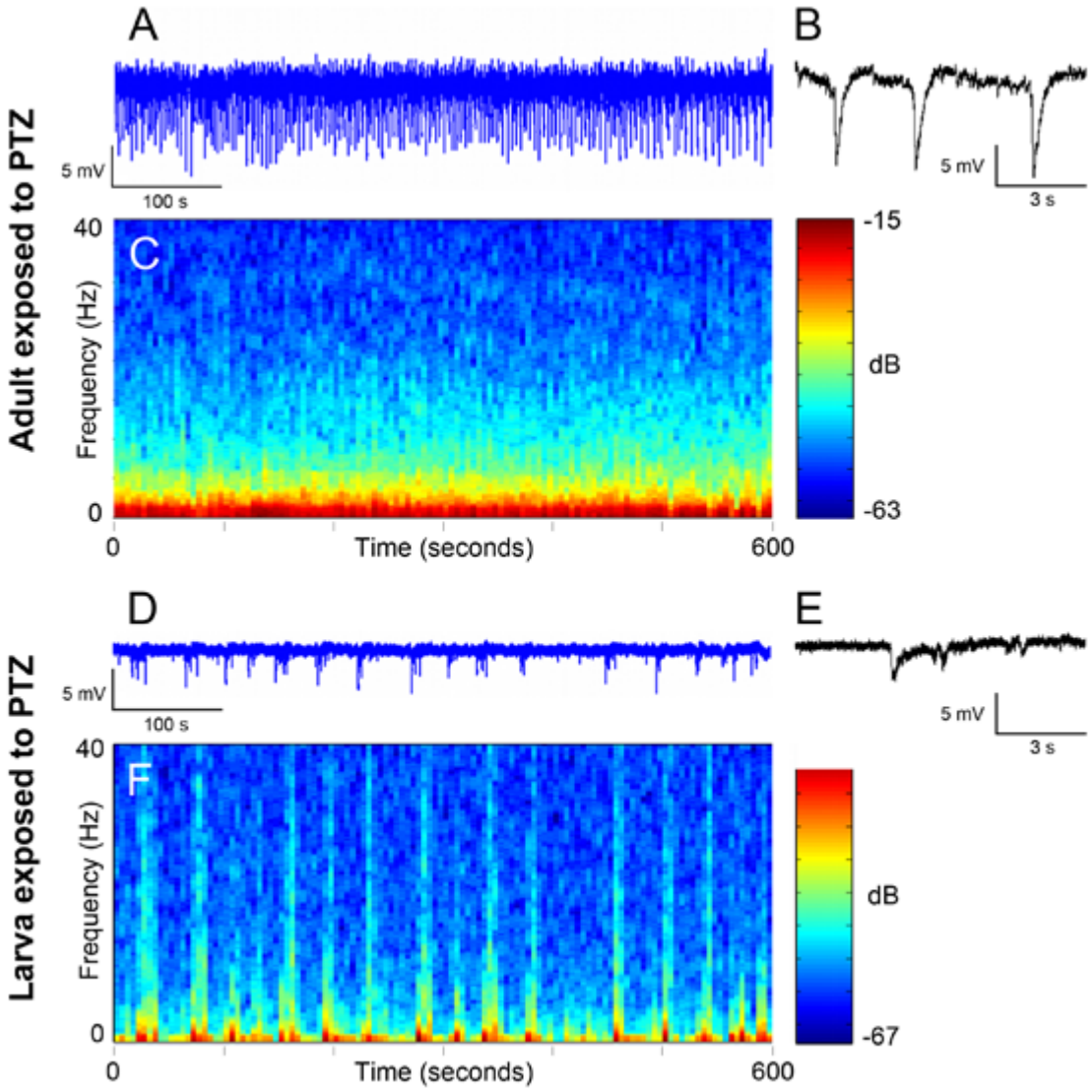


**Figure 4.4: Larvae exhibit fundamentally different seizure dynamics than adults.** (A-C) Adult fish exposed to PTZ. (A) A typical field recording of seizure activity in an adult zebrafish exposed to 15 mM PTZ for 60 minutes. Rapid spikes are evident throughout the recording. (B) Faster time resolution trace. (C) Spectrogram of the field recording in (A). (D-F) Zebrafish larva at 7dpf exposed to PTZ. (D) A typical field recording of seizure activity in a larval (7dpf) zebrafish exposed to 15 mM PTZ for 60 minutes. (E) Faster time resolution trace. (F) Spectrogram of the field recording in (D). Average power was 5 to 8 dB lower in the larva. Note the intermittent bursting activity typical of the larva.

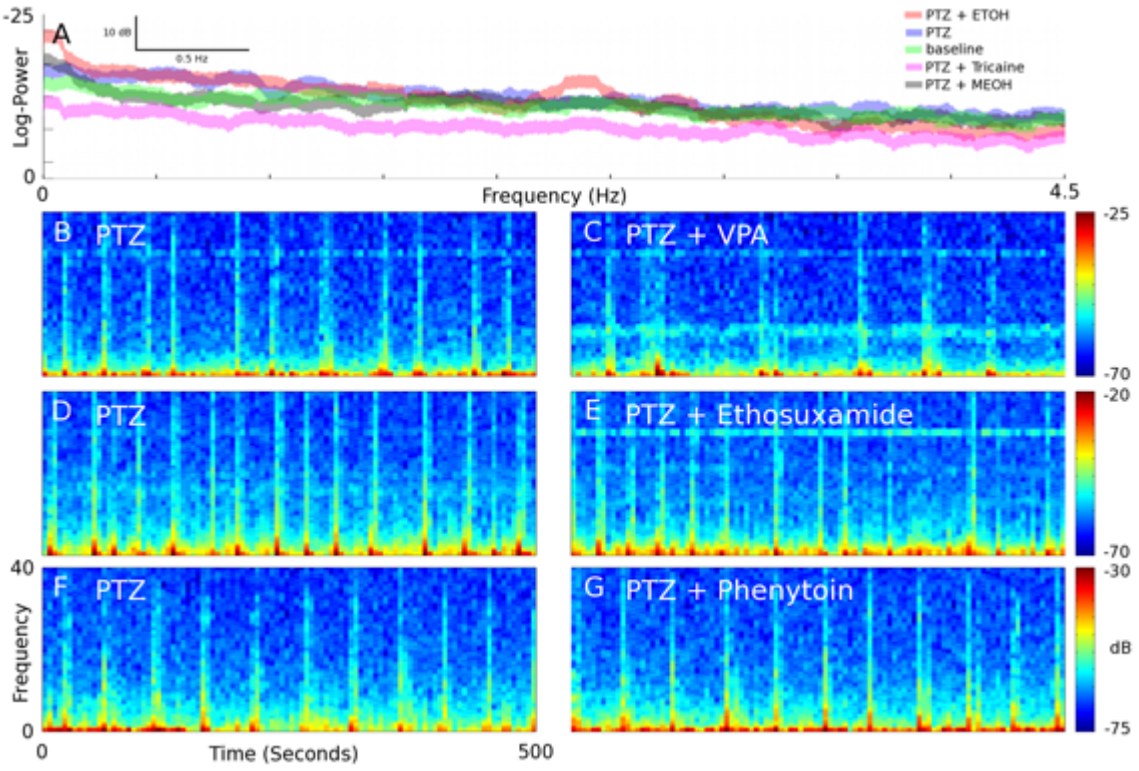


**Figure 4.5: Synaptic pharmacology of PTZ-evoked seizure activity in zebrafish larvae.** (A) Log-spectra of field recordings of larvae exposed to PTZ, PTZ + 5% ETOH, PTZ + 630 µm tris-buffered tricaine, pH 7.2, PTZ + 0.2% MEOH and baseline. Line widths indicate 95% jackknife confidence intervals. PTZ increased power by at least 4 dB relative to baseline across all frequencies. An additional increase in power of up to 5 dB was seen below 1 Hz. Whereas ETOH had little effect at lower frequencies, above 3 Hz, power was reduced by approximately 2-3 dB relative to baseline (5 dB relative to PTZ). Tricaine reduced power below baseline across all frequencies by approximately 10 dB. 0.2% (v/v) methanol reduced power by 3-4dB below 2 Hz. (B-G) Pairs of spectrograms of field recordings of a larva exposed to 15 mM PTZ (B,D,F) followed by 15 mM PTZ plus the AEDs, (C) 5 mM VPA, (E) 10 mM ethosuximide, and (G) 100 µm phenytoin. Note the longer inter-event interval and lower log-power at low frequencies in (C) due to application of VPA. A similar increase in inter-event interval is seen due to ethosuximide, without the concomitant reduction in power. Phenytoin incurred an increase in low frequency power, but had no effect on event intervals.

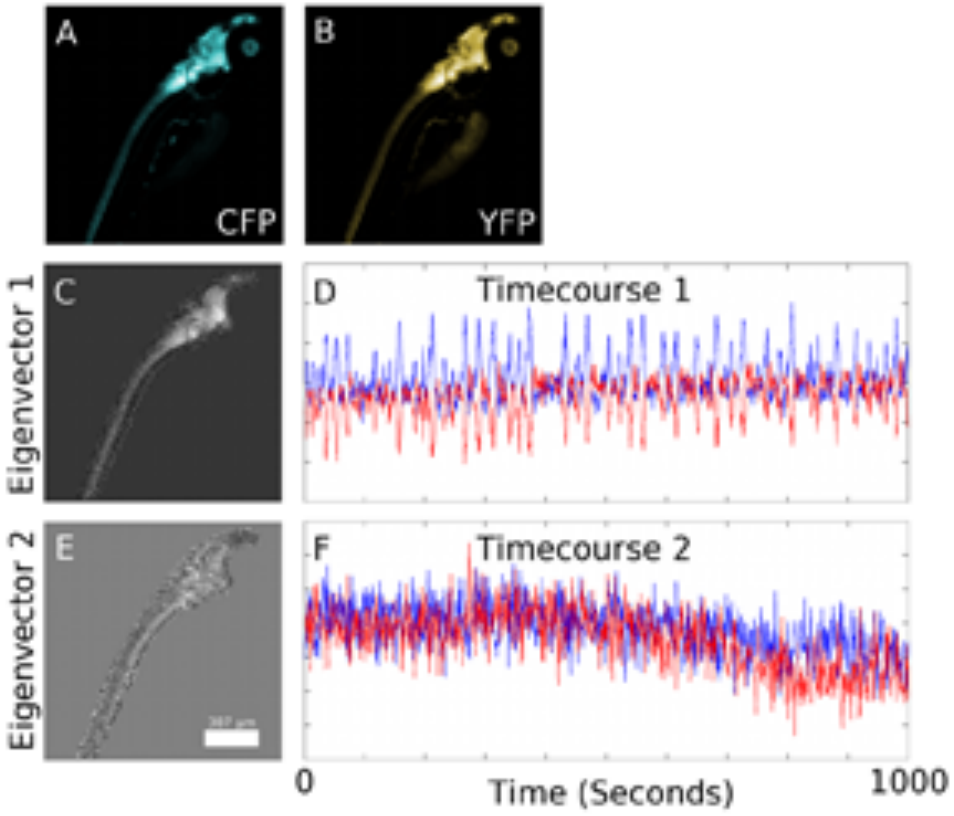


**Figure 4.6: PTZ evokes $Ca^{2+}$ waves in the larval CNS.** (A,B) Cyan and yellow (resp.) mean fluorescence images from a 7 dpf zebrafish larva expressing *cameleon* YC 2.1, a genetically encoded $Ca^{2+}$ indicator, in all neurons. Larvae were exposed to 15 mM PTZ and imaged in cyan (485/40 nm) and yellow (535/30 nm) bands at 1 Hz. Data were analyzed using the SOARS method. The first two eigenvectors (C,E) with time courses (D,F) were statistically significant. The eye, gut and pixels outside the fish were masked out for the SOARS analysis. Cyan fluorescence is shown in red and yellow fluorescence in blue in (D) and (F). The dominant spatial contribution to the dynamics is evident as contiguous bright pixels ranging from the forebrain to the spinal cord in (C). This region exhibited bursts of $Ca^{2+}$ occurring approximately once every 33 seconds, as is evident as the anti-correlated CFP and YFP responses in timecourse 1 (D). This latency interval is comparable to the bursting observed in the electrophysiological recordings of PTZ-evoked activity in larvae (Figs. 4.4 and 4.5 above). Other, subdominant, spatial regions seen in (E) also contributed to the $Ca^{2+}$ signal at higher frequency (F).

## References


Afrikanova T, Serruys AS, Buenafe OE, Clinckers R, Smolders I, de Witte PA, Crawford AD, Esguerra CV (2013) Validation of the zebrafish pentylenetetrazol seizure model: locomotor versus electrographic responses to antiepileptic drugs. PLoS ONE 8:e54166.

Ahrens MB, Orger MB, Robson DN, Li JM, Keller PJ (2013) Whole-brain functional imaging at cellular resolution using light-sheet microscopy. Nat Methods 10:413-420.

Aizenman CD, Cline HT (2007) Enhanced visual activity in vivo forms nascent synapses in the developing retinotectal projection. J Neurophysiol 97:2949-2957.

Akerboom J, Carreras Calderon N, Tian L, Wabnig S, Prigge M, Tolo J, Gordus A, Orger MB, Severi KE, Macklin JJ, Patel R, Pulver SR, Wardill TJ, Fischer E, Schuler C, Chen TW, Sarkisyan KS, Marvin JS, Bargmann CI, Kim DS, Kugler S, Lagnado L, Hegemann P, Gottschalk A, Schreiter ER, Looger LL (2013) Genetically encoded calcium indicators for multi-color neural activity imaging and combination with optogenetics. Frontiers in molecular neuroscience 6:2.

Albuquerque EX, Pereira EF, Alkondon M, Rogers SW (2009) Mammalian nicotinic acetylcholine receptors: from structure to function. Physiol Rev 89:73-120.

Arnolds DE, Zottoli SJ, Adams CE, Dineen SM, Fevrier S, Guo Y, Pascal AJ (2002) Physiological effects of tricaine on the supramedullary/dorsal neurons of the cunner, Tautogolabrus adspersus. The Biological bulletin 203:188-189.

Baier H, Scott EK (2009) Genetic and optical targeting of neural circuits and behavior--zebrafish in the spotlight. Curr Opin Neurobiol 19:553-560.

Baraban SC (2005) Modeling Epilepsy and Seizures in Developing Zebrafish Larvae. In: Models of Seizures and Epilepsy (Pitkänen, A. et al., eds), pp 189-198 30 Corporate Drive, Suite 400, Burlington, MA 01803: Elsevier Academic Press.

Baraban SC (2007) Emerging epilepsy models: insights from mice, flies, worms and fish. Curr Opin Neurol 20:164-168.

Baraban SC, Dinday MT, Castro PA, Chege S, Guyenet S, Taylor MR (2007) A large-scale mutagenesis screen to identify seizure-resistant zebrafish. Epilepsia 48:1151-1157.

Baraban SC, Taylor MR, Castro PA, Baier H (2005) Pentylenetetrazole induced changes in zebrafish behavior, neural activity and c-fos expression. Neuroscience 131:759-768.

Barthel LK, Raymond PA (1990) Improved method for obtaining 3-microns cryosections for immunocytochemistry. J Histochem Cytochem 38:1383-1388.

Baxendale S, Holdsworth CJ, Meza Santoscoy PL, Harrison MR, Fox J, Parkin CA, Ingham PW, Cunliffe VT (2012) Identification of compounds with anti-convulsant properties in a zebrafish model of epileptic seizures. Dis Model Mech 5:773-784.

Berghmans S, Hunt J, Roach A, Goldsmith P (2007) Zebrafish offer the potential for a primary screen to identify a wide variety of potential anticonvulsants. Epilepsy Res 75:18-28.

Birgbauer E, Sechrist J, Bronner-Fraser M, Fraser S (1995) Rhombomeric origin and rostrocaudal reassortment of neural crest cells revealed by intravital microscopy. Development 121:935-945.

Broder J, Majumder A, Porter E, Srinivasamoorthy G, Keith CH, Lauderdale J, Sornborger A (2007) Estimating weak ratiometric signals in imaging data. I. Dual-channel data. J Opt Soc Am A Opt Image Sci Vis 24:2921-2931.

Bryson JL, Coles MC, Manley NR (2011) A method for labeling vasculature in embryonic mice. Journal of visualized experiments : JoVE.

Buckett WR (1968) The pharmacology of pancuronium bromide: a new non-depolarising neuromuscular blocking agent. Irish journal of medical science 7:565-568.

Buckett WR, Marjoribanks CE, Marwick FA, Morton MB (1968) The pharmacology of pancuronium bromide (Org.NA97), a new potent steroidal neuromuscular blocking agent. British journal of pharmacology and chemotherapy 32:671-682.

Buckmaster PS, Jongen-Relo AL (1999) Highly specific neuron loss preserves lateral inhibitory circuits in the dentate gyrus of kainate-induced epileptic rats. The Journal of neuroscience : the official journal of the Society for Neuroscience 19:9519-9529.

Budick SA, O'Malley DM (2000) Locomotor repertoire of the larval zebrafish: swimming, turning and prey capture. J Exp Biol 203:2565-2579.

Carmignoto G, Vicini S (1992) Activity-dependent decrease in NMDA receptor responses during development of the visual cortex. Science 258:1007-1011.

Cline HT, Wu GY, Malinow R (1996) In vivo development of neuronal structure and function. Cold Spring Harb Symp Quant Biol 61:95-104.

Cowan LD (2002) The epidemiology of the epilepsies in children. Ment Retard Dev Disabil Res Rev 8:171-181.

Crunelli V, Leresche N (2002) Block of Thalamic T-Type Ca(2+) Channels by Ethosuximide Is Not the Whole Story. Epilepsy Curr 2:53-56.

Cull-Candy S, Brickley S, Farrant M (2001) NMDA receptor subunits: diversity, development and disease. Curr Opin Neurobiol 11:327-335.

Cull-Candy SG, Leszkiewicz DN (2004) Role of distinct NMDA receptor subtypes at central synapses. Sci STKE 2004:re16.

Danos N, Lauder GV (2007) The ontogeny of fin function during routine turns in zebrafish Danio rerio. J Exp Biol 210:3374-3386.

Destexhe A (2000) Modelling corticothalamic feedback and the gating of the thalamus by the cerebral cortex. J Physiology (Paris) 94:391-410.

Dichter MA, Ayala GF (1987) Cellular mechanisms of epilepsy: a status report. Science 237:157-164.

Douglass AD, Kraves S, Deisseroth K, Schier AF, Engert F (2008) Escape behavior elicited by single, channelrhodopsin-2-evoked spikes in zebrafish somatosensory neurons. Curr Biol 18:1133-1137.

Durand GM, Kovalchuk Y, Konnerth A (1996) Long-term potentiation and functional synapse induction in developing hippocampus. Nature 381:71-75.

Durant NN, Marshall IG, Savage DS, Nelson DJ, Sleigh T, Carlyle IC (1979) The neuromuscular and autonomic blocking activities of pancuronium, Org NC 45, and other pancuronium analogues, in the cat. The Journal of pharmacy and pharmacology 31:831-836.

Dyhrfjeld-Johnsen J, Santhakumar V, Morgan RJ, Huerta R, Tsimring L, Soltesz I (2007) Topological determinants of epileptogenesis in large-scale structural and functional models of the dentate gyrus derived from experimental data. J Neurophysiol 97:1566-1587.

Ewald RC, Cline HT (2009) NMDA Receptors and Brain Development. In: Biology of the NMDA Receptor (AM, V. D., ed) Boca Raton (FL): CRC Press.

Fan X, Majumder A, Reagin SS, Porter EL, Sornborger AT, Keith CH, Lauderdale JD (2007) New statistical methods enhance imaging of cameleon fluorescence resonance energy transfer in cultured zebrafish spinal neurons. Journal of biomedical optics 12:034017.

Feng Z, Durand DM (2004) Suppression of excitatory synaptic transmission can facilitate low-calcium epileptiform activity in the hippocampus in vivo. Brain Res 1030:57-65.

Ferrendelli JA, Holland KD, McKeon AC, Covey DF (1989) Comparison of the anticonvulsant activities of ethosuximide, valproate, and a new anticonvulsant, thiobutyrolactone. Epilepsia 30:617-622.

Forsgren L, Beghi E, Oun A, Sillanpaa M (2005) The epidemiology of epilepsy in Europe - a systematic review. European journal of neurology : the official journal of the European Federation of Neurological Societies 12:245-253.

Fransen E, Tahvildari B, Egorov AV, Hasselmo ME, Alonso AA (2006) Mechanism of graded persistent cellular activity of entorhinal cortex layer v neurons. Neuron 49:735-746.

Frey LC (2003) Epidemiology of posttraumatic epilepsy: a critical review. Epilepsia 44 Suppl 10:11-17.

Friedrich RW, Jacobson GA, Zhu P (2010) Circuit neuroscience in zebrafish. Current biology : CB 20:R371-381.

Galanopoulou AS (2013) Basic mechanisms of catastrophic epilepsy - Overview from animal models. Brain & development.

Garland CM, Foreman RC, Chad JE, Holden-Dye L, Walker RJ (1998) The actions of muscle relaxants at nicotinic acetylcholine receptor isoforms. Eur J Pharmacol 357:83-92.

Granieri E, Rosati G, Tola R, Pavoni M, Paolino E, Pinna L, Monetti VC (1983) A descriptive study of epilepsy in the district of Copparo, Italy, 1964-1978. Epilepsia 24:502-514.

Haas KZ, Sperber EF, Moshe SL (1990) Kindling in developing animals: expression of severe seizures and enhanced development of bilateral foci. Brain research Developmental brain research 56:275-280.

Halpern ME, Rhee J, Goll MG, Akitake CM, Parsons M, Leach SD (2008) Gal4/UAS transgenic tools and their application to zebrafish. Zebrafish 5:97-110.

Hauser WA (1992) Seizure disorders: the changes with age. Epilepsia 33 Suppl 4:S6-14.

Hauser WA (1995) Epidemiology of epilepsy in children. Neurosurg Clin N Am 6:419-429.

Hauser WA, Annegers JF, Kurland LT (1991) Prevalence of epilepsy in Rochester, Minnesota: 1940-1980. Epilepsia 32:429-445.

Hestrin S (1992) Developmental regulation of NMDA receptor-mediated synaptic currents at a central synapse. Nature 357:686-689.

Hewapathirane DS, Dunfield D, Yen W, Chen S, Haas K (2008) In vivo imaging of seizure activity in a novel developmental seizure model. Experimental neurology 211:480-488.

Higashijima S, Masino MA, Mandel G, Fetcho JR (2003) Imaging neuronal activity during zebrafish behavior with a genetically encoded calcium indicator. J Neurophysiol 90:3986-3997.

Hodor PG, Ettensohn CA (1998) The dynamics and regulation of mesenchymal cell fusion in the sea urchin embryo. Developmental biology 199:111-124.

Hortopan GA, Dinday MT, Baraban SC (2010) Zebrafish as a model for studying genetic aspects of epilepsy. Dis Model Mech 3:144-148.

Isaac JT, Crair MC, Nicoll RA, Malenka RC (1997) Silent synapses during development of thalamocortical inputs. Neuron 18:269-280.

Johnston L, Ball RE, Acuff S, Gaudet J, Sornborger A, Lauderdale JD (2013) Electrophysiological Recording in the Brain of Intact Adult Zebrafish. e51065.

Jutkiewicz EM, Baladi MG, Folk JE, Rice KC, Woods JH (2006) The convulsive and electroencephalographic changes produced by nonpeptidic delta-opioid agonists in rats: comparison with pentylenetetrazol. J Pharmacol Exp Ther 317:1337-1348.

Kimmel CB, Ballard WW, Kimmel SR, Ullmann B, Schilling TF (1995) Stages of embryonic development of the zebrafish. Dev Dyn 203:253-310.

Krall RL, Penry JK, White BG, Kupferberg HJ, Swinyard EA (1978) Antiepileptic drug development: II. Anticonvulsant drug screening. Epilepsia 19:409-428.

Lee Y, Kim D, Kim YH, Lee H, Lee CJ (2010) Improvement of pentylenetetrazol-induced learning deficits by valproic acid in the adult zebrafish. Eur J Pharmacol 643:225-231.

Liu YC, Bailey I, Hale ME (2012) Alternative startle motor patterns and behaviors in the larval zebrafish (Danio rerio). Journal of comparative physiology A, Neuroethology, sensory, neural, and behavioral physiology 198:11-24.

Macdonald RL, McLean MJ (1986) Anticonvulsant drugs: mechanisms of action. Adv Neurol 44:713-736.

Mantegazza M, Curia G, Biagini G, Ragsdale DS, Avoli M (2010) Voltage-gated sodium channels as therapeutic targets in epilepsy and other neurological disorders. Lancet neurology 9:413-424.

Mastick GS, Easter SS, Jr. (1996) Initial organization of neurons and tracts in the embryonic mouse fore- and midbrain. Dev Biol 173:79-94.

Mirski MA, Ferrendelli JA (1986) Selective metabolic activation of the mammillary bodies and their connections during ethosuximide-induced suppression of pentylenetetrazol seizures. Epilepsia 27:194-203.

Mitra P, Bokil H (2008) Observed Brain Dynamics. 198 Madison Avenue, New York, NY 10016: Oxford University Press.

Mitra PP, Pesaran B (1999) Analysis of dynamic brain imaging data. Biophys J 76:691-708.

Monyer H, Burnashev N, Laurie DJ, Sakmann B, Seeburg PH (1994) Developmental and regional expression in the rat brain and functional properties of four NMDA receptors. Neuron 12:529-540.

Mueller T, Vernier P, Wullimann MF (2006) A phylotypic stage in vertebrate brain development: GABA cell patterns in zebrafish compared with mouse. J Comp Neurol 494:620-634.

Myers PZ, Bastiani MJ (1993) Growth cone dynamics during the migration of an identified commissural growth cone. Journal of Neuroscience 13:127-143.

Oliver AP, Hoffer BJ, Wyatt RJ (1977) The hippocampal slice: a system for studying the pharmacology of seizures and for screening anticonvulsant drugs. Epilepsia 18:543-548.

Orellana-Paucar AM, Serruys AS, Afrikanova T, Maes J, De Borggraeve W, Alen J, Leon-Tamariz F, Wilches-Arizabala IM, Crawford AD, de Witte PA, Esguerra CV (2012) Anticonvulsant activity of bisabolene sesquiterpenoids of Curcuma longa in zebrafish and mouse seizure models. Epilepsy Behav 24:14-22.

Pandolfo M (2013) Pediatric epilepsy genetics. Curr Opin Neurol 26:137-145.

Parker L, Howlett IC, Rusan ZM, Tanouye MA (2011) Seizure and epilepsy: studies of seizure disorders in Drosophila. International review of neurobiology 99:1-21.

Peterson RT, Fishman MC (2004) Discovery and use of small molecules for probing biological processes in zebrafish. Methods Cell Biol 76:569-591.

Piredda S, Yonekawa W, Whittingham TS, Kupferberg HJ (1986) Effects of antiepileptic drugs on pentylenetetrazole-induced epileptiform activity in the in vitro hippocampus. Epilepsia 27:341-346.

Portugues R, Severi KE, Wyart C, Ahrens MB (2013) Optogenetics in a transparent animal: circuit function in the larval zebrafish. Curr Opin Neurobiol 23:119-126.

Rahman S (2012) Mitochondrial disease and epilepsy. Developmental medicine and child neurology 54:397-406.

Ratzliff A, Santhakumar V, Howard A, Soltesz I (2002) Mossy cells in epilepsy: rigor mortis or vigor mortis? Trends Neurosci 25:140-144.

Roberts EB, Ramoa AS (1999) Enhanced NR2A subunit expression and decreased NMDA receptor decay time at the onset of ocular dominance plasticity in the ferret. J Neurophysiol 81:2587-2591.

Ropireddy D, Bachus SE, Scorcioni R, Ascoli GA (2008) Computational neuroanatomy of the rat hippocampus: implications and applications to epilepsy. In: Computational Neuroscience in Epilepsy (Soltesz, I. and Staley, K., eds), pp 71-85 Amsterdam: Academic Press.

Rosenberg G (2007) The mechanisms of action of valproate in neuropsychiatric disorders: can we see the forest for the trees? Cell Mol Life Sci 64:2090-2103.

Sambrook J, Russell DW (2001) Molecular Cloning: A Laboratory Manual. Cold Spring Harbor: Cold Spring Harbor Laboratory Press.

Sanchez Fernandez I, Ramgopal S, Powell C, Gregas M, Zarowski M, Shah A, Vendrame M, Alexopoulos AV, Kothare SV, Loddenkemper T (2013) Clinical evolution of seizures: distribution across time of day and sleep/wakefulness cycle. Journal of neurology 260:549-557.

Savage DS, Sleigh T, Carlyle I (1980) The emergence of ORG NC 45, 1- [2 beta,3 alpha,5 alpha,16 beta,17 beta)-3, 17-bis(acetyloxy)-2-(1-piperidinyl)-androstan-16-yl]-1-methylpiperidinium bromide, from the pancuronium series. British journal of anaesthesia 52 Suppl 1:3S-9S.

Schindler K, Leung H, Elger CE, Lehnertz K (2007) Assessing seizure dynamics by analysing the correlation structure of multichannel intracranial EEG. Brain 130:65-77.

Scott EK, Mason L, Arrenberg AB, Ziv L, Gosse NJ, Xiao T, Chi NC, Asakawa K, Kawakami K, Baier H (2007) Targeting neural circuitry in zebrafish using GAL4 enhancer trapping. Nat Methods 4:323-326.

Servit Z, Strejckova A (1970a) An electrographic epileptic focus in the fish forebrain. Conditions and pathways of propagation of focal and paroxysmal activity. Brain research 17:103-113.

Servit Z, Strejckova A (1970b) Epileptic focus in the frog forebrain. Triggering of the focal discharge with sensory stimuli. Experimental neurology 28:371-383.

Servit Z, Strejckova A, Volanschi D (1968) An epileptogenic focus in the frog telencephalon. Pathways of propagation of focal activity. Exp Neurol 21:383-396.

Shi J, Aamodt SM, Constantine-Paton M (1997) Temporal correlations between functional and molecular changes in NMDA receptors and GABA neurotransmission in the superior colliculus. J Neurosci 17:6264-6276.

Singh R, Gardner RJ, Crossland KM, Scheffer IE, Berkovic SF (2002) Chromosomal abnormalities and epilepsy: a review for clinicians and gene hunters. Epilepsia 43:127-140.

Sisodiya SM (2004) Malformations of cortical development: burdens and insights from important causes of human epilepsy. Lancet neurology 3:29-38.

Sloviter RS (2008) Hippocampal epileptogenesis in animal models of mesial temporal lobe epilepsy with hippocampal sclerosis: the importance of the "latent period" and other concepts. Epilepsia 49 Suppl 9:85-92.

Sobczyk A, Scheuss V, Svoboda K (2005) NMDA receptor subunit-dependent [Ca2+] signaling in individual hippocampal dendritic spines. J Neurosci 25:6037-6046.

Soltesz I, Staley K (eds.) (2008) Computational Neuroscience in Epilepsy. Amsterdam: Academic Press.

Song J, Tanouye MA (2008) From bench to drug: human seizure modeling using Drosophila. Prog Neurobiol 84:182-191.

Spampanato J, Goldin AL (2008) Computer simulations of sodium channel mutations that cause generalized epilepsy with febrile seizures plus. In: Computational Neuroscience in Epilepsy (Soltesz, I. and Staley, K., eds), pp 143-154 Amsterdam: Academic Press.

Stahl SM (2004) Anticonvulsants as mood stabilizers and adjuncts to antipsychotics: valproate, lamotrigine, carbamazepine, and oxcarbazepine and actions at voltage-gated sodium channels. The Journal of clinical psychiatry 65:738-739.

Steinlein OK (2010) Animal models for autosomal dominant frontal lobe epilepsy: on the origin of seizures. Expert review of neurotherapeutics 10:1859-1867.

Strejckova A (1969) Epileptogenic focus in the fish telencephalon (in the common tench--Tinca tinca). Physiologia Bohemoslovaca 18:209-216.

Sutula TP, Hagen J, Pitkanen A (2003) Do epileptic seizures damage the brain? Current opinion in neurology 16:189-195.

Swinyard EA, Sofia RD, Kupferberg HJ (1986) Comparative anticonvulsant activity and neurotoxicity of felbamate and four prototype antiepileptic drugs in mice and rats. Epilepsia 27:27-34.

Tao L, Lauderdale JD, Sornborger AT (2011) Mapping Functional Connectivity between Neuronal Ensembles with Larval Zebrafish Transgenic for a Ratiometric Calcium Indicator. Front Neural Circuits 5:2.

Traub RD, Miles R (1991) Neuronal Networks of the Hippocampus. New York: Cambridge University Press.

Traub RD, Wong RK (1982) Cellular mechanism of neuronal synchronization in epilepsy. Science 216:745-747.

van Drongelen W, Lee HC, Hereld M, Chen Z, Elsen FP, Stevens RL (2005) Emergent epileptiform activity in neural networks with weak excitatory synapses. IEEE transactions on neural systems and rehabilitation engineering : a publication of the IEEE Engineering in Medicine and Biology Society 13:236-241.

van Drongelen W, Lee HC, Hereld M, Jones D, Cohoon M, Elsen F, Papka ME, Stevens RL (2004) Simulation of neocortical epileptiform activity using parallel computing. Neurocomputing 58-60:1203-1209.

Vannest J, Szaflarski JP, Eaton KP, Henkel DM, Morita D, Glauser TA, Byars AW, Patel K, Holland SK (2013) Functional magnetic resonance imaging reveals changes in language localization in children with benign childhood epilepsy with centrotemporal spikes. Journal of child neurology 28:435-445.

Velisek L, Kusa R, Kulovana M, Mares P (1990) Excitatory amino acid antagonists and pentylenetetrazol-induced seizures during ontogenesis. I. The effects of 2-amino-7-phosphonoheptanoate. Life Sci 46:1349-1357.

Velisek L, Veresova S, Pobisova H, Mares P (1991) Excitatory amino acid antagonists and pentylenetetrazol-induced seizures during ontogenesis. II. The effects of MK-801. Psychopharmacology 104:510-514.

Velluti JC, Costa da Costa J, Russo RE (1997) The cerebral hemisphere of the turtle in vitro. An experimental model with spontaneous interictal-like spikes for the study of epilepsy. Epilepsy Res 28:29-37.

Vermoesen K, Serruys AS, Loyens E, Afrikanova T, Massie A, Schallier A, Michotte Y, Crawford AD, Esguerra CV, de Witte PA, Smolders I, Clinckers R (2011) Assessment of the convulsant liability of antidepressants using zebrafish and mouse seizure models. Epilepsy Behav 22:450-460.

Volanschi D, Servit Z (1969) Epileptic focus in the forebrain of the turtle. Experimental neurology 24:137-146.

Watanabe K, Miura K, Natsume J, Hayakawa F, Furune S, Okumura A (1999) Epilepsies of neonatal onset: seizure type and evolution. Developmental medicine and child neurology 41:318-322.

Watanabe Y, Takechi K, Fujiwara A, Kamei C (2010) Effects of antiepileptics on behavioral and electroencephalographic seizure induced by pentetrazol in mice. Journal of pharmacological sciences 112:282-289.

Wenthold RJ, Prybylowski K, Standley S, Sans N, Petralia RS (2003) Trafficking of NMDA receptors. Annu Rev Pharmacol Toxicol 43:335-358.

Westerfield M (ed.) (2007) The zebrafish book: A guide for the laboratory use of zebrafish (Danio rerio). Eugene, OR: University of Oregon Press.

White HS (2003) Preclinical development of antiepileptic drugs: past, present, and future directions. Epilepsia 44 Suppl 7:2-8.

Winter MJ, Redfern WS, Hayfield AJ, Owen SF, Valentin JP, Hutchinson TH (2008) Validation of a larval zebrafish locomotor assay for assessing the seizure liability of early-stage development drugs. J Pharmacol Toxicol Methods 57:176-187.

Wong M, Yamada KA (2001) Developmental characteristics of epileptiform activity in immature rat neocortex: a comparison of four in vitro seizure models. Brain Res Dev Brain Res 128:113-120.

Wong RK, Traub RD, Miles R (1986) Cellular basis of neuronal synchrony in epilepsy. Adv Neurol 44:583-592.

Wu G, Malinow R, Cline HT (1996) Maturation of a central glutamatergic synapse. Science 274:972-976.

Wullimann MF, Puelles L (1999) Postembryonic neural proliferation in the zebrafish forebrain and its relationship to prosomeric domains. Anat Embryol (Berl) 199:329-348.

Wyart C, Del Bene F, Warp E, Scott EK, Trauner D, Baier H, Isacoff EY (2009) Optogenetic dissection of a behavioural module in the vertebrate spinal cord. Nature 461:407-410.

Zeldenrust F, Wadman WJ (2013) Modulation of spike and burst rate in a minimal neuronal circuit with feed-forward inhibition. Neural networks : the official journal of the International Neural Network Society 40:1-17.

Zhu JJ, Esteban JA, Hayashi Y, Malinow R (2000) Postnatal synaptic potentiation: delivery of GluR4-containing AMPA receptors by spontaneous activity. Nat Neurosci 3:1098-1106.

Supplementary Data

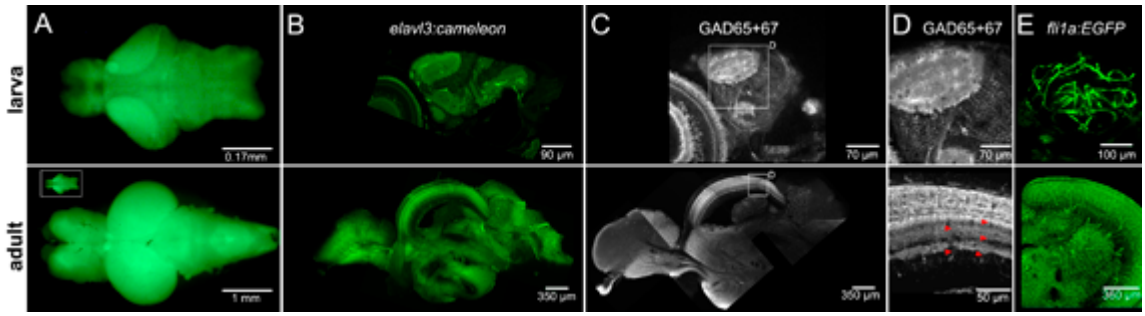


**Supplementary Figure 4.1. Comparison of neuroanatomy and vascular structure between adult and 7 dpf larval zebrafish.** (A) The larval brain at 7 dpf is about 6 times smaller than the brain of the typical adult fish used in these studies. *Lower panel*. To illustrate size differences, brains from a 7 dpf larva (boxed) and adult (~620 mg in body weight) were placed side-by-side and photographed using epifluorescence to visualize the genetically encoded calcium indicator *cameleon* expressed under the control of the pan-neuronal *elavl3* promoter (Higashijima et al., 2003). *Upper panel*. 6X magnified view of same 7 dpf brain to show anatomical features. (B) Parasagittal sections through tecta of larval and adult brains transgenic for*elavl3:cameleon* reveals that the adult tectum is more organized relative to the larva. (C-D) Parasagittal sections through tecta of larval and adult brains immunolabeled using an antibody that reacted specifically with GAD 65 and GAD 67 isoforms from brain. The outer layers (stratum opticum) of the adult tectum expressed visibly more GAD65 + GAD67 than the inner layers (stratum griseum centrale). Regularly spaced GAD65 + GAD67 expressing neurons in the inner neural cell layer projected horizontally into the tectal neuropil (red arrowheads) in the adult. GAD65 + GAD67 was broadly expressed throughout the entire larval tectum. Sparse, individual neurons expressing GAD65 + GAD67 are visible within the tectal neuropil at the level of magnification in this image. (E) Transverse sections through the tecta of larval and adult brains transgenic for*fli1a:EGFP* depicting vascular structure of adult and larval zebrafish tecta. Note the disparity in complexity between adult and larval vascular systems.

# CHAPTER 5

# LITERATURE REVIEW: CRANIOFAICAL DEVELOPMENT

## Craniofacial elements are derived from neural crest cells

In all vertebrates examined, much of the head skeleton and peripheral nervous system develops from migratory cells of the neural crest, with contributions from ectoderm, endoderm and paraxial mesoderm (Schilling et al., 1996, Schilling and Kimmel, 1997, Le Douarin and Kalcheim, 1999, Wada et al., 2005). Neural crest cells arise uniformly along the dorso-lateral edge of closing neural folds. As the neural tube begins to form, the neural crest cells undergo an epithelial-to-mesenchymal transition, whereby they delaminate from the neural tube and begin to migrate to their target destination, where they will then undergo differentiation (Trainor et al., 2003). The population of neural crest cells involved in head development is known as the cranial neural crest (Wada et al., 2005, Saint-Jeannet, 2006, Alexander et al., 2011). These neural crest cells arise from the rostral neural tube and form the anterior neurocranium and segmented pharyngeal skeleton, as well as sensory neurons, glia and pigment cells (Le Douarin and Kalcheim, 1999, Yelick and Schilling, 2002).

The cranial neural crest carry intrinsic differentiation properties acquired prior to migration that influence the skeletal fates along the anterior-posterior axis (Noden, 1983, Trainor et al., 2003). Yet, these cells also require inductive signals from the surrounding endoderm and ectoderm to develop correctly. In avian and mammalian embryos, evidence suggests that cellular diversity within the developing arches is a result of the

positional specification of pharyngeal precursors just after gastrulation (Schilling and Kimmel, 1994). At this time, pharyngeal segmentation is patterned, in part, by the segmental migration of the neural crest that correlates with its rhombomeric point of origin (Lumsden et al., 1991, Schilling, 1997b, Knight and Schilling, 2006). The pharyngeal skeleton then forms within a reiterated series of arches that surround the anterior foregut.

The most anterior population of neural crest, known as the neurocranial precursors, emerge from the midbrain and migrate between the eyes to form the palatal shelves, which also requires mesodermal contributions (Yelick and Schilling, 2002). This population gives rise to the structures that form the braincase. The viscerocranium, on the other hand, is solely derived from cranial neural crest and will give rise to the pharyngeal elements (Wada et al., 2005). Precursors of this region emigrate in three streams from the hindbrain into the mandibular (stream 1), hyoid (stream 2) and five branchial (stream 3) arches. Each of these streams originates adjacent to rhombomeres 2, 4 and 6, respectively (Schilling, 1997a, Trainor et al., 2003). Mixing is never observed between the derivatives of these distinct streams, as rhombomeres 3 and 5 (which are devoid of neural crest due to apoptosis), separate these three populations and ultimately confine the cells to a particular arch primordia (Schilling, 1997b, Graham, 2003). Stream 1 also contributes to the ventral neurocranium (Saint-Jeannet, 2006). The viscerocranial precursors later develop into the structures that support feeding and/or gill-bearing structures within vertebrates (Kimmel et al., 2001). Figure 5.1 shows the neural crest movements and their cartilaginous derivatives in the larval zebrafish.

In neither mouse nor chick is there any evidence of trunk neural crest contributing to the cartilage or bone of the cranium during normal development (Kague et al., 2012). Normal growth of the craniofacial complex is controlled by genetic factors, along with epigenetic, environmental and regulatory mechanisms for morphogenesis of the head and face (Pisano and Greene, 1986). Therefore, dysregulation of the cranial neural crest or alterations within these extrinsic factors often cause craniofacial birth defects, which will be discussed later.

## Mammalian craniofacial development

The pharyngeal arches, which give rise to all craniofacial aspects, are first evident about three to four weeks into human development and by E8.5 in the mouse. It is within these arches that the nerves, skeletal tissue and epithelial specializations of the pharynx are established (Graham, 2003). The first, most anterior arch will give rise to the jaw, while the second forms the hyoid apparatus. The posterior arches develop and become incorporated into the throat. This patterning is the result of the integration between crest-dependent and independent cues, and when dysregulation of these cues occurs, orofacial deformities can develop (Graham, 2003, Dougherty et al., 2013).

In humans, palatal development occurs between the fifth and twelfth weeks of embryonic development, with the most critical period occurring between the sixth and ninth weeks (Merritt, 2005). In mice, this process begins at E10.5, with the critical period occurring just one day later (at E11.5) (Rice, 2005). In the fourth week of human embryonic growth, development of five facial prominences begins when neural crest cells migrate from the dorsal neural tube to the craniofacial region. The five facial prominences include the frontonasal, the paired maxillary, and the paired mandibular

structures (Fig. 5.2A) (Dudas et al., 2007, Mossey et al., 2009, Parker et al., 2010). Near the end of this fourth week, the nasal placodes develop. These structures are ectodermal thickenings on the lower half of the nasal prominence. Nasal pits then develop bilaterally within the placodes, with paired medial and lateral nasal processes developing from the frontonasal process on either side of the nasal placodes (Fig. 5.2B). At the end of the sixth week of gestation, the medial nasal processes fuse, forming the medial cleft of the upper lip (philtrum), and by the end of the eighth week they fuse with the adjacent maxillary processes, forming the upper lip and primary palate (Fig. 5.2C) (Marazita and Mooney, 2004, Merritt, 2005, Dudas et al., 2007, Mossey et al., 2009, Shkoukani et al., 2014).

The secondary palate begins to develop during the sixth week of human gestation and at E12.0 in mice (Rice, 2005). Outgrowths of the bilateral maxillary prominences develop into the palatal shelves, which orient themselves vertically along the lateral edges of the tongue. This process is primarily caused by a significant increase in the proliferation of the mesenchymal cells (Parker et al., 2010). In the following week, the jaw elongates, the tongue descends, and glycosaminoglycans are hydrated, causing the palatal shelves to rise to a horizontal position. The shelves remain adhesion incompetent until they are properly aligned with each other. Once aligned correctly and in contact with each other, the palatal shelves rapidly fuse (Fig. 5.2D-F). This occurs when the medial edge epithelia of the opposing shelves adhere and two epithelial layers are removed along the midline fusion by undergoing apoptosis. The remaining epithelia transdifferentiate into mesenchyme, allowing full fusion of the opposing shelves (Wedden, 1987, Ferguson, 1988, Francis-West et al., 2003, Rice, 2005).

Once fusion of the shelves is complete, the palatal mesenchyme is replaced by intramembranous bone formation, corresponding to the region of the hard palate, while the posterior section does not ossify and will become the soft palate (Merritt, 2005, Mossey et al., 2009, Iwata et al., 2011). When normal development occurs, the secondary palate has completed fusion with the lip and the nasal septum by the tenth week of embryonic development and is fully formed by the twelfth week (van Aalst et al., 2008, Mossey et al., 2009). In the mouse, palatal elevation and fusion begins at E14.0 and is complete by E15.0 (Rice, 2005).

The molecular pathways and processes involved in human craniofacial development seem to be conserved across multiple species, including the mouse, chick, *Xenopus* and zebrafish (Yelick and Schilling, 2002, Chai and Maxson, 2006, Baas et al., 2009, Schilling and Le Pabic, 2009, Szabo-Rogers et al., 2010, Dixon et al., 2011, Ferretti et al., 2011, Weiner et al., 2012). Two amniote models, the domestic chicken and the house mouse reveal striking similarity in the relative contributions of the cranial neural crest and paraxial mesoderm, which populate the discrete and largely non-overlapping territories of the skull (Couly et al., 1993, Noden and Trainor, 2005, Evans and Noden, 2006). A similar pattern of cranial neural crest contribution to the craniofacial skeleton has also been reported in zebrafish, a very distant phylogenetic relative (Kague et al., 2012, Mongera et al., 2013).

## Craniofacial development in the zebrafish

The musculoskeletal system of the zebrafish head, as in other vertebrates, is assembled from cartilage precursors derived primarily from the neural crest and from muscle precursors derived from head and trunk mesoderm (Noden, 1983, Schilling and

Kimmel, 1994, Schilling and Kimmel, 1997). Early in cranial development, three streams of neural crest cells, which arise from the hindbrain, migrate into the pharynx and together with cranial paraxial mesoderm and overlying ectoderm form the seven pharyngeal arches. These arches will develop into the musculoskeletal elements of the jaws and gills. The first two arches give rise to the musculoskeletal elements associated with movements of the jaw, while the third arch is associated with the support and movement of the gills (Schilling and Kimmel, 1997, Hernandez et al., 2005).

Neural crest within the first arch gives rise to the palatoquadrate and Meckel's cartilage, establishing the mandible of the zebrafish. The neural crest cells within the second arch give rise to the hyosymplectic, as well as the different elements of the hyoid (basihyal, interhyal and ceratohyal) process. Finally, neural crest within the third stream give rise to the five cartilaginous ceratobranchial elements associated with the gills (Schilling and Kimmel, 1994, Miller et al., 2003, Hernandez et al., 2005). In contrast to this, the cartilaginous structures that form the base of the skull and upper palate (ethmoid plate and parachordals) are of mixed origin (Fig. 5.1). The parachordal cartilage forms by condensation around the anterior tip of the notochord, but there is no evidence of neural crest contribution to this structure. Yet, the anterior ethmoid plate and trabeculae, which are attached, are neural crest-derived. In contrast to these other cartilages, the population of cells that derives these neurocranial structures originates from the midbrain and is thought to be analogous to the frontonasal process in mammals (Swartz et al., 2011, Kague et al., 2012, Dougherty et al., 2013).

Early in zebrafish development, the neurocranial structures are the first to appear, with the trabecular cartilages being detected at 45-48 hpf. Two parallel, single-cell rows

of chondrocytes form between the eyes of the larvae and fuse in the midline at their anterior ends to form the ethmoid plate around 56 hpf (Schilling and Kimmel, 1997, Wada et al., 2005). These structures seem to be the mammalian equivalent of the upper lip and primary palate, but no secondary palate develops in the fish (Dougherty et al., 2013). Around 50 hpf the parachordal cartilage appears and expands to form a broad basal plate which will fuse with the trabecular cartilages at around 53 hpf (Fig. 5.3A,B). Development then proceeds asynchronously as the palatoquadrate appears first, followed by the ceratohyal, the Meckel's cartilage, the ceratobranchial and the hyosymplectics, which all appear between 53 and 57 hpf. At this time, three sites of chondrification develop within a single hyoid cartilage; these correspond to the ceratohyals, the hyosymplectics and hyomandibular regions (Fig. 5.3C-E). By 68 hpf the symplectic and hyomandibular chondrifications expand and join, and the intherhyal cartilages also chondrify. The more posterior ceratobranchial cartilages differentiate between 60 and 68 hpf (Fig. 5.3F-H). By 74 hpf, the Meckel's cartilage and ceratohyal cartilages elongate and form joints with their contralateral parts. Later, at 90 hpf, the palatoquadrate elongates towards the ethmoid plate and forms a second joint (Fig. 5.3I-K) (Schilling and Kimmel, 1994, Schilling and Kimmel, 1997). Once these cartilages are established the skeleton continues to grow as the larva develops.

When abnormalities develop in the process of cartilage outgrowth or when neural crest cells are perturbed, craniofacial abnormalities generally occur. Zebrafish are now a well-developed model that has been extensively used in the study of human disease and development. This is because the zebrafish form essentially all of the same skeletal and muscle types as their higher vertebrate counterparts, but in a much more simple pattern

(Yelick and Schilling, 2002). It is because the cranial skeleton is so well conserved among vertebrates that the zebrafish can be used to study craniofacial development in humans (Cohen et al., 2014).

## Craniofacial defects

The process of palatogenesis is a very complex process that requires the correct temporal and spatial distribution of a number of growth factors, signaling factors and other biological molecules, as well as appropriately timed cell growth, differentiation, migration, transformation and apoptosis (Shkoukani et al., 2014). Therefore a number of causative factors can be related to the etiology of craniofacial defects. Craniofacial defects are among the most common birth defects in humans, affecting approximately 1 out of every 700 live births (Organization, 2002, Cohen et al., 2014). Most defects are not life threatening, but individuals with craniofacial defects can have difficulties with eating, hearing, speech and respiration that can severely decrease their quality of life.

Orofacial defects develop when individual elements or processes of the embryonic face fail to unite. This early facial development is controlled by tissue-tissue interactions between the epithelium and mesenchyme, and alterations in this signaling can lead to truncated facial development (Wedden, 1987, Francis-West et al., 2003, Rice, 2005). Yet, the etiology of craniofacial defects, including cleft lip and palate, is often complex and can include genetics, teratogen exposure, environmental factors and maternal/paternal age (Cohen et al., 2014, Shkoukani et al., 2014). Cleft palates can also be caused by effects secondary to more ‘distant’ abnormalities, notably in the development of the tongue, mandible or cranial base (Rice, 2005). Despite the number of

identifiable contributing factors, the etiologies of most clefts are multifactorial and remain to be completely delineated (Marazita and Mooney, 2004, Merritt, 2005).

The majority of orofacial malformations develop during the fifth through twelfth week of gestation, but the embryo is most sensitive to teratogen exposure between the third and ninth week of development (Rice, 2005). Diazepam is known to have anticonvulsant activity in both the mouse and in humans (Nicol et al., 1969, Miller and Becker, 1975). When this drug was administered to pregnant mice or women, cleft palate developed in offspring. Yet, the teratogenic effects were only observed when diazepam was administered late in palate development (Miller and Becker, 1975). Similarly, administration of phenytoin, a second anticonvulsant, increased the risk of cleft lip and palate by more than 10 fold in humans (Shkoukani et al., 2014). Under the influence of this drug, the lateral nasal process failed to expand to the size necessary for tight tissue contact with the nasal process (Poswillo, 1988, Rice, 2005). Smoking and alcohol seem to be additional risks.

It has also been proposed that the neurotransmitter GABA plays a role during shelf elevation and fusion in vertebrates. Studies in mice and humans have revealed that mutations in GAD1, but not GAD2, or of the $GABA_A$ receptor, beta 3 (GABARB3) subunit develop cleft palate (Culiat et al., 1995, Asada et al., 1997, Condie et al., 1997, Homanics et al., 1997, Maddox and Condie, 2001, Scapoli et al., 2002, Hagiwara et al., 2003, Kanno et al., 2004, Muhammad et al., 2013). Similarly, drugs known to alter GABA signaling, such as the benzodiazepines or the $GABA_A$ receptor channel blocker picrotoxin, can induce cleft palate when administered to pregnant mice during a critical period of palatogenesis (Miller and Becker, 1975, Wee and Zimmerman, 1983, Ben-

Shachar et al., 1987), or when used during pregnancy in humans (Aarskog, 1975, Safra and Oakley JR, 1975). Both loss-of-function (mutational or channel blocker) and enhancement (benzodiazepine) studies suggest that the processes of palatogenesis require a specific range of GABA signaling during a critical period to allow for normal development.

Studies in mice suggest that GABAergic signaling in the mesenchymal and/or epithelial cells of the developing palate control its development (Wee et al., 1985, Hagiwara et al., 2003, Ding et al., 2004). It is also believed that GABA, which is synthesized and secreted by nonneuronal cells in the palatal epithelium, mediates cellular proliferation during palatal shelf elevation and cell migration/differentiation during palatal fusion (Hagiwara et al., 2003). Together, these studies suggest that GABAergic signaling may play a key role in the mechanisms associated with the cellular proliferation, differentiation and development of the palate by acting through the $GABA_A$ receptor.

Figures

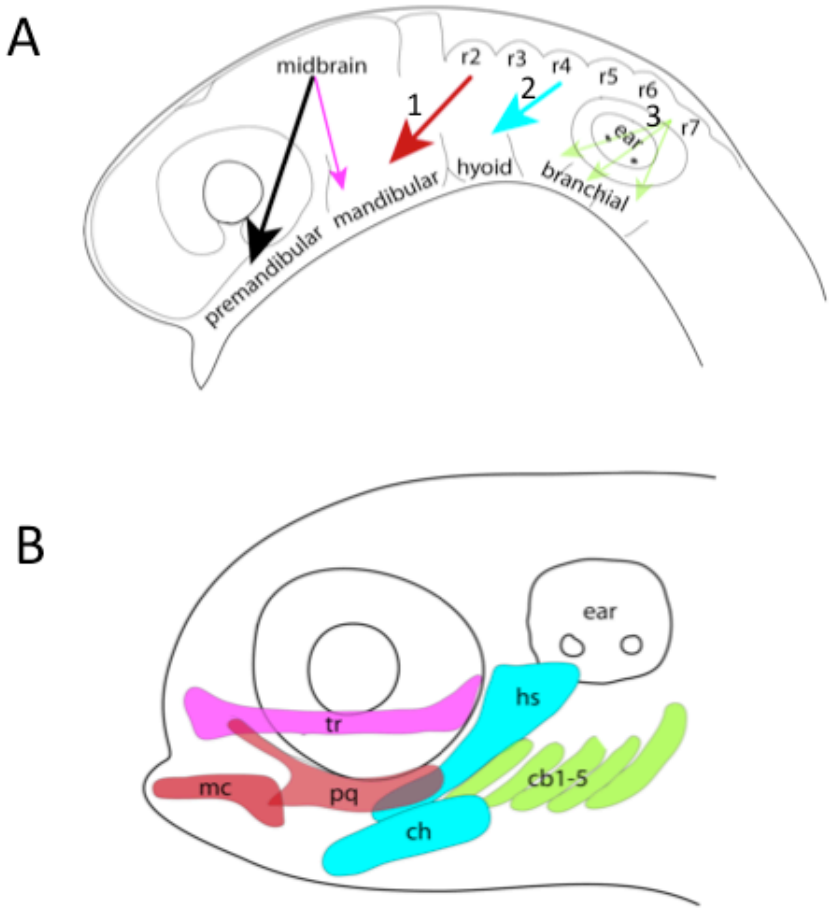


**Figure 5.1. Craniofacial structures in vertebrates are derived from cranial neural crest.** Adapted from J.D. Lauderdale. (A) At 24 hpf in zebrafish, the anterior neural crest (neurocranial precursors) migrate from the midbrain to the mandibular arch (pink arrow). The viscerocranial precursors emigrate in three streams from the hindbrain into the mandibular (stream 1, red arrow), hyoid (stream 2, blue arrow) and five branchial (stream 3, green arrows) arches. (B) At 72 hpf, the cranial neural crest have differentiated and the viscerocranial and neurocranial structures have developed. In zebrafish, these include the tr, mc, pq, ch, hs and cb cartilages. The colored arrows in A correspond to the colored cartilages in B that arise from each neural crest population. cb, ceratobranchial; ch, ceratohyal; hs, hyosymplectic; mc, meckels cartilage; pq, palatoquadrate; tr, trabeculae

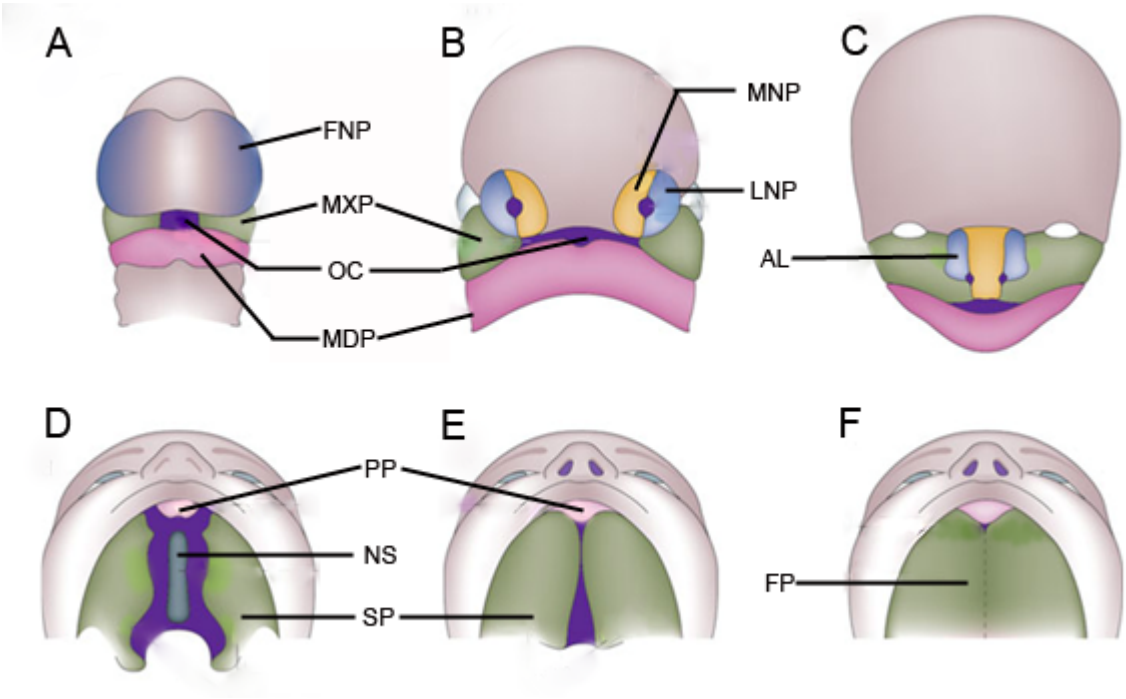


**Figure 5.2. Mammalian craniofacial development.** Adapted from (Wilkie and Morriss-Kay, 2001) (A) During the fourth week of human embryonic growth, five facial prominences develop, including the FNP, bilateral MXPs, and bilateral MDPs. (B) Near the end of the fourth week, nasal pits begin to develop bilaterally. The FNP will give rise to paired MNPs and LNPs on either side of the nasal placodes. (C,D) At the end of the eighth week of gestation, the nasal processes fuse, forming the upper lip and PP. Formation of the SP begins during the sixth week of development. (E) Outgrowths of the MXPs develop into the palatal shelves, extend, and align with each other. (F) Once aligned correctly and in contact with each other, the palatal shelves rapidly fuse. AL, alae; FNP, frontonasal process; FP, fused palate; LNP, lateral nasal process; MDP, mandibular process; MNP, medial nasal process; MXP, maxillary process; NS, nasal septum; OC, oral cavity; PP, primary palate; SP, secondary palate

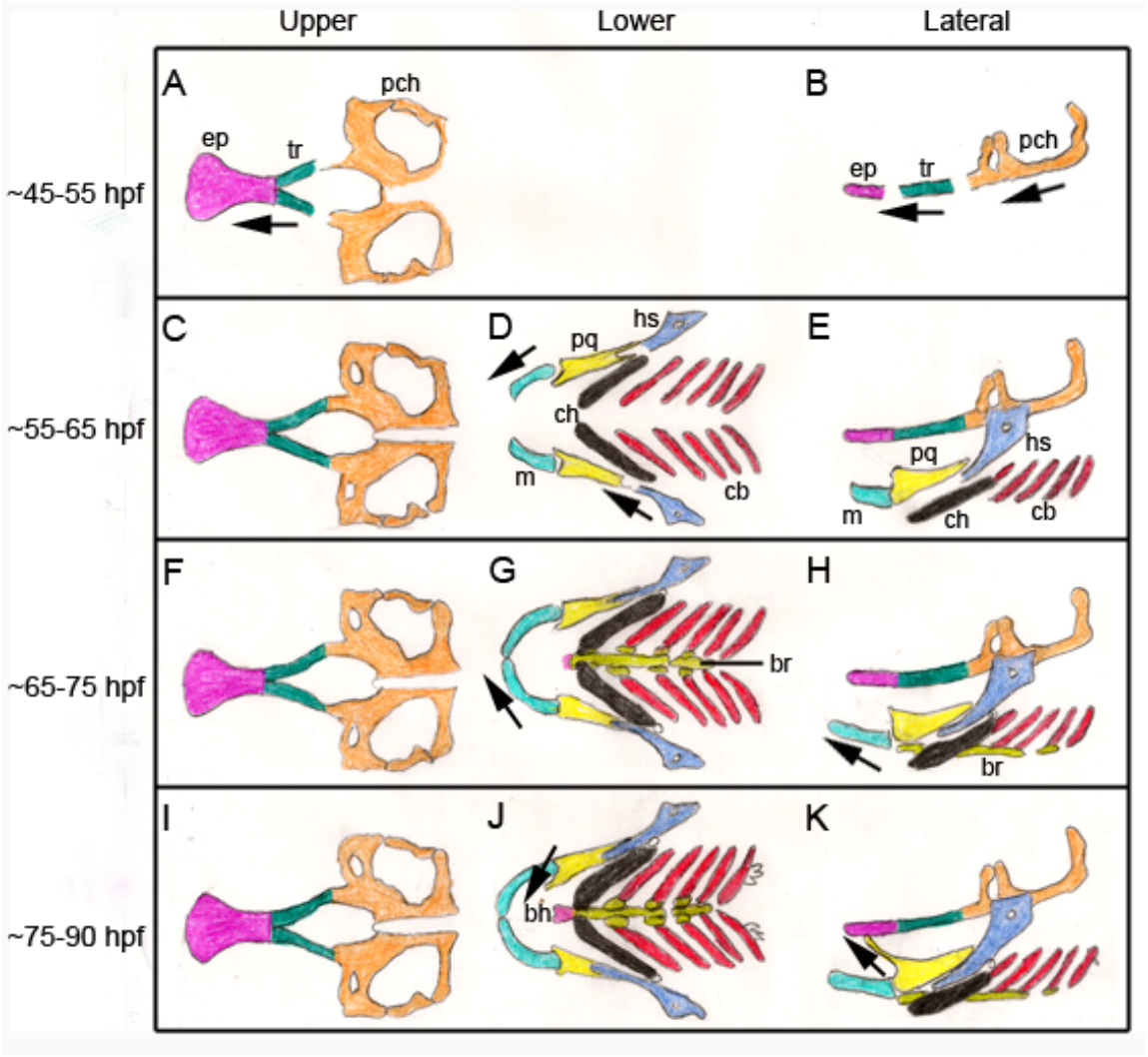


**Figure 5.3. Craniofacial development in the zebrafish.** (A,C,F,I) Development of the neurocranial structures. (D,G,J) Development of the viscerocranial structures. (B,E,H,K) Lateral view of developing cranial cartilages. (A,B) About 45 hpf, two parallel, tr form between the eyes of the larva and fuse in the midline at their anterior ends to form the ep around 56 hpf. Around 50 hpf the pch cartilage appears and expands to form a broad basal plate which will fuse with the tr cartilages at around 53 hpf. (C-E) Development then proceeds asynchronously as the pq appears, followed by the ch, the m cartilage, the cb and the hs, which all appear between 53 and 57 hpf. The more posterior cb cartilages differentiate between 60 and 68 hpf. (F-H) By 68 hpf the symplectic and hyomandibular chondrifications expand and join, and the intherhyal cartilages also chondrify. By 74 hpf, the m cartilage and ch cartilages elongate and form joints. (I-K) Later, by 90 hpf, the pq elongates towards the ep and forms a second joint. Once these cartilages are established the skeleton continues to grow as the larva develops. Black arrows show areas of cartilage extension. bh, basihyal; br, branchial structures; cb, ceratobranchial; ch, ceratohyal; ep, ethmoid plate; hs, hyosymplectic; m, meckels cartilage; pch, parachordal; pq, palatoquadrate; tr, trabeculae

## References


Aarskog D (1975) Association between maternal intake of diazepam and oral clefts. The Lancet 306:921.

Alexander C, Zuniga E, Blitz IL, Wada N, Le Pabic P, Javidan Y, Zhang T, Cho KW, Crump JG, Schilling TF (2011) Combinatorial roles for BMPs and Endothelin 1 in patterning the dorsal-ventral axis of the craniofacial skeleton. Development 138:5135-5146.

Asada H, Kawamura Y, Maruyama K, Kume H, Ding R-G, Kanbara N, Kuzume H, Sanbo M, Yagi T, Obata K (1997) Cleft palate and decreased brain γ-aminobutyric acid in mice lacking the 67-kDa isoform of glutamic acid decarboxylase. Proceedings of the National Academy of Sciences 94:6496-6499.

Baas D, Malbouyres M, Haftek-Terreau Z, Le Guellec D, Ruggiero F (2009) Craniofacial cartilage morphogenesis requires zebrafish *col11a1* activity. Matrix Biology 28:490-502.

Ben-Shachar D, Laufer D, Livne E, Silbermann M (1987) Picrotoxin, a gamma-aminobutyric acid-receptor antagonist, retards craniofacial development in the weaning rat: I. Effect on mandibular bone growth. Journal of craniofacial genetics and developmental biology 8:351-361.

Chai Y, Maxson RE (2006) Recent advances in craniofacial morphogenesis. Developmental Dynamics 235:2353-2375.

Cohen SP, LaChappelle AR, Walker BS, Lassiter CS (2014) Modulation of estrogen causes disruption of craniofacial chondrogenesis in *Danio rerio*. Aquatic Toxicology 152:113-120.

Condie BG, Bain G, Gottlieb DI, Capecchi MR (1997) Cleft palate in mice with a targeted mutation in the γ-aminobutyric acid-producing enzyme glutamic acid decarboxylase 67. Proceedings of the National Academy of Sciences 94:11451-11455.

Couly GF, Coltey PM, Le Douarin NM (1993) The triple origin of skull in higher vertebrates: a study in quail-chick chimeras. Development 117:409-429.

Culiat CT, Stubbs LJ, Woychik RP, Russell LB, Johnson DK, Rinchik EM (1995) Deficiency of the beta 3 subunit of the type A gamma-aminobutyric acid receptor causes cleft palate in mice. Nature genetics 11:344-346.

Ding R, Tsunekawa N, Obata K (2004) Cleft palate by picrotoxin or 3-MP and palatal shelf elevation in GABA-deficient mice. Neurotoxicology and teratology 26:587-592.

Dixon MJ, Marazita ML, Beaty TH, Murray JC (2011) Cleft lip and palate: understanding genetic and environmental influences. Nature Reviews Genetics 12:167-178.

Dougherty M, Kamel G, Grimaldi M, Gfrerer L, Shubinets V, Ethier R, Hickey G, Cornell RA, Liao EC (2013) Distinct requirements for wnt9a and irf6 in extension and integration mechanisms during zebrafish palate morphogenesis. Development 140:76-81.

Dudas M, Li WY, Kim J, Yang A, Kaartinen V (2007) Palatal fusion - where do the midline cells go? A review on cleft palate, a major human birth defect. Acta histochemica 109:1-14.

Evans DJ, Noden DM (2006) Spatial relations between avian craniofacial neural crest and paraxial mesoderm cells. Developmental dynamics : an official publication of the American Association of Anatomists 235:1310-1325.

Ferguson MW (1988) Palate development. Development 103 Suppl:41-60.

Ferretti E, Li B, Zewdu R, Wells V, Hebert JM, Karner C, Anderson MJ, Williams T, Dixon J, Dixon MJ (2011) A conserved Pbx-Wnt-p63-Irf6 regulatory module controls face morphogenesis by promoting epithelial apoptosis. Developmental cell 21:627-641.

Francis-West PH, Robson L, Evans DJ (2003) Craniofacial development: the tissue and molecular interactions that control development of the head. Advances in anatomy, embryology, and cell biology 169:III-VI, 1-138.

Graham A (2003) Development of the pharyngeal arches. American Journal of Medical Genetics Part A 119A:251-256.

Hagiwara N, Katarova Z, Siracusa LD, Brilliant MH (2003) Nonneuronal expression of the $GABA_A$ β3 subunit gene is required for normal palate development in mice. Developmental biology 254:93-101.

Hernandez LP, Patterson SE, Devoto SH (2005) The development of muscle fiber type identity in zebrafish cranial muscles. Anatomy and embryology 209:323-334.

Homanics GE, DeLorey TM, Firestone LL, Quinlan JJ, Handforth A, Harrison NL, Krasowski MD, Rick CE, Korpi ER, Mäkelä R (1997) Mice devoid of γ-aminobutyrate type A receptor β3 subunit have epilepsy, cleft palate, and hypersensitive behavior. Proceedings of the National Academy of Sciences 94:4143-4148.

Iwata J, Parada C, Chai Y (2011) The mechanism of TGF-beta signaling during palate development. Oral diseases 17:733-744.

Kague E, Gallagher M, Burke S, Parsons M, Franz-Odendaal T, Fisher S (2012) Skeletogenic fate of zebrafish cranial and trunk neural crest. PloS one 7:e47394.

Kanno K, Suzuki Y, Yamada A, Aoki Y, Kure S, Matsubara Y (2004) Association between nonsyndromic cleft lip with or without cleft palate and the glutamic acid decarboxylase 67 gene in the Japanese population. American journal of medical genetics Part A 127A:11-16.

Kimmel CB, Miller CT, Moens CB (2001) Specification and morphogenesis of the zebrafish larval head skeleton. Developmental biology 233:239-257.

Knight RD, Schilling TF (2006) Cranial neural crest and development of the head skeleton. Advances in experimental medicine and biology 589:120-133.

Le Douarin N, Kalcheim C (1999) The neural crest: Cambridge University Press.

Lumsden A, Sprawson N, Graham A (1991) Segmental origin and migration of neural crest cells in the hindbrain region of the chick embryo. Development 113:1281-1291.

Maddox DM, Condie BG (2001) Dynamic expression of a glutamate decarboxylase gene in multiple non-neural tissues during mouse development. BMC developmental biology 1:1.

Marazita ML, Mooney MP (2004) Current concepts in the embryology and genetics of cleft lip and cleft palate. Clinics in plastic surgery 31:125-140.

Merritt L (2005) Part 1. Understanding the embryology and genetics of cleft lip and palate. Advances in neonatal care : official journal of the National Association of Neonatal Nurses 5:64-71.

Miller CT, Yelon D, Stainier DY, Kimmel CB (2003) Two endothelin 1 effectors, hand2 and bapx1, pattern ventral pharyngeal cartilage and the jaw joint. Development 130:1353-1365.

Miller RP, Becker BA (1975) Teratogenicity of oral diazepam and diphenylhydantoin in mice. Toxicology and applied pharmacology 32:53-61.

Mongera A, Singh AP, Levesque MP, Chen YY, Konstantinidis P, Nusslein-Volhard C (2013) Genetic lineage labeling in zebrafish uncovers novel neural crest contributions to the head, including gill pillar cells. Development 140:916-925.

Mossey PA, Little J, Munger RG, Dixon MJ, Shaw WC (2009) Cleft lip and palate. Lancet 374:1773-1785.

Muhammad SI, Maznah I, Mahmud R, Zuki AB, Imam MU (2013) Upregulation of genes related to bone formation by gamma-amino butyric acid and gamma-oryzanol in germinated brown rice is via the activation of GABAB-receptors and reduction of serum IL-6 in rats. Clinical interventions in aging 8:1259-1271.

Nicol CF, Tutton JC, Smith BH (1969) Parenteral diazepam in status epilepticus. Neurology 19:332-343.

Noden DM (1983) The role of the neural crest in patterning of avian cranial skeletal, connective, and muscle tissues. Developmental biology 96:144-165.

Noden DM, Trainor PA (2005) Relations and interactions between cranial mesoderm and neural crest populations. J Anat 207:575-601.

Organization WH (2002) The World health report: 2002: Reducing the risks, promoting healthy life.

Parker SE, Mai CT, Canfield MA, Rickard R, Wang Y, Meyer RE, Anderson P, Mason CA, Collins JS, Kirby RS, Correa A, National Birth Defects Prevention N (2010) Updated National Birth Prevalence estimates for selected birth defects in the United States, 2004-2006. Birth defects research Part A, Clinical and molecular teratology 88:1008-1016.

Pisano M, Greene R (1986) HORMONE AND GROWTH-FACTOR INVOLVEMENT IN CRANIOFACIAL DEVELOPMENT. IRCS MEDICAL SCIENCE-BIOCHEMISTRY 14:635-640.

Poswillo D (1988) The aetiology and pathogenesis of craniofacial deformity. Development 103 Suppl:207-212.

Rice DP (2005) Craniofacial anomalies: from development to molecular pathogenesis. Current molecular medicine 5:699-722.

Safra M, Oakley JR G (1975) Association between cleft lip with or without cleft palate and prenatal exposure to diazepam. The Lancet 306:478-480.

Saint-Jeannet J-P (2006) Neural crest induction and differentiation: Springer Science+ Business Media.

Scapoli L, Martinelli M, Pezzetti F, Carinci F, Bodo M, Tognon M, Carinci P (2002) Linkage disequilibrium between GABRB3 gene and nonsyndromic familial cleft lip with or without cleft palate. Human genetics 110:15-20.

Schilling TF (1997a) Genetic analysis of craniofacial development in the vertebrate embryo. BioEssays : news and reviews in molecular, cellular and developmental biology 19:459-468.

Schilling TF (1997b) Genetic analysis of craniofacial development in the vertebrate embryo. BioEssays : news and reviews in molecular, cellular and developmental biology 19:459-468.

Schilling TF, Kimmel CB (1994) Segment and cell type lineage restrictions during pharyngeal arch development in the zebrafish embryo. Development 120:483-494.

Schilling TF, Kimmel CB (1997) Musculoskeletal patterning in the pharyngeal segments of the zebrafish embryo. Development 124:2945-2960.

Schilling TF, Le Pabic P (2009) Fishing for the signals that pattern the face. J Biol 8:101.

Schilling TF, Piotrowski T, Grandel H, Brand M, Heisenberg CP, Jiang YJ, Beuchle D, Hammerschmidt M, Kane DA, Mullins MC, van Eeden FJ, Kelsh RN, Furutani-Seiki M, Granato M, Haffter P, Odenthal J, Warga RM, Trowe T, Nusslein-Volhard C (1996) Jaw and branchial arch mutants in zebrafish I: branchial arches. Development 123:329-344.

Shkoukani MA, Lawrence LA, Liebertz DJ, Svider PF (2014) Cleft palate: A clinical review. Birth defects research Part C, Embryo today : reviews 102:333-342.

Swartz ME, Sheehan‐Rooney K, Dixon MJ, Eberhart JK (2011) Examination of a palatogenic gene program in zebrafish. Developmental Dynamics 240:2204-2220.

Szabo-Rogers HL, Smithers LE, Yakob W, Liu KJ (2010) New directions in craniofacial morphogenesis. Developmental biology 341:84-94.

Trainor PA, Melton KR, Manzanares M (2003) Origins and plasticity of neural crest cells and their roles in jaw and craniofacial evolution. International Journal of Developmental Biology 47:541-553.

van Aalst JA, Kolappa KK, Sadove M (2008) MOC-PSSM CME article: Nonsyndromic cleft palate. Plastic and reconstructive surgery 121:1-14.

Wada N, Javidan Y, Nelson S, Carney TJ, Kelsh RN, Schilling TF (2005) Hedgehog signaling is required for cranial neural crest morphogenesis and chondrogenesis at the midline in the zebrafish skull. Development 132:3977-3988.

Wedden SE (1987) Epithelial-mesenchymal interactions in the development of chick facial primordia and the target of retinoid action. Development 99:341-351.

Wee E, Norman E, Zimmerman E (1985) Presence of gamma-aminobutyric acid in embryonic palates of AJ and SWV mouse strains. Journal of craniofacial genetics and developmental biology 6:53-61.

Wee EL, Zimmerman EF (1983) Involvement of GABA in palate morphogenesis and its relation to diazepam teratogenesis in two mouse strains. Teratology 28:15-22.

Weiner AM, Scampoli NL, Calcaterra NB (2012) Fishing the molecular bases of Treacher Collins syndrome. PloS one 7:e29574.

Wilkie AO, Morriss-Kay GM (2001) Genetics of craniofacial development and malformation. Nat Rev Genet 2:458-468.

Yelick PC, Schilling TF (2002) Molecular dissection of craniofacial development using zebrafish. Critical Reviews in Oral Biology & Medicine 13:308-322.

# CHAPTER 6

# DETERMINING THE ROLE OF GABAERGIC SIGNALING IN THE CRANIOFACIAL DEVELOPMENT OF LARVAL ZEBRAFISH[1]

[1]Beebe, L.L., Ball, R.E., Page, A.T., VanLeuven, A.J., O'Connor, M.J., Dore, T.M., and James D. Lauderdale. To be submitted to *Developmental Cell*.

Abstract

Although best known as an inhibitory neurotransmitter, evidence has implicated GABA as a key signaling molecule in craniofacial development in mammals. However, the mechanism of this process cannot be easily investigated. In our study, translation-blocking morpholinos against the *gad* genes were used to alter GABA expression within larval zebrafish. While *gad2* morphant animals look phenotypically normal, *gad1* morphants exhibit altered cranial structures. Because these structures are neural crest derived, we observed that while expression of early crest markers were only slightly altered, expression of *dlx2a* was significantly delayed. Electrophysiological recordings from *gad1* and *gad2* morphants exhibited abnormal neural activity, when compared to wild type animals. Through the use of caged-morpholinos, cranial deformities could be bypassed when photolyzed at 24 hpf, but morphant animals exhibited abnormal neurological activity. These findings support the idea that *gad1* exhibits a novel function in craniofacial development, independent of its activity in GABA synthesis.

Highlights

- *gad1* is required for proper head outgrowth and arch cartilage patterning
- Knockdown of *gad1* causes disorderly stacking of chondrocytes, suggesting disruption of the earlier stages of chondrogenesis
- *gad1* is required for expression and survival of a subset of neural crest cells migrating to the pharyngeal arches
- Knockdown of *gad1* can be rescued with *gad1* mRNA and *dlx2a* mRNA

## Introduction

Craniofacial anomalies are among the most common birth defects in the human population, with an estimated prevalence of 1 in 600 live births worldwide. These include oral clefts (lip and/or palate), jaw deformities, and defects in the ossification of the facial or cranial bones. Factors that contribute to these conditions are often complex and can include nutrition, drug exposure, environmental factors and heredity (Organization, 2002, Chai and Maxson, 2006, Dixon et al., 2011). The molecular pathways involved in human craniofacial development seem to be conserved across many species including mouse, chick, *Xenopus*, and zebrafish (Miller et al., 2003, Schilling and Le Pabic, 2009, Szabo-Rogers et al., 2010, Ferretti et al., 2011, Swartz et al., 2011). It is believed that some cranial malformations, including oral clefts, could be modulated by neurotransmitters (Ben-Shachar et al., 1987). Studies in humans and rodents have implicated a rather unexpected causal agent in the form of disruptions in γ-aminobutyric acid (GABA) signaling, however the underlying cellular and molecular mechanisms cannot be easily investigated using the existing mouse models or in human patients.

The major pathway through which GABA is synthesized is by the α-decarboxylation of glutamic acid to GABA, by the action of glutamic acid decarboxylase (GAD) (Tillakaratne et al., 1995, Martin et al., 1998, Maddox and Condie, 2001, Kim et al., 2004). In vertebrates, GAD exists in two protein isoforms, each of which is encoded by a separate gene (Bu et al., 1992, Tillakaratne et al., 1995, Martin et al., 1998). In mammals, the GAD1 gene encodes for the protein isoform called GAD67 and the GAD2 gene encodes the protein isoform GAD65 (Erlander et al., 1991, Bu et al., 1992, Asada et al., 1997, Bosma et al., 1999, Maddox and Condie, 2001, Delgado and Schmachtenberg,

2008). These enzymes are highly conserved and have been described in *Drosophila*, avian and mammalian species (Martin et al., 1998). Once synthesized, GABA acts as the ligand for the ionotropic $GABA_A$ receptors, as well as for the metabotropic $GABA_B$ receptor.

Studies in mice and humans have revealed that mutations in *gad1*, but not *gad2*, or of the gene that encodes the $GABA_A$ receptor, *beta 3* (GABARB3) subunit develop cleft palate (Culiat et al., 1995, Asada et al., 1997, Condie et al., 1997, Homanics et al., 1997, Maddox and Condie, 2001, Scapoli et al., 2002, Hagiwara et al., 2003, Kanno et al., 2004, Muhammad et al., 2013). Similarly, drugs known to alter GABA signaling, such as the benzodiazepine drug diazepam (a GABA agonist), can induce cleft palate when administered to pregnant mice during a critical period of palatogenesis (Miller and Becker, 1975, Wee and Zimmerman, 1983), or used during pregnancy in humans (Aarskog, 1975, Safra and Oakley JR, 1975). Both loss-of-function and enhancement studies suggest that the processes of palatogenesis require a specific range of GABA signaling, during a critical period, to allow for normal development. Studies in mice suggest that GABAergic signaling from the mesenchymal and/or epithelial cells of the developing palate control its development (Wee et al., 1985, Hagiwara et al., 2003, Ding et al., 2004). It is believed that GABA, which is synthesized and secreted by nonneuronal cells in the palatal epithelium, mediates cellular proliferation during palatal shelf elevations and cell migration/differentiation during palatal fusion (Hagiwara et al., 2003). Together, these studies propose that GABAergic signaling may play a role in the mechanisms associated with cellular proliferation, differentiation and development of the palate by acting through the $GABA_A$ receptor. Despite this demonstrated importance in

early craniofacial development, the mechanism of how an alteration in GAD or GABA signaling regulates this pathway remains unknown.

In all vertebrates examined, much of the head skeleton and peripheral nervous system develops from migratory cells of the neural crest, with contributions from ectoderm, endoderm and paraxial mesoderm (Schilling et al., 1996b, Schilling and Kimmel, 1997, Le Douarin and Kalcheim, 1999). Neural crest cells arise from the dorsal neural tube and form the anterior neurocranium and segmented pharyngeal skeleton, as well as sensory neurons, glia and pigment cells (Le Douarin and Kalcheim, 1999). In zebrafish, where the central nervous system develops through a process of secondary neurulation, neural crest cells are specified from ectoderm at the dorsal and dorsolateral aspects of the neural keel (Eisen and Weston, 1993, Schilling and Kimmel, 1994). Following the specification of premigratory neural crest, these cells express a unique set of transcription factors, including *Foxd3*, *Snai1b*, *Sox10* and *Tfap2a* (Knecht and Bronner-Fraser, 2002, Barrallo-Gimeno et al., 2004), which aid in further specification and survival of this cell population.

Following specification, the cranial neural crest cells migrate in multiple streams to populate the premandibular region and the seven posterior pharyngeal arches, with the most anterior populations migrating first. This pharyngeal segmentation is patterned, in part, by the segmental migration of the neural crest cells, which correlates with its rhombomeric point of origin (Noden, 1983, Schilling, 1997, Wada et al., 2005). Neurocranial precursors emerge from midbrain levels and migrate between the eyes to form the palatal shelves, while the viscerocranial precursors stream from the hindbrain into the mandibular (stream 1), hyoid (stream 2) and branchial (stream 3-7) arches

(Schilling and Kimmel, 1994, Yelick and Schilling, 2002, Knight and Schilling, 2006). Normal growth of this craniofacial complex is controlled by genetic factors, along with epigenetic, environmental and regulatory mechanisms for morphogenesis of the head and face (Pisano and Greene, 1986).

Here, we focus on the role of *gad1* in early craniofacial development within the zebrafish. Due to premature death of GAD67-/- mice, we used a morpholino-based approach to knockdown *gad1* and *gad2* within the larval zebrafish. Similar to the mouse, *gad2* knockdown did not cause any observable phenotype, while *gad1* morphant animals exhibited dramatically altered craniofacial cartilages. Changes in the craniofacial region were caused by the abnormal patterning of chondrocytes, which led to the development of smaller and misshapen cranial cartilages. This phenotype could be phenocopied when GABA signaling was altered pharamacologically through bath application of $GABA_A$ antagonists to early stage embryos. Early neural crest specification factors were present but slightly altered both in *gad1* morphants and in drug-treated animals. Most dramatically, *dlx2a* expression was delayed in morphant and drug-treated embryos. These changes could be bypassed when caged-morpholinos were photolyzed at 24hpf. Together our findings suggest that altering the levels of GABA by knockdown of *gad1* affects GABAergic signaling through the $GABA_A$ receptor. These alterations seem to cause changes in the migration and differentiation of early neural crest, leading to abnormal patterning of the craniofacial cartilage and pharyngeal arches.

## Results

### *gad1 is required for proper head outgrowth*

To determine the functions of *gad1* and *gad2* during early zebrafish development, translation-blocking morpholinos were injected into 1-4 cell stage embryos and observed during the first 7 days of development. It was determined that knockdown of *gad1*, but not *gad2*, lead to abnormal head outgrowth (Fig. 6.1). While *gad2* morphants looked phenotypically comparable to wild-type animals at all time points observed (Fig. 6.1A,B,E,F,I,J), *gad1* morphant animals did not. This remained true for all concentrations of morpholino tested (SFig. 6.1 and SFig. 6.2). Working concentrations for morpholinos were determined from the concentration that maintained high survivability, while ablating protein presence (as measured by western blot). At 1 dpf, *gad1* morphants exhibited an elongated and abnormally shaped telencephalon and the eye field was diminished and anteriorly rotated when compared to wild-type animals (Fig. 6.1A,C). This phenotype persisted and by 3 dpf, the jaw and mouth failed to extend correctly (Fig. 6.1G). By 7 dpf, the lower jaw in *gad1* morphants had extended, but it caused these animals to have a "pursed" appearance when compared to wild-type animals (Fig. 6.1K).

To confirm the specificity of the phenotype caused by the morpholinos, rescue experiments were carried out using synthetic mRNA for the zebrafish *gad1* gene. The sequence of the translation initiation codon was altered from the wild-type sequence so that the morpholinos would not target them. Embryos were examined for rescue by morphological examination at 1, 3, and 7 dpf (Fig. 6.1) and by alcian blue staining at 7 dpf (Fig. 6.2). The amount of mRNA injected was such that the *gad1* morphant phenotype was rescued and survivability remained high (SFig. 6.3). Animals co-injected

with *gad1* morpholino and *gad1* mRNA exhibited a phenotype comparable to wild-type animals throughout the first week of development (Fig. 6.1D,H,L). Conversely, when *gad1* mRNA was overexpressed, abnormal head development was also observed (data not shown). Together these findings suggest that *gad1*, but not *gad2* is required for normal development of the head within the first week of development in the zebrafish.

***gad1 is required for proper arch cartilage patterning***

To determine which aspects of head development were being affected, we next looked to see if cartilage development was altered at 7 dpf, a time when all head cartilages are present and chondrified (Schilling and Kimmel, 1997). Animals were treated with 1-phenyl 2-thiourea (PTU) during embryogenesis to prevent pigment formation (Karlsson et al., 2001), collected at 7 dpf and alcian stained to observe the gross morphology of the cranial cartilages. For whole-mount analysis, the Meckels, parachordal and ceratohyal cartilages were the structures that were measured. These structures were chosen because they were positioned consistently, allowing for accurate measurements to be obtained. Supplementary Figure 6.4A depicts the measurements collected from whole-mount, alcian stained specimens. All cranial cartilages were present in both *gad1* and *gad2* morphants, yet, the cartilaginous structures of *gad1* morphants were significantly smaller than those of wild-type or *gad2* morphant animals (SFig. 6.4B). These findings lead us to question the cause of these smaller structures: was it due to a lack of cells or abnormal chondrocyte morphology?

To address these questions, the cranial cartilages of alcian stained animals were dissected out and flat mounted (Fig. 6.2). Figure 6.2B depicts a cartoon of the cartilages that make up the neurocranial structures in 7 dpf zebrafish, including the ethmoid plate

(ep), trabeculae (tr) and parachordal cartilages (pch); the corresponding samples are shown in panels D-F. Figure 6.2C depicts a cartoon of the cartilages of the viscerocranium and include the Meckels (m), palatoquadrate (pq), basihyal (bh), ceratohyal (ch), interhyal (ih), hyosymplectic (hs) and the ceratobranchial (cb) cartilages; the corresponding samples are shown in panels G-I. Analysis of the pharyngeal skeleton in *gad1* morphants showed that while all skeletal elements were present and in the correct relative positions, many of these structures were irregularly shaped. Most noticeably, the ep was significantly smaller and abnormally shaped and the tr were elongated and poorly angled when compared to wild-type animals (Fig. 6.2D,E). Similarly, in the viscerocranium, all structures were smaller in *gad1* morphants, and the bh and cb structures were not fully elongated. These abnormalities were also rescued through the co-injection of *gad1* morpholino and *gad1* mRNA (Fig. 6.2F,I). Cell counts were carried out to determine if this abnormal morphology was caused by a lack of cells, but no significant changes in cell number were observed (data not shown).

A lack of change in cell numbers supported the hypothesis that the observed changes in cartilage size and morphology were caused by an abnormal chondrocyte morphology and stacking pattern. High-magnification images of the m cartilage, with small regions of the bh and pq in the field of view, are seen in Supplementary Fig. 6.5. In all of these cartilages, chondrocytes were abnormally elongated and incorrectly patterned. Instead of observing the wild-type morphology, where chondrocytes stack in a single-cell layer and are nicely elongated (SFig. 6.5A), the chondrocytes in *gad1* morphants retained a hexagonal or circular structure and seemed to be arranged in a stacked/overlaping manner. Also, single chondrocytes were smaller throughout the cartilages of *gad1*

morphants (SFig. 6.5B). These changes were apparent in all cartilages of the head skeleton, but easily noticeable in the Meckels region. This morphant phenotype was partially rescued through the co-injection of *gad1* morpholino and *gad1* mRNA; cells within the midline of the Meckels cartilage did not elongate normally, but cells more posterior to this area adapted a wild-type phenotype (SFig. 6.5C). These results demonstrate that *gad1* is required for patterning of the arch cartilage, but not for element identity per se. The disorderly stacking of chondrocytes also suggested that a disruption in the early stages of chondrogenesis was occurring (Thorogood, 1983, Kimmel et al., 1998).

***gad1 is required for normal expression of early cranial neural crest markers***

The head skeleton in zebrafish, as in mammals, is derived from cranial neural crest cells. To determine if these populations of cells were affected from knockdown of *gad1*, early neural crest markers were observed using *in situ* hybridization. For this analysis, the 10-12 somite stage was focused on, as this is a stage before neural crest migration has begun. As shown in Figure 6.3, the presence and expression patterns of *prdm1a, foxd3, tfap2a* and *snai1b* appeared similar between wild-type and *gad1* morphant animals when observed laterally (Fig. 6.3A,C,E,G,I,K,M,O). Yet, when these animals were observed dorsally, it was determined that expression of these markers varied. While *prdm1a* expression remained unaltered in *gad1* morphants (Fig. 6.3A-D), it was determined that these animals exhibited an expanded band of *foxd3* expression within the hindbrain region (Fig. 6.3B,D). The expression of *tfap2a* was also increased within the region of the developing head (Fig. 6.3J,L). When *snai1b* expression was observed, it was found that the level of expression was increased in *gad1* morphant

animals, but this expression did not extend as far anteriorly as was found in wild-type animals (Fig. 6.3N,P). Although the expression of these early neural crest markers varied in *gad1* morphants compared to wild-type animals, they were present, suggesting that these neural crest cell populations were generally in the correct region and at the correct time.

When the neural crest populations were observed at 1 dpf, it was found that the expression patterns of *foxd3* and *sox10* were altered (Fig. 6.4). Although each were present at a level comparable to wild-type animals, the expression patterns for each were disorganized in the region between the eye and the ear of *gad1* morphant animals (Fig. 6.4A-D). We also looked at the level of apoptosis in these *gad1* morphants. At 1 dpf, during the time of neural crest migration, a significant increase in apoptotic cells was observed throughout the cranial region of *gad1* morphants. Most noticeably, a large population of apoptotic cells was present just anterior to the ear in morphant animals (Fig. 6.4E,F). This change was not observed in *gad2* or mismatch morphant animals (data not shown). These findings suggest that *gad1* may have a role during neural crest survival and proliferation.

**_gad1_ is required for _dlx2a_ expression**

To look at the possibility that *gad1* signaling is involved in neural crest survival and proliferation, we next looked at the expression of *dlx2a*, a transcription factor required for the survival of migrating neural crest cells. We found that *dlx2a* expression was significantly delayed in *gad1* morphants (Fig. 6.5). At the 10-12 somite stage*, dlx2a* expression was not detectable within the developing pharyngeal arches of *gad1* morphants (Fig. 6.5A,B). At the 18 somite stage, *dlx2a* expression was observed in these

morphants, but at very low levels when compared to wild-type animals (Fig. 6.5D,E). By 24 hpf, *dlx2a* was expressed in a normal pattern within *gad1* morphants (Fig. 6.5G,H), but it was not until ~30 hpf that expression levels were comparable to wild-type animals (data not shown). These data are consistent with the finding that apoptosis was increased in *gad1* morphant animals (Fig. 6.4E,F). This reduction in *dlx2a* expression was successfully rescued at each time point through the co-injection of *gad1* morpholino and *gad1* mRNA (Fig. 6.5C,F,I). Also, this change in *dlx2a* expression was never observed in *gad2* morphant animals (data not shown). Together, these data suggest that the changes observed in *dlx2a* expression were specific to the knockdown of *gad1*. These findings also support the idea that *gad1* could serve a role in neural crest survival and proliferation, by acting through *dlx2a*.

Previous work in mice has shown that the spatial and temporal expression of *dlx2a* and the *gad* genes overlap (Stühmer et al., 2002, MacDonald et al., 2010). Both *in vitro* and *in vivo* studies suggest that *dlx2a* can act as a key regulator of *gad1* (Stühmer et al., 2002, Sperber et al., 2008, MacDonald et al., 2010). These findings, along with our data, suggest that as *dlx2a* regulates *gad1*, *gad1* can feedback and also act on *dlx2a*. To test this feedback relationship, we carried out a *dlx2a* rescue in our *gad1* morphant zebrafish. Co-injection of *dlx2a* mRNA with the *gad1* morpholino was sufficient to rescue the delayed *dlx2a* expression observed in *gad1* morphant animals at the 10-12 somite stage (Fig. 6.6A-C). Normal *dlx2a* expression was present throughout the pharyngeal arches, but expression was increased throughout the entire embryo due to the presence of excess *dlx2a*. When the craniofacial cartilages of these *dlx2a* rescue animals were observed at 7 dpf, we found that the chondrocyte abnormalities associated with

*gad1* knockdown were not present. These cartilaginous structures were comparable in size and shape to wild-type and *gad1* rescue animals (Fig. 6.2 and 6.6E-H,I-K). In contrast, overexpression of *dlx2a* resulted in ubiquitous expression in 10-12 somite embryos (Fig. 6.6D) and abnormal cranial cartilages at 7 dpf. These structures appeared thickened, possibly due to abnormal chondrocyte stacking, but these alterations were different from those observed in *gad1* morphants (Fig. 6.6H,L). These findings show that not only can knockdown of *gad1* cause a delay in *dlx2a* expression and changes in cranial morphology, but rescue with *dlx2a* mRNA is sufficient to overcome these *gad1* deficiencies.

***Preparation of and photochemical properties of ccMOs***

Cyclic- caged morpholinos were developed and uncaged through exposure to light (SFig. 6.6). BHQ- and CyHQ-caged morpholinos against *gad1* **4a** and **4b** were prepared from their respective linkers **1a** and **1b** as illustrated in Supplementary Figure 6.7. Linker **1a** or **1b** was coupled to the 5¢-amine functionalized end of *gad1* morpholino **2** through displacement of the succinimidyl ester in sodium borate buffer (pH 8.5). After desalting, **3a** or **3b** was cyclized by reducing the disulfide bond in situ with tris(2-carboxyethyl)phosphine (TCEP) to the sulfhydryl, which displaced the chloride on **3a** or **3b** to form the BHQ- or CyHQ-cMO (**4a** or **4b**) in ~50% yield after purification by size exclusion chromatography (NAP-5 column eluting with a water mobile phase).

***Caged-morpholinos can bypass the craniofacial effects of gad1 deficiency***

When caged CyHQ-*gad1* was utilized, we determined that the craniofacial defects observed with the normal *gad1* morpholinos could be bypassed. Caged-morpholinos were injected at the 1-4 cell stage under red light conditions, so as to leave the CyHQ-*gad1*

intact. These injection sets were split in half, allowing one half to be exposed to light immediately and the remaining half to develop in the dark. At 24 hpf, the set of dark-raised embryos were then moved to light for the remainder of the experiment (to release linearized and active *gad1* morpholino). These sets of embryos were analyzed early in development by *in situ* hybridization for changes in neural crest markers and later in development for changes in the craniofacial cartilages.

At the 10-12 somite stage, it was determined that embryos injected with caged CyHQ-*gad1* and raised in the dark exhibited *dlx2a* expression comparable to that of wild-type embryos (Fig. 6.7A,B). Similarly, embryos that were injected with CyHQ-*gad1* morpholino and raised in the light showed significantly reduced *dlx2a* expression, similar to the levels of expression observed in normal *gad1* morphants (Fig. 6.7C,D). Earlier analyses showed that *foxd3* expression was most significantly affected in *gad1* morphant animals when compared to the other neural crest markers used; therefore this marker was chosen for further analysis. Similar to the changes observed with *dlx2a*, embryos that were injected with the CyHQ-*gad1* and reared in the dark exhibited *foxd3* expression comparable to that of wild-type embryos (Fig. 6.7E-H). Those embryos that were injected with CyHQ-*gad1* and raised in the light showed comparable expression to that observed in *gad1* morphant embryos (Fig. 6.7I-L). Together, these findings suggest that the alterations in neural crest expression can be circumvented when the caged-morpholinos remain in the dark and intact.

To determine if the alterations in the craniofacial cartilages could also be bypassed, embryos were injected and raised in either the dark or light, as described above. This methodology is mapped out in Supplementary Figure 6.8. Similar to what

was seen with the *in situ* hybridization analyses, it was determined that when CyHQ-*gad1* was photolyzed at 24 hpf, the cartilage defects observed in *gad1* morphant animals did not develop. In other words, animals that were raised in the dark for the first day of development, and then moved to the light, exhibited cartilaginous structures comparable to those of wild-type animals (SFig. 6.8B,C). Animals that were light-raised for the entire 7 days developed smaller and abnormal cartilaginous structures, comparable to those observed in *gad1* morphants (SFig. 6.8D,E). Not only do these data show that the caged-morpholinos are functional in the developing zebrafish, but they also suggest that the defects in cranial cartilage originate within the first 24 hours of development.

***Alterations of gad1 signaling act through the $GABA_A$ receptor***

To test which GABA receptor was modulating the alterations associated with manipulation of *gad1*, a series of pharmacological agents were bath applied to developing embryos and *dlx2a* expression was observed. At the 10-12 somite stage, *dlx2a* expression was greatly reduced in pentylenetetrazol (PTZ) or picrotoxin (PTX) (both $GABA_A$ receptor antagonists) treated embryos (Fig. 6.8C,D). This decrease in expression was comparable to that observed in *gad1* morphant embryos of the same age (Fig. 6.8B). In contrast to this, treatment with saclofen (a $GABA_B$ antagonsist) did not alter the expression of *dlx2a*. These embryos exhibited comparable expression to wild-type embryos (Fig. 6.8A,E). When muscimol, a $GABA_A$ agonist, was bath applied, *dlx2a* expression was comparable, if not slightly upregulated, when compared to untreated embryos (Fig. 6.8F). These findings support the idea that the alterations we observed during the first 7 days of development are associated with a change in GABA signaling, which is acting through the ionotropic $GABA_A$ receptor.

***Caged-morpholinos can separate craniofacial alterations from the neurological effects of gad1 deficiency***

Because Gad activity is most often associated with neurotransmission, we also looked at the neurological effects associated with knockdown of *gad1* and *gad2*. Extracellular recordings collected from 3 dpf larvae showed that *gad1* morphant animals exhibited an increase in neurological activity. This activity was characterized by an overall increase in the number of high and low amplitude discharges observed in a 30 minute recording period, when compared to wild-type animals (SFig. 6.9A,B). While *gad2* morphant zebrafish looked phenotypically comparable to wild type animals (Fig. 6.1), the animals exhibited spontaneous epileptiform-like activity (SFig. 6.9C). This data mirrored that collected from GAD65-/- mice (Asada et al., 1996, Kash et al., 1997), so our findings were not surprising. When electrophysiological data was collected from *gad1*/*gad2* double morphants, we found a profound increase in neurological activity, when compared to wild-type or single-morphant animals (SFig. 6.9D). The occurrence of very large amplitude and smaller amplitude events was more abundant in these animals.

We next utilized caged CyHQ-*gad1* to separate the craniofacial defects from the neurological defects observed following the knockdown of *gad1*. As previously discussed, when CyHQ-*gad1* was injected and embryos were dark-raised for the first 24 hours of development and then light-raised for the remaining two days, these morphants looked phenotypically comparable to wild- type animals (SFig. 6.8). Yet, these animals exhibited an increase in native neurological activity at 3 dpf (Fig. 6.9A,B). The extracellular recordings of these CyHQ-*gad1* morphants showed more sporadic and large-amplitude events, when compared to wild-type animals. Analyses of these findings

showed that this increased neurological activity lays primarily in the lower delta, theta and alpha frequencies (data not shown). Similar neurological changes were observed in CyHQ-*gad1* morphants raised in the light, but these animals exhibited the craniofacial defects associated with *gad1* knockdown. In contrast, the neurological activity of those CyHQ-*gad1* morphants that were dark-raised for the entire three days displayed neural activity more comparable to wild-type animals (data not shown). Together, these data show that our CyHQ-*gad1* morpholino can be used to separate the craniofacial defects observed in normal *gad1* morphants from the neurological alterations associated with *gad1* knockdown.

## Discussion

In the present study, we show that knockdown of *gad1*, but not *gad2*, leads to changes in craniofacial development within the larval zebrafish, and that this signaling pathway seems to be acting through the $GABA_A$ receptor. These findings are not surprising considering previous work that has been carried out in the mouse. While GAD67 -/- mice die shortly after birth due to the presence of a severe secondary cleft palate, GAD65-/- mice were viable, but exhibited temporal lobe epilepsy (Asada et al., 1997, Condie et al., 1997, Kash et al., 1997, Maddox and Condie, 2001). Similarly, studies in mice and humans have revealed that mutations in GABARB3 develop cleft palate (Culiat et al., 1995, Homanics et al., 1997, Scapoli et al., 2002, Hagiwara et al., 2003, Kanno et al., 2004, Muhammad et al., 2013). Drugs known to alter GABA signaling, such as the benzodiazepine drug diazepam, can induce cleft palate when administered to pregnant mice during a critical period of palatogenesis (Miller and Becker, 1975, Wee and Zimmerman, 1983), or when taken during pregnancy in humans

(Aarskog, 1975, Safra and Oakley JR, 1975). Therefore, it seems likely that similar to mice, GABA signaling may be involved in normal craniofacial development within the zebrafish.

It is well known that cranial neural crest cells (CNC) give rise to the craniofacial cartilages in multiple species (Saint-Jeannet, 2006), including zebrafish (Yelick and Schilling, 2002, Sperber et al., 2008). While neurocranial precursors emerge from the midbrain and migrate between the eyes to form the palatal shelves, viserocranial precursors emigrate in 3 streams from the hindbrain into the mandibular (stream 1), hyoid (stream 2) and 5 branchial (stream 3) arches (Schilling et al., 1996a, Graham, 2003, Saint-Jeannet, 2006, Alexander et al., 2011). In zebrafish, each pharyngeal arch forms from a unique and characteristic set of neural crest-derived cartilages (Schilling et al., 1996a, Yelick and Schilling, 2002), therefore we used a series of early neural crest markers to determine if and how these CNC populations were being affected by *gad1* knockdown. *In situ* hybridization analysis for *prdm1a, snai1b, tfap2a* and *foxd3* showed that neural crest cells were present and expressed in normal patterns at the 10-12 somite stage, a point prior to CNC migration (Schilling and Kimmel, 1994, Baas et al., 2009). There seemed to be a slight increase in the expression of *snai1b, tfap2a* and *foxd3*, but we were unable to determine if this was the outcome of more cells expressing each of these markers or from higher expression within each cell (Fig. 6.3).

We also looked at 1 dpf *gad1* morphants, a point when the CNC have migrated to and begun to populate the pharyngeal arches. At this time, *foxd3* expression in *gad1* morphants was present in a similar region and to a comparable level as that seen in wild-type animals, but the expression pattern was disorganized in the region between the

developing eye and ear (Fig 6.4A,B). Similarly, *sox10* expression, which labels chondrogenic neural crest, was similar between wild-type and *gad1* morphant animals, but the expression pattern was also highly disorganized in the region between the eye and ear (Fig. 6.4C,D). Although there were slight alterations in the expression of each of these transcription factors, these data suggest that the CNC population was present at the correct time and in the appropriate general location in *gad1* morphant animals. Yet, the disorganization observed in these animals at 1 dpf points to the idea that knockdown of *gad1* may be affecting neural crest migration.

Although the neural crest cells were present at these stages, we wanted to determine if the survival and migration patterns of these cells was normal. In zebrafish, the neural crest begin migrating to the pharyngeal arches at ~16 hpf (Schilling and Kimmel, 1994, Baas et al., 2009), and at this time, *dlx2a* is expressed in the 3 major streams of cells that correspond to the 3 pharyngeal arches (Akimenko et al., 1994, Schilling et al., 1996a). Therefore, we used *in situ* probes to visualize changes in *dlx2a* expression during the first day of development. We found that when compared to wild-type animals, *dlx2a* expression was significantly reduced in *gad1* morphants at the 10-12 somite stage. As development continued, *dlx2a* expression increased in both wild-type and morphant animals, but decreased *dlx2a* expression persisted in *gad1* morphants at 18 somites. By 24 hpf, the expression domains of *dlx2a* were comparable between *gad1* morphants and wild-type animals, but a small reduction in expression level was still present (Fig. 6.5). It was not until ~30 hpf that the expression levels were comparable between our morphant and wild-type animals. This data indicates that *dlx2a* expression was delayed, but not absent in *gad1* morphants. This delay could contribute to the

abnormal stacking of chondrocytes observed in our *gad1* morphants, as the disorderly stacking of chondrocytes often suggests a disruption or delay in the early stages of chondrogenesis (Thorogood, 1983, Kimmel et al., 1998, Baas et al., 2009).

When the cranial cartilages of *gad1* morphants were more closely observed we determined that the cartilages of these animals were abnormally shaped and significantly smaller when compared to those of either the *gad2* morphant or wild type animals (Fig. 6.2). These alterations seemed to originate from the fact that individual chondrocytes in *gad1* morphants were abnormally shaped and stacking was disorganized (SFig. 6.5). A similar change in chondrocyte morphogenesis was observed in the zebrafish *dlx2a* morphant (Sperber et al., 2008). Embryos injected with morpholinos against *dlx2a* exhibited a smaller head at 24 hpf, while those injected with *dlx1a* appeared normal. These morphants showed a reduction in anterior facial protrusions and a failure of jaw extension, similar to our observations of 3 and 7 dpf *gad1* morphants (Fig. 6.1). Reduction and malformed cartilage elements (including m, pq, hs, ch) were present in *dlx2a* morphants and chondrocyte stacking was not arrayed in an orderly manner. These *dlx2a* morphants also exhibited a 3-fold increase in the number of apoptotic cells within the migrating neural crest, as shown by TUNEL staining (Sperber et al., 2008). Similar changes were observed in our *gad1* morphant animals (Fig. 6.2, 6.3, SFig. 6.5), suggesting that by knocking down *gad1,* we were altering the subsequent expression of *dlx2a*.

In mice, it has been observed that the spatial and temporal expression of Dlx2a and the Gad genes overlap (Stühmer et al., 2002, MacDonald et al., 2010). In slice culture, ectopic expression of Dlx2 leads to the induction of both Gad1 and Gad2

(Stühmer et al., 2002, MacDonald et al., 2010). Similarly, Dlx2a and Dlx1/2 mutant mice show a loss of Gad1 expression throughout the brain (Sperber et al., 2008, MacDonald et al., 2010). Because the Dlx genes have been found to control the size and shape of the craniofacial skeletal elements (Gordon et al., 2010), it is not surprising that Dlx2a mutant animals exhibit severe craniofacial deformities, including cleft palate, dysmorphic mid ear and jaw bones, which often lead to neonatal lethality (Qiu et al., 1995, Saint-Jeannet, 2006, Verreijdt et al., 2006, Kwakowsky et al., 2007). Together with our findings, these data, suggest that Dlx2a can play a key role in regulating the expression of Gad1 and that a reciprocal relationship may also be present.

To confirm this relationship, we carried out a *dlx2a* rescue in our *gad1* morphant zebrafish. Co-injection of 120 pg *dlx2a* mRNA with 0.3 ng *gad1* morpholino was sufficient to rescue the delayed *dlx2a* expression, as observed by *in situ* hybridization (Fig. 6.6). This amount of mRNA was chosen based upon the amount required to rescue the *dlx2a* morphant phenotype (Sperber et al., 2008). When overexpression of *dlx2a* was observed, it is not surprising that *dlx2a* expression was ubiquitous when compared to wild-type animals (because excess *dlx2a* is present throughout the embryo) (Fig. 6.6D). When the craniofacial cartilages of *dlx2a* rescue animals were observed at 7 dpf, we found that the chondrocyte abnormalities associated with *gad1* knockdown were not present. These cartilaginous structures were comparable in size and shape to wild-type and *gad1* rescue animals. When overexpression animals were observed, we determined that excess *dlx2a* was also sufficient to alter the structure of the cranial cartilages, yet, these changes were different from those observed from *gad1* knockdown. These findings show that not only can knockdown of *gad1* cause a delay in *dlx2a* expression and

changes in cranial morphology, but also that exogenous *dlx2a* expression is sufficient to overcome and rescue these *gad1* deficiencies. It seems that although *dlx2a* sits upstream of, and regulates *gad1*, that *gad1* also has the ability to feedback and act upon *dlx2a*. Therefore, our data, along with that of others, shows that disruption of either *gad1* or *dlx2a* signaling is sufficient to induce cranial skeletal abnormalities in both mice and zebrafish (Condie et al., 1997, Maddox and Condie, 2001, Kwakowsky et al., 2007, Sperber et al., 2008, MacDonald et al., 2010).

To determine which GABA receptor was modulating the effects observed in our *gad1* morphant animals, we bath applied a series of chemicals to alter the effects of different GABA receptors. Due to the toxicity associated with long-term drug exposure, treated animals were collected at the 10-12 somite stage and analyzed by *in situ* hybridization. To determine which GABA receptor was modulating the GABA signaling in our *gad1* morphants, we aimed to phenocopy the delay of *dlx2a* expression observed in these animals. Application of PTZ or PTX resulted in a significant reduction of *dlx2a* expression (Fig. 6.8). Although this decrease was significant when compared to wild-type animals, the change was not quite as severe as that observed in our *gad1* morphants. This outcome is most likely due to the fact that with our morphants, the embryos were exposed to the active morpholino for the entire period of development, whereas drug-treated embryos were only exposed to the antagonists for a short period (4 hours) of time. This shorter exposure period could therefore explain the presence of very low levels of *dlx2a* expression in the PTZ and PTX treated embryos. Bath application of muscimol ($GABA_A$ receptor agonist) resulted in a slight increase in the expression of *dlx2a* throughout the entire embryo, yet when saclofen (a $GABA_B$ receptor antagonist) was applied, *dlx2a*

expression was comparable to that of wild-type animals. These findings support those already established in the mouse. Previous work has shown that mice mutant for the Gabarb3 gene (encoding the $GABA_AR$ β3 subunit) die soon after birth, most likely due to feeding problems associated with a severe secondary cleft palate (Culiat et al., 1995, Homanics et al., 1997, Hagiwara et al., 2003, Addington et al., 2004). Similarly, when GABA agonists, such as diazepam, or antagonists, such as picrotoxin, were administered to pregnant mice, cleft palate was induced in exposed embryos (Miller and Becker, 1975, Wee and Zimmerman, 1983, Jurand and Martin, 1994). Our findings seem to support those observed in mice and they further suggest that deviation from the normal range of GABA signaling can severely affect early development. Our data also suggests that the effects of *gad1* knockdown are acting through the $GABA_A$ receptor.

As GABA signaling is most often associated with neurotransmission and not craniofacial development, we wanted to solidify GABA's role in early craniofacial development by incorporating the caged CyHQ-*gad1* morpholinos. The design of the photoactivatible morpholinos to *gad1* was similar to those morpholinos created by James Chen's laboratory (Ouyang et al., 2009b, Yamazoe et al., 2012), but they included the more sensitive quinoline-based photoremovable protecting groups BHQ and CyHQ, which were developed in the Dore laboratory (Fedoryak and Dore, 2002, Zhu et al., 2006, Davis et al., 2009, Ma et al., 2012). These alterations made the caged-morpholinos more suitable for use in a biological system. Unlike typical morpholinos, photoactivatible morpholinos enable conditional gene silencing, by allowing for controlled timing and targeted illumination (Zhu et al., 2006, Ouyang et al., 2009a, Tomasini et al., 2009, Tallafuss et al., 2012). Therefore, following injection of CyHQ-*gad1* into the zebrafish

embryo, we could control the timing at which we carried out photoactivation, allowing us to separate Gad/GABA's early functions in craniofacial development from its later actions in neurotransmission.

To separate the craniofacial effects associated with the knockdown of *gad1* from its actions in neurotransmission, we photolyzed CyHQ-*gad1* injected embryos that had been raised in the dark at 24 hpf. When uncaging was carried out at this time, we found that the craniofacial defects associated with the original *gad1* morpholinos could be bypassed, whereas those embryos raised in light exhibited the *gad1*-like phenotype at 24 hpf. Similarly, dark-raised CyHQ-*gad1* morphants displayed *dlx2a* expression comparable to wild-type animals, while those CyHQ-*gad1* morphant animals that were raised in the light showed significantly reduced *dlx2a* expression. These light-raised animals exhibited *dlx2a* expression comparable to that of *gad1* morphants (Fig. 6.7). Similarly, when the cartilages of these animals were studied, we found that CyHQ-*gad1* morphants exposed to light at 24 hpf had cranial cartilages that were comparable to wild-type animals, while those raised in the light for the entire 7 days exhibited cartilages comparable to the original *gad1* morphant animals (SFig. 6.6). This data suggests that the observed alterations in cartilage development of *gad1* morphants arose within the first 24 hours of development and that these changes could be bypassed when the caged-morpholino remains intact/inactive until a time after 1 dpf. However, when the neurological activity of these dark-raised (for 24 hpf) CyHQ-*gad1* morphants was observed, we found that these animals displayed significantly increased neural activity, when compared to either wild-type or CyHQ-*gad1* morphants animals that were dark-raised for the first 3 days of development (Fig. 6.9 and data not shown). This increased

activity was more similar to the *gad* morphants, suggesting that photolysis of the CyHQ-*gad1* at 24 hpf could successfully knockdown *gad1* such that its actions in neurotransmission were affected.

In this study, we show that knockdown of *gad1*, but not *gad2*, is sufficient to cause changes in the development of the craniofacial cartilages of larval zebrafish. The cartilages of these animals were significantly reduced and abnormally shaped due to the abnormal development of the chondrocytes. As these cells are derived from the cranial neural crest population, we determined that the early neural crest markers (*prdm1a, tfap2a, foxd3, snai1b*) were present, but expression levels/patterns were just slightly altered. In contrast to this, the expression of *dlx2a*, a factor required for neural crest survival, was significantly delayed in *gad1* morphants. We were able to successfully rescue these abnormal cartilages and *dlx2a* phenotypes with both *gad1* and *dlx2a* mRNA, supporting that these phenotypes were specific to the *gad1* morpholino and that *dlx2a* acts as a key regulator of the GAD genes and GABAergic signaling. Similarly, our pharmacological studies suggest that *gad1's* activity in craniofacial development is modulated through the $GABA_A$ receptor. Finally, we were able to separate GABA's functions in craniofacial development from its later actions in neurotransmission through the use of photoactivatable morpholinos. Our findings suggest that GABA's role in craniofacial development occurs within the first 24 hours of development, whereas its functions in neurotransmission develop after this time. We speculate that GABA's role in craniofacial development occurs at a time after neural crest begin to migrate (16 hpf), but further experiments are needed to determine the critical time period when GABA acts to organize these cartilages.

## Experimental Procedures

### *Zebrafish maintenance*

Adult zebrafish (*Danio rerio*) of WIK strain obtained from the Zebrafish International Research Center (ZIRC) were maintained in an Aquatic Habitats (Apopka, FL) multirack system according to standard procedures . Habitat water consisted of reverse osmosis filtered/sterilized water to which sodium bicarbonate and other salts (Instant Ocean, Aquarium Systems, Inc., Mentor, OH, USA) were added to maintain pH from 7.0 -7.4 and conductivity between 400 and 430 μS. All experimental procedures were conducted in accordance with National Institutes of Health guidelines for use of zebrafish in research under protocols approved by the University of Georgia Institutional Animal Care and Use Committee.

### *Morpholinos and mRNA Rescue*

Morpholino oligonucleotides (MOs) complementary to the translation start site of *gad1* and *gad2* were microinjected into one to two-cell stage embryos. MOs (GeneTools; start sites bolded) used are as follows: *gad1MO*, [5'AAGGTGCAGAAGAC-GC**CAT**CAGTCC-3'], *gad2MO*, [5'-GAAACCAAAACCCGTGTGATGC**CAT**-3'], were diluted in autoclaved MilliQ water, 0.6 mM $Ca(NO_3)_2$ and 0.05% Phenol Red. Embryos were injected with approximately 1 nl at a concentration of 0.3 ng/nl for *gad1MO* and 1ng/nl for *gad2MO*.

To rescue the *gad1* morpholino knockdown phenotype, *gad1* and *dlx2a* mRNA were synthesized *in vitro* and co-injected with the *gad1* morpholino. To make the mRNA, the full-length zebrafish *gad1* ORF was cloned into a pCS2+ vector (primers: 5'CTTGATTTAGGTGACACTATAG-3' and 5'CTTGATTTAGGTGACACTATAG-

3'), which had the CMV promoter removed. Primers were designed to amplify the entire *gad1* ORF while destroying morpholino target site without codon alteration. The *gad1* ORF was then PCR amplified using DreamTaq (Thermo Scientific, Pittsburgh, PA) and cloned into the altered pCS2+ vector cut with EcoRI & XhoI. The clone was linearized by incubating with NotI at 37 $^{o}$C and then heat inactivated at 65 $^{o}$C for 20 minutes. *gad1* mRNA was transcribed using the T7 mMessage mMachineTranscription Kit (Life Technologies, Grand Island, NY).

For rescue, *gad1* mRNA was coinjected with the *gad1MO* at a concentration of 0.05 ng/nl. For overexpression analysis, mRNA was injected at a concentration of 1.66 ng/nl. For rescue with *dlx2a* mRNA, the full-length zebrafish *dlx2a* ORF, which was cloned into a pBS(-) vector, was generously donated by Marc Ekker. The clone was linearized by incubating with ScaI at 37 $^{o}$C and then heat inactivated at 80 $^{o}$C for 20 minutes. *dlx2a* mRNA was transcribed using the T3 mMessage mMachineTranscription Kit (Life Technologies, Grand Island, NY).Based upon previous analyses using *dlx2a* morpholinos (Sperber et al., 2008), a concentration of 120 pg of mRNA was either co-injected with the *gad1* morpholino to rescue the *gad1* phenotype or alone to assess the effects of overexpression.

All embryos were scored at 1dpf to determine phenotype and death rate for each clutch. Samples were later collected at the 12 somite stage, 18 somite stage, 1dpf, 3dpf and 7dpf for in situ hybridization, alcian analysis and western blot analysis.

***Preparation of CyHQ-linked morpholinos***

Preparation of BHQ- and CyHQ-based linkers **1a** and **1b**, $^{1}$H NMR and $^{13}$C NMR spectra, and HPLC chromatograms demonstrating purity of each compound and their intermediates are provided in the Supplemental Information.

***CyHQ-linked morpholinos and photochemical release of gad1MO***

CyHQ-linked morpholinos were utilized to control the timing of morpholino actions. CyHQ-*gad1*, samples were diluted as described above and embyros were injected with approximately 1 nl at a concentration of 0.35 ng/nl-0.45 ng/nl. Working concentrations for CyHQ-*gad1* were determined based upon the concentration that would give comparable phenotypes as observed with *gad1MO*. Embryos were injected and the one to 4-cell stage under red light conditions and separated into two equal sets. One set was raised under light for the first 14 or 24 hours while the second set was raised in the dark. For early neural crest expression analysis, light and dark raised embryos were collected at 12 somites and processed for *in situ* hybridization. For alcian analysis, at 24 hours, dark embryos were exposed to light and all embryos were raised in light until collection at 7 dpf.

***Pharmacology***

GABA activity was altered pharmacologically through the bath application of compounds. Drugs were added to standard egg water (Westerfield, 1993) to make working concentrations and applied to embryos at 10 hpf, directly after the end of gastrulation. Embryos did not survive if drugs were added before this time. Embryos were removed, collected and fixed from bathing solutions at the 10-12 somite stage and analyzed by *in situ* hybridization. Concentrations of drugs utilized were as follows: 15

mM pentylenetetrazol (PTZ) (Baraban et al., 2005, Johnston et al., 2013), 100 μM picrotoxin (PTX) (Wong et al., 2010), 50 μM baclofen (Baraban et al., 2005).

***Electrophysiology***

Electrophysiological recordings were collected from 3 dpf zebrafish as described in Ball et al. (In preparation). Briefly, zebrafish larvae were immobilized in 250 μM α-bungarotoxin and mounted in 1.2% agarose (Thermo Fisher Scientific, Waltham, MA) in Ringer's solution in a 60x15 mm Corning Not-TC treated petri dish (Corning Inc., Tewksbury, MA). Animals were covered with standard egg water (Westerfield, 1993) and a sharp glass pipet microelectrode (15 - 20 MΩ impedance), loaded with 2-3 μL of 2 M potassium chloride, was inserted into the optic tectum (TeO). The optic tectum was chosen to facilitate comparison with previously published data obtained from larval zebrafish (Baraban et al., 2005). A chloride-coated silver wire (0.010" A-M Systems, Inc. Sequim, WA) reference electrode was placed touching the medulla or remaining spinal cord. Field recordings were collected using Molecular Devices' Axoclamp software and data were digitized at 10 kHz, low-pass filtered at 1 kHz, and analyzed with pCLAMP 10.2 software (Axon Instruments, Sunnyvale, CA).

***Western blot analysis and immunodetection of knockdown***

To determine if morpholino injection was successful in knockdown of the Gad67, protein extracts were collected from 3dpf embyros, as expression could not be seen with younger stages. For protein extraction, 30-100 embryos were collected and deyolked (Bradford, 2011) and homogenized in a solution containing 60-100 μL RIPA buffer (Thermo Fisher Scientific Inc., Waltham, MA) with 1 mM EDTA solution and 1 mM protease inhibitor cocktail (Sigma-Aldrich, St. Louis, MO). Samples were centrifuged for

10 min at high speed and the supernatant was collected and stored at -80 $^{o}$C until further use.

Protein concentration was measured by spectrophotometer and determined using a Bradford assay. 10 µg samples were loaded into an upright 10% SDS-polyacrylamide gel and run at 75 volts for 3.5-4.5 hours. A 1X Tris-glycine running buffer (10X Tris-glycine buffer: 250 mM Tris, 2 M glycine, 10% SDS) was used as running buffer for the SDS-PAGE. Protein bands were transferred to a 0.45 µm nitrocellulose membrane (Bio Rad, Hercules, CA) using a transfer rig that was cooled with ice. Ice-cold Towbin transfer buffer (28.8 g glycine, 6.06 g Tris base, 200 mL methanol made up to 2 L with deionized distilled water) was used for the transfer. The transfer was carried out at 130 volts for 1-1.5 hours.

Following transfer, nitrocellulose membranes were blocked with 10% milk block (Bio Rad, Hercules, CA) in 1X TBSTw (1L of 10X TBS: 24g Tris base, 88g NaCl, pH 7.6; to 1X TBS, 0.1% Tween-20 added) overnight at 4 $^{o}$C. Proceeding blocking, membranes were exposed to primary antibodies for 1 hour at RT with gentle rocking. Antibodies used for immunodetection were mouse monoclonal anti-GAD-67 (58531, Santa Cruz Biotechnology Inc., Dallas, TX) and rabbit polyclonal anti-Gad2 (IN) (55772, AnaSpec, Inc., Freemont, CA) used at a dilution of 1:200 and 1:1000 µL in 5% milk block, respectively. Anti-GAPDH (ab9484, Abcam, Cambridge, MA) was used as a loading control. Following exposure to the primary antibody, membranes were washed in TBSTw and incubated with HRP conjugated goat anti-rabbit and goat anti-mouse secondary antibodies (Thermo Fisher Scientific Inc., Waltham, MA) diluted to 1:10,000 and 1:2000 in 5% milk block, respectively. Membranes were exposed to the HRP

secondary antibody for 1 hour at RT with gentle rocking. Following exposure, membranes were washed in 1X TBSTw and exposed to the chemiluminescence substrate Immune-Star WesternC Kit (Bio Rad, Hercules, CA) for 1 min, and the chemiluminescence was developed on X-ray film in a dark room.

***Alcian blue staining of cartilages***

Cartilage staining was performed using a modified protocol of Kimmel et al. (Kimmel et al., 1998). Briefly, larvae were fixed in 4% PFA/PBS pH 7.0 at room temperature for 1 hour. Larvae were washed three times in 70% ethanol (EtOH), and 30% hydrochloric acid (HCl) for five minutes. Larvae were stained overnight in a solution of 0.1% alcian blue, 70% EtOH, and 30% HCl. Samples were then differentiated in 70% EtOH and 30% HCl until no blue color remained in the solution. For whole mount analysis, de-pigmented larvae were stepwise rehydrated to water and then cleared in a series of glycerol/1% KOH. For flat mount analysis, larvae were stepwise rehydrated to water and then rinsed three times in saturated NaBorate solution. Tissues were macerated in 3% trypsin in equal volumes of water and NaBorate for 15-30 minutes. Cartilages were dissected out using fine forceps and samples were rinsed in water before flat mounting.

Whole mount alcian stains were mounted laterally and ventrally in 3% methylcellulose in PBS and imaged on a Leica MZ FLIII fluorescent dissecting microscope connected to a computer running Leica FireCam image capture software (Leica Microsystems, Buffalo Grove, IL). Images were loaded into Adobe PhotoShop (Adobe Systems Incorported, San Jose, CA) and cartilage length was measured for the bones that were not obstructed by tissue. Flat mounted cartilages were digitally photographed using a Zeiss axioscope. The cell counting application in ImageJ 64

(Softonic International, New York, NY) was used to analyze and count cells in flat mount cartilages.

***In situ hybridizations***

Whole-mount RNA *in situ* hybridization (ISH) was performed as previously described (Thisse and Thisse, 2008). Antisense probes for the following genes were generously supplied by Dr. Scott Dougan and Wei-Chia Tseng: *dlx2a, tfap2a, foxd3,* and *snai1b.* DIG-conjugated antisense probes were synthesized from whole-embryo cDNA for the *prdm1a* gene (primers 5' TAATACGACTCACTATAGGGAGATCTGCCC-AGCCAAGTTC-3' and 5'ATTTAGGTGACACTATAGATCCATGGCCTCCTCT GTCT-3'). The T7 and Sp6 promoters were added to these primers to allow for the construction of antisense and sense in situ probes, respectively.

For imaging, whole mount ISH samples were cleared in BABB (1:2 benzyl alcohol: benzyl benzoate) (Fisher Scientific Inc., Pittsburgh, PA) and mounted in Canada balsam (Sigma-Aldrich Co., St. Louis, MO). Images were collected using a SteREO Discovery.V12 (Carl Zeiss Microscopy, LLC, Thornwood, NY) or a Leica MZ FLIII fluorescent dissecting microscope connected to a computer running Leica FireCam image capture software (Leica Microsystems, Buffalo Grove, IL).

Acknowledgements

Grants from the National Institutes of Health (R01 NS070159 to T.M.D. and J.D.L.) and the National Science Foundation (CHE-1012412 and CHE-1317760 to T.M.D.) supported this work. The authors declare no competing interests.

Figures

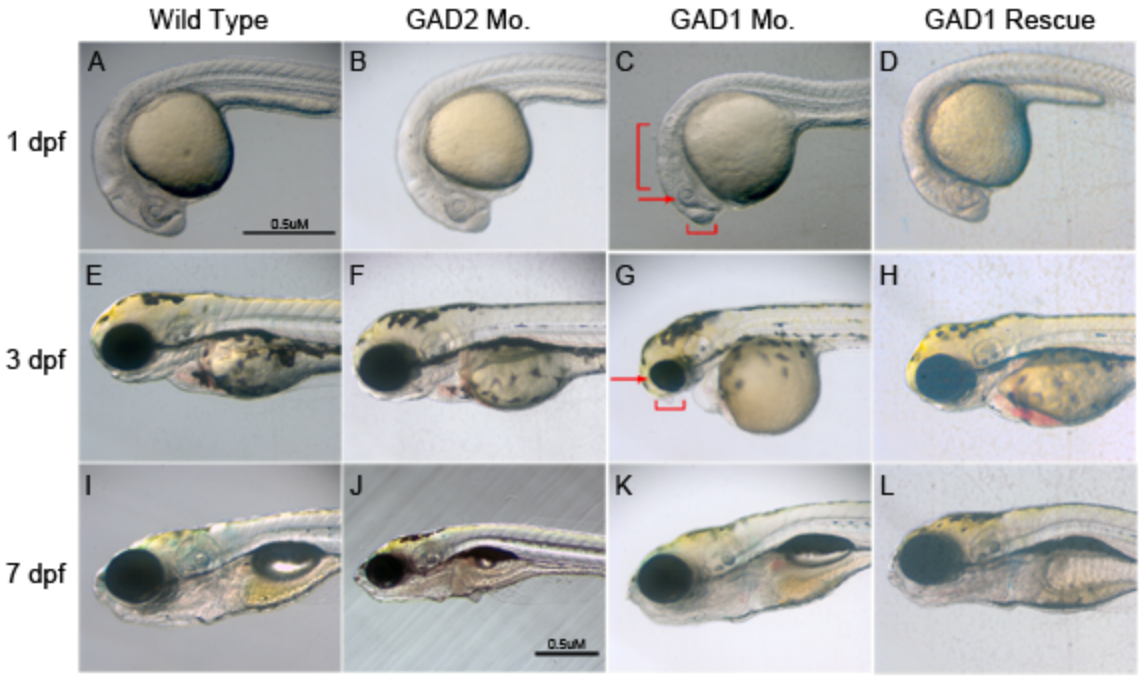


**Figure 6.1. Knockdown of *gad1*, but not *gad2,* causes abnormal craniofacial development.** (A-D) Wild-type, *gad2* morphant, *gad1* morphant and *gad1* rescue animals at 1dpf; (E-H) Wild-type, *gad2* morphant, *gad1* morphant and *gad1* rescue animals at 3dpf; (I-L) Wild-type, *gad2* morphant, *gad1* morphant and *gad1* rescue animals at 7dpf. (A,B) 1dpf wild-type and *gad2* morphant animals look comparable and show normal development; (C) At 1dpf *gad1* morphants exhibit smaller, anteriorly rotated eyes (arrow), an abnormally protruding telencephalon (small bracket) and the rhombencephalon has not correctly segregated from the mesencephalon; (D) This morphant phenotype can be rescued with *gad1* mRNA; (E,F) 3dpf wild-type and *gad2* morphant animals look comparable and show normal development continues; (G) *gad1* morphants continue to exhibit smaller, rotated eyes and the lower jaw does not protrude normally (large bracket); (H) *gad1* rescue animals look comparable to wild-type animals; (I,J) 7dpf wild-type and *gad2* morphant animals look comparable and they exhibit normal development; (K) At 7dpf, *gad1* morphants have developed larger eyes and a protruding jaw; (L) *gad1* rescue animals look comparable to wild-type animals.

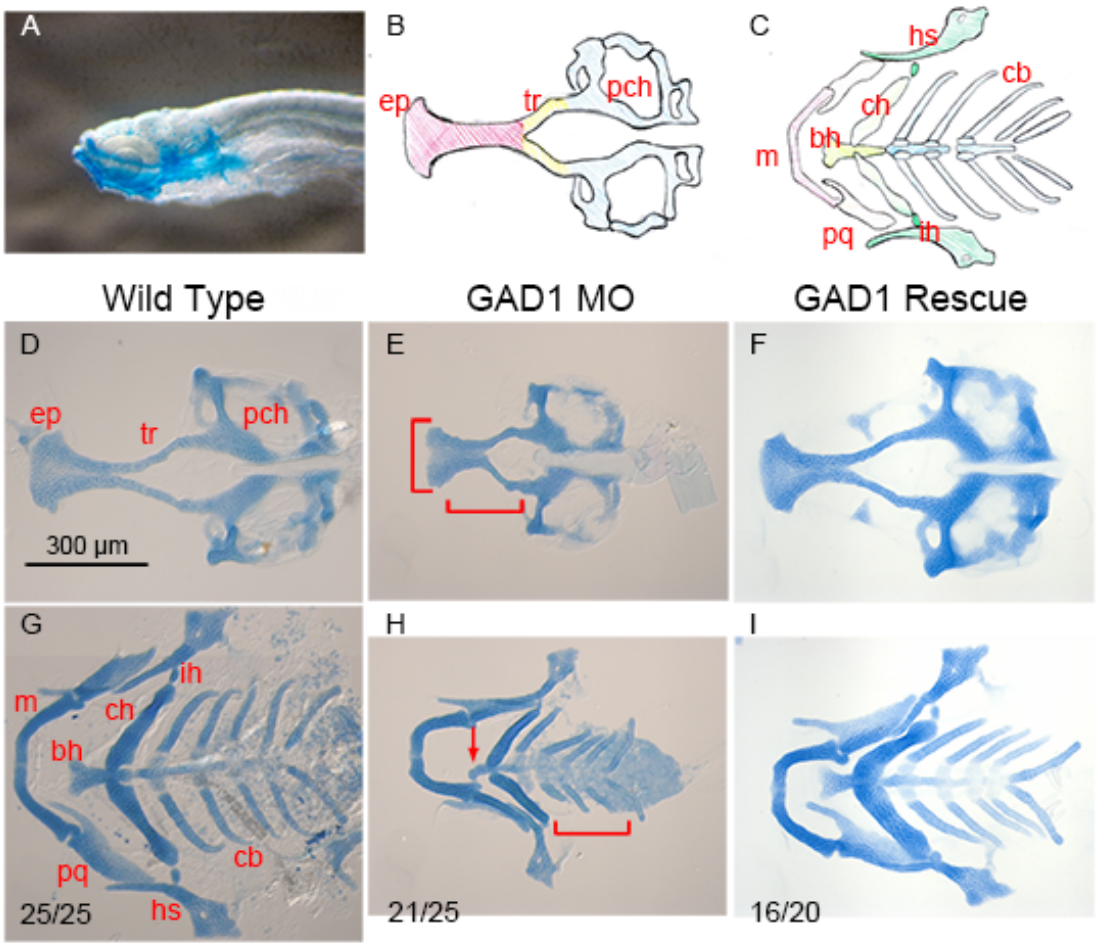


**Figure 6.2. Knockdown of *gad1* causes smaller, abnormally developed cranial cartilages in flat-mounted samples.** (A) Lateral view of 7dpf wild-type alcian stained animal; (B) Cartoon of neurocranial structures present at 7dpf; (C) Cartoon of viscerocranial structures present at 7dpf; (D-H) Flat mounted samples of cranial cartilages at 7dpf. (D,G) Wild-type cranial cartilages show normal morphology; (E,H) Cranial cartilages of *gad1* morphants are significantly smaller than wild-type; (F,I) *gad1* mRNA is sufficient to rescue the small, abnormally shaped cartilage associated with *gad1* knockdown. (E) *gad1* morphants exhibit an abnormally shaped ethmoid plate (vertical bracket) and truncated trabeculae (horizontal bracket); (H) *gad1* morphants display abnormal basihyal cartilage (arrow) and often have truncated ceratobranchial structures (bracket). (bh) basihyal; (cb) ceratobranchial; (ch) ceratohyal; (ep) ethmoid plate; (hs) hyosymplectic; (ih) interhyal; (m) Meckels; (pch) parachordal; (pq) palatoquadrate; (tr) trabeculae

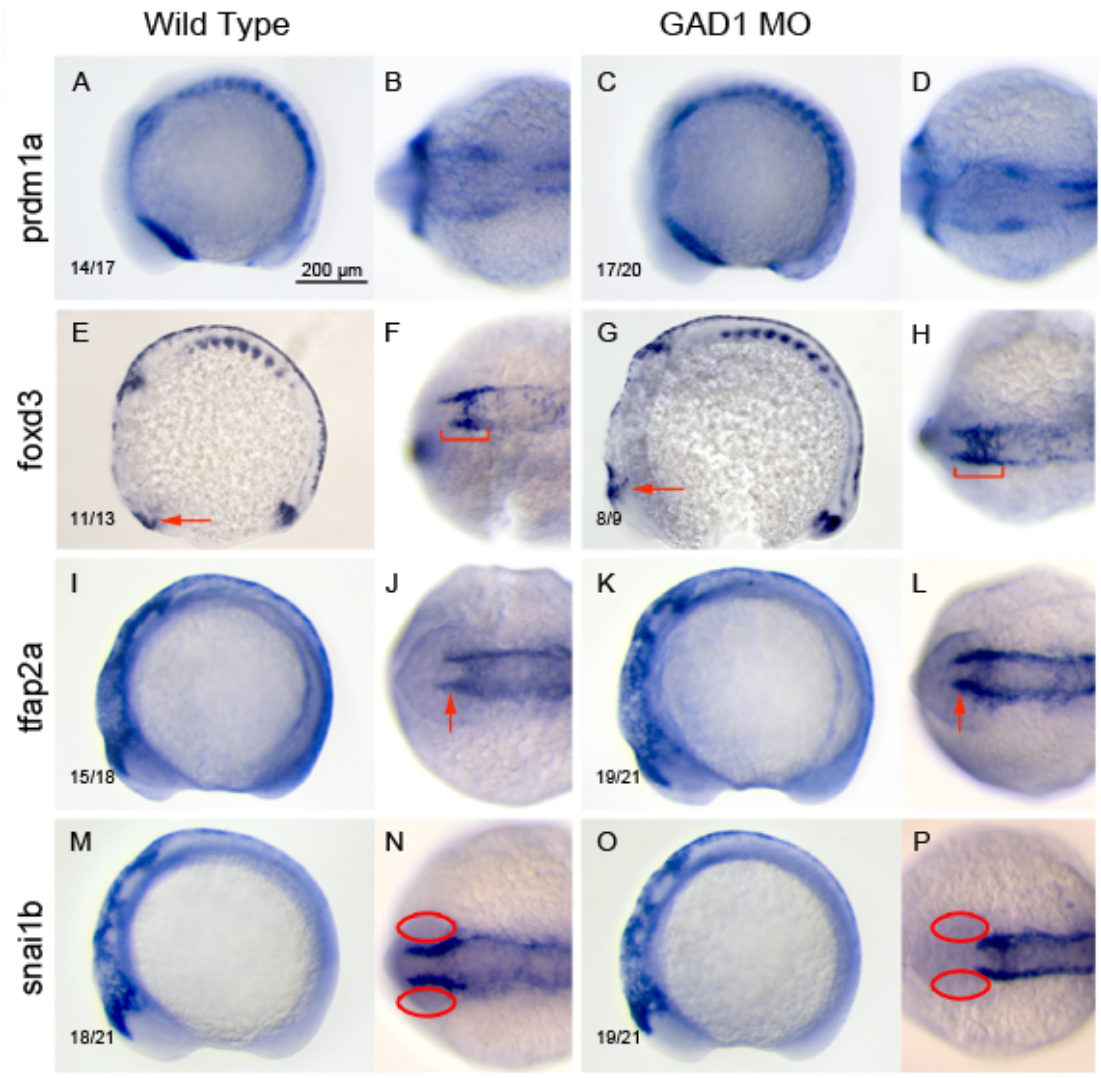


**Figure 6.3. Gene expression abnormalities in premigratory and migrating neural crest cells in *gad1* morphants.** (A-F) Lateral and cranial views of wild-type (A,B,E,F,I,J,M,N) and *gad1* morphant (C,D,G,H,K,L,O,P) embryos at 10-12 somites, showing expression of *prdm1a* (A-D), *foxd3* (E-H) and *tfap2a* (I-L), and *snai1b* (M-P). (A-D) The expression of *prdm1a* is comparable to wild-type animals in both trunk and cranial neural crest populations (D); (E-H) *foxd3* expression is significantly increased in *gad1* morphants. Cranial expression is most significantly affected near the posterior head region (arrows), as shown by a dramatic expansion of *foxd3* expression in this region (red brackets); (I-L) The expression level of *tfap2a* is slightly increased in *gad1* morphants (arrows); (M-P) *snai1b* expression levels are increased in *gad1* morphants, especially throughout the trunk regions. Cranial expression is significantly affected, as *snai1b* expression stops at the posterior edge of the eyes (circles), while expression is retained caudally.

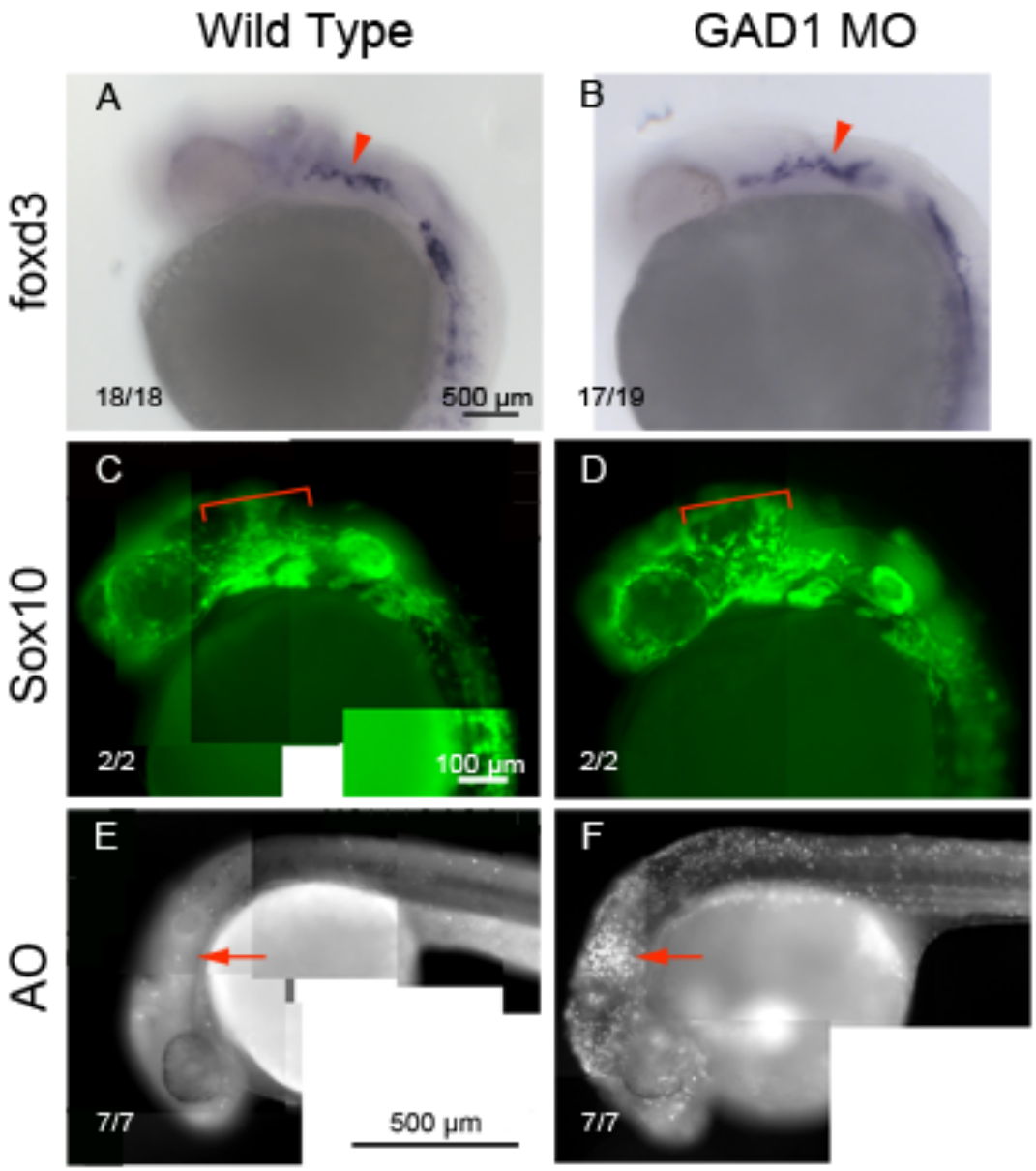


**Figure 6.4. Gene expression abnormalities in migrating and postmigratory neural crest cells in *gad1* morphants.** (A-F) Lateral views of wild-type (A,C,E) and *gad1* morphants (B,D,F) embryos at 1 dpf, showing expression of *foxd3* (A,B), *sox10* (C,D) and acridine orange (E,F). The expression levels of *foxd3* (A,B) and *sox10* (C,D) are comparable between wild-type and *gad1* morphant animals, but expression patterns are disorganized within morphants, especially between the eye and the ear (arrowheads in A and B; brackets in C and D); (E,F) *gad1* morphants exhibit a significant increase in apoptosis, as visualized by acridine orange staining. AO staining is primarily increased within the head and pharyngeal arch regions of *gad1* morphant animals (arrow).
(ao) acridine orange

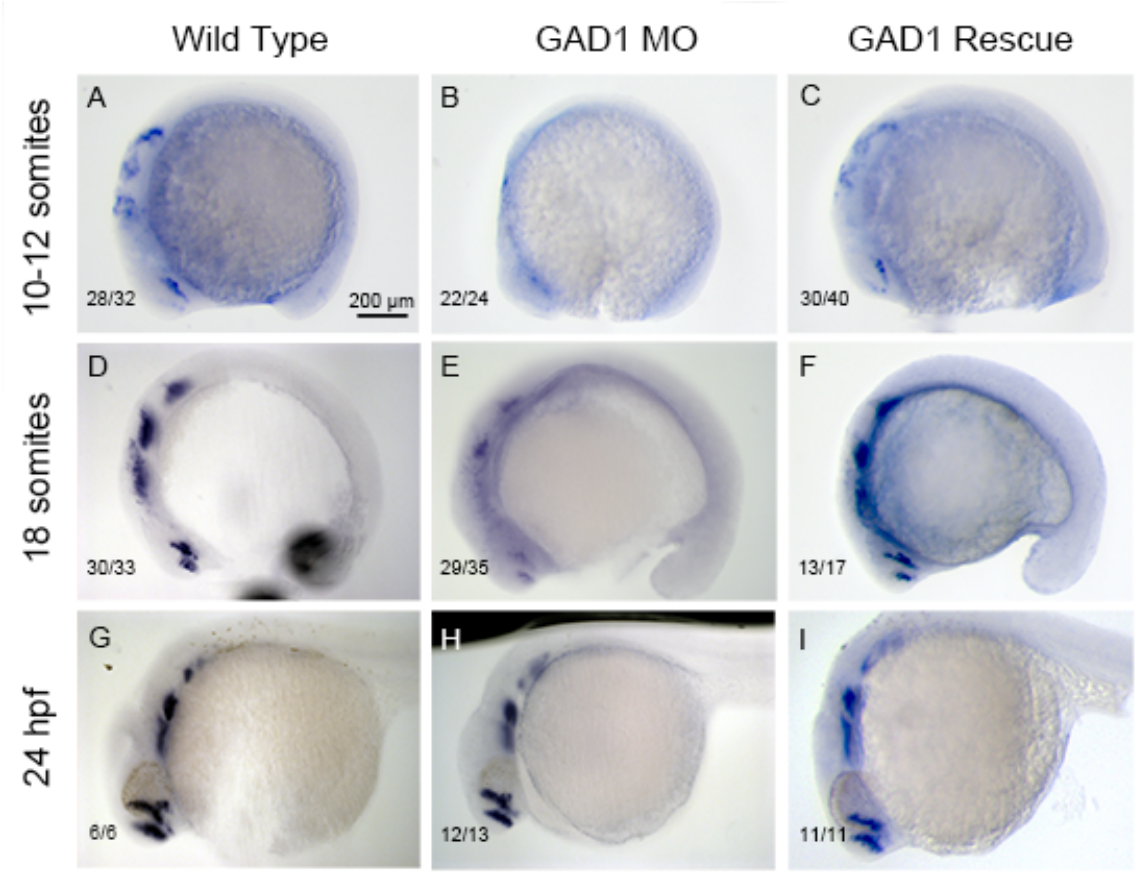


**Figure 6.5. *gad1* knockdown leads to delayed *dlx2a* expression in the pharyngeal arches.** (A-I) Lateral view of *in situ* hybridizations for *dlx2a* in wild-type and *gad1* morphant animals. (A,B) *dlx2a* expression is significantly reduced in *gad1* morphants at 10-12 somites; (D,E) Expression remains reduced in *gad1* morphants at 18 hpf, but light expression is observed within the cranial region and the posterior pharyngeal arches; (G,H) By 24 hpf, expression of *dlx2a* has increased in *gad1* morphants almost to wild-type levels, and expression patterns look comparable to uninjected animals; (C,F,I) The reduction of *dlx2a* expression observed in *gad1* morphants is rescued when Gad1 mRNA is coinjected with the *gad1* morpholino.

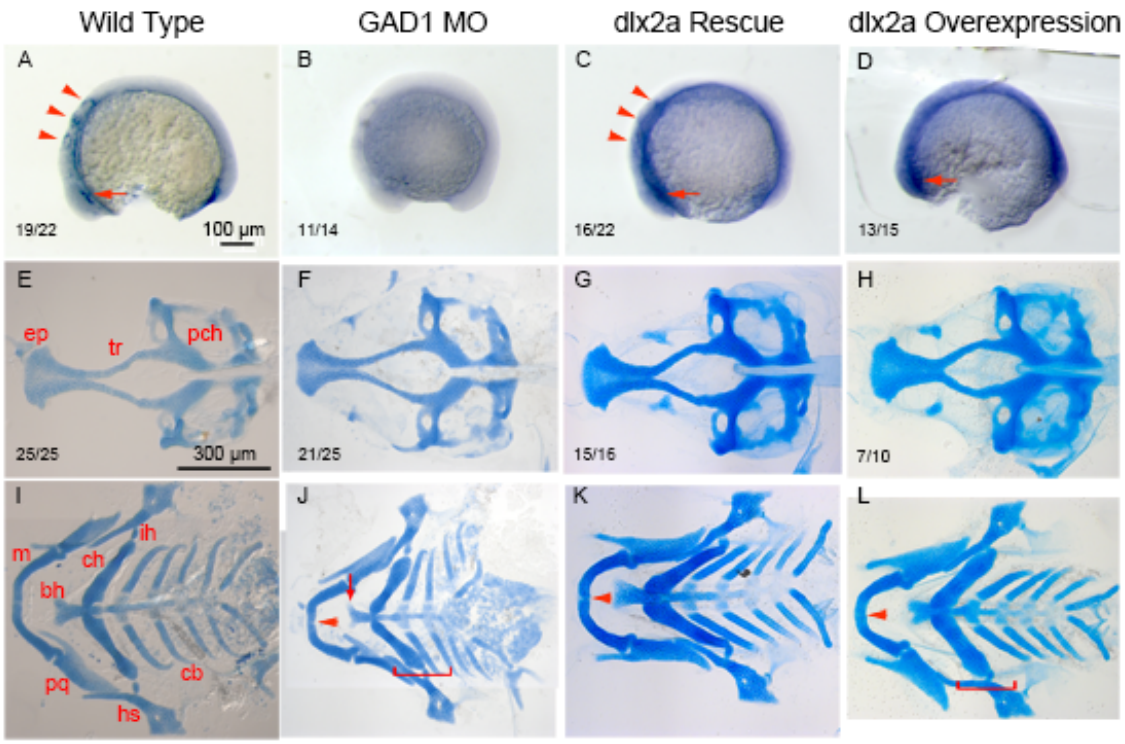


**Figure 6.6. *dlx2a* mRNA can rescue the effects observed with *gad1* knockdown.** (A-D) Lateral view of *in situ* hybridizations in 10-12 somite stage embryos looking *dlx2a* expression. (A) Normal *dlx2a* expression is observed ventral to the eye (red arrow) and in the pharyngeal arches (arrowheads); (B) Expression of *dlx2a* is significantly reduced throughout *gad1* morphant embryos; (C) *dlx2a* expression is rescued ventral to the eye (arrow) and in the 3 arches (arrowheads). Expression is also seen more ubiquitously due to the presence of excess *dlx2a*; (D) Ubiquitous expression of *dlx2a* is observed in animals injected with 120 pg *dlx2a* mRNA. (E-L) Flat mounted samples of cranial cartilages at 7dpf. (E,I) Wild-type cranial cartilages show normal morphology; (F,J) Cranial cartilages of *gad1* morphants are smaller and abnormally shaped when compared to wild-type structures; (G,K) *dlx2a* mRNA is sufficient to rescue the small, abnormally shaped cartilage associated with Gad1 knockdown; (H,L) Injection of 120 pg *dlx2a* mRNA causes truncated and thickened cartilages to develop. (F) *gad1* morphants exhibit an abnormally shaped ethmoid plate and truncated trabeculae; (J) *gad1* morphants display abnormal fusion of the Meckel's cartilage, misshapen basihyal cartilage (arrow) and often have truncated ceratobranchial structures (red bracket); (H,L) *dlx2a* overexpression animals exhibit cartilages that look condensed, when compared to wild-type animals. The cartilages appear much thicker than normal; (H) The ethmoid plate and trabeculae appear thickened and "squashed"; (L) *dlx2a* overexpression causes a thicker fusion point of the Meckel's cartilage (arrowhead) and much wider ceratohyals (bracket). (bh) basihyal; (cb) ceratobranchial; (ch) ceratohyal; (ep) ethmoid plate; (hs) hyosymplectic; (ih) interhyal; (m) Meckels; (pch) parachordal; (pq) palatoquadrate; (tr) trabeculae

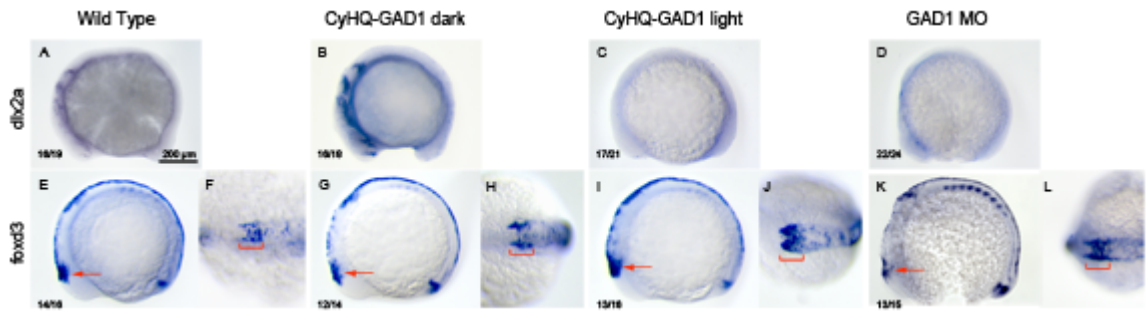


**Figure 6.7. CyHQ-*gad1* morpholinos can bypass changes in early neural crest markers.** (A-D) Lateral view of ISH for *dlx2a* in wild-type, caged CyHQ-*gad1* MO, uncaged CyHQ-*gad1* MO and *gad1*MO animals. (A,B) Expression of *dlx2a* is comparable between wild type and CyHQ-*gad1* morphant animals, where the morpholino remains intact; (C,D) Expression of *dlx2a* is significantly reduced in *gad1* morphant animals and comparable reduction is observed in CyHQ-*gad1* morphants where the morpholino had been uncaged. (E,G,I,K) Lateral view of ISH for *foxd3* in wild-type, caged CyHQ-*gad1* morphant, uncaged CyHQ-*gad1* morphant and *gad1* morphant animals; (E,G) *foxd3* expression is comparable between wild type and CyHQ-*gad1* morphant animals, where the morpholino remains intact (arrows); (I,K) *foxd3* expression is increased in *gad1* and uncaged CyHQ-*gad1* morphant animals. (F,H,J,L) Dorsal view of ISH for *foxd3* in wild-type, caged CyHQ-*gad1* morphant, uncaged CyHQ-*gad1* morphant and *gad1* morphant animals; (F,H) Expression of *foxd3* remains comparable in wild type and CyHQ-*gad1* morphant animals, where the morpholino remains intact (bracket); (J,L) Expression of *foxd3* is significantly increased and comparable in *gad1* and uncaged CyHQ-*gad1* morphants , as shown by the dramatic expansion of *foxd3* expression in the dorsal region between the eye and ear (brackets).

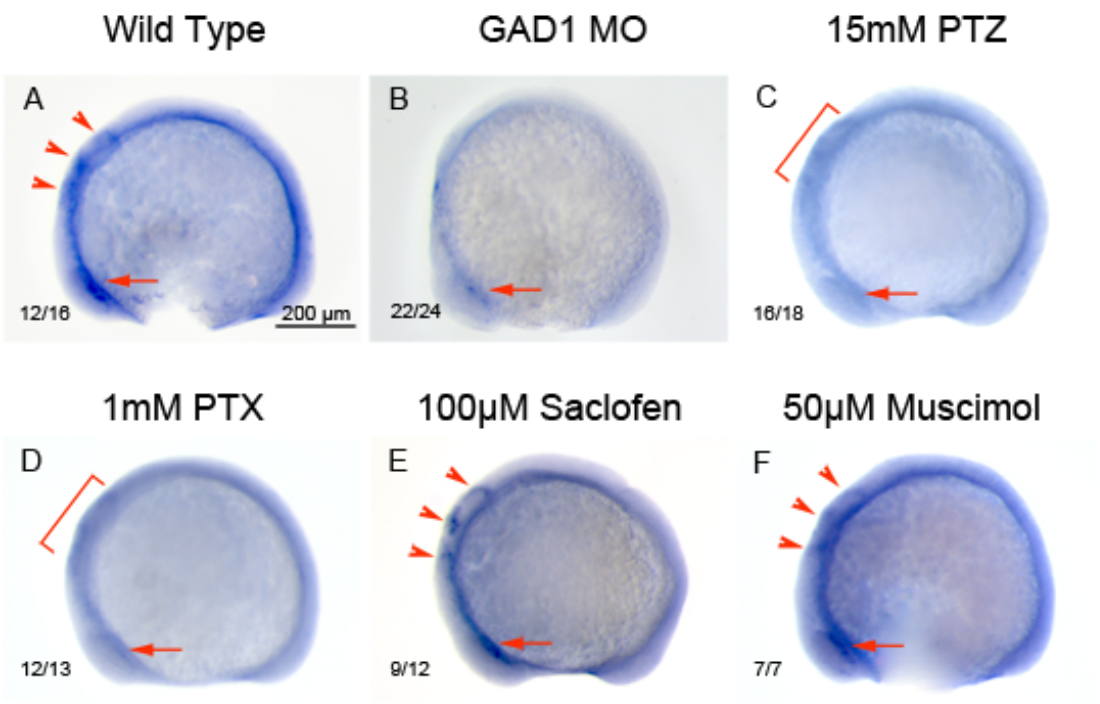


**Figure 6.8. Treatment with $GABA_A$ modulators phenocopy *gad1* knockdown and exhibit reduced expression of *dlx2a.*** (A-F) Lateral view of ISH for *dlx2a* in wild-type, *gad1* morphant, PTZ treated, PTX treated, sacolfen treated and muscimol treated embryos. (A-D) *dlx2a* expression is significantly reduced in embryos treated with 15 mM PTZ or 1 mM PTX, similar to that observed in *gad1* morphant animals (arrow and bracket). Expression in the pharyngeal arches is almost absent, when compared to wild-type animals; (E) Animals treated with 100 µm saclofen exhibited *dlx2a* expression comparable to that of wild type animals (arrow and arrowheads); (F) Animals treated with 50 µm muscimol (a $GABA_A$ agonist) exhibited a modest increase of *dl2a* expression throughout the embryos, when compared to wild type animals.

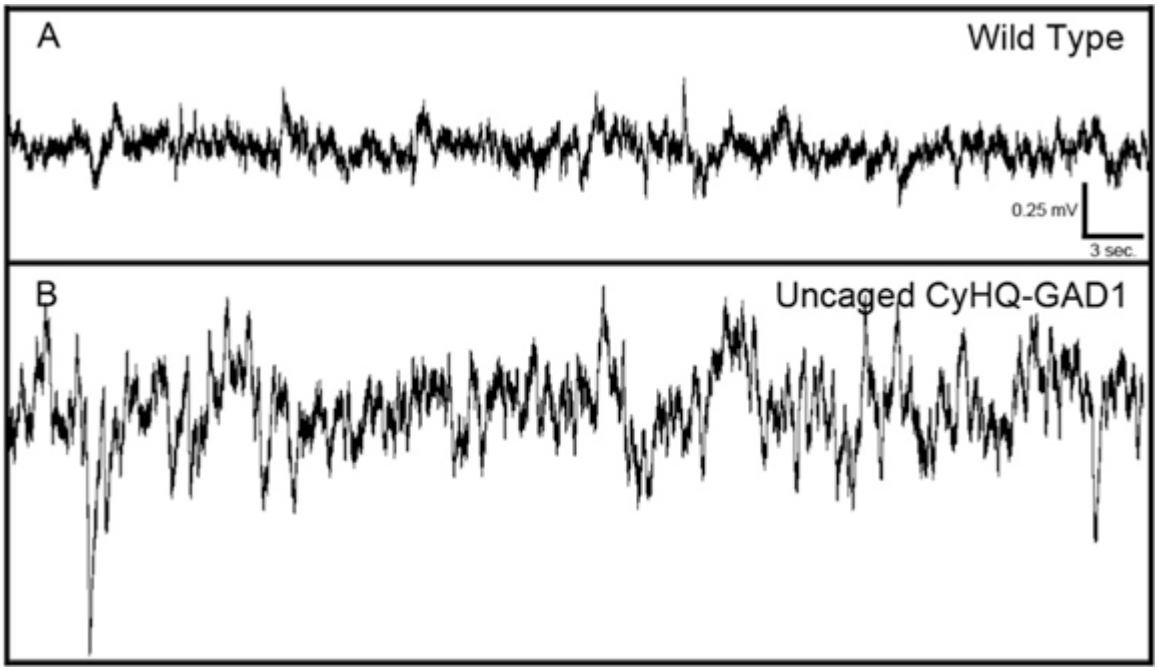


**Figure 6.9. Caged CyHQ-*gad1* can separate the activity of *gad1* in craniofacial development from its activities in neurotransmission.** (A) A 1 minute recording collected from the optic tectum of a wild-type 3 dpf larval zebrafish. Spontaneous activity, with amplitude no larger than 0.25 mV, is observed; (B) The neurological activity observed within the optic tectum of a 3 dpf CyHQ-*gad1* morphant animal that was raised in the dark for the first 24 hours of development. This animal looked phenotypically comparable to wild-type animals, but the native neurological activity within these animals was significantly higher than the wild-type animals. Larger amplitude (> 0.4 mV) events were observed consistently throughout the recording period.

References

Aarskog D (1975) Association between maternal intake of diazepam and oral clefts. The Lancet 306:921.

Addington A, Gornick M, Duckworth J, Sporn A, Gogtay N, Bobb A, Greenstein D, Lenane M, Gochman P, Baker N (2004) GAD1 (2q31. 1), which encodes glutamic acid decarboxylase (GAD67), is associated with childhood-onset schizophrenia and cortical gray matter volume loss. Molecular psychiatry 10:581-588.

Akimenko MA, Ekker M, Wegner J, Lin W, Westerfield M (1994) Combinatorial expression of three zebrafish genes related to distal-less: part of a homeobox gene code for the head. The Journal of neuroscience 14:3475-3486.

Alexander C, Zuniga E, Blitz IL, Wada N, Le Pabic P, Javidan Y, Zhang T, Cho KW, Crump JG, Schilling TF (2011) Combinatorial roles for BMPs and Endothelin 1 in patterning the dorsal-ventral axis of the craniofacial skeleton. Development 138:5135-5146.

Asada H, Kawamura Y, Maruyama K, Kume H, Ding R-g, Ji FY, Kanbara N, Kuzume H, Sanbo M, Yagi T (1996) Mice lacking the 65 kDa isoform of glutamic acid decarboxylase (GAD65) maintain normal levels of GAD67 and GABA in their brains but are susceptible to seizures. Biochemical and biophysical research communications 229:891-895.

Asada H, Kawamura Y, Maruyama K, Kume H, Ding R-G, Kanbara N, Kuzume H, Sanbo M, Yagi T, Obata K (1997) Cleft palate and decreased brain γ-aminobutyric acid in mice lacking the 67-kDa isoform of glutamic acid decarboxylase. Proceedings of the National Academy of Sciences 94:6496-6499.

Baas D, Malbouyres M, Haftek-Terreau Z, Le Guellec D, Ruggiero F (2009) Craniofacial cartilage morphogenesis requires zebrafish *col11a1* activity. Matrix Biology 28:490-502.

Ball R, Page AT, Acuff S, Singer R, Gaudet J, Beebe LL, Keith CH, Sornborger AT, Lauderdale JD (In preparation) A Comparison of Evoked Seizure Activity in the Mature and Immature Zebrafish Brains.

Baraban SC, Taylor MR, Castro PA, Baier H (2005) Pentylenetetrazole induced changes in zebrafish behavior, neural activity and c-fos expression. Neuroscience 131:759-768.

Barrallo-Gimeno A, Holzschuh J, Driever W, Knapik EW (2004) Neural crest survival and differentiation in zebrafish depends on mont blanc/tfap2a gene function. Development 131:1463-1477.

Ben-Shachar D, Laufer D, Livne E, Silbermann M (1987) Picrotoxin, a gamma-aminobutyric acid-receptor antagonist, retards craniofacial development in the weaning rat: I. Effect on mandibular bone growth. Journal of craniofacial genetics and developmental biology 8:351-361.

Bosma PT, Blázquez M, Collins MA, Bishop J, Drouin G, Priede IG, Docherty K, Trudeau VL (1999) Multiplicity of glutamic acid decarboxylases (GAD) in vertebrates: molecular phylogeny and evidence for a new GAD paralog. Molecular biology and evolution 16:397-404.

Bradford Y, Conlin, T., Dunn, N., Fashena, D., Frazer, K., Howe, D.G., Knight, J., Mani, P., Martin, R., Moxon, S.A., Paddock, H., Pich, C., Ramachandran, S., Ruef, B.J., Ruzicka, L., Bauer Schaper, H., Schaper, K., Shao, X., Singer, A., Sprague, J., Sprunger, B., Van Slyke, C., and Westerfield, M. (2011) ZFIN: enhancements and updates to the zebrafish model organism database. Nucleic Acids Res 39:D822-D829.

Bu D-F, Erlander MG, Hitz BC, Tillakaratne N, Kaufman DL, Wagner-McPherson CB, Evans GA, Tobin AJ (1992) Two human glutamate decarboxylases, 65-kDa GAD and 67-kDa GAD, are each encoded by a single gene. Proceedings of the National Academy of Sciences 89:2115-2119.

Chai Y, Maxson RE (2006) Recent advances in craniofacial morphogenesis. Developmental Dynamics 235:2353-2375.

Condie BG, Bain G, Gottlieb DI, Capecchi MR (1997) Cleft palate in mice with a targeted mutation in the γ-aminobutyric acid-producing enzyme glutamic acid decarboxylase 67. Proceedings of the National Academy of Sciences 94:11451-11455.

Culiat CT, Stubbs LJ, Woychik RP, Russell LB, Johnson DK, Rinchik EM (1995) Deficiency of the beta 3 subunit of the type A gamma-aminobutyric acid receptor causes cleft palate in mice. Nature genetics 11:344-346.

Davis MJ, Kragor CH, Reddie KG, Wilson HC, Zhu Y, Dore TM (2009) Substituent Effects on the Sensitivity of a Quinoline Photoremovable Protecting Group to One- and Two-Photon Excitation. Journal of Organic Chemistry 74:1721-1729.

Delgado L, Schmachtenberg O (2008) Immunohistochemical localization of GABA, GAD65, and the receptor subunits GABAAα1 and GABAB1 in the zebrafish cerebellum. The Cerebellum 7:444-450.

Ding R, Tsunekawa N, Obata K (2004) Cleft palate by picrotoxin or 3-MP and palatal shelf elevation in GABA-deficient mice. Neurotoxicology and teratology 26:587-592.

Dixon MJ, Marazita ML, Beaty TH, Murray JC (2011) Cleft lip and palate: understanding genetic and environmental influences. Nature Reviews Genetics 12:167-178.

Eisen JS, Weston J (1993) Development of the neural crest in the zebrafish. Developmental biology 159:50-59.

Erlander MG, Tillakaratne NJ, Feldblum S, Patel N, Tobin AJ (1991) Two genes encode distinct glutamate decarboxylases. Neuron 7:91-100.

Fedoryak OD, Dore TM (2002) Brominated hydroxyquinoline as a photolabile protecting group with sensitivity to multiphoton excitation. Organic Letters 4:3419-3422.

Ferretti E, Li B, Zewdu R, Wells V, Hebert JM, Karner C, Anderson MJ, Williams T, Dixon J, Dixon MJ (2011) A conserved Pbx-Wnt-p63-Irf6 regulatory module controls face morphogenesis by promoting epithelial apoptosis. Developmental cell 21:627-641.

Gordon CT, Brinas IM, Rodda FA, Bendall AJ, Farlie PG (2010) Role of Dlx genes in craniofacial morphogenesis: Dlx2 influences skeletal patterning by inducing ectomesenchymal aggregation in ovo. Evolution & development 12:459-473.

Graham A (2003) Development of the pharyngeal arches. American Journal of Medical Genetics Part A 119A:251-256.

Hagiwara N, Katarova Z, Siracusa LD, Brilliant MH (2003) Nonneuronal expression of the $GABA_A$ β3 subunit gene is required for normal palate development in mice. Developmental biology 254:93-101.

Homanics GE, DeLorey TM, Firestone LL, Quinlan JJ, Handforth A, Harrison NL, Krasowski MD, Rick CE, Korpi ER, Mäkelä R (1997) Mice devoid of γ-aminobutyrate type A receptor β3 subunit have epilepsy, cleft palate, and hypersensitive behavior. Proceedings of the National Academy of Sciences 94:4143-4148.

Johnston L, Ball RE, Acuff S, Gaudet J, Sornborger A, Lauderdale JD (2013) Electrophysiological Recording in the Brain of Intact Adult Zebrafish. e51065.

Jurand A, Martin LVH (1994) Cleft palate and open eyelids inducing activity of lorazepam and the effect of flumazenil, the benzodiazepine antagonist. Pharmacology & toxicology 74:228-235.

Kanno K, Suzuki Y, Yamada A, Aoki Y, Kure S, Matsubara Y (2004) Association between nonsyndromic cleft lip with or without cleft palate and the glutamic acid decarboxylase 67 gene in the Japanese population. American journal of medical genetics Part A 127A:11-16.

Karlsson J, von Hofsten J, Olsson P-E (2001) Generating transparent zebrafish: a refined method to improve detection of gene expression during embryonic development. Marine Biotechnology 3:522-527.

Kash SF, Johnson RS, Tecott LH, Noebels JL, Mayfield RD, Hanahan D, Baekkeskov S (1997) Epilepsy in mice deficient in the 65-kDa isoform of glutamic acid decarboxylase. Proceedings of the National Academy of Sciences 94:14060-14065.

Kim Y-J, Nam R-H, Yoo YM, Lee C-J (2004) Identification and functional evidence of GABAergic neurons in parts of the brain of adult zebrafish (*Danio rerio*). Neuroscience letters 355:29-32.

Kimmel CB, Miller CT, Kruze G, Ullmann B, BreMiller RA, Larison KD, Snyder HC (1998) The shaping of pharyngeal cartilages during early development of the zebrafish. Developmental biology 203:245-263.

Knecht AK, Bronner-Fraser M (2002) Induction of the neural crest: a multigene process. Nature Reviews Genetics 3:453-461.

Knight RD, Schilling TF (2006) Cranial neural crest and development of the head skeleton. Advances in experimental medicine and biology 589:120-133.

Kwakowsky A, Schwirtlich M, Zhang Q, Eisenstat DD, Erdélyi F, Baranyi M, Katarova ZD, Szabó G (2007) GAD isoforms exhibit distinct spatiotemporal expression patterns in the developing mouse lens: correlation with Dlx2 and Dlx5. Developmental Dynamics 236:3532-3544.

Le Douarin N, Kalcheim C (1999) The neural crest: Cambridge University Press.

Ma J, Rea AC, An H, Ma C, Guan X, Li M-D, Su T, Yeung CS, Harris KT, Zhu Y, Nganga JL, Fedoryak OD, Dore TM, Phillips DL (2012) Unraveling the Mechanism of the Photodeprotection Reaction of 8-Bromo- and 8-Chloro-7-hydroxyquinoline Caged Acetates. Chem—Eur J 18:6854-6865.

MacDonald RB, Debiais-Thibaud M, Talbot JC, Ekker M (2010) The Relationship Between dlx and gad1 Expression Indicates Highly Conserved Genetic Pathways in the Zebrafish Forebrain. Developmental Dynamics 239:2298-2306.

Maddox DM, Condie BG (2001) Dynamic expression of a glutamate decarboxylase gene in multiple non-neural tissues during mouse development. BMC developmental biology 1:1.

Martin SC, Heinrich G, Sandell JH (1998) Sequence and expression of glutamic acid decarboxylase isoforms in the developing zebrafish. The Journal of comparative neurology 396:253-266.

Miller CT, Yelon D, Stainier DY, Kimmel CB (2003) Two endothelin 1 effectors, hand2 and bapx1, pattern ventral pharyngeal cartilage and the jaw joint. Development 130:1353-1365.

Miller RP, Becker BA (1975) Teratogenicity of oral diazepam and diphenylhydantoin in mice. Toxicology and applied pharmacology 32:53-61.

Muhammad SI, Maznah I, Mahmud R, Zuki AB, Imam MU (2013) Upregulation of genes related to bone formation by gamma-amino butyric acid and gamma-oryzanol in germinated brown rice is via the activation of GABAB-receptors and reduction of serum IL-6 in rats. Clinical interventions in aging 8:1259-1271.

Noden DM (1983) The role of the neural crest in patterning of avian cranial skeletal, connective, and muscle tissues. Developmental biology 96:144-165.

Organization WH (2002) The World health report: 2002: Reducing the risks, promoting healthy life.

Ouyang X, Shestopalov IA, Sinha S, Zheng G, Pitt CL, Li WH, Olson AJ, Chen JK (2009a) Versatile synthesis and rational design of caged morpholinos. Journal of the American Chemical Society 131:13255-13269.

Ouyang X, Shestopalov IA, Sinha S, Zheng G, Pitt CLW, Li W-H, Olson AJ, Chen JK (2009b) Versatile Synthesis and Rational Design of Caged Morpholinos. Journal of the American Chemical Society 131:13255-13269.

Pisano M, Greene R (1986) HORMONE AND GROWTH-FACTOR INVOLVEMENT IN CRANIOFACIAL DEVELOPMENT. IRCS MEDICAL SCIENCE-BIOCHEMISTRY 14:635-640.

Qiu M, Bulfone A, Martinez S, Meneses JJ, Shimamura K, Pedersen RA, Rubenstein J (1995) Null mutation of Dlx-2 results in abnormal morphogenesis of proximal first and second branchial arch derivatives and abnormal differentiation in the forebrain. Genes & development 9:2523-2538.

Safra M, Oakley JR G (1975) Association between cleft lip with or without cleft palate and prenatal exposure to diazepam. The Lancet 306:478-480.

Saint-Jeannet J-P (2006) Neural crest induction and differentiation: Springer Science+ Business Media.

Scapoli L, Martinelli M, Pezzetti F, Carinci F, Bodo M, Tognon M, Carinci P (2002) Linkage disequilibrium between GABRB3 gene and nonsyndromic familial cleft lip with or without cleft palate. Human genetics 110:15-20.

Schilling TF (1997) Genetic analysis of craniofacial development in the vertebrate embryo. BioEssays : news and reviews in molecular, cellular and developmental biology 19:459-468.

Schilling TF, Kimmel CB (1994) Segment and cell type lineage restrictions during pharyngeal arch development in the zebrafish embryo. Development 120:483-494.

Schilling TF, Kimmel CB (1997) Musculoskeletal patterning in the pharyngeal segments of the zebrafish embryo. Development 124:2945-2960.

Schilling TF, Le Pabic P (2009) Fishing for the signals that pattern the face. J Biol 8:101.

Schilling TF, Piotrowski T, Grandel H, Brand M, Heisenberg C-P, Jiang Y-J, Beuchle D, Hammerschmidt M, Kane DA, Mullins MC (1996a) Jaw and branchial arch mutants in zebrafish I: branchial arches. Development 123:329-344.

Schilling TF, Piotrowski T, Grandel H, Brand M, Heisenberg CP, Jiang YJ, Beuchle D, Hammerschmidt M, Kane DA, Mullins MC, van Eeden FJ, Kelsh RN, Furutani-Seiki M, Granato M, Haffter P, Odenthal J, Warga RM, Trowe T, Nusslein-Volhard C (1996b) Jaw and branchial arch mutants in zebrafish I: branchial arches. Development 123:329-344.

Sperber SM, Saxena V, Hatch G, Ekker M (2008) Zebrafish< i> dlx2a</i> contributes to hindbrain neural crest survival, is necessary for differentiation of sensory ganglia and functions with *dlx1a* in maturation of the arch cartilage elements. Developmental biology 314:59-70.

Stühmer T, Anderson SA, Ekker M, Rubenstein JL (2002) Ectopic expression of the Dlx genes induces glutamic acid decarboxylase and Dlx expression. Development 129:245-252.

Swartz ME, Sheehan‐Rooney K, Dixon MJ, Eberhart JK (2011) Examination of a palatogenic gene program in zebrafish. Developmental Dynamics 240:2204-2220.

Szabo-Rogers HL, Smithers LE, Yakob W, Liu KJ (2010) New directions in craniofacial morphogenesis. Developmental biology 341:84-94.

Tallafuss A, Gibson D, Morcos P, Li Y, Seredick S, Eisen J, Washbourne P (2012) Turning gene function ON and OFF using sense and antisense photo-morpholinos in zebrafish. Development 139:1691-1699.

Thisse C, Thisse B (2008) High-resolution in situ hybridization to whole-mount zebrafish embryos. Nature protocols 3:59-69.

Thorogood P (1983) Morphogenesis of cartilage. Cartilage 2:223-254.

Tillakaratne NJ, Medina-Kauwe L, Gibson KM (1995) Gamma-aminobutyric acid (GABA) metabolism in mammalian neural and nonneural tissues. Comparative Biochemistry and Physiology Part A: Physiology 112:247-263.

Tomasini AJ, Schuler AD, Zebala JA, Mayer AN (2009) PhotoMorphs: a novel light-activated reagent for controlling gene expression in zebrafish. Genesis 47:736-743.

Verreijdt L, Debiais‐Thibaud M, Borday‐Birraux V, Sire JY, Huysseune A (2006) Expression of the dlx gene family during formation of the cranial bones in the zebrafish (Danio rerio): differential involvement in the visceral skeleton and braincase. Developmental Dynamics 235:1371-1389.

Wada N, Javidan Y, Nelson S, Carney TJ, Kelsh RN, Schilling TF (2005) Hedgehog signaling is required for cranial neural crest morphogenesis and chondrogenesis at the midline in the zebrafish skull. Development 132:3977-3988.

Wee E, Norman E, Zimmerman E (1985) Presence of gamma-aminobutyric acid in embryonic palates of AJ and SWV mouse strains. Journal of craniofacial genetics and developmental biology 6:53-61.

Wee EL, Zimmerman EF (1983) Involvement of GABA in palate morphogenesis and its relation to diazepam teratogenesis in two mouse strains. Teratology 28:15-22.

Westerfield M (1993) The zebrafish book : a guide for the laboratory use of zebrafish (Brachydanio rerio). Eugene, OR: M. Westerfield.

Wong K, Stewart A, Gilder T, Wu N, Frank K, Gaikwad S, Suciu C, Dileo J, Utterback E, Chang K, Grossman L, Cachat J, Kalueff AV (2010) Modeling seizure-related behavioral and endocrine phenotypes in adult zebrafish. Brain research 1348:209-215.

Yamazoe S, Shestopalov IA, Provost E, Leach SD, Chen JK (2012) Cyclic caged morpholinos: conformationally gated probes of embryonic gene function. Angewandte Chemie, International Edition 51:6908-6911.

Yelick PC, Schilling TF (2002) Molecular dissection of craniofacial development using zebrafish. Critical Reviews in Oral Biology & Medicine 13:308-322.

Zhu Y, Pavlos CM, Toscano JP, Dore TM (2006) 8-Bromo-7-hydroxyquinoline as a photoremovable protecting group for physiological use: mechanism and scope. Journal of the American Chemical Society 128:4267-4276.

Supplementary Methods

***Preparation of CyHQ-gad1 cMO***

Preparation of BHQ-gad1cMO (**4a**) and CyHQ-Gad1cMO (**4b**) from linker **1a** and **1b**. A 25-base *Gad1* MO oligomer with 5¢-amine and 3¢-disulfide functionalization (**2**, 5¢-AAGGTGCAGAAGACGCCATCAGTCC-3¢, 15 nmol, Gene-Tools) was dissolved in 0.1 M $Na_2B_4O_7$, pH 8.5 (100 mL). Photocleavable linker **1a** or **1b** (1.0 mmol, 20 eq) in DMSO (15.0 mL) was added, and the reaction was shaken in the dark until LC-MS indicated that it was complete. The resulting mixture was purified on a NAP-5 gel-filtration column and lyophilized; the resulting white solid was dissolved in water (200 mL). Acetic acid (2.00 mL) was added to the solution, which was then washed successively with chloroform (3 × 200 mL) and EtOAc (2 × 200 mL), and then neutralized with 10% aq. $NH_4OH$. The solution was lyophilized to dryness, affording the conjugated product **3a** or **3b** as a white solid, which was taken directly to the next step without further purification.

*BHQ-Gad1MO (**3a**)*: MS-ESI-LC-MS-Q-TOF (*m*/*z*) $[M+H]^+$ calcd for $C_{349}N_{165}O_{106}H_{534}P_{25}ClBrS_2$ 9688, found 9688.

*CyHQ-Gad1MO (**3b**)*: MS-ESI-LC-MS-Q-TOF (*m*/*z*) $[M+H]^+$ calcd. for $C_{350}N_{163}O_{106}H_{534}P_{25}ClS_2$ 9634, found 9634.

Gel-immobilized TCEP (100 mL) (Pierce Biotechnology) was washed with 0.1 M Tris-HCl buffer, pH 8.4 (3 x 100 mL) in a centrifuge filter tube. BHQ-*Gad1*MO (**3a**) or CyHQ-*Gad1*MO (**3b**) was dissolved in 0.1 M Tris-HCl buffer, pH 8.4 (100 mL) and added to the washed gel; the reaction was shaken for 10 h in the dark. The supernatant was collected by centrifuge at 1000 rpm for 30 s. The gel slurry was washed with 0.1 M

Tris-HCl buffer, pH 8.4 (3 × 100 mL), and the eluted fractions were combined with the supernatant. This mixture was purified on a NAP-5 gel-filtration column and lyophilized to afford **4a** (8.2 nmol, 56%) or **4b** (11.7 nmol, 56%). *BHQ-Gad1cMO (**4a**)*: MS-ESI-LC-MS-Q-TOF (*m*/*z*) $[M+H]^+$ calcd for $C_{337}N_{161}O_{105}H_{518}P_{25}BrS$ 9431, found 9433. *CyHQ-Gad1cMO (**4b**)*: MS-ESI-LC-MS-Q-TOF (*m*/*z*) $[M+H]^+$ calcd for $C_{338}N_{162}O_{105}H_{518}P_{25}S$ 9374, found 9376.

Supplementary Figures

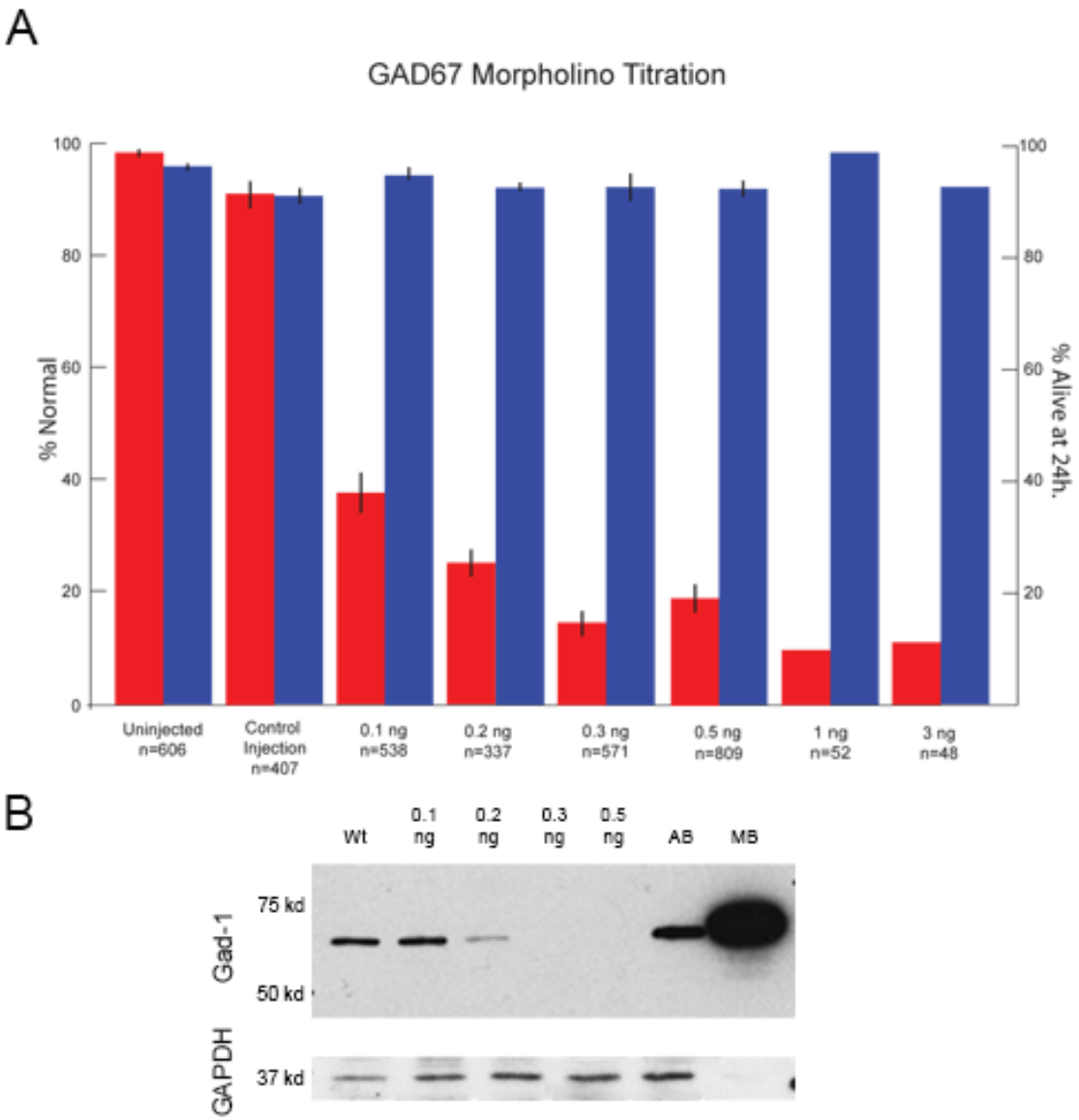


**Supplementary Figure 6.1. Titration of *gad1* morpholino and survivability at 24 hpf.** (A) Red bars represent percent of injected animals (out of 100) that showed normal morphology; Blue bars represent the percent of injected animals alive at 24hpf; (B) Western blot analysis of morpholino titration and the corresponding GAPDH control at 3 dpf; At 0.1ng of *gad1* morpholino, only 38% of animals looked normal, but protein was still present. At 0.3 ng of *gad1* morpholino, less than 20% of animals exhibited normal phenotypes, but all Gad67 protein was gone, according to western blot analysis. (AB) adult zebrafish brain extract; (MB) positive control mouse brain extract; (Wt) 3dpf wild-type zebrafish brain extract

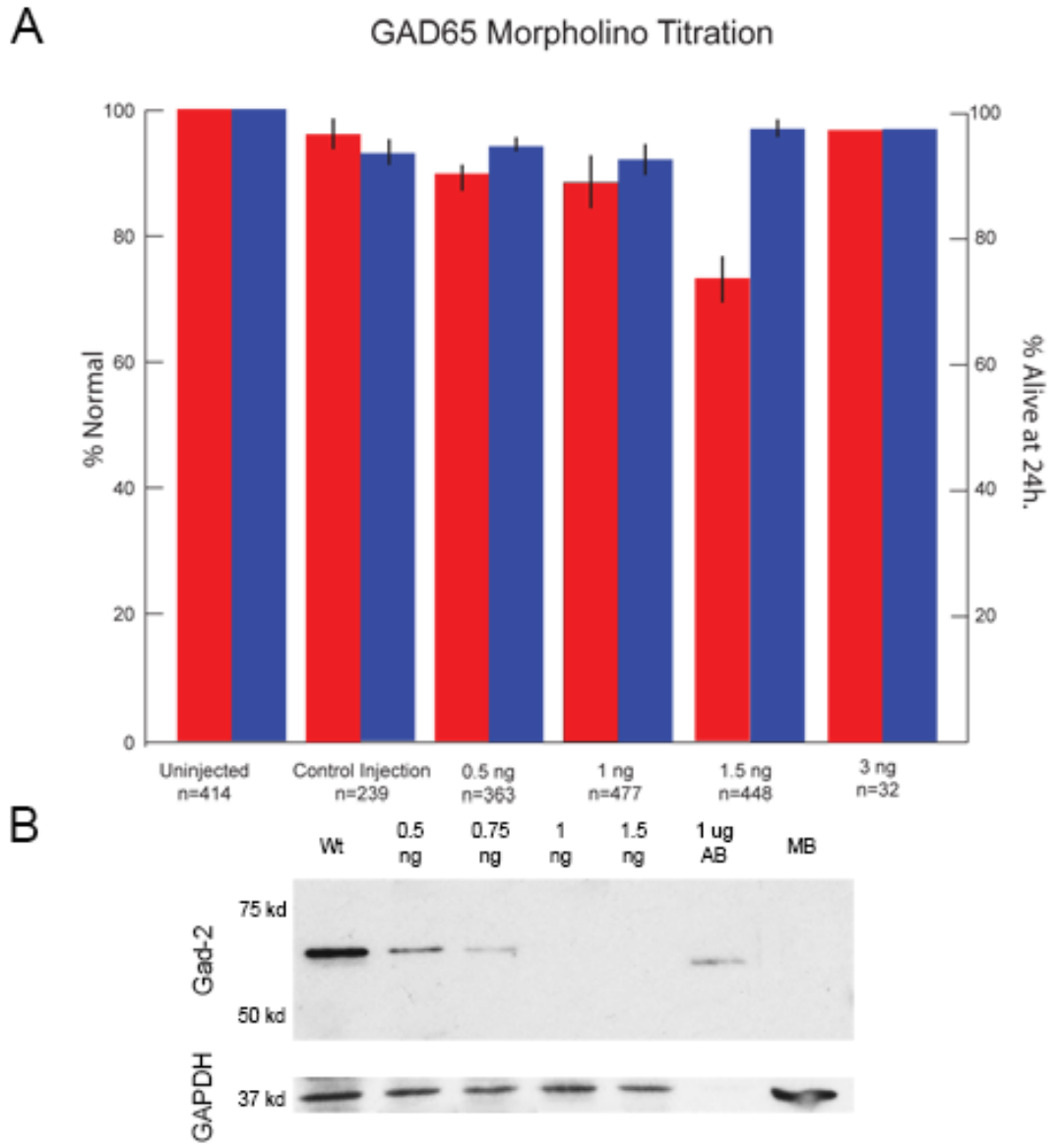


**Supplementary Figure 6.2. Titration of *gad2* morpholino and survivability at 24 hpf.** (A) Red bars represent the percent of injected animals (out of 100) that showed normal morphology; Blue bars represent the percent of injected animals alive at 24hpf; (B) Western blot analysis of morpholino titration and the corresponding GAPDH control at 3 dpf; At all concentration of *gad2* morpholino, between 90 and 100% of animals looked normal. According to western blot analysis, Gad65 protein was present up to a concentration of 1ng, which was used as the working concentration. (AB) adult zebrafish brain extract; (MB) positive control mouse brain extract; (Wt) 3dpf wild-type zebrafish brain extract

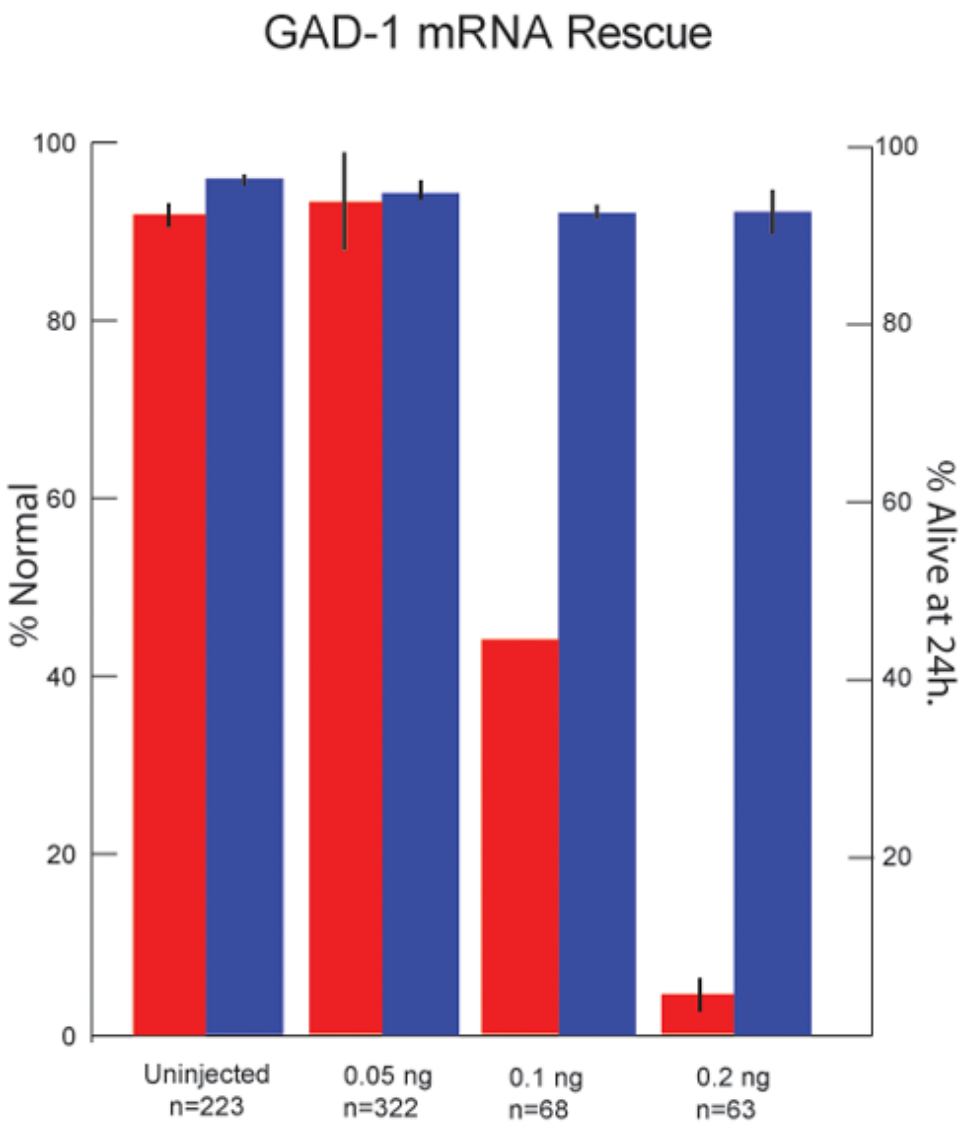


**Supplementary Figure 6.3. Titration of *gad1* mRNA and survivability at 24 hpf.** Red bars represent the percent of injected animals (out of 100) that showed normal morphology; Blue bars represent the percent of injected animals alive at 24 hpf.

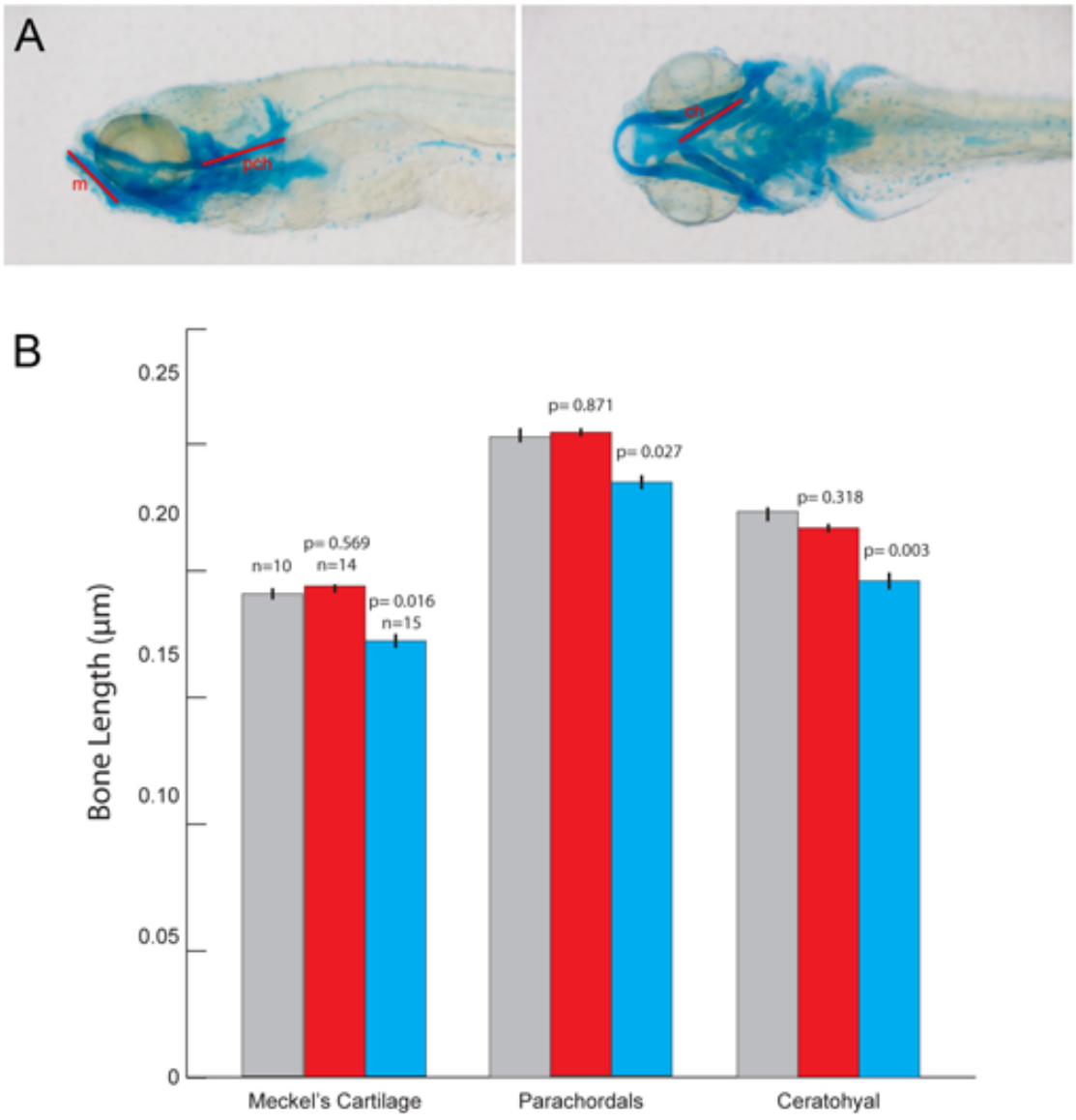


**Supplementary Figure 6.4. Knockdown of *gad1*, but not *gad2,* leads to smaller cranial cartilages.** (A) Left panel: Lateral view of a wild-type alcian stained animal; Right panel: ventral view of wild-type alcian stained animal. Red lines demarcate where whole-mount measurements were taken; (B) Knockdown of *gad1* causes Meckels cartilage, Parachordal cartilage and ceratohyal cartilages to be significantly smaller than in wild-type and *gad2* morphant animals. (m) Meckels cartilage; (pch) parachordal cartilage; (ch) ceratohyal cartilage

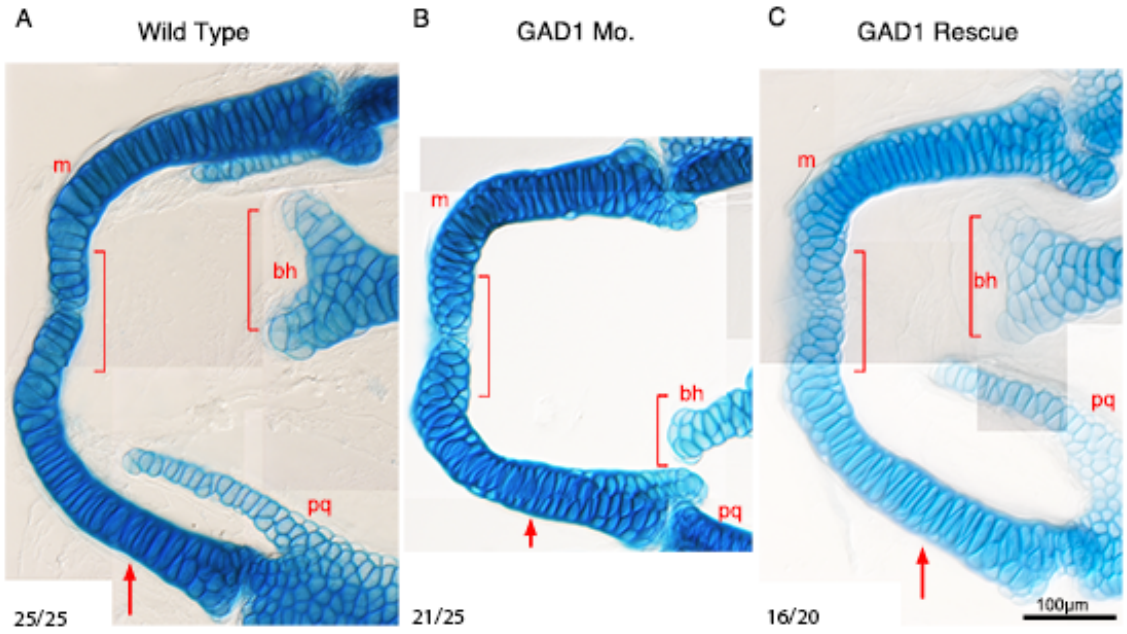


**Supplementary Figure 6.5. Knockdown of *gad1* causes aberrant chondrocyte morphology and stacking.** (A-C) Flat mounted samples of Meckels cartilages from 7dpf animals and imaged at 70x. (A) Wild-type Meckels cartilage consists of chondrocytes that are elongated and stacked in a planar fashion (arrow). Fusion and elongation points of the Meckels cartilage and exhibit normal morphology (brackets); (B) *gad1* morphants display abnormally shaped and aberrant stacking patterns of cranial chondrocytes (arrow). The fusion point of the Meckels cartilage is thickened due to small, abnormally stacked chondrocytes and the basihyal is greatly misshapen and not fully extended (brackets); (C) Co-injection of *gad1* morpholino and *gad1* mRNA partially rescues the morphant phenotype. Most chondrocytes regain a normal morphology and stacking pattern, but the midline fusion of the Meckels cartilage retains the abnormal chondrocyte morphology. (bh) basihyal; (m) Meckels; (pq) palatoquadrate

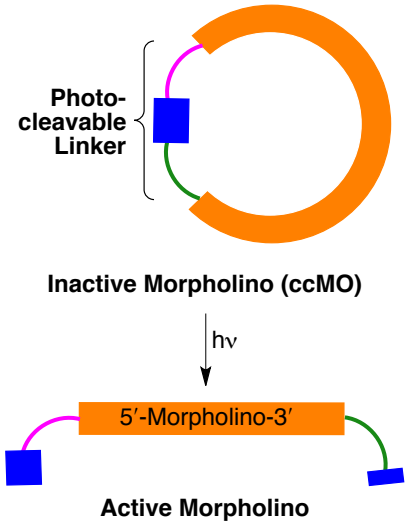


**Supplementary Figure 6.6**. **Photoactivation of a caged, cyclic morpholino (ccMO).** When intact, the caged morpholino exists as a circular entity, and because of this structure, cannot adequately target and bind to the complementary mRNA. Once exposed to light, the BHQ-caging moiety is cleaved, allowing linearization and subsequent targeting and binding of the morpholino to its complementary sequence.

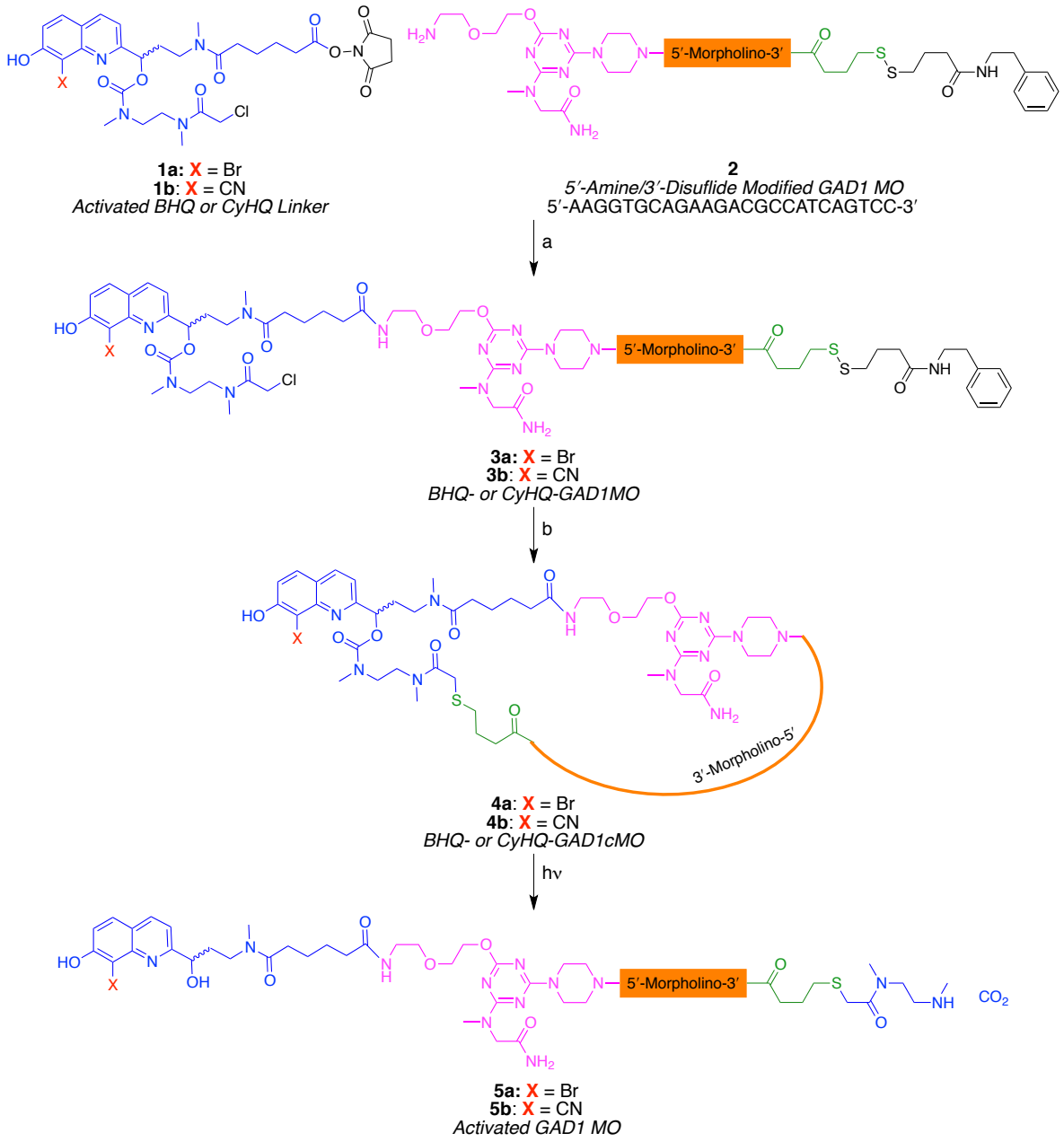


**Supplementary Figure 6.7**. **Preparation and activation of ccMOs.** (A) 0.1 M $NaB_4O_7$, pH 8.5, DMSO, functionalized MO with 5¢ amino and 3¢ disulfide (**2**); (B) tris (2-carboxyethyl)phosphine (TCEP), resin, 0.1 M Tris-HCl buffer, pH 8.4. Preparations of **1a** and **1b** are described in Supplemental Methods.

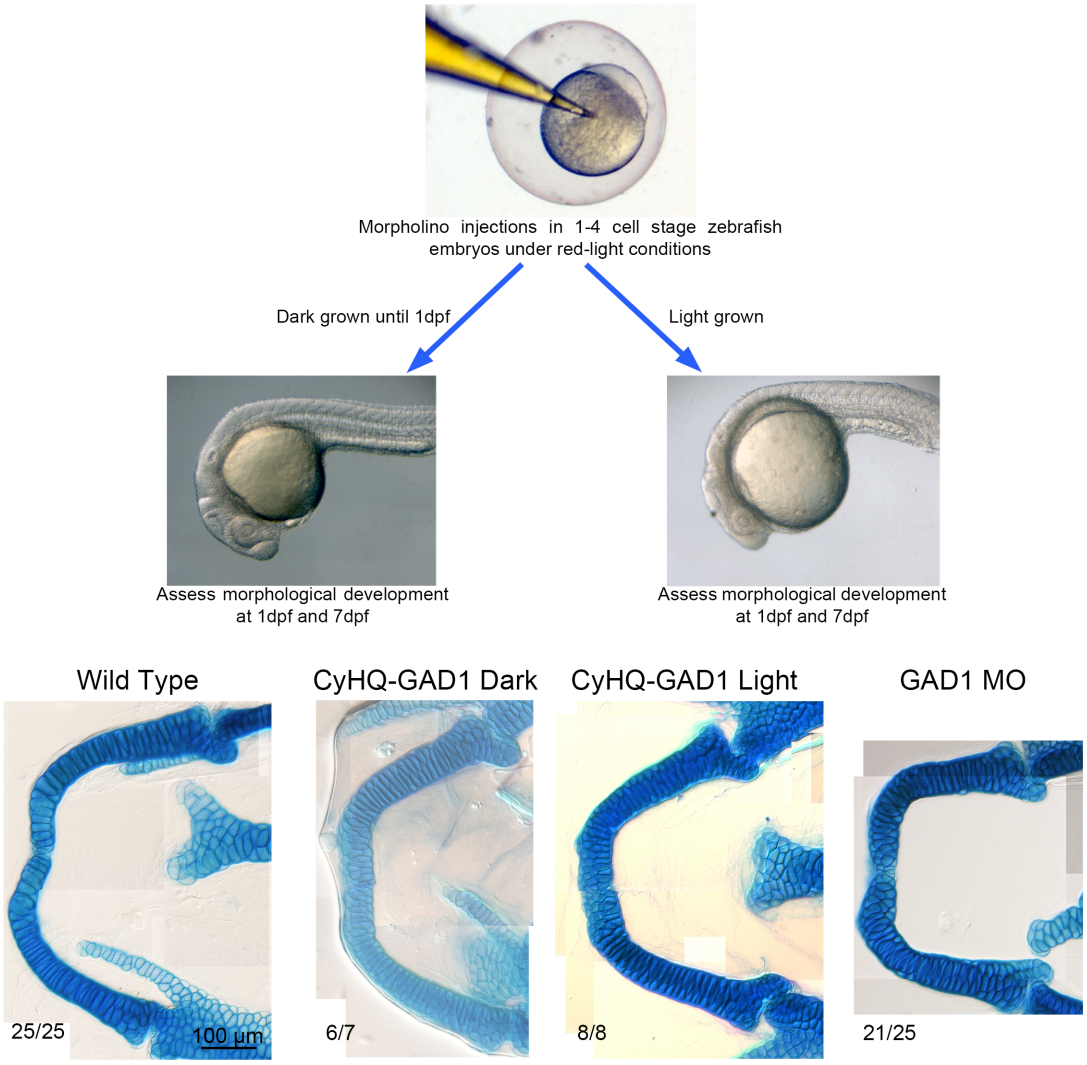


**Supplementary Figure 6.8. Caged CyHQ-*gad1* morpholinos can bypass the *gad1* morphant phenotype.** (A) Schematic of uncaging paradigm. CyHQ-*gad1* morpholino injected into 1-4 cell stage embryos under red-light conditions. Half of the embryos were raised in dark for first 24 hours and then exposed to light for the remainder of the experiment. The remaining half was raised in light. Morphology of animals was assessed at 1 dpf and 7 dpf. (B-E) Flat mounted samples of Meckels cartilage from 7dpf animals; (B) Wild-type animals displayed normal cartilage morphologies; (C) Animals injected with CyHQ-*gad1* and dark-raised for 24 hours and then in the light exhibited normal morphology of cranial cartilages; (D) Animals injected with CyHQ and raised in the light exhibited abnormal chondrocyte morphology and stacking, similar to *gad1* morphants (E).

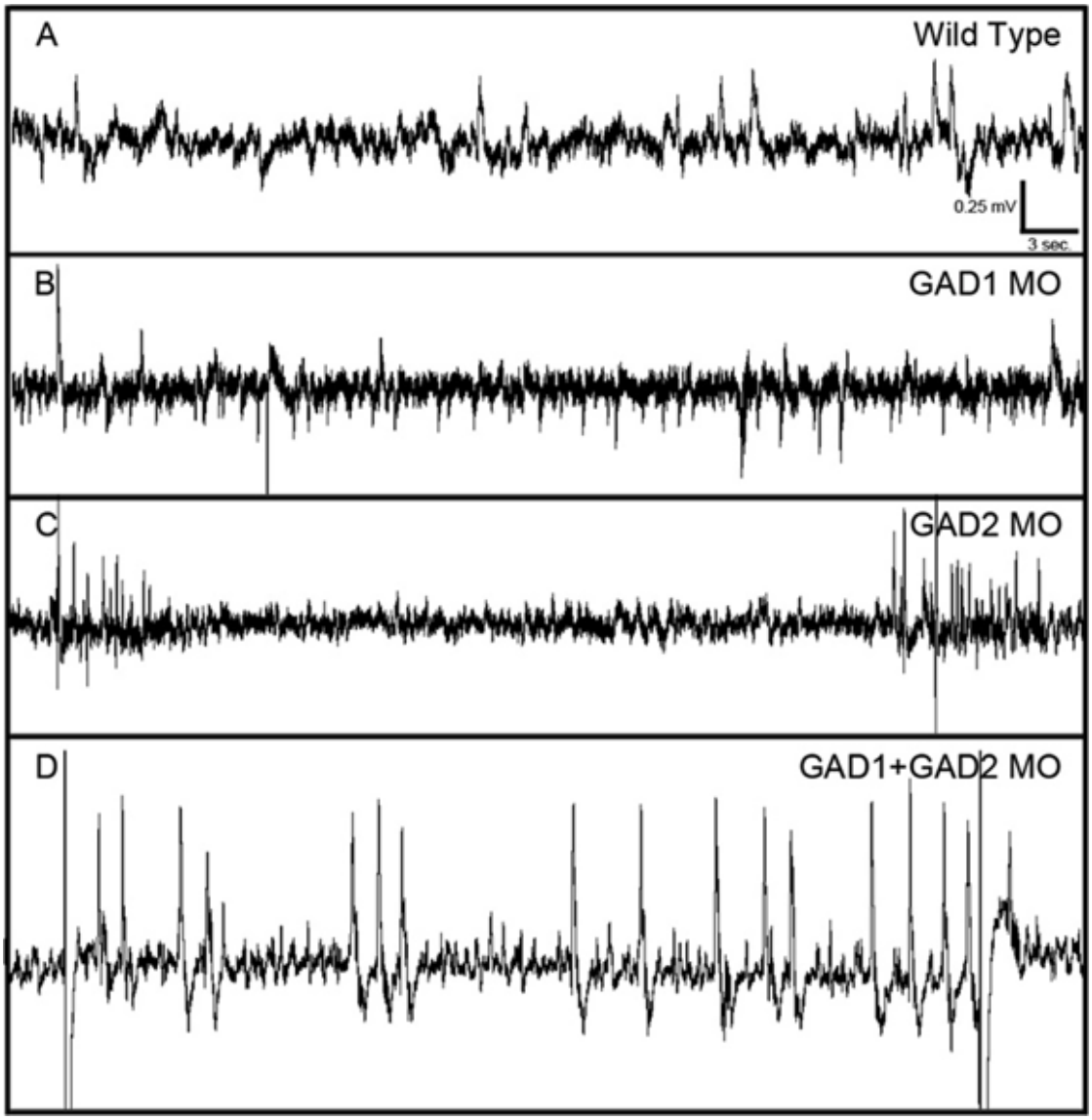


**Supplementary Figure 6.9. Knockdown of *gad1* and *gad2* causes an increase in native neurological activity in 3 dpf zebrafish larvae** (A) Native neurological activity within the optic tectum of 3 dpf wild-type animals. This recording shows spontaneous electrical discharges, no larger than 0.25 mV; (B) Knockdown of *gad1* causes an increase in the native activity observed in the optic tectum. Events on the order of 0.15-0.25 mV occur more often and larger amplitude (> 0.3 mV) events develop; (C) Knockdown of *gad2* leads to the development of epileptic-like events, where clusters of large (> 0.3 mV) events develop and are separated by a period of quieter, baseline-level activity; (D) *gad1/gad2* double morphants exhibit a significant increase in neurological activity, when compared with either wild-type or single morphant animals. Large amplitude (> 0.6 mV) events develop and occur in small clusters, separated by smaller (0.15 mV) events.

# CHAPTER 7

# CONCLUSION

Through this work, I have shown that *gad1* is involved in a variety of roles during early zebrafish development. Specifically, I determined that GABA signaling is not only involved in the later processes of neurotransmission, but I have uncovered a second role in early craniofacial development. This finding is not surprising, as previous work in the mouse has suggested GABA's role in craniofacial development, but the mechanism involved has remained elusive.

Studies in mice and humans have revealed that mutations in *gad1*, but not *gad2*, or in the $GABA_A$ receptor, *beta 3* (GABARB3) subunit develop cleft palate (Culiat et al., 1995, Asada et al., 1997, Condie et al., 1997, Homanics et al., 1997, Maddox and Condie, 2001, Scapoli et al., 2002, Hagiwara et al., 2003, Kanno et al., 2004, Muhammad et al., 2013). Similarly, drugs known to alter GABA signaling, such as the benzodiazepines or the $GABA_A$ receptor channel blocker picrotoxin, can induce cleft palate when administered to pregnant mice during a critical period of palatogenesis (Miller and Becker, 1975, Wee and Zimmerman, 1983, Ben-Shachar et al., 1987), or when taken during pregnancy in humans (Aarskog, 1975, Safra and Oakley JR, 1975). Both loss-of-function and enhancement studies using $GABA_A$ receptor antagonists and agonists suggest that the processes of palatogenesis require a specific range of GABA signaling during a critical period to allow for normal palate development.

Similar to these findings, my data shows that knockdown of *gad1*, but not *gad2*, is sufficient to induce cranial changes within the larval zebrafish. These alterations manifest as abnormal head outgrowth and underdevelopment of the eyes at 1 dpf, and by 7 dpf, smaller cranial cartilages are observed. The cartilaginous structures of the head region are misshapen and smaller due to the abnormal shape and stacking pattern of the chondrocytes. These changes are also observed when $GABA_A$ receptor antagonists are bath applied early in development (~10 hpf). Based upon these results, this pathway appears to be signaling through the $GABA_A$ receptor. Because it is known that the cranial cartilages develop from the cranial neural crest population, I looked at early neural crest markers to determine if these cells were being affected or if the observed changes occurred later in cartilage development. The most striking finding, and what provided the first insight into the mechanism involved, was that *dlx2a* expression was significantly delayed in *gad1* morphant animals. This delay could contribute to the abnormal stacking pattern of chondrocytes that is observed in the *gad1* morphants. Even though disorderly stacking of chondrocytes often suggests a disruption or delay in the early stages of chondrogenesis (Thorogood, 1983, Kimmel et al., 1998, Baas et al., 2009), the exact role of GABA signaling in this early developmental process remains unknown.

Studies in mice suggest that GABAergic signaling in the mesenchymal and/or epithelial cells of the developing palate can play a role in its development (Wee et al., 1985, Hagiwara et al., 2003, Ding et al., 2004). This work suggests that GABA, which is synthesized and secreted by nonneuronal cells in the palatal epithelium, could mediate cellular proliferation during palatal shelf elevations and cell migration/differentiation during palatal fusion (Hagiwara et al., 2003). Although zebrafish do not develop a

secondary palate, this data suggests that GABAergic signaling, through the $GABA_A$ receptor, may play a role in the mechanisms associated with cellular proliferation, differentiation and early vertebrate development.

I speculate that the abnormal development observed in the *gad1* morphant zebrafish results from changes in the cellular proliferation and differentiation of the cranial neural crest cells. This idea is primarily based upon work carried out in stem cell culture populations, as well as in embryonic mice. In this work, Andäng and colleagues determined that autocrine/paracrine GABA signaling, by means of the $GABA_A$ receptor, could negatively control stem cell proliferation, resulting in attenuation of the neuronal progenies from the stem cell niche (2008).

Andäng and colleagues first showed that the $GABA_A$ receptor was present in stem cells and that its activity could induce a hyperpolarizing current through an influx of chloride ions. They went on to show that application of muscimol (a potent $GABA_A$ agonist) to stem cell preparations caused a significant decrease in the number of mitotic events observed, and the majority of normal cell proliferation was blocked (Snodgrass, 1978, Andäng et al., 2008). Similarly, knockdown of GABARB3 or GABA by RNAi or bicuculline, respectively, lead to an increase in the number of cells and mitotic events within a two-hour period following exposure. The rapid changes in cell cycle observed following application of muscimol suggested that the mechanism was likely acting in late S, G2 or M phase. Cell cycle distribution analysis, by flow cytometry, revealed either an accumulation or a decrease in the number of stem cells in S phase following six hours of activation or inhibition of the $GABA_A$ receptor, respectively. The buildup of cells in S phase (following activation of $GABA_A$) also resulted in a rapid decrease in cellular

proliferation. Together, these findings suggested that while the S phase was being affected, the G1-S transition was not. It seems that activation of the $GABA_A$ receptor in stem cells leads to hyperpolarizing activity and a subsequent increase in cell volume, followed by control of cell proliferation through regulation of the progression through S phase (Andäng et al., 2008).

This group went on to analyze the active phosphorylated histone H2AX (γ-H2AX), which is a critical component of the S-G2 DNA-damage checkpoint complex (Fernandez-Capetillo et al., 2004, Lowndes and Toh, 2005). Following exposure to muscimol, γ-H2AX levels rapidly increased in nuclear foci of the stem cells. Additionally, this activity could be inhibited through exposure to $GABA_A$ antagonists, yet, DNA tail comet assays revealed no apparent DNA damage following these treatments. H2AX is phosphorylated by the phosphatidylinositol-3-OH kinase-related kinase (PIKK) family, including ataxia telangiectasia mutated (ATM), ataxia telangiectasia, Rad3-related (ATR) and DNA protein kinase (DNA-PK) (Bartek et al., 2004, Fernandez-Capetillo et al., 2004, Lowndes and Toh, 2005, Lovejoy and Cortez, 2009). In stem cell preparations, the cell cycle distribution response to muscimol was abolished following siRNA against ATR. Because ATR activates ATM in response to replication fork stalling, they also looked at phosphorylated ATM (P-ATM) (Stiff et al., 2006). P-ATM was increased after muscimol treatment. Also, exposure of an ATM/DNA-PK inhibitor (blocks phosphorylation of ATM) decreased γ-H2AX levels and significantly reduced the number of cells in the S phase (Andäng et al., 2008). These findings suggest that the PIKK family of kinases mediates $GABA_A$ receptor activation of H2AX in the absence of DNA damage.

Finally, Andäng and colleagues determined that GABA's effect on cellular proliferation was critically dependent on H2AX. Knockdown of H2AX by RNAi eliminated the effect that muscimol had in stem cells, causing a decrease in the number of cells in S phase. This outcome could result from either the stem cells spending more time in other cell cycle phases or by cells progressing through S phase at a faster rate. The latter was shown to be correct, as evidenced by an elevation in BrdU incorporation in these RNAi treated cells. Similarly, blocking GABA with bicuculline resulted in an almost two fold increase in BrdU incorporation, *in vivo* (Andäng et al., 2008). Together, these findings suggest that endogenously produced GABA, acting through the PIKK-family proteins and H2AX, has the following functions: 1) regulates stem cell proliferation, 2) determines early embryo size and 3) determines proliferation *in vivo*, resulting in direct consequences on progeny cell number. This S phase-based mechanism may provide control of proliferation, independent of differentiation or DNA-damage.

Although I have not directly looked at the cell cycle and proliferation of the cranial neural crest cells, Andäng's findings suggest that GABA signaling, acting through the $GABA_A$ receptor, plays a key role in modulating progression through the cell cycle. My data shows that when GABA signaling is knocked down: 1) *dlx2a* expression is delayed, 2) there is a significant increase in apoptosis, and 3) chondrocytes of the cranial cartilages retain an undifferentiated morphology. Together these data suggest that although neural crest development is delayed, which could explain the observed increase in apoptosis, these cells eventually achieve *dlx2a* expression comparable to wild-type animals. Therefore, it seems likely that the process of cranial neural crest development and differentiation is delayed in *gad1* morphant animals. The abnormal round shape of

the chondrocytes seems to suggest that although chondrocyte differentiation occurs, it is developmentally delayed (Thorogood, 1983, Kimmel et al., 1998, Baas et al., 2009). This is supported by the fact that *gad1* morphant animals exhibit defects in the columnar organization of the chondrocytes in the cranial cartilages.

To confirm that the differentiation and/or proliferation of the cranial neural crest cells are developmentally delayed within *gad1* morphant animals, further analyses need to be carried out. Because Andäng determined that when GABA levels were low, fewer cells stalled in the S phase, and rapid proliferation took place (Andäng et al., 2008), it will be necessary to look at many of the cell cycle markers used in his work. It is well known that GABA signaling is involved in many developmental processes prior to inhibitory neuronal synapse formation. These processes include the generation of stem cells, cell cycle regulation, neuronal proliferation and outgrowth, and craniofacial development (Asada et al., 1997, Condie et al., 1997, Kwakowsky et al., 2007, Andäng et al., 2008, Benes, 2010). Although I can only speculate about the mechanism involved in the changes observed in *gad1* morphant animals, I find it intriguing that GABA signaling is involved in early cranial development within multiple vertebrates, including zebrafish. Thus, the zebrafish may lend itself as a good model to further study and determine the mechanism by which GABAergic signaling influences craniofacial development.

References

Aarskog D (1975) Association between maternal intake of diazepam and oral clefts. The Lancet 306:921.

Andäng M, Hjerling-Leffler J, Moliner A, Lundgren TK, Castelo-Branco G, Nanou E, Pozas E, Bryja V, Halliez S, Nishimaru H (2008) Histone H2AX-dependent GABAA receptor regulation of stem cell proliferation. Nature 451:460-464.

Asada H, Kawamura Y, Maruyama K, Kume H, Ding R-G, Kanbara N, Kuzume H, Sanbo M, Yagi T, Obata K (1997) Cleft palate and decreased brain γ-aminobutyric acid in mice lacking the 67-kDa isoform of glutamic acid decarboxylase. Proceedings of the National Academy of Sciences 94:6496-6499.

Baas D, Malbouyres M, Haftek-Terreau Z, Le Guellec D, Ruggiero F (2009) Craniofacial cartilage morphogenesis requires zebrafish *col11a1* activity. Matrix Biology 28:490-502.

Bartek J, Lukas C, Lukas J (2004) Checking on DNA damage in S phase. Nature reviews Molecular cell biology 5:792-804.

Ben-Shachar D, Laufer D, Livne E, Silbermann M (1987) Picrotoxin, a gamma-aminobutyric acid-receptor antagonist, retards craniofacial development in the weaning rat: I. Effect on mandibular bone growth. Journal of craniofacial genetics and developmental biology 8:351-361.

Benes FM (2010) Relationship of GAD67regulation to cell cycle and DNA repair in GABA neurons in the adult hippocampus: Bipolar disorder versus schizophrenia. Cell Cycle 9:625-627.

Condie BG, Bain G, Gottlieb DI, Capecchi MR (1997) Cleft palate in mice with a targeted mutation in the γ-aminobutyric acid-producing enzyme glutamic acid decarboxylase 67. Proceedings of the National Academy of Sciences 94:11451-11455.

Culiat CT, Stubbs LJ, Woychik RP, Russell LB, Johnson DK, Rinchik EM (1995) Deficiency of the beta 3 subunit of the type A gamma-aminobutyric acid receptor causes cleft palate in mice. Nature genetics 11:344-346.

Ding R, Tsunekawa N, Obata K (2004) Cleft palate by picrotoxin or 3-MP and palatal shelf elevation in GABA-deficient mice. Neurotoxicology and teratology 26:587-592.

Fernandez-Capetillo O, Lee A, Nussenzweig M, Nussenzweig A (2004) H2AX: the histone guardian of the genome. DNA Repair 3:959-967.

Hagiwara N, Katarova Z, Siracusa LD, Brilliant MH (2003) Nonneuronal expression of the $GABA_A$ β3 subunit gene is required for normal palate development in mice. Developmental biology 254:93-101.

Homanics GE, DeLorey TM, Firestone LL, Quinlan JJ, Handforth A, Harrison NL, Krasowski MD, Rick CE, Korpi ER, Mäkelä R (1997) Mice devoid of γ-aminobutyrate type A receptor β3 subunit have epilepsy, cleft palate, and hypersensitive behavior. Proceedings of the National Academy of Sciences 94:4143-4148.

Kanno K, Suzuki Y, Yamada A, Aoki Y, Kure S, Matsubara Y (2004) Association between nonsyndromic cleft lip with or without cleft palate and the glutamic acid decarboxylase 67 gene in the Japanese population. American journal of medical genetics Part A 127A:11-16.

Kimmel CB, Miller CT, Kruze G, Ullmann B, BreMiller RA, Larison KD, Snyder HC (1998) The shaping of pharyngeal cartilages during early development of the zebrafish. Developmental biology 203:245-263.

Kwakowsky A, Schwirtlich M, Zhang Q, Eisenstat DD, Erdélyi F, Baranyi M, Katarova ZD, Szabó G (2007) GAD isoforms exhibit distinct spatiotemporal expression patterns in the developing mouse lens: correlation with Dlx2 and Dlx5. Developmental Dynamics 236:3532-3544.

Lovejoy CA, Cortez D (2009) Common mechanisms of PIKK regulation. DNA Repair 8:1004-1008.

Lowndes NF, Toh GW (2005) DNA repair: the importance of phosphorylating histone H2AX. Current biology : CB 15:R99-R102.

Maddox DM, Condie BG (2001) Dynamic expression of a glutamate decarboxylase gene in multiple non-neural tissues during mouse development. BMC developmental biology 1:1.

Miller RP, Becker BA (1975) Teratogenicity of oral diazepam and diphenylhydantoin in mice. Toxicology and applied pharmacology 32:53-61.

Muhammad SI, Maznah I, Mahmud R, Zuki AB, Imam MU (2013) Upregulation of genes related to bone formation by gamma-amino butyric acid and gamma-oryzanol in germinated brown rice is via the activation of GABAB-receptors and reduction of serum IL-6 in rats. Clinical interventions in aging 8:1259-1271.

Safra M, Oakley JR G (1975) Association between cleft lip with or without cleft palate and prenatal exposure to diazepam. The Lancet 306:478-480.

Scapoli L, Martinelli M, Pezzetti F, Carinci F, Bodo M, Tognon M, Carinci P (2002) Linkage disequilibrium between GABRB3 gene and nonsyndromic familial cleft lip with or without cleft palate. Human genetics 110:15-20.

Snodgrass SR (1978) Use of 3H-muscimol for GABA receptor studies.

Stiff T, Walker SA, Cerosaletti K, Goodarzi AA, Petermann E, Concannon P, O'Driscoll M, Jeggo PA (2006) ATR-dependent phosphorylation and activation of ATM in response to UV treatment or replication fork stalling. The EMBO journal 25:5775-5782.

Thorogood P (1983) Morphogenesis of cartilage. Cartilage 2:223-254.

Wee E, Norman E, Zimmerman E (1985) Presence of gamma-aminobutyric acid in embryonic palates of AJ and SWV mouse strains. Journal of craniofacial genetics and developmental biology 6:53-61.

Wee EL, Zimmerman EF (1983) Involvement of GABA in palate morphogenesis and its relation to diazepam teratogenesis in two mouse strains. Teratology 28:15-22.

# APPENDIX A:

# LIGHT ACTIVATED SEROTONIN FOR EXPLORING ITS ACTION IN BIOLOGICAL SYSTEMS [1,2]

[1]Rea, A.C., Vandenberg, L.N., Ball, R.E., Snouffer, A.A., Hudson, A.G., Zhu, Y., McLain, D.E., Johnston, L.L, Lauderdale, J.D., Levin, M and Dore, T. M.. 2013. *Chemistry & biology*. *20*(12):1536-1546.
Reprinted here with permission of the publisher.

[2] Previously published as Lindsey L. Johnston (maiden name)

## Abstract

Serotonin (5-HT) is a neuromodulator involved in regulating mood, appetite, memory, learning, pain, and establishment of left-right (LR) asymmetry in embryonic development. To explore the role of 5-HT in physiology, we have created two forms of "caged" 5-HT, BHQ-*O*-5HT and BHQ-*N*-5HT. When exposed to 365 or 740 nm light, BHQ-*O*-5HT releases 5-HT through one- or two-photon excitation, respectively. BHQ-*O*-5HT mediated changes in neural activity in cultured mouse primary sensory neurons and the trigeminal ganglion and optic tectum of intact zebrafish larvae in the form of high-amplitude spiking in response to light. In *Xenopus laevis* embryos, light-activated 5-HT increased the occurrence of LR patterning defects. Maximal rates of LR defects were observed when 5-HT was released at stage 5 compared with stage 8. These experiments show the potential for BHQ-caged serotonins in studying 5-HT-regulated physiological processes.


## Graphical Abstract

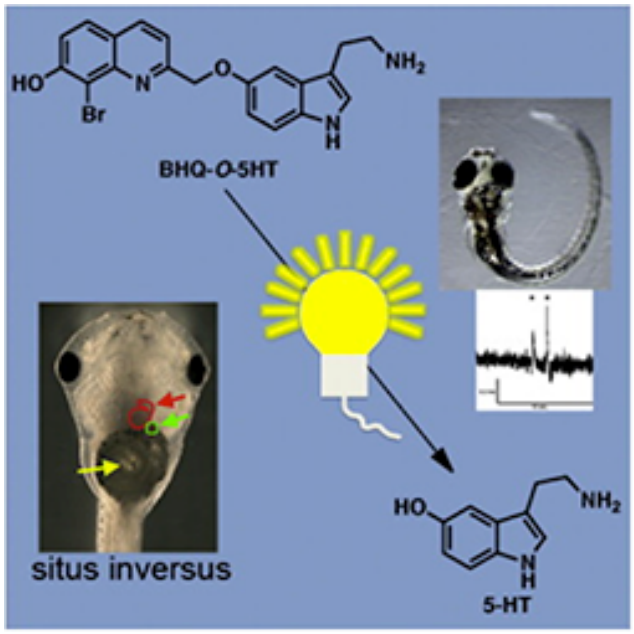

## Introduction

Serotonin (5-hydroxytyptamine or 5-HT) is an ancient biogenic amine found in wide variety of eukaryotes, including animals, plants, fungi, and pathogenic amoebae (Barnes and Sharp, 1999, Feldberg and Toh, 1953, Hoyer et al., 1994, Jackson and Yakel, 1995, McGowan et al., 1983 and Roshchina, 2001). In vertebrates, 5-HT is a neurotransmitter within both the central and peripheral nervous systems, and it also acts as a hormone in diverse tissues (Barnes and Sharp, 1999). In the brain, neurons in the raphe nuclei region produce 5-HT (Barnes and Sharp, 1999 and Frazer and Hensler, 1999). These neurons project into the cortex and hippocampus and influence an enormous network of excitatory and inhibitory neurotransmission (Frazer and Hensler, 1999) involved in regulating mood, appetite, memory, learning, and other cognitive functions (Barnes and Sharp, 1999, Daubert and Condron, 2010, Feldberg and Toh, 1953, Kang et al., 2009, McGowan et al., 1983 and Rapport et al., 1948). Serotonin in the CNS and periphery plays a complex role in mediating pain, both by acting as an algesic by exciting the peripheral terminations of primary afferent neurons, and in pain suppression via descending pathways (Bardin, 2011 and Basbaum and Fields, 1978). Interestingly, 5-HT also is involved in embryonic development and the establishment of left-right (LR) asymmetry (Levin et al., 2006 and Vandenberg and Levin, 2010). This diversity of function implicates 5-HT in several physiological and pathological processes.

In mammals and other vertebrates, 5-HT function is mediated by a large number of different receptors. In mammals, there are 14 structurally and pharmacologically distinct 5-HT receptor subtypes that are grouped into seven major families of 5-HT receptors, designated 5-$HT_{1–7}$ (Hoyer et al., 1994). One of these families, the 5-

$HT_3$ receptors, comprises ligand-gated ion channels that mediate fast synaptic transmission (Barnes and Sharp, 1999) through a transient inward current that rapidly depolarizes the cell. The remaining six receptor families are members of the G protein-coupled receptor superfamily and mediate a wide range of physiological and pharmacological responses (Barnes and Sharp, 1999). Several classes of antidepressant, antipsychotic, anxiolytic, and antimigraine drugs target these 5-HT signaling systems (Barnes and Sharp, 1999).

To explore the role of 5-HT in a variety of physiological contexts, a light-activated form of it would be useful. This can be achieved by covalently connecting a photoremovable protecting group (PPG) to 5-HT, thereby blocking or "caging" its action (Ellis-Davies, 2007, Klán et al., 2013, Kramer and Chambers, 2011, Lee et al., 2009, Mayer and Heckel, 2006, Specht et al., 2009 and Young and Deiters, 2007). Exposure to light releases or "uncages" 5-HT in its active form. Ideally, the caged 5-HT would be highly sensitive to light at wavelengths not detrimental to biological systems; release 5-HT rapidly; and in quantitative yield upon light exposure, exhibit no off-target effects, and be completely stable under physiological conditions in the dark. In addition, sensitivity to 5-HT release through two-photon excitation (2PE) is desirable for localization of release to subcellular levels (Bort et al., 2013, Dore, 2005, Dore and Wilson, 2011 and Warther et al., 2010). Four caged 5-HTs are known in the literature: 2-((2-(5-hydroxy-1*H*-indol-3-yl)ethyl)amino)-2-(2-nitrophenyl)acetic acid (*N*-CNB-5HT), 2-((3-(2-aminoethyl)-1*H*-indol-5-yl)oxy)-2-(2-nitrophenyl)acetic acid (*O*-CNB-5HT), 1-(2-nitrophenyl)ethyl (2-(5-hydroxy-1*H*-indol-3-yl)ethyl)carbamate (NPEC-*N*-5HT) (Boahen and MacDonald, 2005 and Breitinger et al., 2000), and

$[Ru(bpy)_2(5HT)_2]^{2+}$ (Zayat et al., 2006) (Figure A.1). Hess and coworkers synthesized *N*-CNB-5HT and *O*-CNB-5HT to study the kinetics of the 5-$HT_3$ligand-gated ion channel (Breitinger et al., 2000). The rate constant for release of 5-HT from *N*-CNB-5HT was too slow for that compound to be useful in the study, but *O*-CNB-5HT had sufficiently rapid release kinetics, albeit low photolysis $Q_u$ and molar absorptivity. The preparation and photolysis of 2-(5-(1-(2-nitrophenyl)ethoxy)-1*H*-indol-3-yl)ethanamine (NPE-*O*-5HT) (Boahen and MacDonald, 2005) and $[Ru(bpy)_2(5HT)_2]^{2+}$ (Zayat et al., 2006) were reported by MacDonald and Etchenique, respectively, and Tocris Bioscience sells NPEC-*N*-5HT commercially (catalog no. 3991), but the use of these compounds in a study of 5-HT physiology has not yet been reported.

We report the preparation of two (8-bromo-7-hydroxyquinolin-2-yl)methyl (BHQ)-protected 5-HT compounds 2-(((3-(2-aminoethyl)-1*H*-indol-5-yl)oxy)methyl)-8-bromoquinolin-7-ol (BHQ-*O*-5HT) and (8-bromo-7-hydroxyquinolin-2-yl)methyl (2-(5-hydroxy-1*H*-indol-3-yl)ethyl) carbamate (BHQ-*N*-5HT) (Figure A.1) and their suitability for spatially and temporally controlling the release of 5-HT through one-photon excitation (1PE) and 2PE within a biological system. We found that BHQ-*O*-5HT depolarized sensory neurons when photolyzed in culture and in larval zebrafish (*Danio rerio*) comparable to that observed by 5-HT by itself. Light-induced release of 5-HT from BHQ-*O*-5HT in stage 5 *Xenopus laevis*embryos significantly increases the rate of LR patterning defects in the frog. Activation of 5-HT at later stages had a less significant effect.

## Results and Discussion

We chose 8-bromo-7-hydroxyquinoline (BHQ) as the caging group for 5-HT because it has good sensitivity to 1PE-mediated photolysis at biologically compatible wavelengths (>350 nm) (Fedoryak and Dore, 2002 and Zhu et al., 2006) and rapid release kinetics (Ma et al., 2012). High sensitivity to light is important for working in thick or pigmented biological tissues, such as whole larval zebrafish or *X. laevis* embryos. Rapid release kinetics is critical for studying fast signaling events initiated by neurotransmitters and for taking advantage of BHQ's sensitivity to 2PE (Fedoryak and Dore, 2002 and Zhu et al., 2006), a sensitivity that is better than that of many groups currently used in biological studies, yet not as sensitive as others (Dore, 2005, Dore and Wilson, 2011, Klán et al., 2013 and Warther et al., 2010). To take advantage of the tight spatial release that 2PE affords, the release kinetics must be faster than diffusion out of the excitation volume. BHQ's moderate sensitivity to 2PE and rapid release kinetics could be advantageous for future biological studies.

Typically, phenols and alcohols require a carbonate linker for efficient release from the caging group after photoexcitation, but the initially released carbonate must first decarboxylate to yield the free phenol or alcohol. This slow step of the release process ($\tau$ = 240–270 μs for phenols) is not optimal (Zhao et al., 2006). It would be better to release phenol directly. To test this, we synthesized 8-bromo-2-(phenoxymethyl)quinolin-7-ol (BHQ-OPh) from bromo-7-(methoxymethoxy)quinolin-2-yl)methanol (MOM-BHQ-OH) (Figure A.2A). MOM-BHQ-OH, prepared from 8-bromo-7-hydroxyquinaldine as described previously (Ma et al., 2012), was converted to the corresponding mesylate that was subsequently displaced by phenol in good yield to provide the desired phenyl ether.

Removal of the methoxymethyl ether (MOM) protecting group with trifluoroacetic acid (TFA) in methanol afforded BHQ-OPh. BHQ-OPh was reasonably stable under simulated physiological conditions consisting of 100 mM potassium 3-(*N*-morpholino) propanesulfonate (KMOPS) buffer at pH 7.2, with a time constant for hydrolysis in the dark ($\tau_{dark}$) = 95 hr. BHQ-OPh photolyzes with a quantum efficiency ($Q_u$) = 0.19 at 365 nm and a 2PE photolysis uncaging action cross-section ($\delta_u$) = 0.56 GM [GM = $10^{-50}$ ($cm^4$ s)/photon] at 740 nm in KMOPS buffer (Figure A.2A). Figure A.S1 shows the time course of photolysis of BHQ-OPh by 1PE and 2PE. These results demonstrated that phenols were sufficiently good leaving groups for light-mediated release from BHQ and that protection and release of the phenol on 5-HT (and other neuromodulators) from BHQ were feasible.

We prepared two versions of the photoactivatable 5-HT: BHQ-*O*-5HT and BHQ-*N*-5HT from MOM-BHQ-OH and an appropriately protected 5-HT (Figures A.2B and A.2C). These compounds are distinguished by the type of linkage between the PPG and 5-HT. The *O*-version has a phenolic ether linkage, whereas the *N*-version uses a carbamate linker. The latter would place limitations on the use of BHQ-*N*-5HT that are discussed below. To synthesize BHQ-*O*-5HT, MOM-BHQ-OH was converted to the corresponding mesylate and displaced by the Boc-protected serotonin *tert*-butyl (2-(5-hydroxy-1*H*-indol-3-yl)ethyl)carbamate (*N*-Boc-5HT) that was prepared as described previously (Breitinger et al., 2000), to generate the doubly protected compound *tert*-butyl (2-(5-((8-bromo-7-(methoxymethoxy)quinolin-2-yl)methoxy)-1*H*-indol-3-yl)ethyl)carbamate [MOM-BHQ-*O*-5HT(*N*-Boc)]. Global deprotection with TFA in dichloromethane provided BHQ-*O*-5HT (Figure A.2B).

BHQ-*N*-5HT was prepared by activating the primary alcohol with carbonyldiimidazole and then treating the resulting carbamate (MOM-BHQ-carbonylimidazole) with triisopropylsilyl (TIPS)-protected serotonin 2-(5-((triisopropylsilyl)oxy)-1*H*-indol-3-yl)ethanamine [5HT(*O*-TIPS)] that was prepared as described previously ( Ho et al., 2003). Removal of first the TIPS protecting group with tetra-*n*-butylammonium fluoride (TBAF) was followed by the MOM deprotection in acidic methanol to provide BHQ-*N*-5HT (Figure A.2C).

Selected photophysical and photochemical properties of the two forms of caged 5-HT were examined (Table A.1) and compared with previously reported caged 5-HTs (Boahen and MacDonald, 2005, Breitinger et al., 2000 and Zayat et al., 2006). In contrast to the CNB- and NPE-protected 5-HTs, the BHQ-protected 5-HTs have absorbance maxima ($\lambda_{max}$) above 350 nm and larger molar absorptivities ($\varepsilon$), but not as high as $[Ru(bpy)_2(5HT)_2]^{2+}$ that is more absorbent in the visible region (Table A.1). BHQ-*O*-5HT and BHQ-*N*-5HT were each photolyzed under simulated physiological conditions (KMOPS buffer [pH 7.2]) with 370 nm light from a mercury lamp (1PE) and 740 nm light from a pulsed Ti:sapphire laser (2PE) (Chameleon Ultra II, Coherent) (Figure A.3). The time course of the reaction was monitored by high-performance liquid chromatography (HPLC), measuring the disappearance of the caged compound and appearance of 5-HT (Figure A.4). From these data, the 1-photon quantum efficiencies of photolysis ($Q_u$) and the 2PE photolysis action cross-sections ($\delta_u$) were calculated using previously described methods (Davis et al., 2009,Fedoryak and Dore, 2002, Furuta et al., 1999, Lu et al., 2003 and Zhu et al., 2006). Compared with the CNB- and NPE-protected 5-HTs and $[Ru(bpy)_2(5HT)_2]^{2+}$, both BHQ-caged 5-HTs demonstrated superior $Q_u$ and

sensitivity to light ($Q_u \times \varepsilon$) at biologically compatible wavelengths. The sensitivity of the NPE-protected 5-HTs was not explicitly reported (Boahen and MacDonald, 2005), but the sensitivity of a related compound, NPE-protected phenylephrine, is 682 at 272 nm ( Walker et al., 1993), a shorter wavelength not well suited for biological experiments. The absorbance spectrum of NPE-caged ATP drops precipitously as the wavelength increases (Kaplan et al., 1978), indicating that NPE-protected 5-HTs also have low sensitivity at $\lambda > 300$ nm. BHQ-*O*-5HT was found to be the most sensitive of all seven caged 5-HTs at 368 nm. Both BHQ-protected 5-HTs were stable in the dark in buffered aqueous media. The $\delta_u$ values were not reported for the CNB-, NPE-, and $Ru(bpy)_2$-protected 5-HTs, but the CNB and NPE groups are not considered sensitive to 2PE ($\delta_u \leq$ 0.04 GM) (Dore, 2005, Dore and Wilson, 2011, Kiskin et al., 2002 and Warther et al., 2010), and other conjugates of $Ru(bpy)_2$ are only slightly more sensitive ($\delta_u$ = 0.01–0.14 GM) (Nikolenko et al., 2005 and Salierno et al., 2010). The $\delta_u$ values of BHQ-*O*-5HT and BHQ-*N*-5HT were at least an order of magnitude larger than CNB- and NPE-protected 5-HT at 740 nm and sufficiently sensitive for use in biological systems. The time course for 2PE is in minutes because the excitation volume is smaller than the sample size, and more time is required for a sufficient amount of starting material to be photolyzed to detectable levels.

BHQ-*N*-5HT might be less useful in applications using 2PE or activating the ionotrophic 5-HT receptors, because release of 5-HT from BHQ-*N*-5HT upon light exposure is slow. Initially formed carbamic acid intermediates typically decompose to $CO_2$ and the amine on a 6–7 ms timescale (Papageorgiou and Corrie, 1997), a timescale that is slower than the diffusional escape time from the focal volume of 2PE excitation

(estimated at 113–900 μs; Kiskin and Ogden, 2002) and the opening of ionotrophic 5-HT-gated ion channels (5-$HT_3$ receptors open on the order of 1–2 ms timescales and remain open for up to 10 ms; Jackson and Yakel, 1995). Time-resolved studies on BHQ-caged acetate (Ma et al., 2012) suggest that BHQ-*O*-5HT releases 5-HT on nanosecond timescales—orders of magnitude shorter than diffusional timescales.

To test the biological effects of BHQ-*O*-5HT on neural activity, extracellular recordings were obtained from dissociated sensory neurons prepared from mouse dorsal root ganglia (DRGs) and the trigeminal ganglion or optic tectum in intact zebrafish larva during exposure to 5-HT, BHQ-*O*-5HT, or 8-bromo-2-(hydroxymethyl)quinolin-7-ol (BHQ-OH). Previous studies have shown that 5-HT elicits depolarizing responses in small-diameter trigeminal ganglion neurons in mammals and type A and C primary afferent neurons in the DRGs of mammals and frogs (Holz and Anderson, 1984, Holz et al., 1985, Todorović and Anderson, 1990 and Tsutsui et al., 2008). 5-HT is also known to increase a hyperpolarization-activated cation current in type Aα and Aβ DRG neurons (Cardenas et al., 1999, Harper and Lawson, 1985a, Harper and Lawson, 1985b, Scroggs et al., 1994 and Villière and McLachlan, 1996). Figure A.5 depicts the results for DRG neurons. For these experiments, recordings were obtained from DRG neurons with soma 19 ± 2 μm in diameter (Figure A.5A) that are largely nociceptive afferent (C and Aδ) neurons, but they can include Aα/Aβ neurons (Harper and Lawson, 1985a, Harper and Lawson, 1985b and Lawson and Waddell, 1991). Therefore, neurons were first tested for a response to 100 μM 5-HT, and then the same neurons were exposed to 500 μM BHQ-*O*-5HT or BHQ-OH (Figure A.3), a control to test for the effects of the caging group. All compounds were administered by pressure ejection of 1 nl of solution from a

micropipette, the tip of which was located 90–110 μm from the neuron cell body to minimize potential artifacts associated with the pressure ejection. Cells were exposed to a 1 ms pulse of 365 nm light 10 s after application of the compound. In all cases, pressure ejection of BHQ-*O*-5HT induced small changes in baseline activity DRG neurons that were likely due to small amounts of uncaged 5-HT in the solution; however, activity comparable to uncaged 5-HT was observed only after exposure to a 1 ms pulse of 365 nm light (compare Figure A.5B to Figure A.5C). For DRG neurons of this size class, application of 5-HT resulted in a negative extracellular potential (i.e., depolarization) in 26/34 neurons tested and a positive potential (i.e., hyperpolarization-activated cation current) in 8/34 neurons tested. In 17 cases, where there were multiple cells in the field, biphasic responses were recorded. 5-HT and uncaged BHQ-*O*-5HT elicited the same effect for any given neuron. Application of the caged compound and uncaging could be performed repeatedly on the same neuron under perfusion conditions. No significant change in neuronal activity was observed after ejection of solvent (Ringer's solution with 1% DMSO) or BHQ-OH, or upon exposure to 1PE in the absence of BHQ-*O*-5HT (Figure A.5B and data not shown). Together, these results demonstrated that BHQ-*O*-5HT could be used to modulate the activity of mammalian neurons in culture. A cell viability assay (Freshney, 1987) showed no statistical difference (t test, $p < 0.01$) in the percentage of dying cells between BHQ-*O*-5HT-treated and untreated control cultures, suggesting that mammalian neurons in culture tolerate BHQ-*O*-5HT well.

Figure A.6 depicts the results of using BHQ-*O*-5HT to control neural activity in vivo. For these experiments, zebrafish larvae were immobilized in agar at 5 days postfertilization (dpf), and solutions containing 5-HT (100 μM), BHQ-*O*-5HT (1 mM), or

BHQ-OH (1 mM) dissolved in Ringer's solution containing 1% DMSO were microinjected in the vicinity of the maxillary nerve (Figure A.6A). Electrical activity was monitored with a field electrode placed under visual guidance on the ventral aspect of the trigeminal ganglion (Figure A.6A). This placement also likely detects electrical activity from the anterodorsal lateral line ganglion (Raible and Kruse, 2000). Whereas injection of 5-HT typically induced a characteristic change in the electrographic activity (n = 6/7), injection of BHQ-*O*-5HT did not significantly affect baseline activity until after photolysis using 365 nm light (n = 6/6). In some experiments, a short-lived electrographic response was observed immediately after injection of BHQ-*O*-5HT but before exposure to light, suggesting that a small amount of 5-HT was released during handling or injection; however, in these cases, exposure to light also resulted in a significant electrographic response, indicating that the majority of the compound had remained in a caged state. In these experiments, repeated exposure to light resulted in repeated induction of neural activity (Figure A.6C) for up to ten trials; however, as expected, the amount of activity began to diminish with time and the number of exposures to light. This suggests that enough caged compound remained after illumination to permit repeated stimulation experiments in intact preparations. No change in baseline activity was observed after injection with BHQ-OH or by exposing the larva to flashes of light in the absence of BHQ-*O*-5HT. Comparable results were obtained for experiments directed toward the optic tectum (Figure A.S2). We observed no mortality resulting from injection or an obvious increase in cell death in the vicinity of the injection site (n = 47) during the course of the experiments, indicating that the zebrafish tolerate BHQ-*O*-5HT.

Because 5-HT signaling is required for LR patterning in *X. laevis* embryos (Fukumoto et al., 2005a,Fukumoto et al., 2005b and Vandenberg et al., 2013), we used this endpoint and animal model to assay the physiological action of caged 5-HT molecules. To test the effects of BHQ-*O*-5HT on LR patterning, embryos were soaked in BHQ-*O*-5HT (1 mM) from the one-cell through 32-cell stage (stage 5), washed, and then both the top and bottom of the embryos were exposed to light for 1 hr using a broad-spectrum lamp to uncage 5-HT. LR patterning was assessed at stage 45 via inspection of three asymmetric organs: the heart, stomach, and gall bladder (Figure A.7A). In contrast to embryos soaked in 5-HT, no LR patterning defects were observed, indicating that BHQ-*O*-5HT does not penetrate the cell membrane of the *Xenopus* embryo and is not taken up via the serotonin transporter (Figure A.7B). Additional embryos were injected with BHQ-*O*-5HT at the one-cell stage, and 5-HT was uncaged starting at the 16-cell stage using the broad-spectrum lamp. LR defects including situs inversus and heterotaxia were observed in BHQ-*O*-5HT-injected embryos after uncaging with a similar percentage of affected embryos as those observed when 5-HT is injected (Figure A.7C). A low rate of LR defects was also observed in embryos injected with BHQ-*O*-5HT that were maintained in the dark throughout the experiment, suggesting that a small amount of 5-HT is released during handling, injection, or incubation. To verify temporal control of BHQ-*O*-5HT uncaging, embryos were injected at the one-cell stage and then maintained in the dark until two later stages of development: 32-cell stage (stage 5) and early blastula (stage 8). Significant increases in LR patterning defects were observed only when uncaging occurred at stage 5 (Figure A.7D).

Under all conditions, BHQ-*O*-5HT produced very low levels of toxicity, including few dead or deformed embryos or tadpoles. In experiments where embryos were soaked in BHQ-*O*-5HT, toxicity rates were 5%–6% either when maintained in the dark or uncaged, rates that were similar to the rates observed in untreated controls (7%, $p > 0.05$). Likewise, when BHQ-*O*-5HT was injected, low toxicity (4%–12%) was observed whether maintained in the dark or uncaged, similarly to rates observed in controls (5%–7%, $p > 0.05$). Injections with BHQ-OH produced few LR patterning defects (2%–3%, see Figure A.7D) and little toxicity (4%–6% compared with 5% in untreated controls, $p > 0.05$). Soaking and injection experiments were also conducted with BHQ-*N*-5HT, but uncaging this molecule did not disrupt LR patterning in any experiment, regardless of which treatment route was used (data not shown). This might be due to the inability of light to penetrate the pigment in early cleavage stage embryos with enough intensity to release 5-HT from BHQ-*N*-5HT.

Significance

Based on the ability of the BHQ protecting group to photochemically release phenol through both 1PE and 2PE, the two forms of caged 5-HT prepared, BHQ-***O***-5HT and BHQ-***N***-5HT, have higher ***Q***uand δuvalues than previously reported caged 5-HTs. BHQ-***O***-5HT was found to be more sensitive to light at 368 and 740 nm than BHQ-***N***-5HT, and based on the behavior of similar compounds (Ma et al., 2012), its release kinetics is expected to be faster than diffusion rates and the opening of 5-HT3receptors. BHQ-***O***-5HT mediated the light activation of 5-HT, subsequently depolarizing mammalian neurons in culture or in the nervous system of intact larval zebrafish (5–7

dpf). In the developing *Xenopus* embryo, light-induced release of 5-HT disrupted LR patterning maximally at stage 5 of development.

Taken together, these experiments demonstrate the potential of BHQ-caged 5-HT to enable the advanced study of 5-HT's physiological role in a variety of biological contexts, whole animal studies in particular. For example, BHQ-caged 5-HT could enable the exploration of mechanisms involved in the propagation of coherent neural activity (i.e., seizures) in the brain, potentially impacting our understanding of epilepsy and other seizure disorders. More broadly, BHQ-caged 5-HT could be used to explore the role of 5-HT in modulating mood, appetite, memory, learning, and other cognitive functions. In addition, 5-HT has been shown to play important roles in early developmental patterning events outside of neural tissue, such as LR patterning and melanocyte differentiation. Thus, BHQ-caged 5-HT, which can be manipulated both spatially and temporally, provides significant experimental power to dissect and understand the mechanisms behind 5-HT-mediated signaling in the developing embryo. The BHQ-caged serotonins are relatively nontoxic, have relatively little leakage, and can be released using standard laboratory equipment, enabling biologists to better probe the role of 5-HT signaling pathways in the brain and in early developmental processes.

## Experimental Procedures

### *Preparation of BHQ-OPh*

#### *(8-bromo-7-(methoxymethoxy)quinolin-2-yl)methyl Methanesulfonate*

To prepare (8-bromo-7-(methoxymethoxy)quinolin-2-yl)methyl methanesulfonate (MOM-BHQ-OMs), MOM-BHQ-OH (0.526 g, 1.76 mmol) was dissolved in

tetrahydrofuran (THF). Ethyldiisopropylamine (0.61 ml, 3.52 mmol) and methanesulfonyl chloride (0.20 ml, 2.64 mmol) were successively added dropwise, followed by stirring at room temperature (RT) for 2 hr. The reaction was concentrated, and the residue was purified over silica gel with a gradient from 100% hexanes to 2:3 ethyl acetate (EtOAc)/hexanes, collecting the product as a white solid (0.446 g, 68%): $^{1}$H nuclear magnetic resonance ($^{1}$H NMR) (400 MHz, $CDCl_3$) δ 8.19 (d, 1H), 7.79 (d, 1H), 7.55 (d, 1H), 7.52 (d, 1H), 5.57 (s, 2H), 5.43 (s, 2H), 3.58 (s, 3H), 3.23 (s, 3H); $^{13}$C NMR (101 MHz, $CDCl_3$) δ 155.8, 155.7, 146.1, 137.9, 128.2, 124.9, 118.7, 118.0, 112.5, 95.6, 72.4, 56.9, 38.7; high-resolution mass spectrometry-electrospray ionization (HRMS-ESI) (*m*/*z*) calcd for $[M+H]^+$ 375.9849, 377.9828; found 375.9846, 377.9825.

*8-bromo-7-(methoxymethoxy)-2-(phenoxymethyl)quinoline*

To prepare 8-bromo-7-(methoxymethoxy)-2-(phenoxymethyl)quinoline (MOM-BHQ-OPh), MOM-BHQ-OMs (0.035 g, 0.093 mmol) was dissolved in THF (2 ml). Phenol (0.016 g, 0.17 mmol) was added, followed by 1 M potassium hydroxide solution (170 µl), and the reaction was stirred at RT for 12 hr. The solvent was removed on a rotary evaporator, and the remaining residue was taken up in EtOAc that was washed successively with water and brine. The EtOAc was removed on a rotary evaporator, and the remaining residue was purified by column chromatography with 9:1 hexanes/EtOAc. Fractions were collected and concentrated to yield a residue on the flask wall (0.025 g, 0.067 mmol, 72%): $^{1}$H NMR (400 MHz, $CDCl_3$) δ 8.13 (d, $J$ = 8.2 Hz, 1H), 7.75 (d, $J$ = 9.0 Hz, 1H), 7.65 (d, $J$ = 8.2 Hz, 1H), 7.50 (d, $J$ = 9.0 Hz, 1H), 7.30 (m, 2H), 7.05 (d, $J$ = 7.8 Hz, 2H), 6.97 (t, $J$ = 7.4 Hz, 1H), 5.46 (s, 2H), 5.42 (s, 2H), 3.59 (s, 3H); $^{13}$C NMR (101 MHz, $CDCl_3$) δ 160.0, 158.6, 155.4, 146.0, 137.3, 129.8, 128.2, 124.7, 121.4, 118.3,

117.4, 115.110,112.3, 95.6, 71.4, 56.9; HRMS-ESI (*m*/*z*) calcd for $[M+H]^+$ 374.0386, 376.0366; found 374.0401, 376.0382.

*BHQ-OPh*

MOM-BHQ-OPh (0.025 g, 0.067 mmol) was dissolved in $CH_3OH$ (1 ml). TFA (0.5 ml) was added, and the reaction was stirred for 30 min. The solvent was evaporated, and the remaining residue was taken up in EtOAc, washed successively with water and brine, and concentrated. The remaining residue was purified by column chromatography with 8:2 hexanes/EtOAc. Fractions were collected and concentrated to yield a residue on the flask wall: $^1$H NMR (400 MHz, $CDCl_3$) δ 8.11 (d, *J* = 8.6 Hz, 1H), 7.71 (d, *J* = 8.6 Hz, 1H), 7.61 (d, *J* = 8.6 Hz, 1H), 7.31 (m, 3H), 7.04 (d, *J* = 7.8 Hz, 2H), 6.98 (t, *J* = 7.4 Hz, 1H), 5.35 (s, 2H); $^{13}$C NMR (101 MHz, $CDCl_3$) δ 159.8, 158.6, 154.4, 145.5, 137.4, 129.8, 128.6, 123.9, 121.4, 117.9, 117.7, 115.1, 108.0, 71.3; HRMS-ESI (*m*/*z*) calcd for $[M+H]^+$ 330.0124, 332.0104; found 330.0136, 332.0123.

***Preparation of BHQ-N-5HT***

(8-bromo-7-(methoxymethoxy)quinolin-2-yl)methyl 1*H*-imidazole-1-carboxylate To prepare (8-bromo-7-(methoxymethoxy)quinolin-2-yl)methyl 1*H*-imidazole-1-carboxylate (MOM-BHQ-carbonylimidazole), MOM-BHQ-OH (0.100 g, 0.34 mmol) was dissolved in THF. Carbonyldiimidazole (0.082 g, 0.50 mmol) was added, and the reaction stirred at RT for 2 hr. The reaction was concentrated, and the residue was dissolved in EtOAc, washed successively with water and brine, dried over $MgSO_4$, filtered, and concentrated in vacuo. The crude product was purified by column chromatography with silica gel, eluting with a gradient from 1:1 EtOAc/hexanes to 100% EtOAc, yielding a white solid (0.084 g, 63%):$^1$H NMR (400 MHz, $CDCl_3$) δ 8.28 (s, 1H),

8.14 (d, $J$ = 8.4 Hz, 1H), 7.74 (d, $J$ = 9.0 Hz, 1H), 7.55 (s, 1H), 7.50 (d, $J$ = 9.0 Hz, 1H), 7.39 (d, $J$ = 8.4 Hz, 1H), 7.11 (s, 1H), 5.75 (s, 2H), 5.39 (s, 2H), 3.56 (s, 3H); $^{13}$C NMR (101 MHz, $CDCl_3$) δ 155.8, 155.4, 148.9, 146.1, 137.6, 137.6, 131.0, 128.0, 124.7, 118.0, 117.7, 117.6, 112.6, 95.6, 69.9, 56.8; HRMS-ESI (*m*/*z*) calcd for $[M+H]^+$ 392.0246, 394.0225; found 392.0262, 394.0244.

*(8-bromo-7-(methoxymethoxy)quinolin-2-yl)methyl (2-(5-((triisopropylsilyl)oxy)-1H-indol-3-yl)ethyl)carbamate*

To prepare (8-bromo-7-(methoxymethoxy)quinolin-2-yl)methyl (2-(5-((triisopropylsilyl)oxy)-1*H*-indol-3-yl)ethyl)carbamate [MOM-BHQ-*N*-5HT(*O*-TIPS)], 5HT(*O*-TIPS) (0.067 g, 0.020 mmol) was dissolved in a small amount of *N*,*N*-dimethylformamide (DMF). MOM-BHQ-carbonylimidazole (0.100 g, 0.25 mmol) was added, and the reaction was heated to 60°C and stirred overnight. The solvent was removed in vacuo, and the residue was partitioned between EtOAc and water. The EtOAc layer was dried over $MgSO_4$, filtered, and concentrated in vacuo. The crude product was purified by column chromatography with silica gel, eluting with a gradient from 100% hexanes to 1:1 EtOAc/hexanes, yielding the product as a solid (0.0859 g, 65%): $^1$H NMR (400 MHz, $CDCl_3$) δ 8.07 (d, $J$ = 8.4 Hz, 1H), 7.95 (s, 1H), 7.72 (d, $J$ = 9.0 Hz, 1H), 7.48 (d,$J$ = 9.0 Hz, 1H), 7.36 (d, $J$ = 8.4 Hz, 1H), 7.18 (d, $J$ = 8.7 Hz, 1H), 7.04 (s, 1H), 7.00 (s, 1H), 6.81 (d, $J$ = 8.7 Hz, 1H), 5.44 (s, 2H), 5.40 (s, 2H), 5.02 (br, 1H), 3.58 (t, $J$ = 6.6 Hz, 2H), 3.57 (s, 3H), 2.95 (t, $J$ = 6.6 Hz, 2H), 1.26 (m, $J$ = 7.3 Hz, 3H), 1.11 (d, $J$ = 7.3 Hz, 18H); $^{13}$C NMR (126 MHz, $CDCl_3$) δ 158.8, 156.2, 155.2, 149.7, 145.8, 137.0, 131.8, 127.9, 127.8, 124.4, 122.9, 118.1, 117.2, 116.3, 112.3, 111.4, 107.8, 95.4, 77.2,

67.5, 56.6, 41.2, 25.7, 18.1, 12.7; HRMS-ESI (*m*/*z*) calcd for $[M+H]^+$ 656.2155, 658.2135; found 656.2171, 658.2154.

*(8-bromo-7-(methoxymethoxy)quinolin-2-yl)methyl (2-(5-hydroxy-1H-indol-3-yl)ethyl)carbamate*

To prepare (8-bromo-7-(methoxymethoxy)quinolin-2-yl)methyl (2-(5-hydroxy-1*H*-indol-3-yl)ethyl)carbamate (MOM-BHQ-*N*-5HT), MOM-BHQ-*N*-5HT(*O*-TIPS) (85.9 mg, 0.13 mmol) was dissolved in a small amount of THF. TBAF (0.2 ml, 1.0 M in THF) was added slowly, and the reaction stirred at RT for 15 min. The reaction was concentrated, and the residue was partitioned between EtOAc and water. The organic layer was washed with water and brine, dried over anhydrous $MgSO_4$, filtered, and concentrated in vacuo. The crude product was purified by column chromatography with silica gel, eluting with a gradient from 100% hexanes to 1:1 EtOAc/hexanes, yielding the product as a solid (55 mg, 85%): $^1$H NMR (400 MHz, $CDCl_3$) δ 8.06 (s, 1H), 8.02 (d, *J* = 8.3 Hz, 1H), 7.97 (d, *J* = 9.1 Hz, 1H), 7.67 (d, *J* = 9.0 Hz, 1H), 7.45 (d, *J* = 9.1 Hz, 1H), 7.31 (d, *J* = 8.5 Hz, 1H), 7.13 (d, *J* = 8.6 Hz, 1H), 6.96 (d, *J* = 13.2 Hz, 1H), 6.74 (dd, *J* = 9.1, 14.4 Hz, 1H), 5.41 (s, 2H), 5.38 (s, 2H), 5.18 (br, 1H), 3.56 (s, 3H), 3.48 (q, *J* = 6.6 Hz, 2H), 2.92 (d, *J* = 26.8 Hz, 1H), 2.84 (t, *J* = 6.8 Hz, 2H); $^{13}$C NMR (101 MHz, $CDCl_3$) δ 158.8, 156.7, 155.5, 149.8, 145.9, 137.4, 131.8, 128.1,126.2, 124.6, 123.4, 118.3, 117.5, 115.8, 112.3, 112.1, 103.2, 103.3, 95.6, 67.7, 56.9, 41.6, 26.0; HRMS-ESI (*m*/*z*) calcd for $[M+H]^+$ 500.0821, 502.0801; found 500.0823, 502.0810.

*BHQ-N-5HT*

MOM-BHQ-*N*-5HT (45 mg, 0.090 mmol) was dissolved in $CH_3OH$. A small amount of concentrated HCl was added, and the reaction was stirred overnight. The

reaction was diluted with EtOAc and washed successively with saturated $NaHCO_3$ and brine, dried over anhydrous $MgSO_4$, filtered, and concentrated in vacuo. The crude product was purified by HPLC with 50% $CH_3CN$/50% $H_2O$ (with 0.1% TFA) and the first peak (retention time 4.5 min) was collected and concentrated (22.5 mg, 55%): $^1$H NMR [500 MHz, $(CD_3)_2CO$] δ 9.63 (br, 1H), 8.11 (d, *J* = 8.3 Hz, 1H), 7.68 (d, *J* = 8.8 Hz, 1H), 7.26 (t, *J* = 8.3 Hz, 2H), 7.23 (d,*J* = 8.8 Hz, 1H), 7.07 (d, *J* = 8.6 Hz, 1H), 6.98 (s, 1H), 6.88 (s, 1H), 6.57 (d, *J* = 8.6 Hz, 1H), 6.48 (br, 1H), 5.22 (s, 2H), 3.34 (t, *J* = 7.3 Hz, 2H), 2.79 (t, *J* = 7.3 Hz, 2H); $^{13}$C NMR (101 MHz, $(CD_3)_2CO$) δ 159.1, 156.2, 155.8, 150.7, 145.9, 137.1, 131.6, 128.5, 128.1, 127.6, 123.2, 118.6, 116.8, 111.6, 111.5, 106.9, 102.6, 66.8, 41.6, 29.7, 25.9; HRMS-ESI (*m*/*z*) calcd for $[M+H]^+$ 456.0559, 458.0538; found 456.0574, 458.0567.

***Preparation of BHQ-O-5HT***

*MOM-BHQ-O-5HT(N-Boc)*

*N*-Boc-5HT (97 mg, 0.35 mmol) was dissolved in $CH_3CN$, and potassium carbonate (86 mg, 0.62 mmol) was added. MOM-BHQ-OMs (188 mg, 0.50 mmol) was added in one portion, and the reaction was stirred at reflux for 2 days. The reaction was allowed to cool and then filtered and concentrated. The residue was purified by column chromatography with silica gel, eluting with a gradient from 100% hexanes to 3:1 EtOAc/hexanes, yielding a yellow oil (151 mg, 78%): $^1$H NMR (400 MHz, $CDCl_3$) δ 8.14 (d, *J* = 8.4 Hz, 1H), 7.97 (s, 1H), 7.76 (d, *J* = 9.0 Hz, 1H), 7.74 (d, *J* = 8.4 Hz, 1H), 7.50 (d, *J* = 9.0 Hz, 1H), 7.23 (s, 1H), 7.02 (m, 2H), 5.50 (s, 2H), 5.42 (s, 2H), 3.59 (s, 3H), 3.42 (t, *J* = 6.5 Hz, 2H), 2.90 (t, *J* = 6.5 Hz, 2H), 1.43 (s, 9H); $^{13}$C NMR (101 MHz, $CDCl_3$) δ 170.7, 161.2, 161.1, 160.6, 156.1, 155.3, 153.0, 146.0, 137.2, 131.9, 128.2,

124.7, 118.5, 117.3, 112.8, 112.1, 103.5, 102.6, 95.6, 77.4, 72.2, 56.9, 40.8, 28.7, 26.0; HRMS-ESI (*m*/*z*) calcd for $[M+H]^+$ 556.1447, 558.1427; found 556.1432, 558.1420.

*BHQ-O-5HT*

MOM-BHQ-*O*-5HT(*N*-Boc) (0.047 g, 0.085 mmol) was dissolved in $CH_2Cl_2$. Trifluoroacetic acid was added, and the reaction stirred at RT for 1 hr. The solvent was removed in vacuo, and the residue was purified by HPLC with 50% $CH_3CN$/50% $H_2O$ (with 0.1% TFA). Fractions containing only one peak were combined and concentrated (0.020 g, 57%): $^1$H NMR (600 MHz, $CD_3OD$) δ 8.29 (d, *J* = 8.4 Hz, 1H), 7.80 (d, *J* = 8.8 Hz, 1H), 7.67 (d, *J* = 8.3 Hz, 1H), 7.31 (d, *J* = 7.6 Hz, 1H), 7.30 (d, *J* = 8.8 Hz, 1H), 7.24 (d, *J* = 2.1 Hz, 1H), 7.15 (s, 1H), 6.98 (dd, *J* = 8.8, 2.2 Hz, 1H), 5.46 (s, 2H), 3.20 (m, 2H), 3.06 (t, *J* = 7.3 Hz, 2H); $^{13}$C NMR (150 MHz, $CD_3OD$) δ 162.2, 161.8, 151.6, 147.5, 138.9, 133.3, 131.5, 129.0, 125.3, 125.2, 122.2, 117.6, 113.1, 112.9, 109.6, 103.3, 98.9, 61.6, 41.2, 24.7; HRMS-ESI (*m*/*z*) calcd for $[M+H]^+$ 412.0661, 414.0640; found 412.0651, 414.0626.

$^1$H NMR spectra for all compounds and an HPLC chromatogram for BHQ-*O*-5HT demonstrating purity are provided in the Supplemental Information.

***Photochemistry***

*Determination of ε*

A weighed portion of BHQ-*O*-5HT was dissolved in $CH_3OH$. A measured aliquot of this solution was withdrawn and placed in KMOPS buffer (3.0 ml) and mixed thoroughly to generate a 100 μM solution of BHQ-*O*-5HT. The absorbance (A) of this solution at $\lambda_{max}$ = 368 nm was measured. This method was repeated twice with different

masses of BHQ-*O*-5HT. The three absorbance values obtained were averaged, and the molar extinction coefficient (ε) value at $\lambda_{max}$ = 368 nm was calculated to be 2,000 $M^{-1}$ $cm^{-1}$ using the equation A = εlc, where A is the absorbance, l is the path length of the cuvette, and c is the concentration of the solution. The ε value of BHQ-OPh and BHQ-*N*-5HT was measured similarly. See Figure A.S3 for representative UV-visible (vis) spectra of BHQ-OPh, BHQ-*N*-5HT, and BHQ-*O*-5HT.

*Determination of* $\tau_{dark}$

Three 100 μM solutions of BHQ-*O*-5HT in KMOPS were created and stored in the dark. Aliquots (20 μl) were removed periodically from each solution and analyzed by HPLC. The concentration of BHQ-*O*-5HT (measured by external standard) for each time point for each solution was averaged and plotted versus time. A simple single exponential decay curve provided the best fit and was used to determine the $\tau_{dark}$value. The $\tau_{dark}$ value of BHQ-OPh and BHQ-*N*-5HT was measured similarly.

*Determination of the Uncaging* $Q_u$

As described previously (Adams et al., 1988, Davis et al., 2009, Fedoryak and Dore, 2002, Furuta et al., 1999, Lu et al., 2003 and Zhu et al., 2006), the $Q_u$ value was calculated using the equation $Q_u = (I\sigma t_{90\%})^{-1}$, where $I$ is the irradiation intensity in einstein·$cm^{-2}$·$s^{-1}$, σ is the decadic extinction coefficient (1,000 times ε), and $t_{90\%}$ is the time in seconds required for the conversion of 90% of the starting material to product. To find$t_{90\%}$, a solution of BHQ-*O*-5HT in KMOPS was prepared and placed in a cuvette along with a small stir bar. While stirring, the solution was irradiated with UV light from a mercury lamp (Spectroline SB-100P, Spectronics) equipped with two glass filters (CS0-52, CS7-60, Ace Glass) so that the wavelength was restricted to 365 ± 15 nm.

Periodically, 20 µl aliquots were removed and analyzed by HPLC. The time points collected were as follows: 0, 20, 40, 60, 90, and 120 s. The concentration of BHQ-*O*-5HT remaining (measured by external standard) was plotted versus time of photolysis. A simple single exponential decay curve provided the best fit for the data and was used to extrapolate $t_{90\%}$. The lamp's $I$ value was measured using potassium ferrioxalate actinometry ( Hatchard and Parker, 1956). Initially, 6 mM potassium ferrioxalate solution (3 ml) was irradiated with the mercury lamp for 60 s. A portion of this solution (2 ml) was combined with aqueous buffer (3 ml), 0.1% phenanthroline solution (3 ml), and 2 M KF solution (1 m) in a 25 ml volumetric flask. Deionized water was added to generate a 25 ml solution. A blank solution was also prepared using the same method, but the potassium ferrioxalate used in the blank was not irradiated. Both solutions rested for 1 hr, and the blank was then used as a baseline against which the absorbance of the irradiated solution was measured at 510 nm. The following equation was used to calculate lamp intensity:

$$I = \frac{V_3 \Delta D_{510}}{1{,}000 \varepsilon_{510} V_2 \phi_{Fe} t},$$

where $V_3$ is the volume of dilution (25 ml), $V_2$ is the volume of irradiated potassium ferrioxalate solution taken for analysis (2 ml), $\Delta D_{510}$ is the absorption of the solution at 510 nm, $\varepsilon_{510}$ is the actinometry extinction coefficient ($1.11 \times 10^4$ $M^{-1}$ $cm^{-1}$), $\phi Fe$ is the quantum yield for production of ferrous ions from potassium ferrioxalate at 365 nm, and $t$ represents the time of irradiation. The $\Delta D_{510}$ value used for calculations is the average of two measurements taken before and after irradiation of BHQ-*O*-5HT. The$Q_u$ of BHQ-OPh and BHQ-*N*-5HT was measured similarly.

*Determination of $\delta_u$*

The $\delta_u$ values were measured using previously described methods (Davis et al., 2009, Fedoryak and Dore, 2002, Furuta et al., 1999, Lu et al., 2003 and Zhu et al., 2006) using fluorescein as an external standard to estimate the pulse parameters of the laser. A portion of BHQ-*O*-5HT was dissolved in KMOPS buffer, and the concentration of the solution was found using UV-vis absorption in conjunction with Beer's law. Aliquots (25 µl) of this solution were placed in a microcuvette (10 × 1 × 1 mm illuminated dimensions) and irradiated with an fs-pulsed and mode-locked Ti:sapphire laser with 740 nm light at an average power of 300 mW. Three samples were irradiated for each of the following time periods: 0, 10, 20, 30, and 40 min. The samples (20 µl aliquots) were analyzed by HPLC as in the $Q_u$ measurement to determine the extent of photolysis at each time point. A solution of fluorescein at pH 9.0 was prepared to act as a standard because of its well-characterized $\delta_u$ ($\delta_{aF}$ = 30 GM at 740 nm) and quantum yield ($Q_{F2}$ = 0.9). UV-vis absorption at 488 nm was used to determine the fluorescein concentration. Aliquots (25 µl) of fluorescein solution were placed in the microcuvette and irradiated by the laser in the same apparatus used for the BHQ-*O*-5HT photolysis. The fluorescence emission from the solution was measured with a radiometer (SED033 detector on an IL-1700, International Light) before and after the BHQ-*O*-5HT samples were irradiated, and the two values were averaged. The following equation was used to calculate the $\delta_u$ value for BHQ-*O*-5HT:

$$\delta_u = \frac{N_p \phi Q_{F2} \delta_{aF} C_F}{\langle F(t) \rangle C_S},$$

where *Np* is the number of product molecules formed per second (determined by HPLC), $\phi$ is the collection efficiency of the detector on the radiometer used to measure the

fluorescence of fluorescein passing through the cuvette window and through a 535/545 nm bandpass filter at a right angle to the laser's beam, *CF* is the concentration of fluorescein, $\langle F(t) \rangle$ is the time-averaged fluorescent photon flux (photons per second) of fluorescein measured by the radiometer, and *CS* is the initial concentration of the caged compound. The $\delta_u$ value of BHQ-OPh and BHQ-*N*-5HT was measured similarly.

### *Electrophysiological Recordings*

#### *DRG Neurons*

Dissociated primary sensory neurons were prepared from mouse DRGs as described previously (Malin et al., 2007), and plated on lysine/laminin-coated coverslips. For extracellular recordings, the slips with cells were mounted in a horizontal perfusion chamber (PC-H, Siskiyou) with a chloride-coated silver reference electrode attached, and then placed on the stage of an upright microscope (Examiner.Z1, Zeiss). Solutions of 5-HT (100 μM), BHQ-*O*-5HT (500 μM), or BHQ-OH (500 μM) in normal Ringer's solution containing 1% DMSO were delivered focally to the desired cell by pressure ejection (Picospritzer II, Parker Hannifin) of 1 nl volumes from a fine-tipped glass micropipette, the tip of which was placed 100 ± 10 μm from the cell of interest. Flash photolysis was achieved using a Cairn Flash Photolysis System and OptoSource xenon and mercury/xenon mixed-gas arc light source (Cairn Research) equipped with a 365/10 nm bandpass filter (Chroma) and coupled by a fiber optic cable to the Examiner.Z1 microscope through the external port of a Colibri illumination system. Light was focused on the cells of interest using the microscope optics and water immersion lenses (20×, 40×, or 63×) with UV transmission properties. Extracellular recordings were

made using glass microelectrodes (15–20 MΩ impedance) loaded with normal Ringer's solution (116 mM NaCl, 2.9 mM KCl, 1.8 mM $CaCl_2$, 5.0 mM HEPES [pH 7.2]) that were gently affixed to the soma by suction. Electrical activity was recorded using an Axoclamp 900a amplifier (Axon Instruments). The amplified voltage was passed through a Hum Bug Noise Eliminator (AutoMate Scientific), bandpass-filtered from 1 Hz to 0.1 kHz, and digitized at 10 kHz using a Digidata 1440 interface and stored on a PC using pClamp version 10.3 software (Axon Instruments). For all experiments, the set-up procedure was carried out in dark room conditions at RT (23°C).

*Assessment of Toxicity*

The DRG neurons in culture were exposed to BHQ-*O*-5HT (1 mM) followed by incubation in the dark for 8–12 hr. Viable cell counts were made using trypan blue, a dye that is excluded from living cells (Freshney, 1987). The percentage of dead cells was determined by dividing the number of trypan blue-stained cells by the total number of cells on a 22 × 22 mm coverslip.

*Larval Zebrafish*

Larval zebrafish of the WIK strain were obtained from animals maintained in the University of Georgia Zebrafish Facility following standard procedures (Westerfield, 2007). Embryos and larvae were staged using standard staging criteria (Kimmel et al., 1995 and Westerfield, 2007). All experiments conformed to the guidelines on the ethical use of animals. All experimental procedures were conducted according to National Institutes of Health guidelines under protocols approved by the University of Georgia

Institutional Animal Care and Use Committee and were designed to minimize animal suffering.

Larval zebrafish, 5 dpf, were immobilized by exposure to alpha bungarotoxin (Trapani and Nicolson, 2010) and mounted in 1.2% agarose made with normal Ringer's solution in a 35 mm petri dish. A sharp glass microelectrode (15–20 MΩ impedance), loaded with normal Ringer's solution, was placed under visual guidance on the ventral aspect of the trigeminal ganglion, and the chloride-coated silver reference wire was placed was placed touching a dorsal region of the tail. For drug delivery, a second sharp glass pipette was inserted in the vicinity of the maxillary nerve. After a 2 min baseline was recorded, 0.5 nl of 5-HT (100 μM), BHQ-*O*-5HT (1 mM), or BHQ-OH (1 mM) dissolved in Ringer's solution containing 1% DMSO was pressure injected (Picospritzer II), and the neurological responses were recorded. Flash photolysis was achieved, and electrical activity was recorded as described above. As with the DRG experiments, these experiments were carried out under dark room conditions and at RT.

*Assessment of Toxicity*

The mortality of the zebrafish larvae after injection of BHQ-*O*-5HT into the trigeminal nerve or the optic tectum was used as a measure of the toxicity of BHQ-*O*-5HT. Cell death at the injection site was assessed by differential interference contrast microscopy, acridine orange staining, or both.

***In Vivo Assay of LR Patterning in X. laevis Embryos***

*Animals*

*Xenopus* embryos were collected and fertilized according to standard protocols ( Sive et al., 2000) in 0.1× modified Marc's Ringer (MMR) at pH 7.8 containing 0.1%

gentamicin and staged according to Nieuwkoop and Faber (1967). This study was carried out in strict accordance with the recommendations in the Guide for the Care and Use of Laboratory Animals of the National Institutes of Health. The protocol was approved by Tufts University's Institutional Animal Care and Use Committee (M2011-70).

*Microinjection of Xenopus Embryos*

Single-cell embryos were placed in 3% Ficoll in 1× MMR and injected in the animal pole using standard methods (50–100 ms pulses with borosilicate glass needles calibrated for a bubble pressure of 50–70 kPa in water). Injections occurred under a red lamp to prevent spurious uncaging of the molecules and were otherwise protected from light. For 5-HT, 30 ng was injected; for BHQ-*O*-5HT, 50 ng was injected; for BHQ-OH, 40 ng was injected. After injections, embryos were washed and incubated at 18°C in the dark.

*Embryo Soaking*

Single-cell embryos were placed in 1× MMR containing 5-HT (5 mM) or BHQ-*O*-5HT (1 mM). Embryos were washed at stage 5 or stage 8 and returned to 0.1× MMR. After treatment, embryos were washed and kept in 0.1× MMR at 18°C in the dark.

*Uncaging 5-HT from BHQ-O-5HT*

After soaking or injection with BHQ-*O*-5HT, embryos were placed on a platform and subjected to high-intensity broad-spectrum light from two light sources: one source was located below the embryos and one source was located above the embryos. Light treatment progressed for 1 hr, and embryos were then washed and returned to a dark 18°C incubator.

*Laterality Assay*

At stage 45, *Xenopus* embryos were analyzed for position of the heart (looping to the left), stomach (coiling to the left), and gall bladder (positioned on the right). Heterotaxia was defined as the reversal in position of one or more organs. Only embryos with normal dorsoanterior patterning were scored. The percentage with LR patterning defects was calculated as the absolute number of heterotaxic embryos divided by the total number of scorable embryos. A chi-square test with Pearson correction for increased stringency was used to compare absolute counts of heterotaxic embryos.

*Assessment of Toxicity*

The number of embryos and tadpoles that died or that were otherwise malformed (abnormal dorsoanterior patterning, edema, spina bifida, etc.) was counted for each treatment group. The toxicity rate was calculated as the absolute number of dead and malformed embryos divided by the total number of embryos. A chi-square test with Pearson's correction for increased stringency was used to compare toxicity rates between treated and untreated groups.

Acknowledgments

We thank Matthew J. O'Connor for technical assistance. This work was supported by grants from the National Institutes of Health (R01 NS070159 to J.D.L. and T.M.D. and GM077425 to M.L.), the American Heart Association (0740088N to M.L.), and the National Science Foundation (CHE-1012412 and CHE-1317760 to T.M.D.).

Tables

**Table A.1. Selected Photophysical and Photochemical Properties of Caged 5-HTs**

| Caged 5-HT | $\lambda_{max}$ (nm) | ε ($M^{-1}$ $cm^{-1}$) | $Q_u$ | Sensitivity ($Q_u \times \varepsilon$) | $\delta_u$ (GM) | $\tau_{dark}$ (hr) |
|---|---|---|---|---|---|---|
| *O*-CNB-5HT | 280 | 800 at 337 nm | 0.03 | 24 | NR | NR |
| $[Ru(bpy)_2(5HT)_2]^{2+}$ | 488 | 9,880 | 0.023 | 227 | NR | NR |
| BHQ-OPh | 369 | 3,200 | 0.19 | 608 | 0.56 | 95 |
| BHQ-*O*-5HT | 368 | 2,000 | 0.30 | 600 | 0.50 | 260 |
| BHQ-*N*-5HT | 370 | 2,100 | 0.10 | 210 | 0.42 | 300 |

UV-vis spectra (Figure A.S3) and photolysis data on BHQ-OPh (Figure A.S1), BHQ-*O*-5HT, and BHQ-*N*-5HT were acquired in KMOPS buffer at pH 7.2. Absolute values of $\delta_u$ are estimated to be accurate within a factor of two (Furuta et al., 1999), but the relative magnitudes of the values are consistent when measured on the same apparatus as is the case here. Data for *N*-CNB-5HT, NPE-*O*-5HT, and NPEC-*N*-5HT are not reported. Data for *O*-CNB-5HT and $[Ru(bpy)_2(5HT)_2]^{2+}$ are from Breitinger et al. (2000) and Zayat et al. (2006), respectively. NR, not reported.

Figures

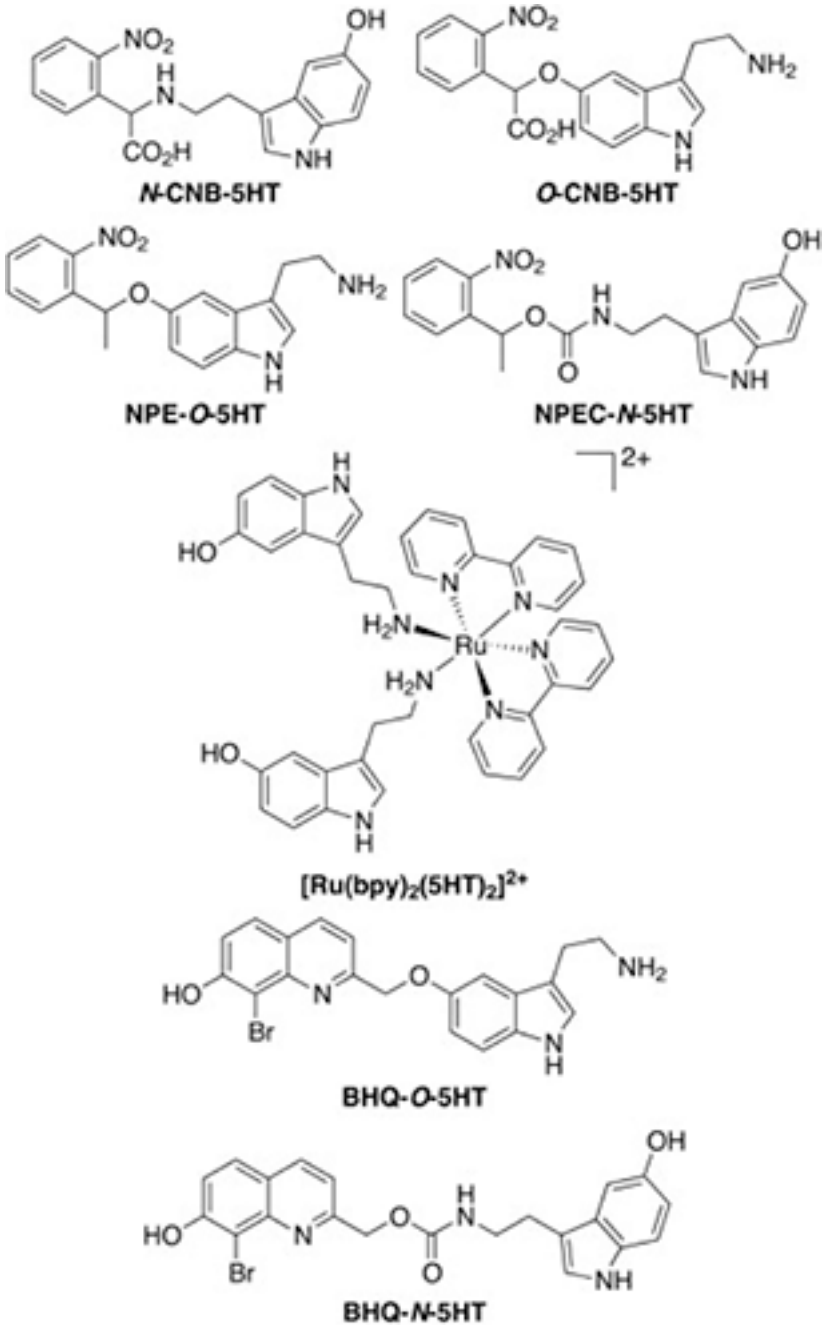


**Figure A.1. Caged serotonins**

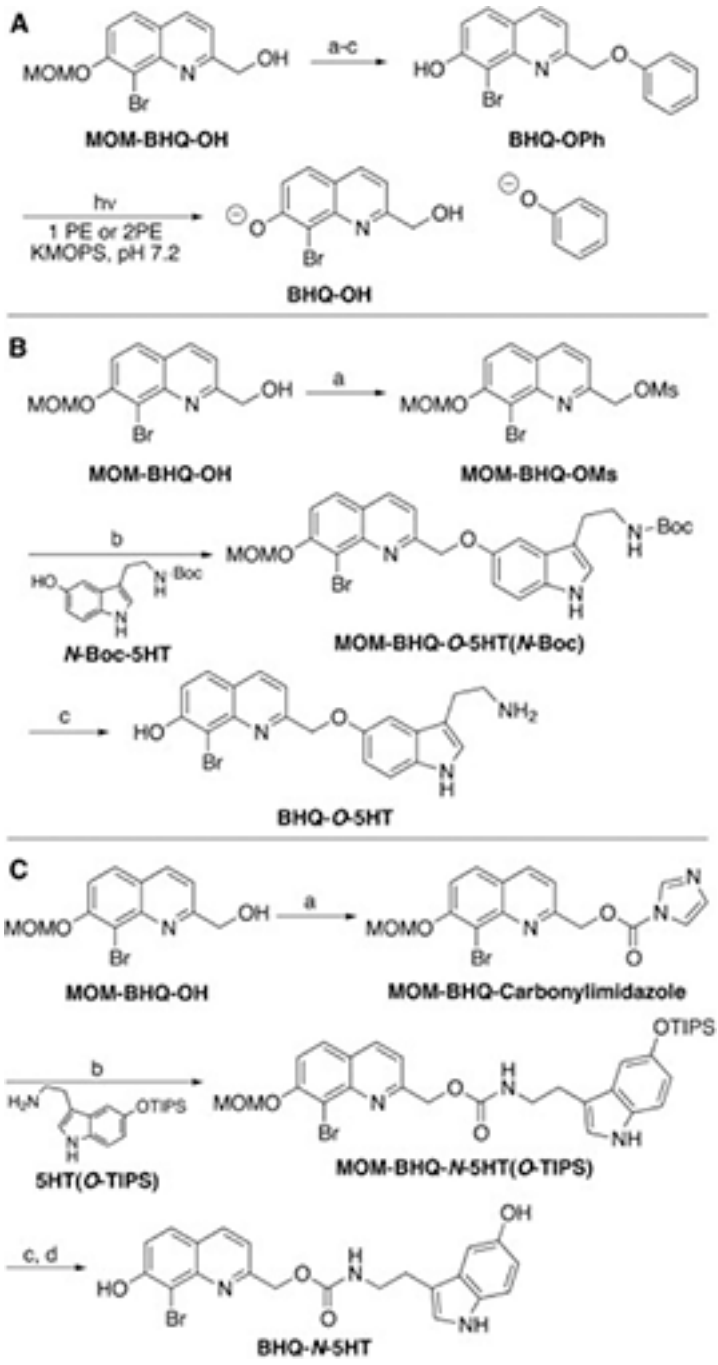


**Figure A.2. Synthesis and Photolysis of BHQ-OPh and Syntheses of BHQ-*O*-5HT and BHQ-*N*-5HT.** (A) Preparation and photolysis of BHQ-OPh. (a) Methanesulfonyl chloride (MsCl), ethyldiisopropylamine (DIEA), THF, RT, 2 hr, 68%. (b) Phenol, 1 M KOH (aqueous), THF, 72%. (c) TFA, $CH_3OH$. Time courses for the photolysis of BHQ-OPh are shown in Figure A.S1. (B) Preparation of BHQ-*O*-5HT. (a) MsCl, DIEA, THF, RT, 2 hr, 68%. (b) $K_2CO_3$, $CH_3CN$, reflux, 48 hr, 78%. (c) TFA, $CH_2Cl_2$, RT, 1 hr, 57%. (C) Preparation of BHQ-*N*-5HT. (a) carbonyldiimidazole, THF, RT, 2 hr, 63%. (b) DMF, 60°C, 12 hr, 65%. (c) TBAF, THF, RT, 15 min, 85%. (d) Concentrated HCl (trace), $CH_3OH$, RT, 12 hr, 55%.

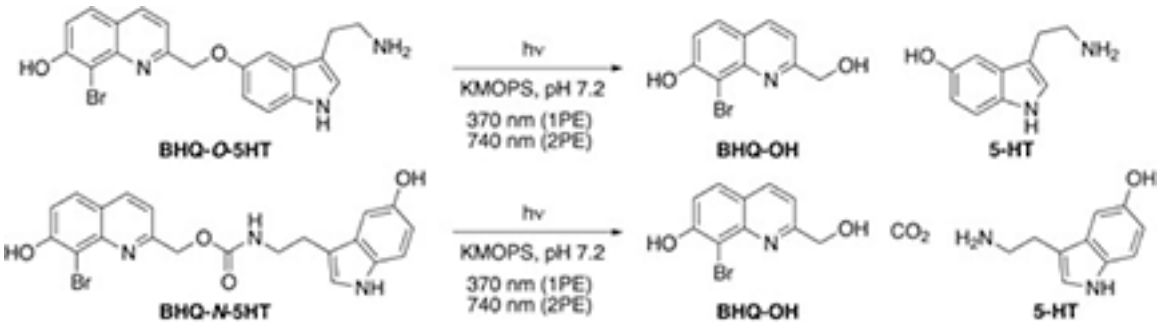


**Figure A.3. Photolysis Reaction of BHQ-*O*-5HT and BHQ-*N*-5HT**

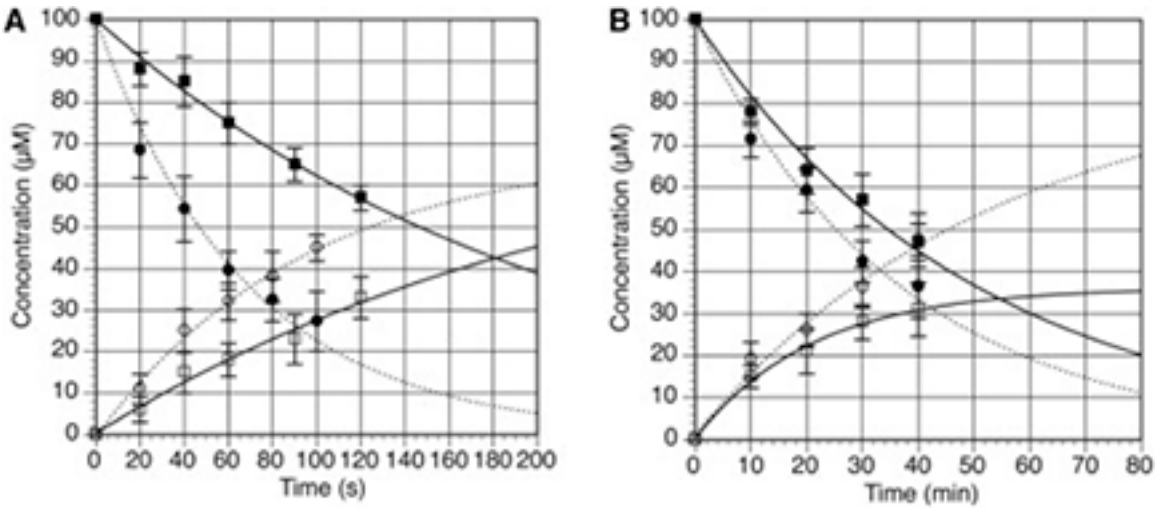


**Figure A.4. Time Course for Photolysis of BHQ-*O*-5HT and BHQ-*N*-5HT**

Time course for photolysis of BHQ-*O*-5HT (closed circles) and BHQ-*N*-5HT (closed squares) at (A) 365 nm (1PE) and (B) 740 nm (2 PE) in KMOPS buffer (pH 7.2) and the rise of 5-HT from BHQ-*O*-5HT (open circles) and BHQ-*N*-5HT (open squares), respectively. The concentration was determined by HPLC using an external standard and is the average of at least three runs. Lines are least-squares fits of a single exponential decay or a single exponential rise to max. From the decay curves, $Q_u$ and $\delta_u$were calculated. Error bars represent the SD of the measurement.

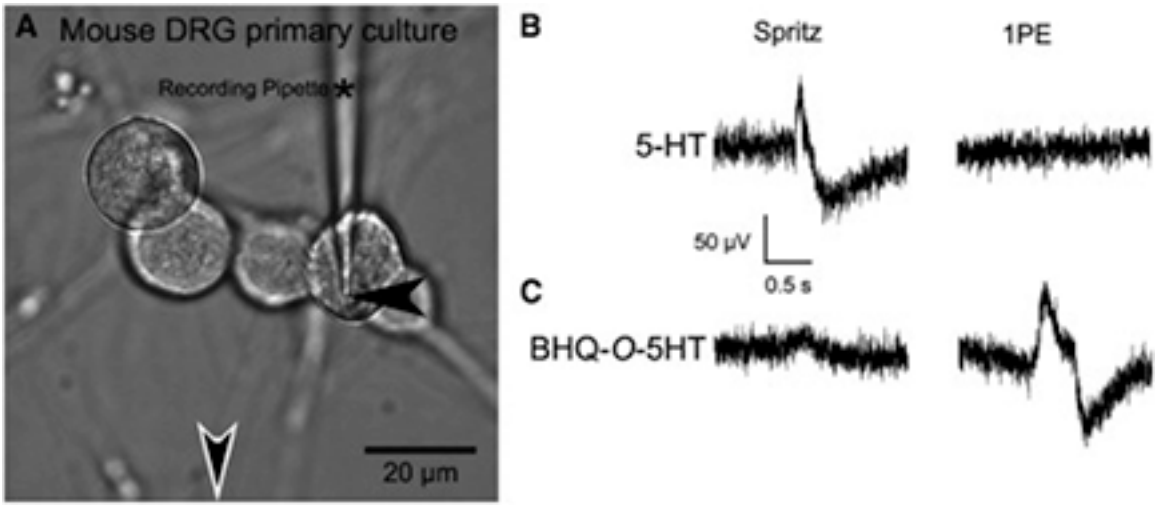


**Figure A.5. BHQ-*O*-5HT Acts on Mouse DRG Neurons in Culture.** (A) Brightfield image of mouse DRG neurons in culture showing placement of the field recording pipette (black arrowhead) and direction toward the microinjection pipette (open white arrowhead) that was located 100 µm from the cells and is out of the field of view. (B) Pressure injection of 1 nl of a 100 µM buffered 5-HT solution induced activity in the medium-sized DRG neuron shown in (A), but no change in activity was observed upon exposure to a 1 ms pulse of 365 nm light (1PE). (C) Although pressure ejection of a 1 mM buffered BHQ-*O*-5HT solution induced a small change baseline activity in the same neuron as (B), a significant change in activity was observed after exposure to a 1 ms pulse of 365 nm light. The traces comparing 5-HT to BHQ-*O*-5HT are temporally aligned to facilitate comparison.

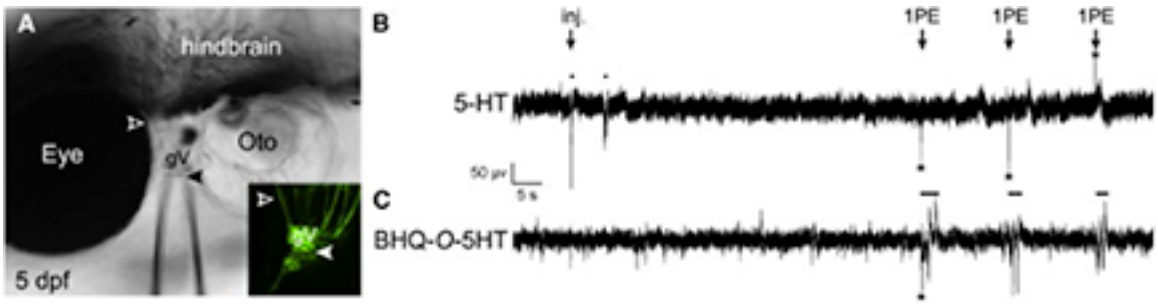


**Figure A.6. BHQ-*O*-5HT Excites Trigeminal Neurons in Intact Zebrafish Larva.** (A) Lateral brightfield view of a zebrafish larva at 5 dpf showing placements of the field recording (black arrowhead) and microinjection (open white arrowhead) pipettes relative to the trigeminal ganglion (gV). Dorsal is up and anterior is left, with the eye, hindbrain and ear (Oto, otocyst) indicated for reference. The inset is a confocal fluorescence image of the trigeminal ganglion obtained from a comparable experiment using a 5 dpf larva expressing the *cameleon* calcium indicator in all neurons. Placements of the recording (arrowhead) and injection (open arrowhead) pipettes are indicated. (B and C) In vivo extracellular field recordings of 5-HT-induced changes in trigeminal ganglion activity. (B) Baseline recordings from the ventral aspect of the trigeminal ganglion show low-amplitude neural activity. Microinjection (inj.) of 0.5 nl of a 1 mM buffered 5-HT solution in the region of the putative maxillary nerve elicited a brief bust of high-amplitude spiking; in some cases, this initial discharge was followed by a second burst within a few seconds of the injection. Bars above traces denote significant changes from baseline activity. No change in activity was observed upon exposure to three 1 ms pulses of 365 nm light (1PE) spaced ~15 s apart. Electronic spikes associated with the lamp discharge are denoted with asterisks; these occur about 60% of the time. (C) Microinjection of 1 nl of a 500 mM buffered BHQ-*O*-5HT solution did not alter baseline activity. Photolysis of BHQ-*O*-5HT by exposure to 1 ms pulses of 365 nm light elicited high-amplitude spiking that typically lasted a few seconds (bars). The traces comparing 5-HT to BHQ-*O*-5HT are temporally aligned to facilitate comparison. A similar experiment was carried out in the optic tectum of 7 dpf zebrafish larva (Figure A.S2).

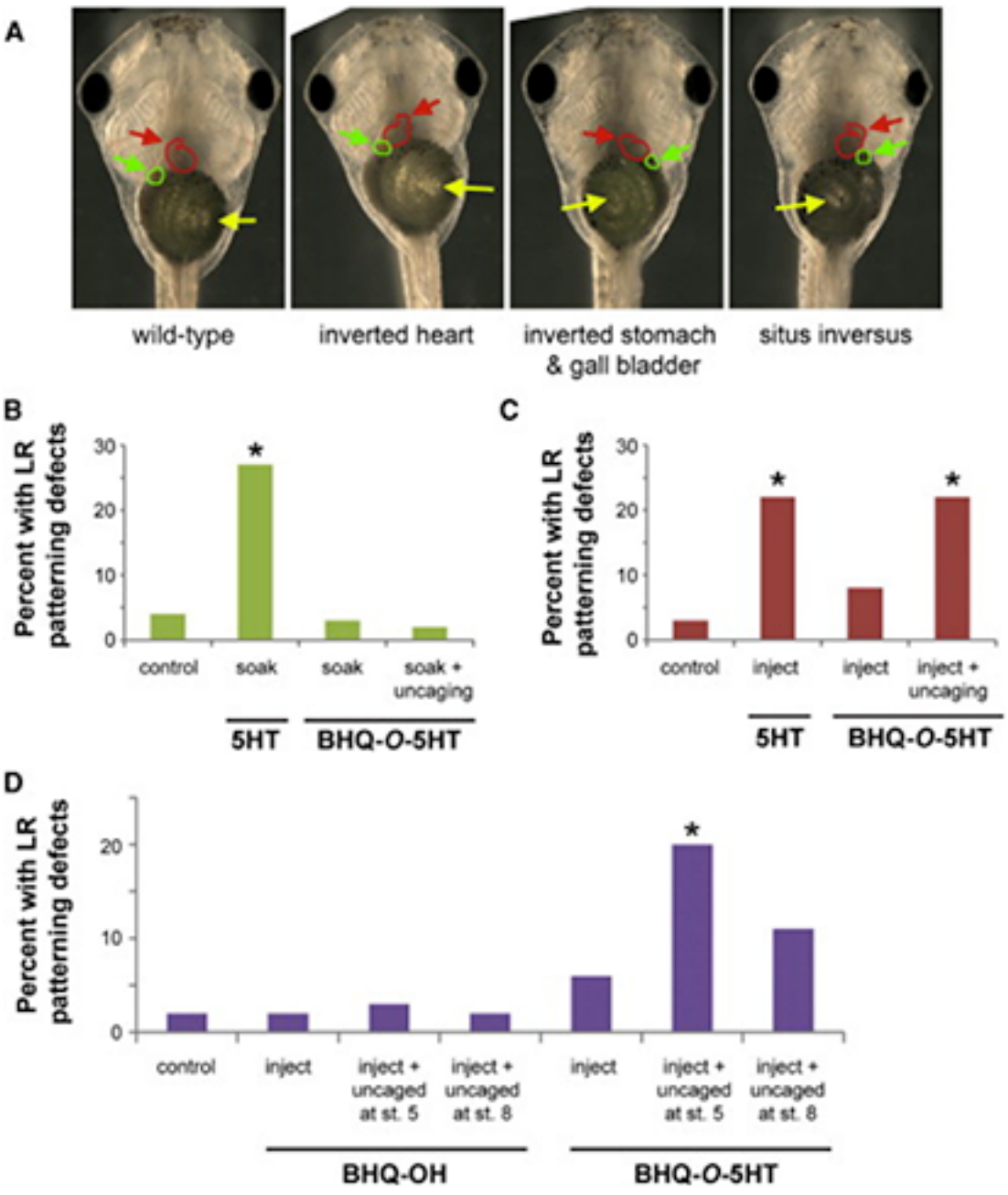


**Figure A.7. BHQ-*O*-5HT Disrupts LR Patterning in *X. laevis* Embryos.** (A) Position of three organs (heart, red arrow; stomach, yellow arrow; gall bladder, green arrow) in wild-type tadpoles and tadpoles with LR patterning defects. (B and C) Single-cell embryos were soaked (B) or injected (C) with 5-HT or BHQ-*O*-5HT, and LR defects were assessed after uncaging. (D) Temporal assessment of BHQ-*O*-5HT uncaging indicates a critical period for the effect of 5-HT on LR patterning. Treatment with BHQ-OH ruled out effects of the PPG and the uncaging light treatment in LR defects.
*$p < 0.01$ relative to controls, chi-square test.

References

Adams, S.R., Kao, J.P.Y., Grynkiewicz, G., Minta, A., and Tsien, R.Y. (1988). Biologically useful chelators that release Ca2+ upon illumination. J. Am. Chem. Soc. 110, 3212–3220. Bardin, L. (2011). The complex role of serotonin and 5-HT receptors in chronic pain. Behav. Pharmacol. 22, 390–404.

Barnes, N.M., and Sharp, T. (1999). A review of central 5-HT receptors and their function. Neuropharmacology 38, 1083–1152.

Basbaum, A.I., and Fields, H.L. (1978). Endogenous pain control mechanisms: review and hypothesis. Ann. Neurol. 4, 451–462.

Boahen, Y.O., and MacDonald, G.M. (2005). A concise approach to caged serotonin for Fourier transform infrared (FT-IR) difference photolysis studies. J. Ghana Sci. Assoc. 7, 54–59.

Bort, G., Gallavardin, T., Ogden, D., and Dalko, P.I. (2013). From one-photon to two-photon probes: ‘‘caged’’ compounds, actuators, and photoswitches. Angew. Chem. Int. Ed. Engl. 52, 4526–4537.

Breitinger, H.-G.A., Wieboldt, R., Ramesh, D., Carpenter, B.K., and Hess, G.P. (2000). Synthesis and characterization of photolabile derivatives of serotonin for chemical kinetic investigations of the serotonin 5-HT(3) receptor. Biochemistry 39, 5500–5508.

Cardenas, C.G., Mar, L.P., Vysokanov, A.V., Arnold, P.B., Cardenas, L.M., Surmeier, D.J., and Scroggs, R.S. (1999). Serotonergic modulation of hyperpolarization-activated current in acutely isolated rat dorsal root ganglion neurons. J. Physiol. 518, 507–523.

Daubert, E.A., and Condron, B.G. (2010). Serotonin: a regulator of neuronal morphology and circuitry. Trends Neurosci. 33, 424–434.

Davis, M.J., Kragor, C.H., Reddie, K.G., Wilson, H.C., Zhu, Y., and Dore, T.M. (2009). Substituent effects on the sensitivity of a quinoline photoremovable protecting group to one- and two-photon excitation. J. Org. Chem. 74, 1721–1729.

Dore, T.M. (2005). Multiphoton phototriggers for exploring cell physiology. In Dynamic Studies in Biology: Phototriggers, Photoswitches, and Caged Biomolecules, M. Goeldner and R.S. Givens, eds. (Weinheim, Germany: Wiley-VCH), pp. 435–459.

Dore, T.M., and Wilson, H.C. (2011). Chromophores for the delivery of bioactive molecules with two-photon excitation. In Photosensitive Molecules for Controlling Biological Function, J.J. Chambers and R.H. Kramer, eds. (New York: Humana Press), pp. 57–92.

Ellis-Davies, G.C.R. (2007). Caged compounds: photorelease technology for control of cellular chemistry and physiology. Nat. Methods 4, 619–628.

Fedoryak, O.D., and Dore, T.M. (2002). Brominated hydroxyquinoline as a photolabile protecting group with sensitivity to multiphoton excitation. Org. Lett. 4, 3419–3422.

Feldberg, W., and Toh, C.C. (1953). Distribution of 5-hydroxytryptamine (serotonin, enteramine) in the wall of the digestive tract. J. Physiol. 119, 352–362.

Frazer, A., and Hensler, J.G. (1999). Understanding the neuroanatomical organization of serotonergic cells in brain provides insight into the functions of this neurotransmitter. In Basic Neurochemistry, Sixth Edition, G.J. Siegel, B.W. Agranoff, R.W. Albers, S.K. Fisher, and M.D. Uhler, eds. (Philadelphia, PA: Lippincott-Raven), pp. 264–268.

Freshney, R.I. (1987). Culture of Animal Cells: A Manual of Basic Technique, Second Edition. (New York: A. R. Liss).

Fukumoto, T., Blakely, R., and Levin, M. (2005a). Serotonin transporter function is an early step in left-right patterning in chick and frog embryos. Dev. Neurosci. 27, 349–363.

Fukumoto, T., Kema, I.P., and Levin, M. (2005b). Serotonin signaling is a very early step in patterning of the left-right axis in chick and frog embryos. Curr. Biol. 15, 794–803.

Furuta, T., Wang, S.S.H., Dantzker, J.L., Dore, T.M., Bybee, W.J., Callaway, E.M., Denk, W., and Tsien, R.Y. (1999). Brominated 7-hydroxycoumarin-4- ylmethyls: photolabile protecting groups with biologically useful crosssections for two photon photolysis. Proc. Natl. Acad. Sci. USA 96, 1193–1200.

Harper, A.A., and Lawson, S.N. (1985a). Conduction velocity is related to morphological cell type in rat dorsal root ganglion neurones. J. Physiol. 359, 31–46.

Harper, A.A., and Lawson, S.N. (1985b). Electrical properties of rat dorsal root ganglion neurones with different peripheral nerve conduction velocities. J. Physiol. 359, 47–63.

Hatchard, C.G., and Parker, C.A. (1956). A new sensitive chemical actinometer. II. Potassium ferrioxalate as a standard chemical actinometer. Proc. R. Soc. Lond. A. Math. Phys. Sci. 235, 518–536.

Ho, K.-k., Baldwin, J.J., Bohnstedt, A.C., Kultgen, S.G., McDonald, E., Guo, T., Morphy, J.R., Rankovic, Z., Horlick, R., and Appell, K.C. February 2003. Preparation of 2-(aminomethyl) arylamide analgesics. U.S. Patent Application 10/364,039.

Holz, G.G.I., 4th, and Anderson, E.G. (1984). The actions of serotonin on frog primary afferent terminals and cell bodies. Comp. Biochem. Physiol. C. Comp. Pharmacol. Toxicol. 77, 13–21.

Holz, G.G.I., 4th, Shefner, S.A., and Anderson, E.G. (1985). Serotonin depolarizes type A and C primary afferents: an intracellular study in bullfrog dorsal root ganglion. Brain Res. 327, 71–79.

Hoyer, D., Clarke, D.E., Fozard, J.R., Hartig, P.R., Martin, G.R., Mylecharane, E.J., Saxena, P.R., and Humphrey, P.P.A. (1994). International Union of Pharmacology classification of receptors for 5-hydroxytryptamine (Serotonin). Pharmacol. Rev. 46, 157–203.

Jackson, M.B., and Yakel, J.L. (1995). The 5-HT3 receptor channel. Annu. Rev. Physiol. 57, 447–468.

Kang, K., Park, S., Kim, Y.S., Lee, S., and Back, K. (2009). Biosynthesis and biotechnological production of serotonin derivatives. Appl. Microbiol. Biotechnol. 83, 27–34.

Kaplan, J.H., Forbush, B., 3rd, and Hoffman, J.F. (1978). Rapid photolytic release of adenosine 50 -triphosphate from a protected analogue: utilization by the Na:K pump of human red blood cell ghosts. Biochemistry 17, 1929– 1935.

Kimmel, C.B., Ballard, W.W., Kimmel, S.R., Ullmann, B., and Schilling, T.F. (1995). Stages of embryonic development of the zebrafish. Dev. Dyn. 203, 253–310.

Kiskin, N.I., and Ogden, D. (2002). Two-photon excitation and photolysis by pulsed laser illumination modelled by spatially non-uniform reactions with simultaneous diffusion. Eur. Biophys. J. 30, 571–587.

Kiskin, N.I., Chillingworth, R., McCray, J.A., Piston, D., and Ogden, D. (2002). The efficiency of two-photon photolysis of a ‘‘caged’’ fluorophore, o-1-(2-nitrophenyl)ethylpyranine, in relation to photodamage of synaptic terminals. Eur. Biophys. J. 30, 588–604.

Kla´ n, P., Solomek, T., Bochet, C.G., Blanc, A., Givens, R., Rubina, M., Popik, V., Kostikov, A., and Wirz, J. (2013). Photoremovable protecting groups in chemistry and biology: reaction mechanisms and efficacy. Chem. Rev. 113, 119–191.

Kramer, R.H., and Chambers, J.J., eds. (2011). Photosensitive Molecules for Controlling Biological Function (New York: Humana Press).

Lawson, S.N., and Waddell, P.J. (1991). Soma neurofilament immunoreactivity is related to cell size and fibre conduction velocity in rat primary sensory neurons. J. Physiol. 435, 41–63.

Lee, H.-M., Larson, D.R., and Lawrence, D.S. (2009). Illuminating the chemistry of life: design, synthesis, and applications of ‘‘caged’’ and related photoresponsive compounds. ACS Chem. Biol. 4, 409–427.

Levin, M., Buznikov, G.A., and Lauder, J.M. (2006). Of minds and embryos: left-right asymmetry and the serotonergic controls of pre-neural morphogenesis. Dev. Neurosci. 28, 171–185.

Lu, M., Fedoryak, O.D., Moister, B.R., and Dore, T.M. (2003). Bhc-diol as a photolabile protecting group for aldehydes and ketones. Org. Lett. 5, 2119– 2122.

Ma, J., Rea, A.C., An, H., Ma, C., Guan, X., Li, M.-D., Su, T., Yeung, C.S., Harris, K.T., Zhu, Y., et al. (2012). Unraveling the mechanism of the photodeprotection reaction of 8-bromo- and 8-chloro-7-hydroxyquinoline caged acetates. Chem.– Eur. J. 18, 6854–6865.

Malin, S.A., Davis, B.M., and Molliver, D.C. (2007). Production of dissociated sensory neuron cultures and considerations for their use in studying neuronal function and plasticity. Nat. Protoc. 2, 152–160.

Mayer, G., and Heckel, A. (2006). Biologically active molecules with a ‘‘light switch’’. Angew. Chem. Int. Ed. 45, 4900–4921.

McGowan, K., Kane, A., Asarkof, N., Wicks, J., Guerina, V., Kellum, J., Baron, S., Gintzler, A.R., and Donowitz, M. (1983). Entamoeba histolytica causes intestinal secretion: role of serotonin. Science 221, 762–764.

Nieuwkoop, P.D., and Faber, J. (1967). Normal Table of Xenopus laevis (Daudin). (Amsterdam: North-Holland Publishing Company).

Nikolenko, V., Yuste, R., Zayat, L., Baraldo, L.M., and Etchenique, R. (2005). Two-photon uncaging of neurochemicals using inorganic metal complexes. Chem. Commun. (Camb.) (13), 1752–1754.

Papageorgiou, G., and Corrie, J.E.T. (1997). Synthesis and properties of carbamoyl derivatives of photolabile benzoins. Tetrahedron 53, 3917–3932.

Raible, D.W., and Kruse, G.J. (2000). Organization of the lateral line system in embryonic zebrafish. J. Comp. Neurol. 421, 189–198.

Rapport, M.M., Green, A.A., and Page, I.H. (1948). Serum vasoconstrictor, serotonin; isolation and characterization. J. Biol. Chem. 176, 1243–1251.

Roshchina, V.V. (2001). Neurotransmitters in Plant Life. (Enfield: Science Publishers).

Salierno, M., Marceca, E., Peterka, D.S., Yuste, R., and Etchenique, R. (2010). A fast ruthenium polypyridine cage complex photoreleases glutamate with visible or IR light in one and two photon regimes. J. Inorg. Biochem. 104, 418–422.

Scroggs, R.S., Todorovic, S.M., Anderson, E.G., and Fox, A.P. (1994). Variation in IH, IIR, and ILEAK between acutely isolated adult rat dorsal root ganglion neurons of different size. J. Neurophysiol. 71, 271–279.

Sive, H.L., Grainger, R.M., and Harland, R.M. (2000). Early Development of Xenopus laevis: A Laboratory Manual. (Cold Spring Harbor: Cold Spring Harbor Laboratory Press).

Specht, A., Bolze, F., Omran, Z., Nicoud, J.-F., and Goeldner, M. (2009). Photochemical tools to study dynamic biological processes. HFSP J. 3, 255–264.

Todorovic, S., and Anderson, E.G. (1990). 5-HT2 and 5-HT3 receptors mediate two distinct depolarizing responses in rat dorsal root ganglion neurons. Brain Res. 511, 71–79.

Trapani, J.G., and Nicolson, T. (2010). Physiological recordings from zebrafish lateral-line hair cells and afferent neurons. Methods Cell Biol. 100, 219–231.

Tsutsui, Y., Ikeda, M., Takeda, M., and Matsumoto, S. (2008). Excitability of small-diameter trigeminal ganglion neurons by 5-HT is mediated by enhancement of the tetrodotoxin-resistant sodium current due to the activation of 5- HT(4) receptors and/or by the inhibition of the transient potassium current. Neuroscience 157, 683–696.

Vandenberg, L.N., and Levin, M. (2010). Far from solved: a perspective on what we know about early mechanisms of left-right asymmetry. Dev. Dyn. 239, 3131–3146.

Vandenberg, L.N., Lemire, J.M., and Levin, M. (2013). Serotonin has early, cilia-independent roles in Xenopus left-right patterning. Dis. Model. Mech. 6, 261–268.

Villie`re, V., and McLachlan, E.M. (1996). Electrophysiological properties of neurons in intact rat dorsal root ganglia classified by conduction velocity and action potential duration. J. Neurophysiol. 76, 1924–1941.

Walker, J.W., Martin, H., Schmitt, F.R., and Barsotti, R.J. (1993). Rapid release of an a-adrenergic receptor ligand from photolabile analogues. Biochemistry 32, 1338–1345.

Warther, D., Gug, S., Specht, A., Bolze, F., Nicoud, J.F., Mourot, A., and Goeldner, M. (2010). Two-photon uncaging: new prospects in neuroscience and cellular biology. Bioorg. Med. Chem. 18, 7753–7758.

Westerfield, M., ed. (2007). The Zebrafish Book: A Guide for the Laboratory Use of Zebrafish (Danio rerio), Fifth Edition (Eugene: University of Oregon Press).

Young, D.D., and Deiters, A. (2007). Photochemical control of biological processes. Org. Biomol. Chem. 5, 999–1005.

Zayat, L., Salierno, M., and Etchenique, R. (2006). Ruthenium(II) bipyridyl complexes as photolabile caging groups for amines. Inorg. Chem. 45, 1728–1731.

Zhao, J., Gover, T.D., Muralidharan, S., Auston, D.A., Weinreich, D., and Kao, J.P.Y. (2006). Caged vanilloid ligands for activation of TRPV1 receptors by 1- and 2-photon excitation. Biochemistry 45, 4915–4926.

Zhu, Y., Pavlos, C.M., Toscano, J.P., and Dore, T.M. (2006). 8-Bromo-7-hydroxyquinoline as a photoremovable protecting group for physiological use: mechanism and scope. J. Am. Chem. Soc. 128, 4267–4276.

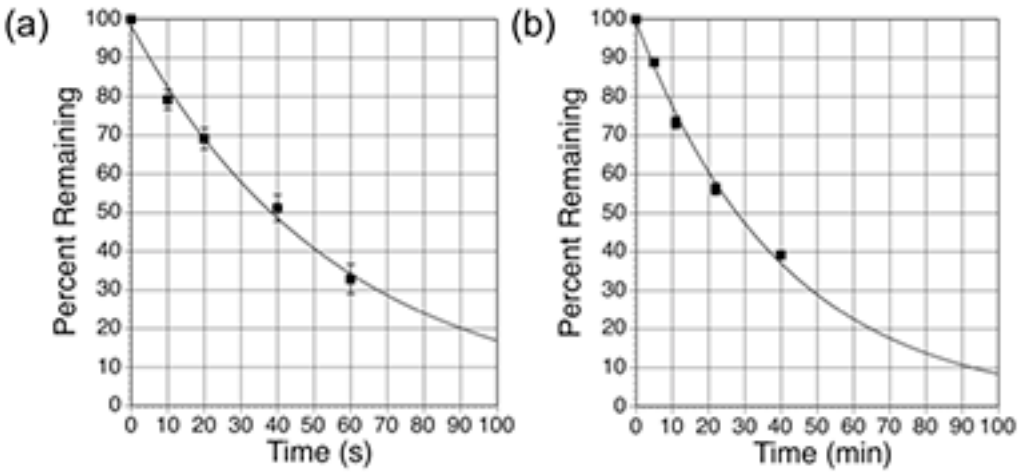


**Figure A.S1.** Time course for photolysis of BHQ-OPh at (a) 365 nm (1PE) and (b) 740 nm (2 PE) in KMOPS buffer (pH 7.2) to accompany Figure A.2a and Table 1 in the main text. The percent remaining was determined by HPLC and is the average of at least 3 runs. Lines are least-squares fits of a single exponential decay. From these curves, $Q_u$ and $\delta_u$ were calculated. Error bars represent the standard deviation of the measurement.

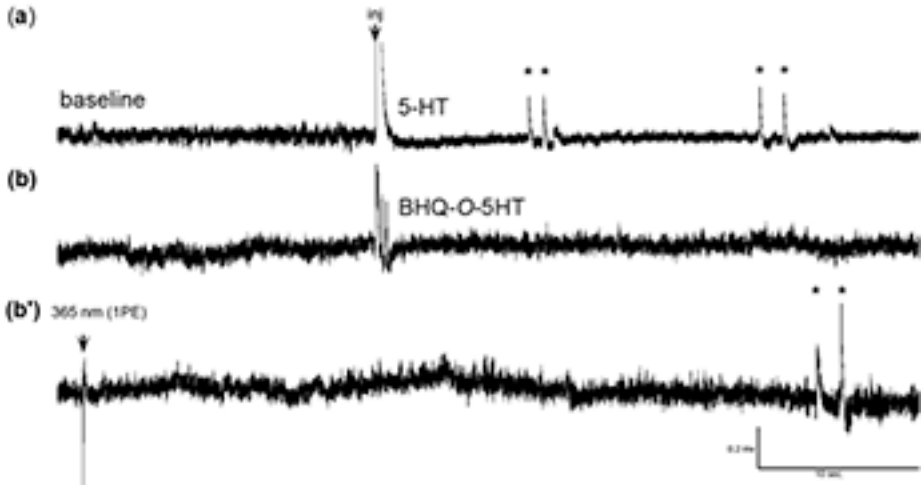


**Figure A.S2.** In vivo extracellular field recordings of 5-HT induced changes in neural activity in the optic tectum of 7-day old zebrafish larva to accompany Figure A.6 in the main text. Baseline recordings from the optic tectum of 7-day old larvae show low amplitude neural activity. **(a)** Micro-injection of 1 nL of a 250-μM buffered 5-HT solution into the optic tectum elicited periodic high amplitude spiking (asterisks) within 10 s of the injection. Response shown was observed in 27 out of 29 experiments. **(b)** Micro- injection of 1 nL of a 500-μM buffered BHQ-*O*-5HT solution did not alter baseline activity. Response shown was observed in 12 out of 12 experiments. **(b′′)** Photolysis of BHQ-*O*-5HT by exposure of the embryo to four 1-ms pulses of 365-nm light elicited periodic high amplitude spiking (asterisks) within 20-30 s. Response shown was observed in 12 out of 12 experiments.

**Electrophysiology in the Optic Tectum of 7 dpf Larval Zebrafish (Figure A.S2)**

*Animals.* Larval zebrafish (*Danio rerio*) of the WIK strain were obtained from animals maintained in the University of Georgia Zebrafish Facility following standard procedures (Westerfield, 2007). Embryos and larvae were staged using standard staging criteria (Kimmel, et al., 1995; Westerfield, 2007). All experiments conformed to the guidelines on the ethical use of animals. All experimental procedures were conducted according to National Institutes of Health guidelines under protocols approved by the University of Georgia Institutional Animal Care and Use Committee and were designed to minimize animal suffering.

*Solutions*. The 5-HT used for this study was purchased from Sigma-Aldrich (St. Louis, MO). The concentration of 5-HT used was 250 μM for each experiment. All neurotransmitters were dissolved in phosphate buffered saline (137 mM NaCl, 10 mM phosphate, 2.7 mM KCl, pH 7.4) containing 0.5% dimethyl sulfoxide. Solid BHQ-*O*-5HT was dissolved in phosphate buffered saline containing 0.5% dimethyl sulfoxide, making a 500 μM solution.

*Electrophysiology*. Larval zebrafish, 7 days post-fertilization (7 dpf) of age, were immobilized by exposure to 0.5 mM pancuronium bromide in normal Ringer's solution (116 mM NaCl, 2.9 mM KCl, 1.8 mM $CaCl_2$, 5.0 mM HEPES, pH 7.2.) and mounted in 1.2% agarose made with normal Ringer's in a 35-mm petri dish, to which 2850 μL Ringer's solution was added. A sharp glass pipet microelectrode (15–20 MΩ impedance), loaded with normal Ringer's solution, was inserted into the optic tectum and the chloride-coated silver reference wire was placed was placed touching a dorsal region of the tail. For drug delivery, a second sharp glass pipet was inserted into the optic tectum in close proximity to the primary electrode. After a 2-minute baseline was recorded, 1 nL of the test compounds were microinjected into the optic tectum and the neurological responses recorded. To control for light flashes used in the uncaging experiments, a fiber optic cable was used to flash the larval set-up (400 V, 2,000 mF × 4 at 2-s intervals) one min after microjection. To test the ability of caged 5-HT to alter the neurological activity of the larvae, BHQ-*O*-5HT was microinjected into the optic tectum of a larval zebrafish. It was observed that injection of the caged-compound did not disrupt or alter the native electrophysiological state of the larvae. Once it had been established that microinjection of the caged-compound would not disrupt the native neural activity, the BHQ-*O*-5HT was photolysed (400 V, 2,000 mF × 4 at 2-s intervals) using a fiber optic cable to flash the larval set-up. For all experiments, the set-up procedure was carried out in dark room conditions. Electrical activity was recorded using an Axoclamp 900a amplifier (Axon Instruments, Union City, Ca, USA). The amplified voltage was passed through a Hum Bug Noise Eliminator (AutoMate Scientific, Berkley, CA, USA), band-pass filtered from 1 Hz–0.1 kHz, and digitized at 10 kHz using a Digidata 1440 interface and stored on a PC using pClamp software (version 10.3, Axon).

*References*

Kimmel, C.B., Ballard, W.W., Kimmel, S.R., Ullmann, B., and Schilling, T.F. (1995). Stages of embryonic development of the zebrafish. Dev. Dyn. *203*, 253-310.

Westerfield, M. ed. (2007). The Zebrafish Book: A Guide for the Laboratory Use of Zebrafish (*Danio rerio*), 5th Edition (Eugene, OR: University of Oregon Press).

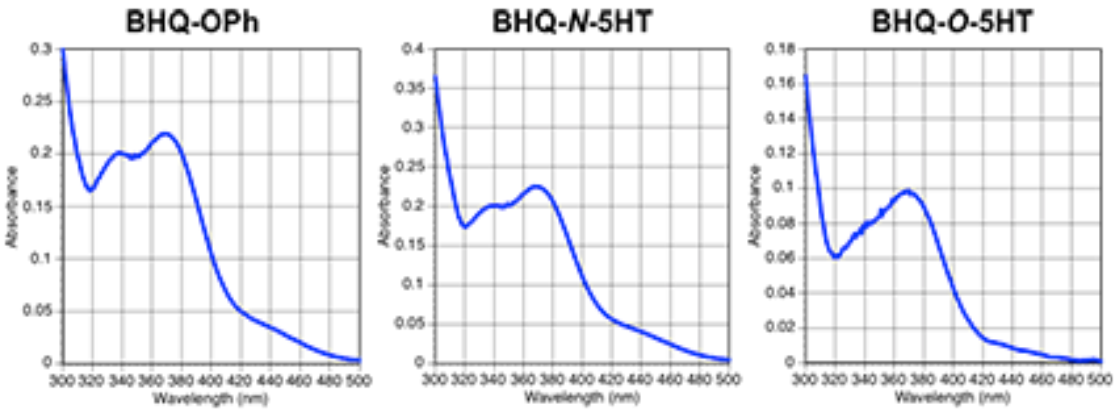


**Figure A.S3.** Representative UV-vis spectra of BHQ-OPh (68 μM), BHQ-*N*-5HT (110 μM), and BHQ-*O*-5HT (49 μM) in KMOPS buffer (pH 7.2) to accompany Table A.1.

$^{1}$**H NMR Spectra** (see synthetic preparations in the Experimental Procedures section)
*MOM-BHQ-OMs (chloroform-d)*

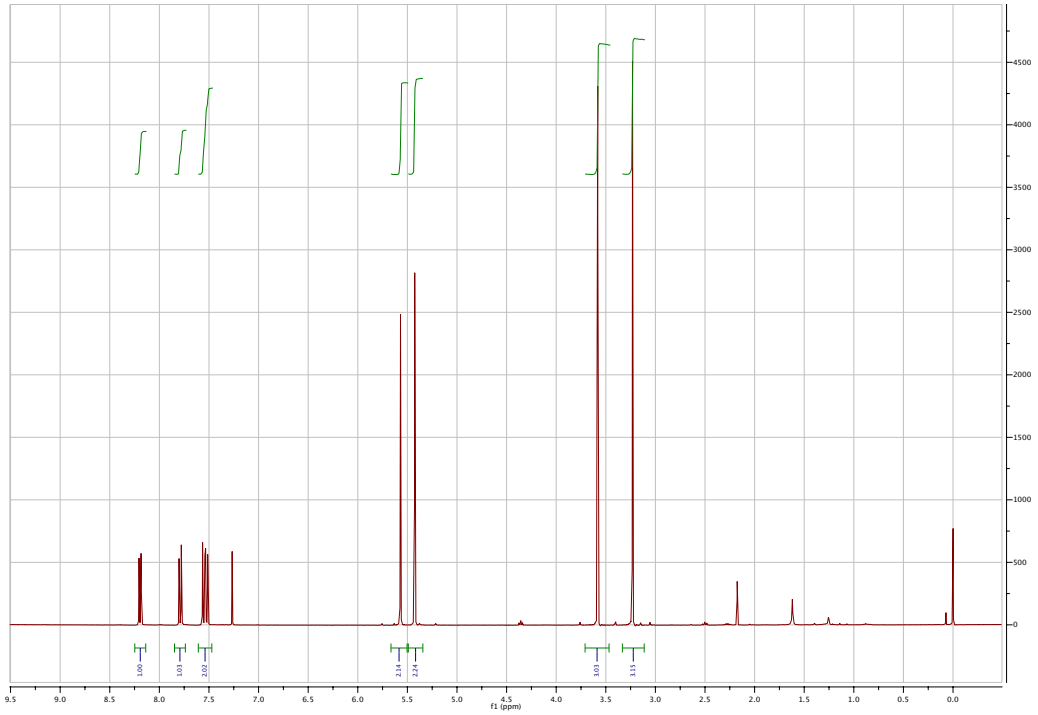

*MOM-BHQ-OPh (chloroform-d)*


*BHQ-OPh (chloroform-d)*

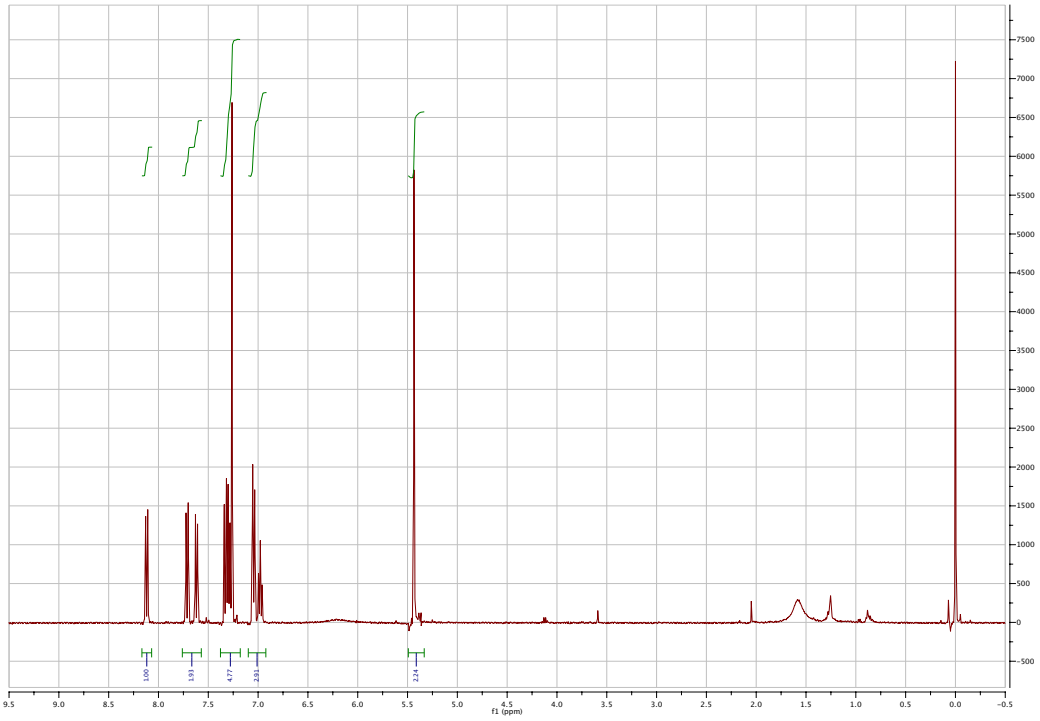

*MOM-BHQ-Carbonylimidazole (chloroform-d)*

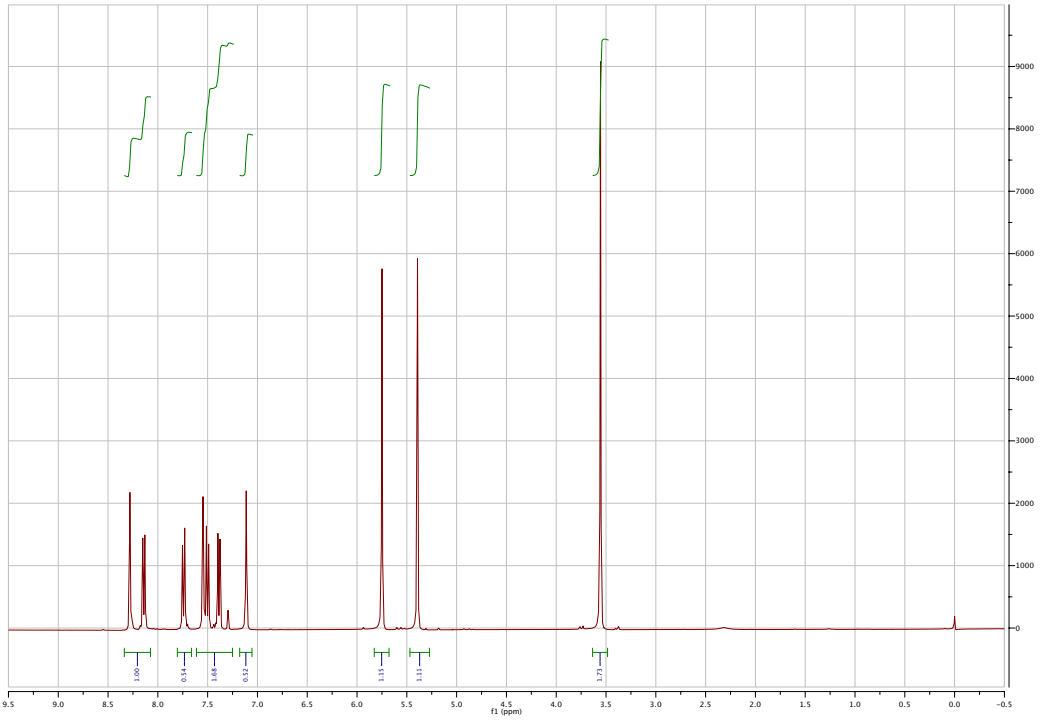


*MOM-BHQ-N-5HT(O-TIPS) (chloroform-d)*

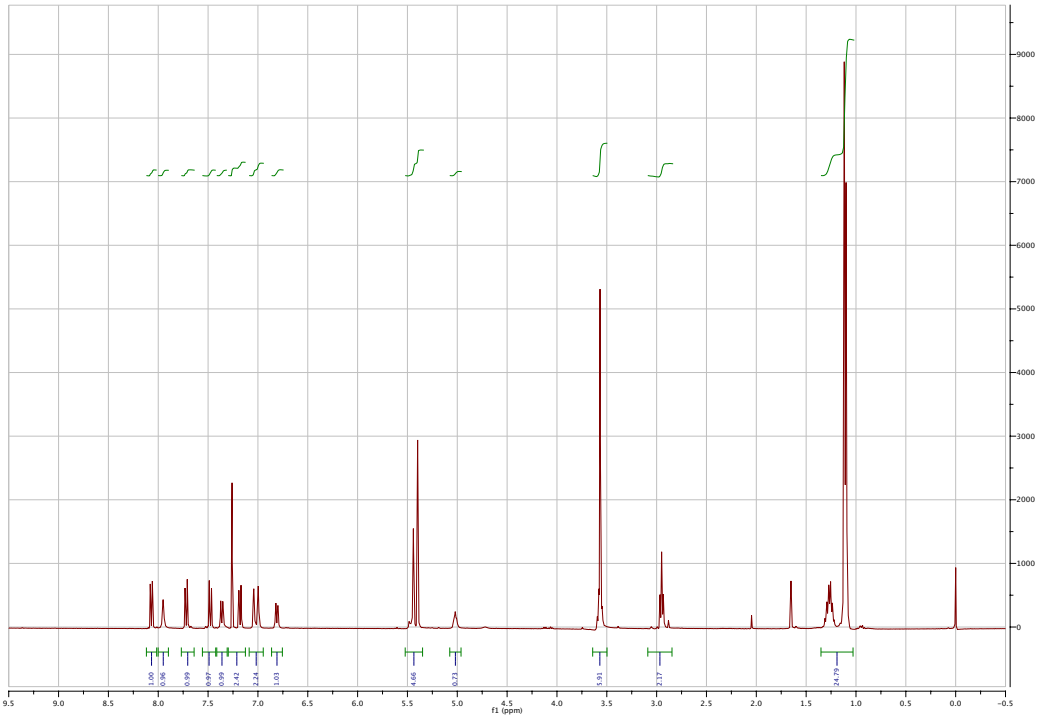

*MOM-BHQ-*N*-5HT (chloroform-d)*

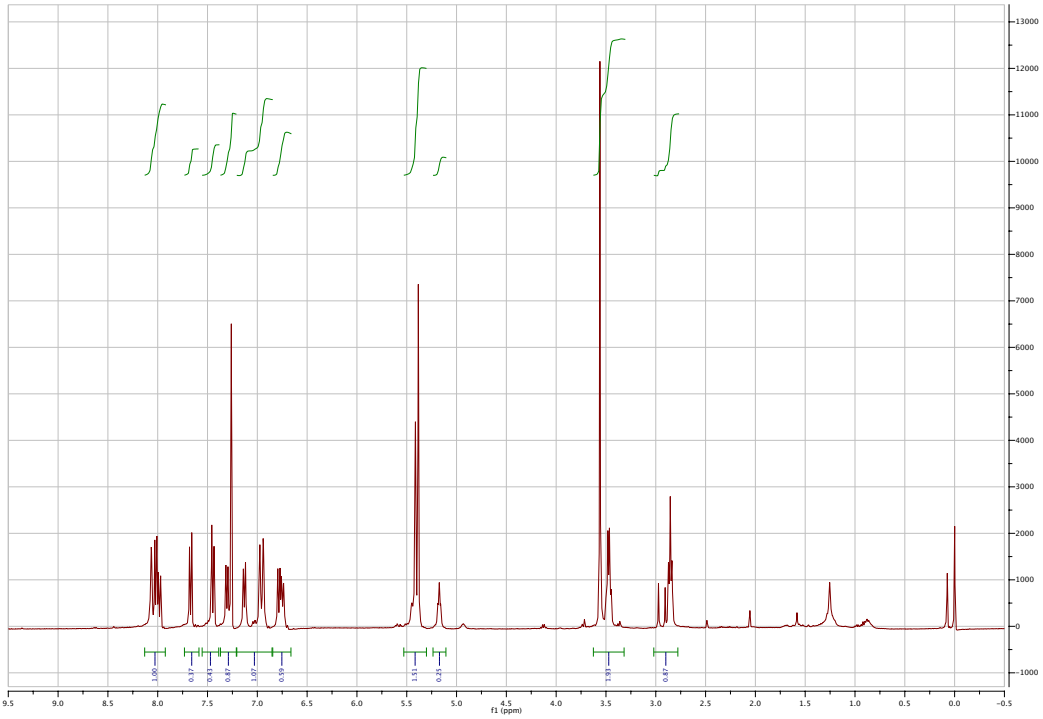

*BHQ-N-5HT (acetone-d6)*

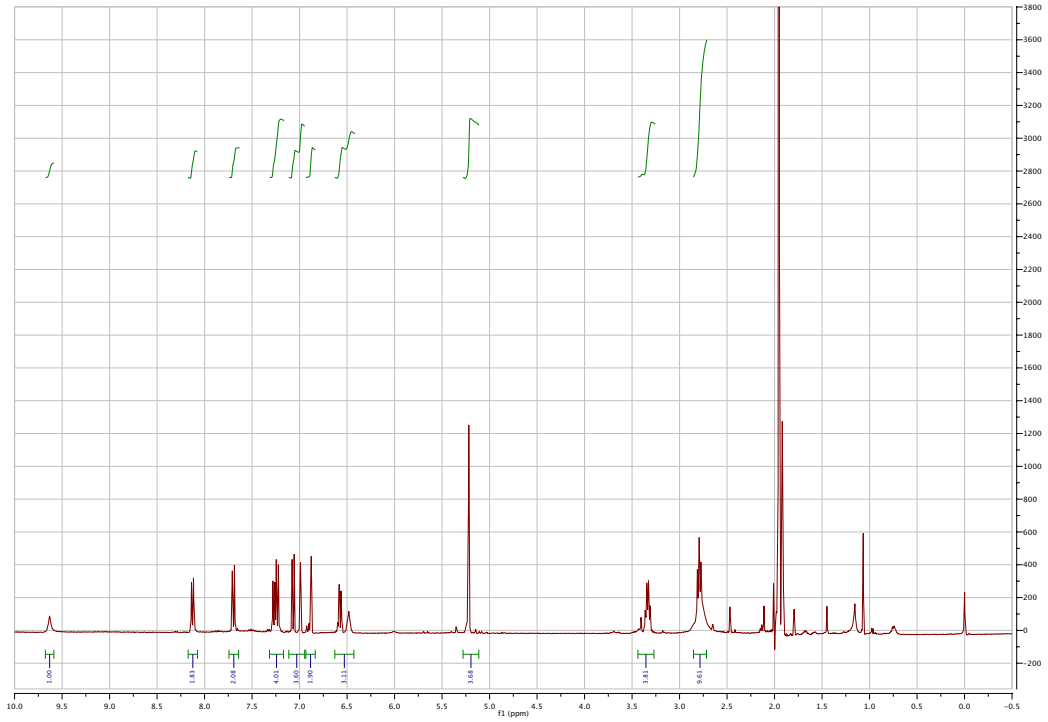

*BHQ-O-5HT(*N-*Boc) (chloroform-d)*

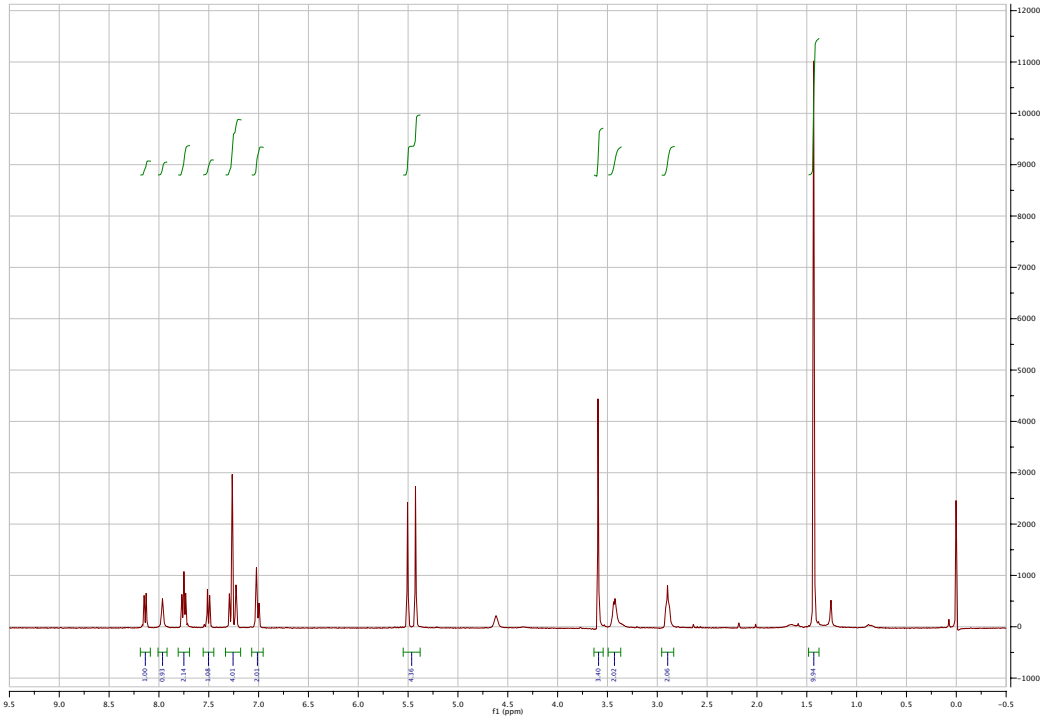

*BHQ-O-5HT (methanol-d4)*

**HPLC Data** (see synthetic preparations in the Experimental Procedures section)

*BHQ-O-5HT*

Microsorb-MV 100-5 C18 250 × 4.6 mm column 40% $CH_3CN$/60% $H_2O$ (w/ 0.1 % TFA) isocratic, 1 mL/min flow rate